ALFRED-WEGENER-INSTITUT
HELMHOLTZ-ZENTRUM FÜR POLAR- UND MEERESFORSCHUNG

725
2018

Berichte
zur Polar- und Meeresforschung

Reports on Polar and Marine Research

Russian-German Cooperation: Expeditions to Siberia in 2017

Edited by

Jens Strauss, Julia Boike, Dmitry Yu. Bolshiyanov, Mikhail N. Grigoriev, Hassan El-Hajj, Anne Morgenstern, Pier Paul Overduin and Annegret Udke
with contributions of the participants

HELMHOLTZ GEMEINSCHAFT

Die Berichte zur Polar- und Meeresforschung werden vom Alfred-Wegener-Institut, Helmholtz-Zentrum für Polar- und Meeresforschung (AWI) in Bremerhaven, Deutschland, in Fortsetzung der vormaligen Berichte zur Polarforschung herausgegeben. Sie erscheinen in unregelmäßiger Abfolge.

Die Berichte zur Polar- und Meeresforschung enthalten Darstellungen und Ergebnisse der vom AWI selbst oder mit seiner Unterstützung durchgeführten Forschungsarbeiten in den Polargebieten und in den Meeren.

Die Publikationen umfassen Expeditionsberichte der vom AWI betriebenen Schiffe, Flugzeuge und Stationen, Forschungsergebnisse (inkl. Dissertationen) des Instituts und des Archivs für deutsche Polarforschung, sowie Abstracts und Proceedings von nationalen und internationalen Tagungen und Workshops des AWI.

Die Beiträge geben nicht notwendigerweise die Auffassung des AWI wider.

Herausgeber
Dr. Horst Bornemann

Redaktionelle Bearbeitung und Layout
Birgit Reimann

Alfred-Wegener-Institut
Helmholtz-Zentrum für Polar- und Meeresforschung
Am Handelshafen 12
27570 Bremerhaven
Germany

www.awi.de
www.reports.awi.de

The Reports on Polar and Marine Research are issued by the Alfred Wegener Institute, Helmholtz Centre for Polar and Marine Research (AWI) in Bremerhaven, Germany, succeeding the former Reports on Polar Research. They are published at irregular intervals.

The Reports on Polar and Marine Research contain presentations and results of research activities in polar regions and in the seas either carried out by the AWI or with its support.

Publications comprise expedition reports of the ships, aircrafts, and stations operated by the AWI, research results (incl. dissertations) of the Institute and the Archiv für deutsche Polarforschung, as well as abstracts and proceedings of national and international conferences and workshops of the AWI.

The papers contained in the Reports do not necessarily reflect the opinion of the AWI.

Editor
Dr. Horst Bornemann

Editorial editing and layout
Birgit Reimann

Alfred-Wegener-Institut
Helmholtz-Zentrum für Polar- und Meeresforschung
Am Handelshafen 12
27570 Bremerhaven
Germany

www.awi.de
www.reports.awi.de

Titel: Das neu installierte klimatisierte Feldobservatorium-Iglu auf der Insel Samoylov, Lena Delta, beherbergt empfindliche Messgeräte, die an den meteorologischen Messturm im Hintergrund angeschlossen sind (Foto: Peter Schreiber, AWI).

Cover: The newly installed and climate-controlled observatory igloo on Samoylov Island, Lena Delta, houses sensitive measuring devices connected to the meteorological instrument tower in the background (Photo: Peter Schreiber, AWI).

Russian-German Cooperation: Expeditions to Siberia in 2017

Edited by

Jens Strauss, Julia Boike, Dmitry Yu. Bolshiyanov, Mikhail N. Grigoriev,

Hassan El-Hajj, Anne Morgenstern, Pier Paul Overduin and Annegret Udke

with contributions of the participants

Please cite or link this publication using the identifiers

http://hdl.handle.net/10013/epic.d436b7c2-6fb6-4543-813e-39e022d17bd5 and
https://doi.org/10.2312/BzPM_0725_2018

ISSN 1866-3192

Expeditions to Siberia in 2017

Research Station Samoylov Island and Lena Delta 02.04 - 26.09.2017

Drilling Campaign on Bykovsky Peninsula: Spring 2017 06.04 - 24.04.2017

Summer campaign on Bykovsky Peninsula 09.07 - 08.08.2017

Chief scientists

Julia Boike (AWI Potsdam), Dmitry Bolshiyanov (AARI), Svetlana Evgrafova (SIF), Alexey Fage (IPGG, NSU), Mikhail Grigoriev (MPI, IPGG), Guido Grosse (AWI Potsdam), Nikolay Mikhaltsov (IPGG, NSU), Anne Morgenstern (AWI Potsdam), Pier Paul Overduin (AWI Potsdam), Lasse Sander (AWI Sylt), Jens Strauss (AWI Potsdam)

Contents

Chapter 1

Introduction

Anne Morgenstern [1], Pier Paul Overduin [1], Jens Strauss [1], Julia Boike [1], Dmitry Y. Bolshiyanov [2], Mikhail N. Grigoriev [3,4,5]

[1] Alfred Wegener Institute Helmholtz Center for Polar and Marine Research, Potsdam, Germany

[2] Arctic and Antarctic Research Institute, St. Petersburg, Russian Federation

[3] Melnikov Permafrost Institute, Siberian Branch, Russian Academy of Sciences, Russian Federation

[4] Trofimuk Institute for Petroleum Geology and Geophysics, Siberian Branch, Russian Academy of Sciences, Russian Federation

[5] North-Eastern Federal University, Yakutsk, Russian Federation

Overview

This report provides an overview of the study locations, scientific objectives and field activities of the joint Russian-German expeditions to Siberia in 2017, which investigated the biology, geology, geomorphology, coastal dynamics, ecology and paleo-enviroment of the Lena Delta region, with a focus on Samoylov Island. Co-operative Russian-German geo-science research in Siberia resulted in annual expeditions to Yakutia and the Siberian Arctic since 1993. An expedition to the Lena River Delta in 1998 within the framework of the Russian-German Cooperation SYSTEM LAPTEV SEA, supported by the research ministries of both countries was the first in the series of annual joint Russian-German expeditions LENA. This first expedition laid the foundation for the establishment of a permafrost observatory on Samoylov Island in the central Lena Delta and the operation of a research station, which has been serving as a scientific and logistical base for the LENA expeditions ever since. Permafrost conditions, micrometeorology, trace gas exchange, biology, and many other parameters are monitored at long-term measurement sites on the island and have been providing important data for the expeditions and the research community as a whole, for example through publication via data portals such as PANGAEA (https://www.pangaea.de/) or integration into international data bases, such as the Global Terrestrial Network for Permafrost (GTN-P; http://gtnp.arcticportal.org/). In 2017, the LENA expedition covered the period from April to September. It was coordinated by Prof. Dr. Guido Grosse (Alfred Wegener Institute Helmholtz Center for Polar and Marine Research - AWI, Potsdam), Prof. Dr. Dmitry Bolshiyanov (Arctic and Antarctic Research Institute - AARI, St. Petersburg) and Dr. Mikhail N. Grigoriev (Melnikov Permafrost Institute, Siberian Branch, Russian Academy of Sciences – MPI SB RAS, Yakutsk) and led by Dmitry Bolshiyanov and Waldemar Schneider. In addition to research on Samoylov Island, field sites included other locations within the Lena River Delta and adjacent to it. Larger efforts focused on water bodies along the southern coast of the Bykovsky Peninsula, where a drilling expedition took place in the spring (April-May) followed by a summer expedition (July-August). This report is split

into three chapters devoted to work in the Lena Delta, focused around Research Station Samoylov Island (Chapter 2), to the spring drilling expedition on the Bykovsky Peninsula (Chapter 3) and to the summer expedition to the Bykovsky Peninsula (Chapter 4). Participants and their affiliations are listed in the appendix, which also lists all the collected samples and measurements made in 2017.
The Research Station Samoylov Island is operated by the Trofimuk Institute for Petroleum Geology and Geophysics, Siberian Branch, Russian Academy of Sciences (IPGG SB RAS), and provided a logistics staging base, laboratories for field work and accommodation for the scientists, technicians and students.
This report contains contributions from the participants. The authors are responsible for content and correctness.

Figure 1-1: *Samoylov Island and Lena Delta Campaign Logo - Bykovsky Peninsula Campaign Logo*

Expedition Lena 2017 – Participants and itinerary
75 scientists, technicians and students participated in the 2017 LENA expedition, of which 35 were based at Russian research institutions and universities, 32 were from Germany and 8 from Switzerland.
Jens Strauss (AWI Potsdam) and Mikhail Grigoriev (MPI Yakutsk) led the Drilling Campaign on Bykovsky Peninsula, which was taking place from 06 April to 24 April 2017. In total, a group of 26 participants (12 German and 14 Russian) took part in the drilling campaign with a maximum number of 22 at the same time. The expedition group started in Tiksi from where the group was transferred to Uomullyakh-Kyuel Lagoon (06 April 2017), Polar Fox Lagoon (13 April 2017) and Goltsovoye Lake (19 April 2017).
The Summer Campaign on Bykovsky Peninsula with 11 participants (3 German and 8 Russian) was led by Pier Paul Overduin (AWI Potsdam) from 09 July to 08 August 2017. The group camped at Uomullyakh-Kyuel Lagoon from 11 July to 5 August 2017. At the beginning of August, work was also done aboard the Yacht Nicole in Tiksi Bay, Buor Khaya Bay and the Lena River Delta for six days.

Figure 1-2: *Samoylov Island Spring Team*

Figure 1-3: *Samoylov Island July Team - 1*

Figure 1-4: *Samoylov Island July Team - 2*

Figure 1-5: *Samoylov Island August Team - 1*

Figure 1-6: *Samoylov Island August Team - 2*

Figure 1-7: *Samoylov Island August Team with members of the delegation of AWI and IPGG directors and German general consulate in Novosibirsk visiting the station*

Figure 1-8: *Samoylov Island September Team*

Figure 1-9: *Bykovsky Spring Campaign Team - 1*

Figure 1-10: *Bykovsky Spring Campaign Team - 2*

Figure 1-11: *Bykovsky Summer Campaign Team*

Acknowledgements
The LENA 2017 expedition depended on essential support of the Russian and German organizing institutions, funding agencies, authorities and individuals. In particular, we would like to express our appreciation to the staff of the Research Station Samoylov Island, the Lena Delta Reserve, the Tiksi Hydrobase, and Arctica GeoCenter.

Chapter 2

Research Station Samoylov Island and Lena Delta

Edited by: Julia Boike, Leonid Tsibizov, Ingeborg Bussmann, Christophe Praz, Svetlana Evgrafova, Lasse Sander, Anne Morgenstern

2.1 Introduction

Julia Boike[1]

[1] Alfred Wegener Institute Helmholtz Center for Polar and Marine Research, Potsdam, Germany

The Lena River Delta is one of the key regions for the understanding of the dynamic of the Arctic climate system. Thus, the continuation of the Russian-German investigations and long term observations since 1998 are prerequisite for understanding the observed processes and changes. The field research started at the research base Samoylov on April (spring) when snow and ice still covered the ground and ended the end of September when the first freezing of the tundra took place. In addition to experimental work carried out on Samoylov, several teams used the research base on Samoylov to access the adjacent islands (Kurungnakh) and the inner part of the Lena River, collecting data on permafrost and soils, lakes and rivers, atmospheric fluxes and thermokarst.

2.2 ISOARC: Maintenance of the *in situ* water vapour isotopic analyser on Samoylov Island

Jean-Louis Bonne[1], Hanno Meyer[2], Kirstin Hoffmann[2] (Martin Werner[1], Sepp Kipfstuhl[1], Benjamin Rabe[1], Melanie Behrens[1], Lutz Schoenicke[2]: not in the field)

[1] Alfred Wegener Institute Helmholtz Center for Polar and Marine Research, Bremerhaven, Germany

[2] Alfred Wegener Institute Helmholtz Center for Polar and Marine Research, Potsdam, Germany

Fieldwork period and location
April 2nd to April 21st and August 25th to August 28th, 2017 (on Samoylov Island)

Objectives
The project ISOARC, supported by AWI strategy fund, aims at understanding the water transport pathways in the Arctic with a focus on Northern Eurasia. The *in situ* water vapour isotopic analyzers, installed at Samoylov Station and on-board the Polarstern in July 2015. These analyzers are associated with a network of ground stations in Eurasian Arctic from collaborating institutes, provide a dataset of specific humidity, $H_2{}^{18}O$ and HDO, covering a transect of approx. 6,000 km in the eastern Arctic. This will allow a quantitative assessment of the Eurasian Arctic water cycle, its isotopic variations and imprint in various climate archives.

Fieldwork
A Cavity Ring Down Spectroscopy (CRDS) analyser (Picarro, Inc. L2140-i) has been running continuously since July 2015. It alternately measures stable oxygen and hydrogen isotopes of either ambient air (sampled through a heated tube, with an inlet located at about 5 meters height above ground level) or air coming from one of the two custom-made calibration units. Two independent calibration systems have been installed for a better resilience of the instrument: a vaporizer system allowing for a four-point calibration and a custom-made dew point generator, later named bubbler, allowing for a one-point standard calibration (see setup on Figure 2.2-1). Two types of calibrations are performed: (i) correction of the humidity concentration-dependence by measuring each standard across a range of humidity values covering the expected ambient air humidity values, and (ii) repeated corrections of the deviation from the VSMOW-SLAP scale by fitting a linear regression between the known values and the measured values of a set of water standards, also allowing for the correction of the instrumental drift. This follows the recommendations of Bailey et al. (2015).

Troubles with the dry air source for the calibration unit, lowering the stability of the calibrations and their precision at low humidity, have been noticed in September 2016. In order to improve the dry air base level, a chemical desiccant unit has been installed downstream of the dry air generator in April 2017. This new device now provides a very stable and low humidity level. After selection of the valid experiments, the concentration dependency has been estimated, as shown on Figure 2.2-2.

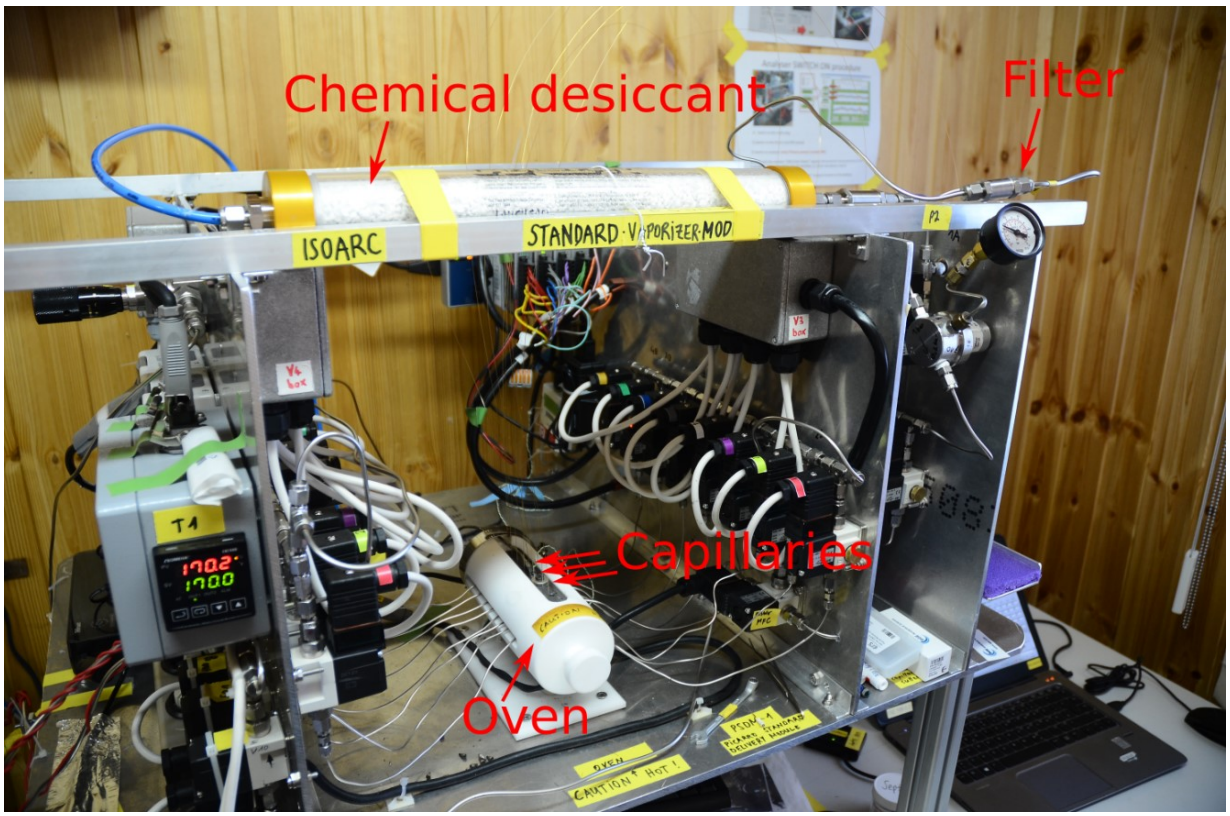

Figure 2.2-1: *Vaporizer calibration system with newly installed chemical desiccant and air filters*

Since summer 2016, the bubbler calibration system has been used on a daily basis. A slow drift of the isotopic composition has been noticed on the standard. This effect can be corrected in the future as samples of the standard have been taken during each visit on site and measured afterwards in Potsdam.

In order to attempt limiting the frequency of clogging of the fused silica capillaries, which are used to deliver liquid water standards for the calibration, new filters have also been installed after the dry air source to prevent particles from entering the calibration unit. However, regular control and small maintenance of the instrument is always needed, as the mentioned problem could not yet be solved completely. Improvements of the system regarding the capillaries could still be worthwhile in the future. Additionally, routine maintenance of different consumables (including pumps membranes, filters, dry air generator, glass capillaries) has also been done on site in April 2017, and Kirstin Hoffmann has been trained at the full instrument maintenance. In addition to the water vapour observations, a snow sampling campaign was conducted for a period of 12 consecutive days in April 2017 in order to obtain new insights into the spatial and temporal variability of the stable water isotope composition of the snow cover. At six different sites in the surroundings of the research station, the upper 5 cm of the snow cover were sampled, first four times a day (8 am, 12 pm, 4 pm and 8 pm) and then due to time shortage three times a day (8 am, 2 pm and 8 pm). In addition, samples of snow precipitation were collected when occurring. After their arrival in Germany, all samples were analysed for their stable water isotope composition at the Stable Isotope Laboratory of AWI Potsdam.

In the end of August 2017, a second full maintenance of the dry air generator and of the inlet pump (KNF) has been carried out and the Drierite chemical desiccant tube has been exchanged. This latter step reduced the humidity level from about 150 ppm to 65 ppm. Two additional isotope-humidity response curves have been measured on lines 1A and 2A. In summary, the system has been maintained and tested from August 24th to 28th 2017, then routine measurement were started again.

Preliminary results

Data acquired since July 2017, as shown on Figure 2.2-3, clearly depict variability on multiple time scales. Yearly cycles on specific humidity and δ^{18}O reveal seasonal variations of large amplitudes. In addition to the seasonal variations, meteorological conditions lead to large increases of specific humidity and δ^{18}O, with duration from a few days to weeks and amplitudes comparable to the seasonal cycles.

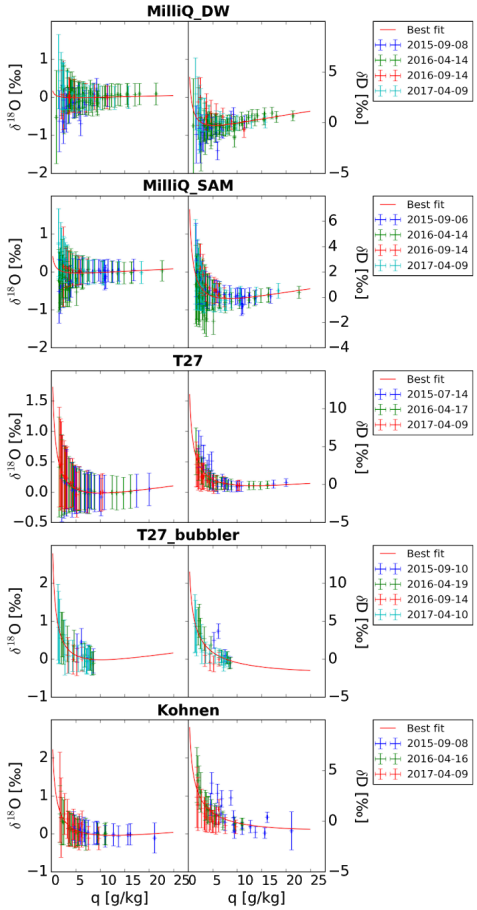

Figure 2.2-2: *Results of the concentration dependency experiments after manual selection of the valid tests based on dry air base level stability for the different standards (top to bottom: MilliQ_DW at -9.45 % in δ18O, MilliQ_SAM at -20.71 % , T27 at -34.24 %, T27 used with the bubbler system, Kohnen at -44.37 %). δ18O (left column) and δD (right column) deviations in % as a function of the specific humidity (in g/kg). Real measurements are shown with error bars in colors depending on the time of the test. The red line shows the estimated concentration dependency function.*

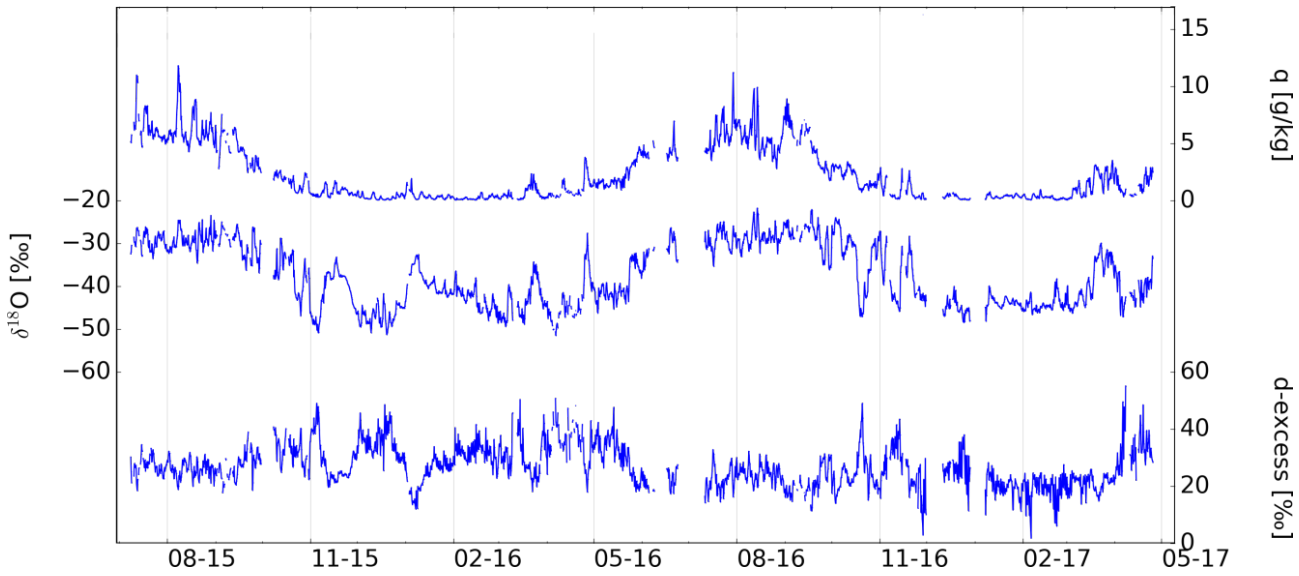

Figure 2.2-3: *Time series of water vapour isotopic observations on Samoylov Island from July 2015 to April 2017*

2.3 Samoylov long term meteorology, soil, and greenhouse gas observatory

Julia Boike[1], (Lars Kutzbach[2]: not in the field), Torsten Sachs[3], Lutz Beckebanze[2], Niko Bornemann[1], Oliver Kaufmann[2], Zoé Rehder[2], Norman Rüggen[2], Peter Schreiber[1], Christian Wille[3]

[1] Alfred Wegener Institute Helmholtz Centre for Polar and Marine Research, Potsdam, Germany

[2] Institute of Soil Science (IFB), Universität Hamburg, Germany

[3] Helmholtz-Zentrum Potsdam - GFZ German Research Center for Geosciences, Potsdam, Germany

Fieldwork period and location
September 03rd to September 26th, 2017 (near Samoylov research station, Lena River Delta)

Objectives
The goal of our research was to provide a continuation of long-term meteorological, hydrological, soil physical, and carbon and energy exchange flux measurements at Samoylov Island. The continuation of this data series is important for analyzing the intra- and inter-annual variability of e.g. meteorological and soil conditions, hydrology, and the atmospheric fluxes of energy and H_2O, CO_2, and CH_4. Only on the basis of long-term measurements, we are able to give generalized conclusions about e.g. the state of the permafrost soils and the carbon balance of this tundra environment as well as climatic influences on those properties.

1. *Eddy Covariance Measurements of Greenhouse Gas and Energy Fluxes*

   Fieldwork summary
   It is a major issue to cover the strongly contrasting seasons in the Arctic by year-round measurements. This is only possible with regular maintenance and calibration of the GHG flux monitoring instruments. In 2017, maintenance work was performed during expeditions in April, July, and September.

   Preliminary results
   Meteorological, soil, and eddy-covariance systems were in operation from 18.09.2016 (end of 2016 field campaigns) through 21.09.2017 (end of 2017 field campaigns). Due to technical problems the data series are not continuous - data availability is listed in Table 2.3.1. The processing of eddy-covariance raw data, and the quality control and gap-filling of fluxes and meteorological data will be finalized after the field work.

Table 2.3.1: Data availability during the period 09.2016 - 09.2017

Data type	Data available period
1-minute meteorological data	18.09.2016 - 12.02.2017, 08.04.2017 - 21.09.2017
30-minute met/soil data	18.09.2016 - 12.02.2017, 16.03.2017 - 21.09.2017
open-path EC raw data CO_2, H_2O	18.09.2016 - 05.11.2016, 07.04.2017 - 21.09.2017
open-path EC raw data CH_4	10.04.2017 - 11.09.2017
closed-path EC raw data CO_2, H_2O, CH_4	18.09.2016 - 05.11.2016, 07.04.2017 - 21.09.2017

2. *Lateral Fluxes of Water, Carbon and Nutrients*
   Fieldwork summary
   Three discharge gauging weirs, dating from 2012 and located at the border between the river terrace and the floodplain about 1 km north of the research station, were repaired during September 2017. The V-shaped gauging weirs enable the determination of the discharge rate based on water level measurements. The position of the weirs are given in Table 2.3.2. The weirs are planned to be put in operation again in 2018.

Table 2.3.2: Positions of Weirs

Weir	GPS Coordinates
1	N 72.37588 E 126.47879
2	N 72.38015 E 126.48145
3	N 72.37997 E 126.48098

3. *New climate controlled field lab IGLOO and instrumentation of the Tower*
   Fieldwork summary
   Close to the new research tower, installed in 2016, a specially streamlined igloo shaped field lab has been placed on a wooden platform close to the already installed boardwalk (Figure 2.3-1). To be able to house high precision instruments under constant temperature conditions, the glass fiber construction was isolated from the inside and an additional heating system integrated. During the warmer summer periods, the igloo will be air conditioned to compensate for the radiation impact and the all-time present waste heat. Therefore, the Igloo is connected to the Main power source that supplies from the Samoylov Research Station. To ensure that continuous power is being delivered to the scientific instruments and the Igloos infrastructure, an elaborate power and temperature management system was installed which controls the lab temperature and different power supplied under all possible conditions, taking into account the possible year round weather conditions. In preparation of the relocation of the Eddy Covariance Measurement System from the Old to the New tower, several instruments for meteorological parameters where installed at different heights. The sensors measure air temperature and humidity, wind speed and wind direction, incoming and outgoing short- and longwave radiation.

Figure 2.3-1: *IGLOO Field Lab (foreground) and Tower (Background)*

2.4 Hydrological work in the Lena River Delta in April 2016

Irina Fedorova[1,2], Dmitry Bolshiyanov[1], Stepan Romanov[2]

[1] Arctic and Antarctic Research Institute, St. Petersburg, Russian Federation
[2] Saint Petersburg State University, St. Petersburg, Russian Federation

Fieldwork period and location
From April 07th to April 29th, 2016 (in the Lena Delta)

Objectives
Hydrological measurements were carried out during the expedition to the Lena Delta in April 2016. These measurements were a continuation of previous investigations of hydrological, hydrochemical and bed-evolution processes in lakes and channels of the Lena River Delta.
This study was a part of the “Scientific station Samoylov” and “CarboPerm” projects and was supported by a grant of Russian Foundation for Basic Research: No. 14-05-00787.
During April 2016, the following investigations have been carried out: measurements of water discharge and total suspended matter in Main Channel (4.7 km from Stolb Island) and Olenekskaya Channel, water and sediment sampling from Samoylov Island lakes and Lena river channels, laboratory analysis of water samples. Areas of hydrological studies are presented in Figure 2.4-1 (channels) and Figure 2.4-2 (lakes); coordinates of sampling points are in Table 2.4.1.
Our studies included four main steps:

1. Measurements of water discharge and suspended supply on the Olenekskaya Channel (near Chay-Tumus Station of The Lena Delta Reserve) and on the Main Channel of the Lena River (4.7 km from Stolb Island).
2. Water sampling in lakes, channels, and taliks; snow and river/lake ice sampling.
3. Processing of water samples in the laboratory of the Samoylov Station: mineralization, pH, dissolved oxygen, permanganate oxidation and chromaticity.
4. Preparation of water samples for transport to the Otto Schmidt Laboratory for further analysis: CDOM, DOC, content of biogenic elements, main ions, isotopes.

Table 2.4.1: Measurement points of water and suspended material sampling

Point	Date	Latitude [N]	Longitude [E]	Location
Lake Banya-2	20.04.16	72.36872	126.50144	Lake on Samoylov Island
Lake Banya-1	22.04.16	72.36897	126.48669	Lake on Samoylov Island
Molo Lake	20.04.16	72.37833	126.49678	Lake on Samoylov Island
Fish Lake	22.04.16	72.37392	126.48678	Lake on Samoylov Island
Lake N.10	21.04.16	72.38422	126.48954	Lake on Samoylov Island
Lake Banya-3	22.04.16	72.37019	126.51872	Lake on Samoylov Island
Lake N.11	23.04.16	72.37539	126.51941	Lake on Samoylov Island
Lake N.9	22.04.16	72.36879	126.51254	Lake on Samoylov Island
Chay-Tumus	15.04.16	72.359	125.67117	Station on Olenekskaya Channel
Main Channel	09-12.04.16	72.37803	126.75733	The Lena River
Olenekskaya Channel	15-16.04.16	72.29614	126.09444	The Lena River

Methods

Measurement of water discharge

Water discharge measurements were carried out in two Lena River channels. Profiles were located in representative channel parts. Coordinates of the locations were traced using GPS. The first profile was a standard hydrometeorological profile on the Main Channel in 4.7 km upstream from Stone Island. The second profile was located on the Olenekskaya Channels near old Chay-Tumus Station of the Lena Delta Reserve. Hydrometrical work included cleaning the ice cover, drilling wells (ice-holes) for depth and velocity measurements, as well as for water and suspended material sampling.

Depth measurements were made with an echo-sounding device (Garmin). Special bed relief points were fixed as hydrometric verticals for the next step of water discharge measurements. There were three measured verticals on the Main Channel and only one vertical on the Olenekskaya Channel. Water flow speed measurements were taken in three horizons at the each vertical: 0.2H; 0.6H; 0.8H using a Hydrological speed recorder (GR-21). Water discharges were calculated according to the recommendations for Russian hydrometeorological stations (A.2-2).

Water sampling in the channels and lakes - laboratory analysis

Samples for total suspended matter were collected in chosen verticals of the River and observed lakes. Water samples were collected by plastic and glass bathometers, and were later filtered in the laboratory through a pre-prepared paper filters (diameter 10 cm) to ”Kuprin” filtration device or through glass microfiber or polycarbonate filters (GF pore size of 0.45 nm, diameter 4.7 cm and PC). Further filters were dried and weighed in the laboratory. Turbidity was determined as the difference between full and empty filters divided by the volume of the sample. According to the calculated water discharge and turbidity, suspended supply was determined.

Water conductivity and pH were measured in laboratory using multiparametrical device (WTW 340i). Chemical methods have been used to determine indicators such as the dissolved oxygen, permanganate index and chromaticity.

Preliminary results

In April 2016, hydrological field measurements were carried out to extend previous investigations and included standard hydrometrical measurements, confirmation of previous results, and collecting new information.

We measured water and sediment discharge on Main and Olenekskaya Channel in winter low period. Water discharge on Main Channel (1384 m^3/sec) was slightly lower than the long-term average (1515 m^3/sec); suspended supply was 4.84 kg/sec. There was no water velocity and water discharge in Olenekskaya Channel in April 2016. Only 5 discharges of Roshydromet (Habarova/ Stolb SFOletation) measurements over years between 1977-2004 can be noticed. It could be due to freezing of shallow channel parts in the Olenekskaya mouth or a surge of the shoreline and backing-up of water in channels. These reasons should be better analyzed and measured.

Conductivity values in the lakes in April 2016 varies between 140 and 277 μS/cm in comparison to summer volumes that vary between 23 and 120 μS/cm. Conductivity in the channels (Main and Olenekskaya) was 494-581 μS/cm (and 103-160 μS/cm in summer period).

Some analyses had been done for snow and river-like ice as well as for talik water. Talik drilling had been done by M.Grigoriev (see other part of the same report) with colleagues from Permafrost Institute. Mud mineralized water on 6 m was analyzed: mineralization was 333-828 mg/liter. Chromaticity of channel water was 27-44 pt-co degrees and 33-178 pt-co degrees for lakes. pH value varies from 5.05 for snow up to 9.46 in the third Banya Lake. Dissolved oxygen concentration changed from 52 % on the bottom of Fish Lake to 139 % on the surface of Molo Lake.

The complete list of taken samples is shown in Table A.2-1. Results of some hydrochemical express analyses that had been done in the field and on Samoylov Station in April 2016 are presented in the Table A.2-2. Currently, the continuation of water analyses are being processed.

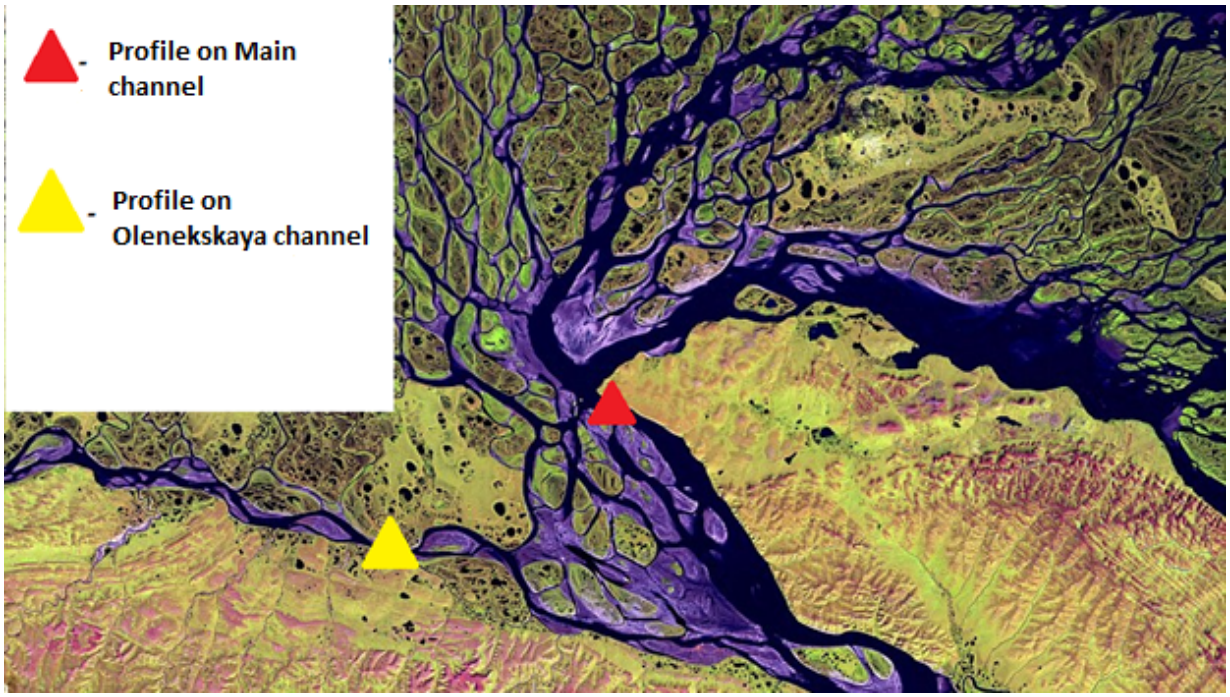

Figure 2.4-1: *Measurement points on the Lena River Channels*

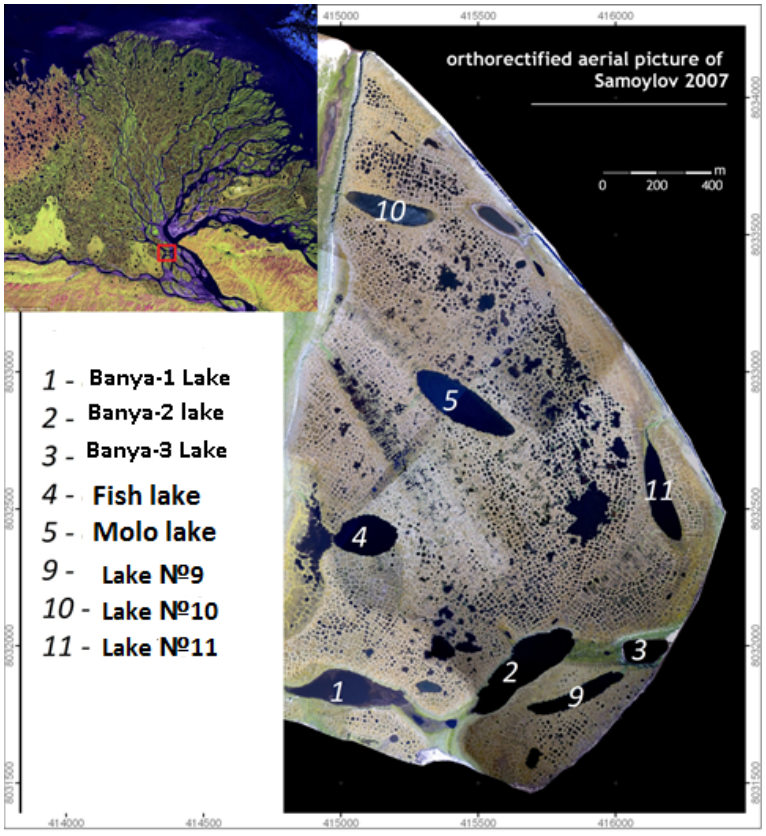

Figure 2.4-2: *Measurement points on Lake*

2.5 Hydrological work in the Lena River Delta in April 2017

Irina Fedorova[1], Denis Aybulatov[2], (Natalia Alekseeva[1]: not in the field)

[1] Arctic and Antarctic Research Institute, St. Petersburg, Russia Federation

[2] Moscow State University, Moscow, Russian Federation

Fieldwork period
April 14th to April 29th, 2017 (Main Channel of the Lena Delta (profile 4.7 km upstream of Stolb Island); Bykovskaya, Olenekskaya and Tumatskaya Channels, lakes on Samoylov Island)

Objectives
Field measurements aimed to obtain new data on the hydrology and hydrochemistry of channels and lakes of the Lena River Delta under winter situation. These observations were already performed in April 2015, 2016 and 2017, to reveal interannual variability. Due to difficult field / ice conditions in April 2017, some of the hydrometrical and hydrological measurements are different from the previous measurements.
The Polar Station of Roshydromet Stolb/Khabarovo observes the water surface level under ice only in the Bykovskaya Channel. Thus we performed our water discharge measurements also in this channel. Therefore, we now can compare our results with the long-term data of the Stolv/Khabarovo Station and better predict changes. The monitoring of ice thickness on lakes of Samoylov Island and under ice hydrochemistry were also extended.

Methods
Measurements of water discharge and conductivity
Water discharge measurements were carried out in three Lena River channels (Bykovskaya, Olenekskaya and Tumatskaya) as well as on a profile across the Main Channel, 4.7 km upstream of Stolb Island (Figure 2.5-1). Profiles were located at representative (standard) channel positions where Russian Hydrometeorological Service has been measuring since 1951 (for the Main Channel and Bykovskaya Channel) and since 1977 (for Trofimovskaya and Tumatskaya Channels). Time schedule of measurements in April 2017 are presented in Table 2.5.1. Hydrometrical work included the measuring of a snow thickness and its temperature. After drilling ice-holes with a moto auger, the water depth was determined and depth profiles of water temperature and water velocity were measured. Afterwards, water samples were taken near the surface at intermediate depths and near the bottom (Table A.2-3). Water velocity and discharge were determined with an ISP-1 (unspecified), water depth with an echo finder (Garmin).
The Expert-002 conductometer was used for determination of conductivity and water temperature at different depths with a dipping sensor. It measures the specific conductance (UEP) on a broad range of conductivity and water temperatures. The conductometer is capable to quickly and precisely measure the UEP, and convert it to standard temperature (25 °C) resulting in the UEP25. Conductivity should be recalculated for standard temperature as conductivity is dependent on temperature. For example, if conductivity is 281 μSm/cm at a temperature of -0.7 °C, converting this to standard temperature 25 °C results in a conductivity of 582.1 μSm/sm.

Water sampling in the channels and lakes, laboratory analysis
Samples for total suspended matter were collected in chosen verticals. These depth profiles were chosen according to the depth profile of the channel, the number of verticals depends on the channel width, however, the distance between vertical never exceeded 500 m. Sampling was done in the different river channels and in lakes of Samoylov Island (Figure 2.5-2).

Water samples were collected by plastic and glass bathometers. In the laboratory, water was filtered through pre-weighted paper filters (d. 10 cm), filters were dried and weighed in the laboratory. For geochemistry, water was filtered through glass microfiber or polycarbonate filters (pore size of 0.45 nm, d. 4.7 cm). Turbidity (g/m^3) was calculated according to the difference in the weight of the filters before and after filtering the sampled water volume. Sediment load (g/sec) was calculated by multiplying the turbidity with water discharge.
pH was measured in the laboratory with multiparameter device (WTW 340i). Dissolved oxygen, permanganate index and chromaticity were determined with the auto titration instrument of the station (Mettler G20, Mettler Toledo). Samples for cations and DOC were preserved with HNO_3 and HCl and stored at 4 °C. Nutrient samples were kept frozen. These samples were transported to St. Petersburg for later analyses.

Preliminary results
In April 2017, hydrological field measurements were carried out to extend previous investigations and included standard hydrometrical measurements. Sampling sites were located at the Main Channel, Bykovskaya, Olenekskaya and Tumatskaya branches.
Ice thickness on the channels ranged from 1 m nearshore of the Main Channel to 2.5 m in the middle of the Main Channel (Table A.2-4). Maximal snow thickness on the ice was 1.23 m (at North-East Lake). On the Bykovsky Channel, most stations were without any snow at all. Snow temperature profiles are presented in Figure 2.5-3. The top layer usually had the same temperature as the air on the date of measurement and mostly decreased towards the ice.
Maximal water depth was observed in the Main Channel with -25.3 m, while the Oleneksaya Channel was only approx. 4 m deep. Water velocity in the channels was 0.114 m/sec in the Main Channel, 0.182 m/sec in the Bykovskaya Channel, 0.042 m/sec in Olenekskaya Channel, and no velocity was measured in Tumatskaya Channel. This is in contrast to the findings in 2016, when no water velocity was measured in the Olenekskaya Channel.
Water temperature in the Main, Bykovskaya and Olenekskaya Channels was -0.7 °C to -0.8 °C. Water temperature of Tumatskaya Channel changed from -0.3 °C under ice to -0.7 °C at intermediate depth and 0 °C near bottom (Figure 2.5-4).
The conductivity of channel water had a mean value of -272.8 μS/cm, when measured on site at low water temperature (about -0.7 °C). If this value is corrected to standard temperature (25 °C), the conductivity was more than 500 μS/cm. For example, the observed conductivity 272.1 at a temperature of -0.7 °C has a normalized conductivity of 560.3 μS/cm. The measurements were compared with the WTW meter of the Samoylov Island equipment. The corrected values were in accordance with the lab-values, which are shown in Table A.2-4. Conductivity ranged from 411 μS/cm in Tumatskaya Channel to 532 μS/cm in the Main Channel. These data show that high concentration of ions accumulate in the channels under the ice. In summer, the average conductivity is much lower (103-160 μS/cm). pH was neutral in all channels. Dissolved oxygen ranged from 3.97 mg/l in Tumatskaya Channel to 7.7 mg/l in Olenekskaya Channel (near Samoylov Island).
In the lakes, conductivity ranged from 90 μS/cm in Shallow Lake to 240 μS/cm in South Lake. These values are 2-3 times lower than in channel waters. The highest conductivity had a polygonal crack that was drilled by Katya Abramova. pH of lacustrine water was quite similar for all lakes. Dissolved oxygen ranged from 1.52 mg/l at the bottom of South Lake to 11.09 mg/l – at the surface of Banya-2 Lake (Figure 2.5-5). Ice thickness, water depth and planned analyses of water chemistry are shown in Table A.2-5.
Concentrations of carbon dioxide in water are shown in Figure 2.5-6. In the channels CO_2 concentrations were lower than in the lakes. Maximal values were observed in North-East, Molo and Bannoe-1 Lakes, with 16.5, 17.2, and 15.7 mg/l respectively.
Data for Permanganate oxidation (as analogon to DOC) are presented in Table A.2-6. Minimal value was observed in Fish Lake with 2.95 mgO/l. Maximal value for Permanganate oxidation (PO) was observed in the Main Channel near to left shallow bank with 10.1 mgO/l. According to the long-term

measurements of PO in April - May at the Kyusyur cross section (since 1953), PO never exceeded 20 mgO/l. According to Bobrova (2014) PO for the river channels in summer was 18-22 mg/l, for lakes - 15 - 22 mg/l, in pore waters (the Fish Lake catchment) the concentration was higher - 47 - 48 mg/l. Quite high DOC concentrations were observed in the channels and in lakes with active planktonic life under ice. The average DOC concentration in Arctic lakes is about 13.11 mg/l (Ask et al., 2009; Seekell et al., 2015). The parameter DOC is usually a little bit higher than PO. In this season, samples for both analyses (PO and DOC) had been taken. This comparison will allow to calculate a correlation between DOC and PO, and further long-term PO data of Roshydromet can be compared with recent DOC measurements.

Conclusion

Several new measurements have been performed in April 2017. These data will add further information about the ice-covered period and give background information for further investigations. The calculation of the water discharge under ice will allow to budget ion and gas fluxes during the underestimated winter processes on the big Arctic rivers.

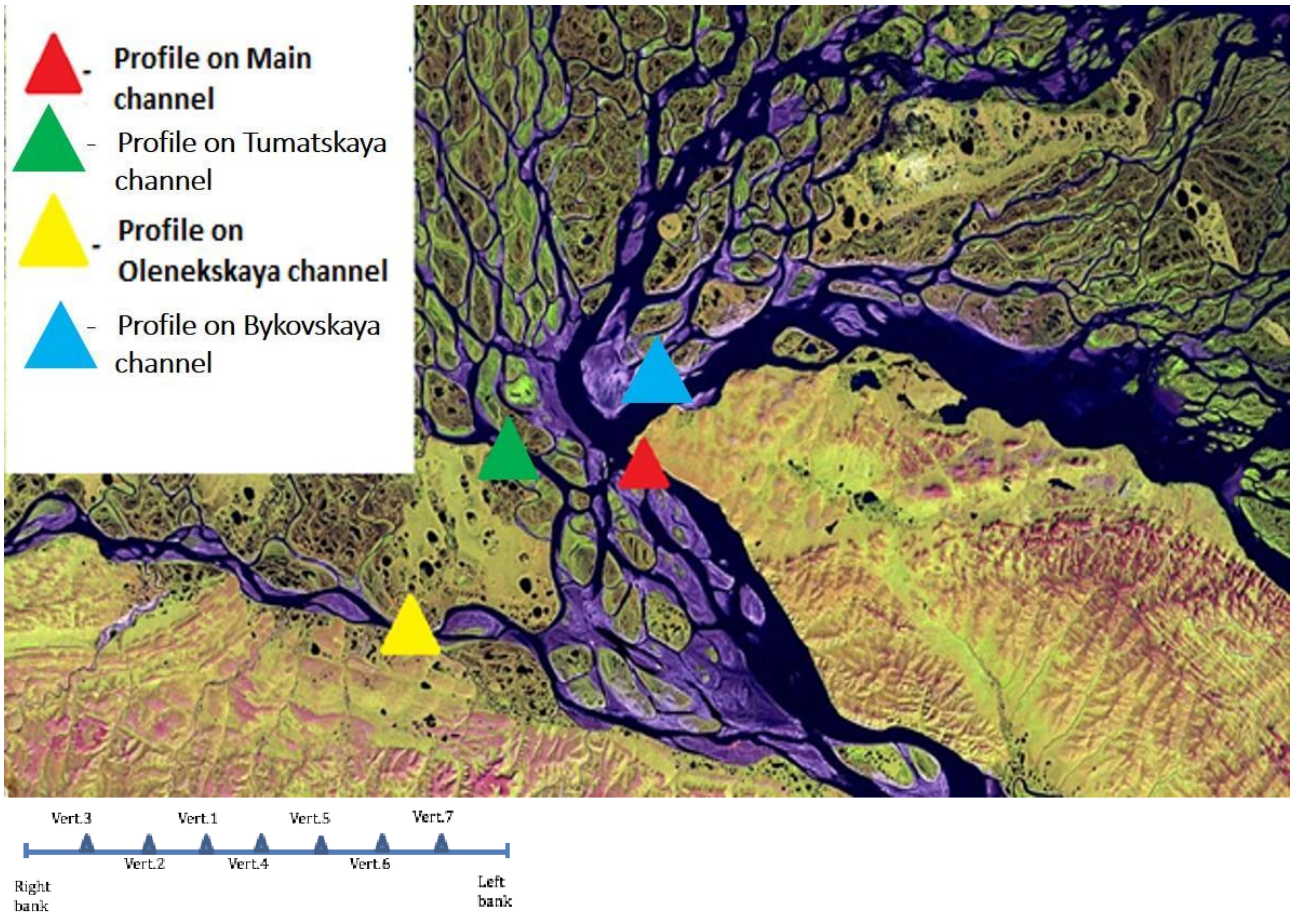

Figure 2.5-1: *Location of the sampling transects on the Lena River channels, inlet shows position of the different vertical sampling.*

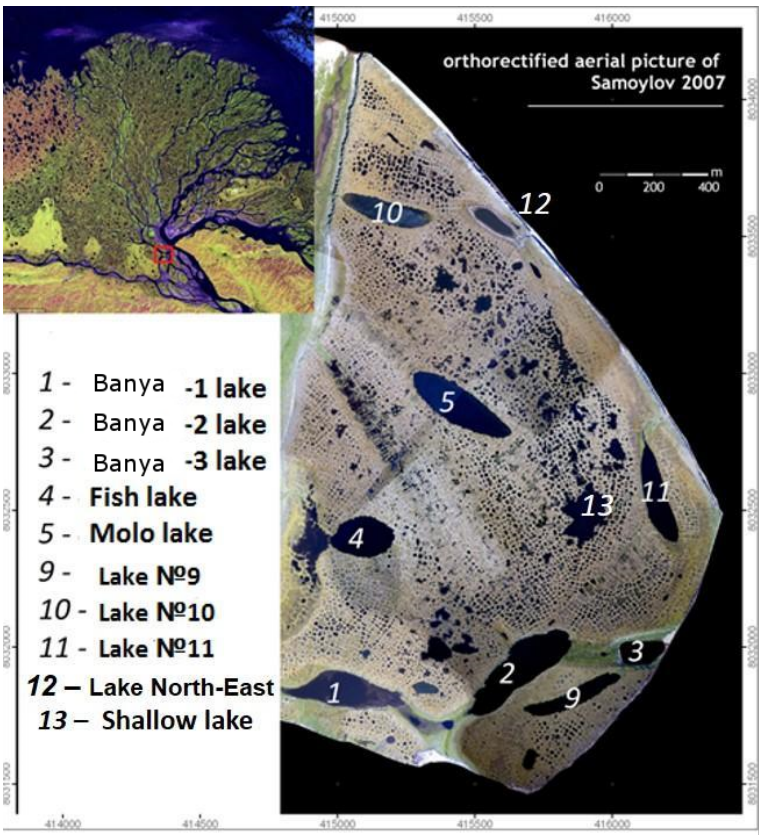

Figure 2.5-2: *Sampled lakes on Samoylov Island*

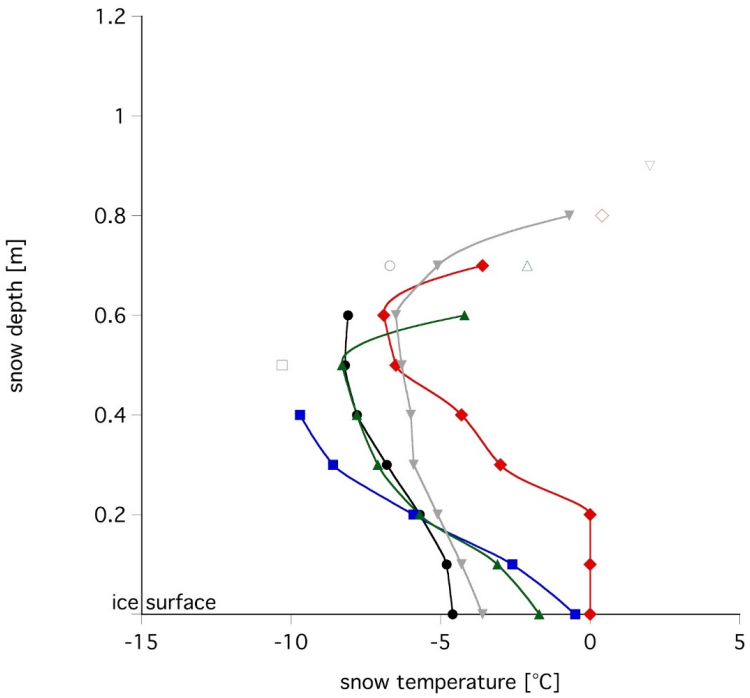

Figure 2.5-3: *Snow temperatures above the ice on different locations of the Main Channel. Open sympbols indicate the respective air temperature.*

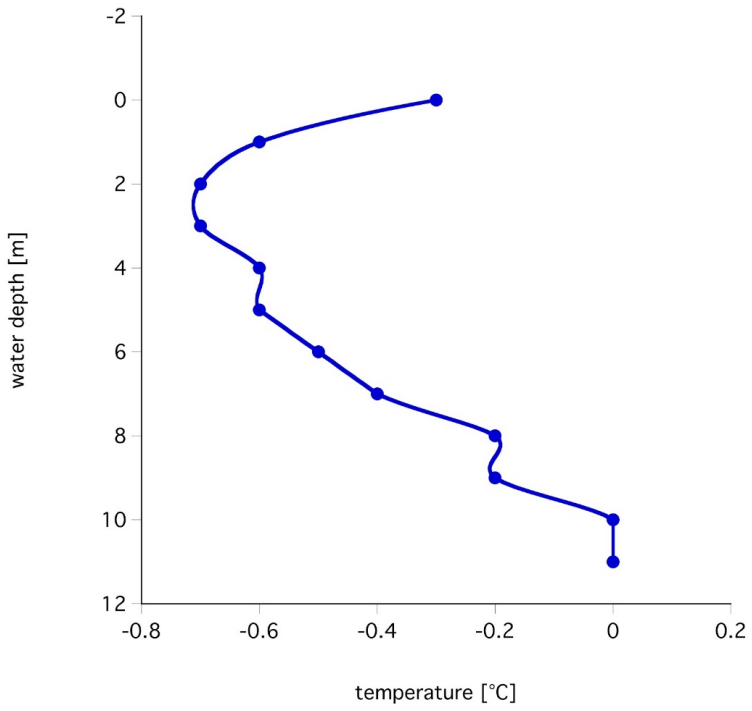

Figure 2.5-4: *Temperature in the water column of the Tumatskaya Channel on 17.04.2017*

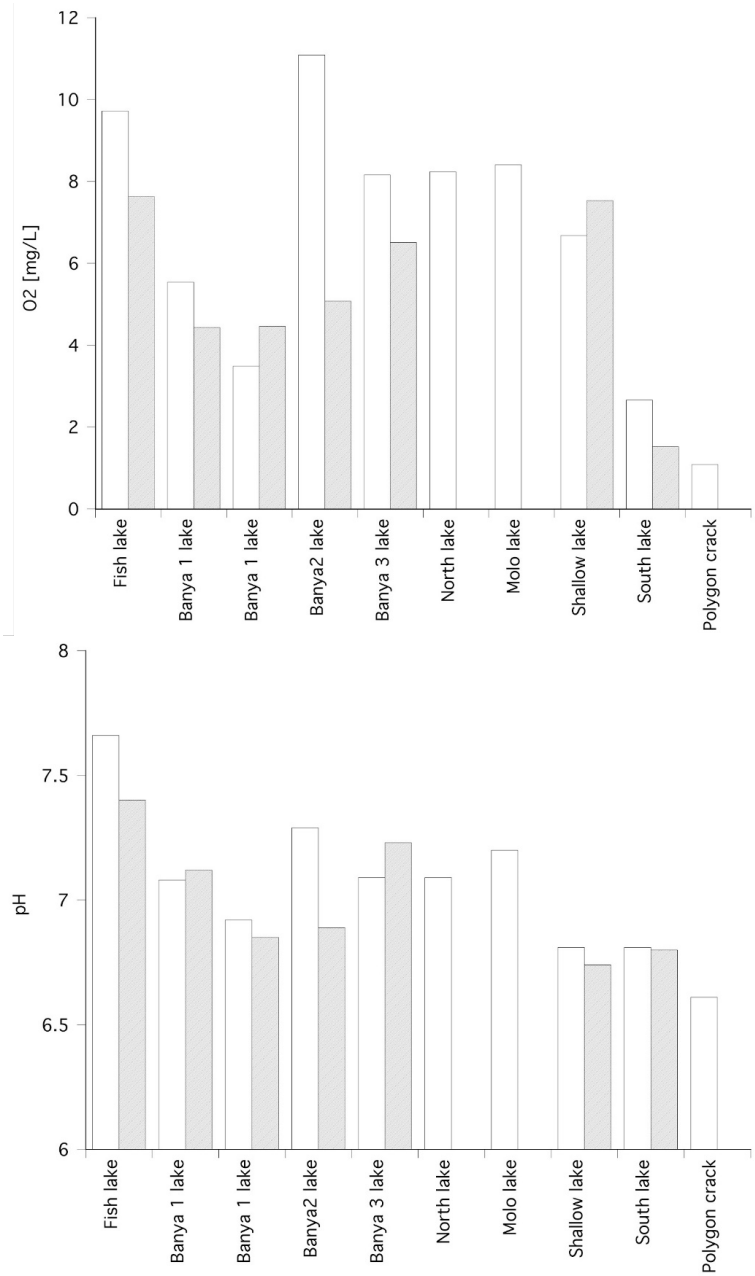

Figure 2.5-5: *Oxygen concentration and pH in the surface water (white bars) and bottom water (shaded bars) of different lakes*

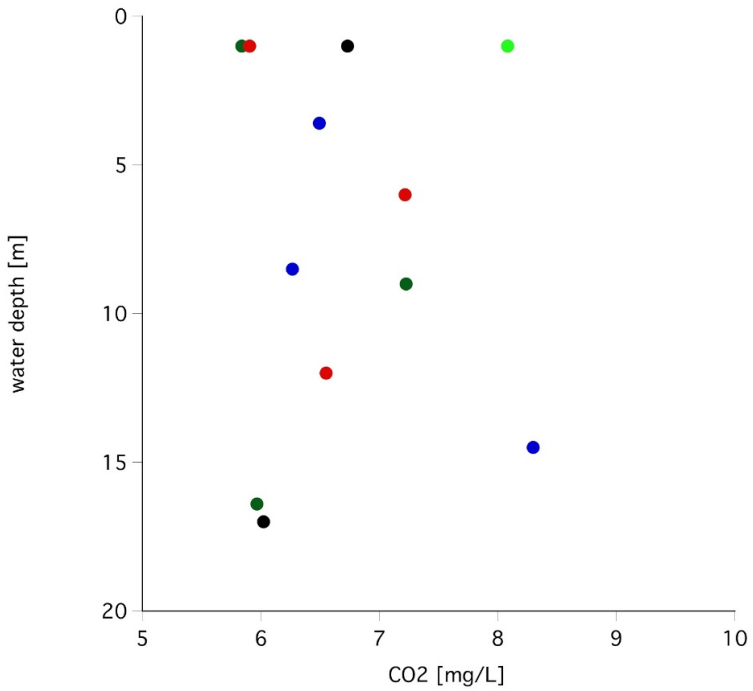

Figure 2.5-6: *Water column concentration of CO_2 at different verticals on the Main Channel*

Table 2.5.1: Sampling stations on various channels and Samoylov Island lakes

Station	Date	Remarks
Tumatskaya Channel	17.04.17	Standard cross section of Roshydromet
Main Channel. vertical 1	18.04.17	Vertical 1
Main Channel. vertical 2	19.04.17	Vertical 2 between right bank and vert.1
Main Channel. vertical 3	19.04.17	Vertical 3. close to the right bank
Main Channel. vertical 4	20.04.17	Border of the ice hummock
Main Channel. vertical 5	20-21.04.17	Vertical 4. close to the left bank
Main Channel. vertical 6	21.04.17	Vertical 5
Main Channel. vertical 7	21.04.17	Vertical 6
Bykovskaya Channel. vertical 1	22.04.17	Vertical 1
Polygonal crack	23.04.17	-
Banya-2 Lake	23.04.17	-
Banya-1 Lake	23.04.17	-
Molo Lake	23.04.17	-
Fish Lake	23.04.17	-
North Lake n.10	23.04.17	-
Banya-3 Lake	23.04.17	-
East Lake n.11	23.04.17	-
North-East Lake n.12	23.04.17	-
South Lake n.9	24.04.17	-
Shallow Lake n.13	24.04.17	-

2.6 Hydrological work in the Lena River Delta in July 2016

Irina Fedorova[1,3], Larisa Frolova[2], Miron Makushin[3]

[1] Arctic and Antarctic Research Institute, St. Petersburg, Russian Federation

[2] Kazan Federal University, Kazan, Russian Federation

[3] Saint Petersburg State University, St. Petersburg, Russian Federation

Fieldwork period and location
From July 03rd to July 30th, 2016 (in the Lena River Delta)

Objectives
The Lena River Delta is a very interesting and important object for the world's scientific community. A lot of hydrological, geochemical, and geological research was conducted in this area over the years. In the 20th c., numerous hydrological stations were placed in all the channels of the Delta to record hydrometeorological measurements; however, nowadays these stations are closed, with the contemporary research in the Lena River Delta based in new the 'Samoylov Island' Research Station, opened in 2013. During the expedition in July 2016, measurements of water discharge and suspended sediment load were completed in Olenekskaya, Bykovskaya, Trofimovskaya and Tumatskaya Channels. Daily measurements of water level were organized in the vicinity of the station. Additionally, water samples were collected from all the channels and lakes in Samoylov and Kurungnakh Islands, as well as bottom soil columns from Molo Lake and Kurungnakh-2 Lake. Areas of hydrological researching are shown in Figure 2.6-1 (channels) and Figure 2.6-2 (lakes) while coordinates are listed in Table 2.4.1.
The following types of field work were conducted in July 2016:

1. Measurements of water discharge and sediment discharge in Olenekskaya, Bykovskaya, Trofimovskaya and Tumatskaya Channels;
2. Collection of water samples in all channels and lakes in Samoylov and Kurungnakh Islands, as well as bottom soil columns of Molo Lake and Kurungnakh-2 Lake.
3. Conservation of water samples for analyses of CDOM, DOC, nutrients, ionic composition and isotopes.

Methods
The work can be divided into several types: measurement of water flow in the channels, the sampling in the channels and lakes, and sample analysis in the laboratory.
Hydrometric observations were made in the Bykovskaya, Trofimovskaya, Tumatskaya and Olenekskaya Channels; samples were collected from 12 lakes on Samoylov Island and 2 lakes on Kurungnakh Island. The geographical coordinates of the channels and lakes are listed in Table A.2-7 - A.2-10. Water discharge measurements were carried out on all the channels of the delta on standard gauge line of Roshydromet. On Olenekskaya Channel, additional cross-sections were also chosen from an old post, Gusinka, located downstream of Gusinka, Chay-Tumus and Olenekskyi gauging stations. Spot Soundings were performed using the sonar "Garmin", pinpoints of the depths were made every 20 meters. The profiles of channels were modelled based on the data collected above.

Multiple verticals were selected based on the characteristics of bottom points, the number of verticals and length between them depends on the width of channels. Flow velocity measurements were carried out using the hydrological turntables GR-21 to standard horizons: 0.2 H, 0.6 H, 0.8 H (where H means: depth on a vertical). Furthermore, flow discharge was calculated according to the flow velocity and area of profiles. Calculation of sediment load was completed based on data of flow discharge and water turbidity.
Water samples from various depths of lakes and channels were collected using Niskin-type Water Sample PWS. Water samples were filtrated in a laboratory through a pre-prepared (dried and weighed) paper filters ("white band") on the "Kuprin" device or through special filters GF / F (glass microfiber filters) on the filter system (a pore size of 0.45 m button, diameter 4.7 cm). Further filters were dried and weighed in the laboratory. The flow of suspended sediments was calculated based on turbidity and water flow data. The total amount of samples for the turbidity was 78 pcs. GF / F filters will later be used to carry out tests to determine the geochemical composition of suspended solids. In total, 22 samples were selected for geochemical analysis.
The Gravity corer was used on the Molo Lake and Kurungnakh-2 Lake to collect lacustrine sediment columns. Water samples for colored dissolved organic matter (CDOM), dissolved organic carbon (DOC), nutrients, isotope analysis and ionic analysis from lakes and channels were also performed. Samples for nutrients and ion analysis were filtered through the CA-filter (cellulose acetate filters a pore diameter of 0.45 μm), while the samples for the CDOM, DOC and isotopic analysis were filtered through a GF/f-filter (glass microfiber filters - a pore size of 0.70 μm) and sent to St. Petersburg. These samples are expected to be treated at the Otto Schmidt Laboratory, AARI.

Preliminary results
Flow discharge and sediment discharge were calculated based on data of measurements. Analytical method of calculation was used (three-point method of calculation of velocity on a vertical):

$$V = 0.25 \times V_{0.2} + 2 \times V_{0.6} + 2 \times V_{0.8} \tag{2.1}$$

A calibration formula for GR-21: V=0.182n+0.016, where n – number of rings per second.
Flow discharge of water was calculated in all big channels of the delta. Flow discharge of Bykovskaya Channel was 7.551 m^3/sec compared to the long-term average (1977-2004) 10.564 m^3/sec. A profile of the cross-section is illustrated in figure 2.6-3. Flow discharges in Olenekskaya Channel were measured in four locations: 1.550 m^3/s 40 km downstream of Gusinka, 1.985 m^3/s on the site of the old post Gusinka, 1.772 m^3/s near post Chay-Tumus, 2.815 m^3/s in the Olenekskaya gauging station. Additional cross-section profiles are illustrated in Figures 2.6-6 and 2.6-9. The flow discharge in Tumatskaya Channel was also calculated to be 3.437 m^3/s. The calculation results are illustrated in Figure 2.6-3, 2.6-4 and 2.6-10. There is a tendency to reduce the water flow while comparing the measured discharge of the channels with average annual values. The average annual consumption of water in July for Olenekskaya Channels for the period 1977-2004 was 2.856 m^3/s, which is 1.5-2 times higher than the value of the measured water consumption. Measured flow of Olenekskaya gauging station was approx. equal to the average annual values. The measured water flow in the Bykovskaya Channel also decreased compared to average annual values. The measured flow rate was 7.551 m^3/s, which is slightly less than the average annual rate for July (10.564 m^3/s for 1951-2004). Average annual water discharge in Trofimovskaya Channel in July was 24.767 m^3/s in July, for the period 1977-2004, more than the measured flow rate for July 2016, amounting to 21.110 m^3/s. The results from July 2016 and comparisons are shown in Table A.2-11. Results of measurements pH, conductivity, dissolved oxygen (mg/l and %) and oxidation-reduction potential are illustrated in Table A.2-12. One can see differences between channels and lakes in the delta. In general, we can assume that the water in the channels are slightly alkaline pH (values from 7.58 in Tumatskaya Channel to 8.06 in Trofimovskaya). The water is saturated with oxygen, the water flow can be attributed to be clean and very clean. The degree of oxygen saturation percentage ranges from 82.5 % in Tumatskaya Channel to 119.4 % in Olenekskaya Channel. Water in the lakes can be considered

slightly alkaline. The amplitude of the oscillation of pH range from 7.33 in the Fish Lake to 8 in the Kurungnakh-2 Lake. pH below 7 was observed in the Northern and Northeastern lakes, indicating that they contain weakly acidic water. The Northern Lake is heavily saturated with oxygen, saturation values range from 86.2 to 125.3 %. The lake water can be classified as clean and very clean based on the levels of oxygen saturation. However, in the Banya-2 Lake, the degree of oxygen saturation was 72.1 %, which indicates that the lake is considered moderately polluted. This is mainly due to using the lake water for the station necessities. List of taken samples is shown in Table A.2-9.

Figure 2.6-1: *Measurement points on the Lena River channels*

Figure 2.6-2: *Measurement points on Samoylov Island lakes*

Figure 2.6-3: *Measurement points on Kurungnakh Island lakes*

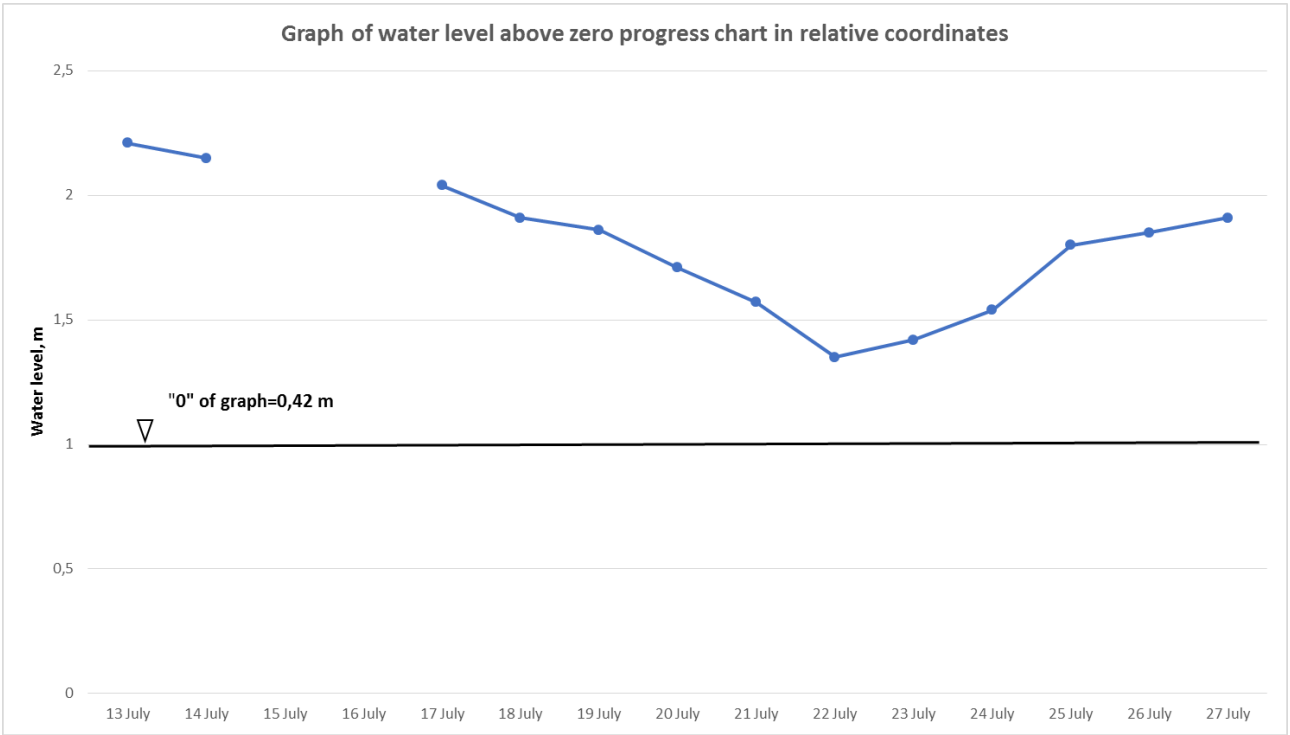

Figure 2.6-4: *Graph of water level above zero progress chart in relative coordinates*

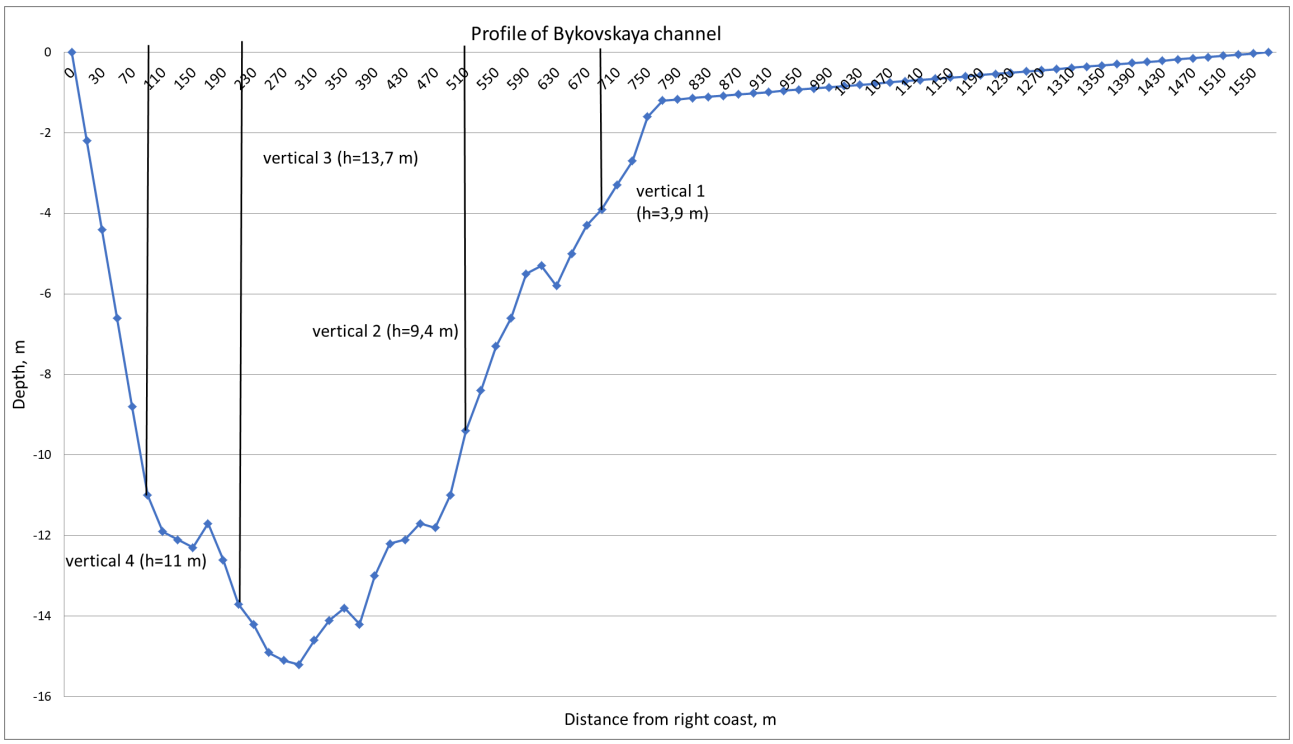

Figure 2.6-5: *Profile of Bykovskaya Channel*

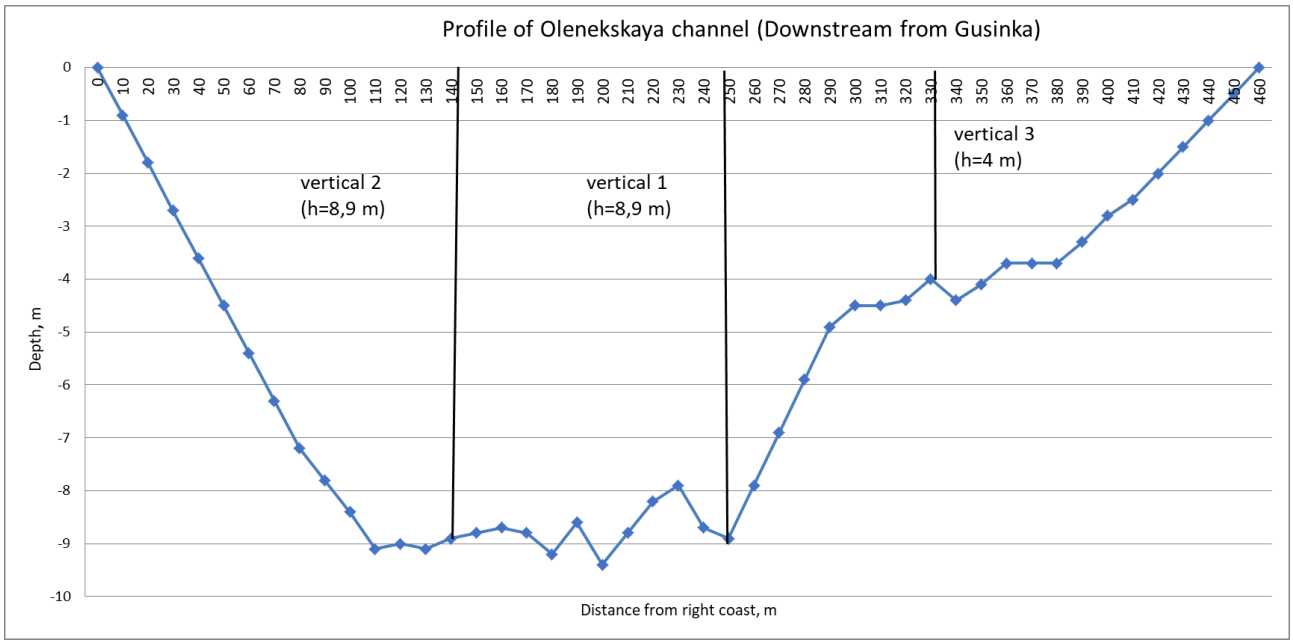

Figure 2.6-6: *Profile of Olenekskaya Channel (40 km downstream of Gusinka)*

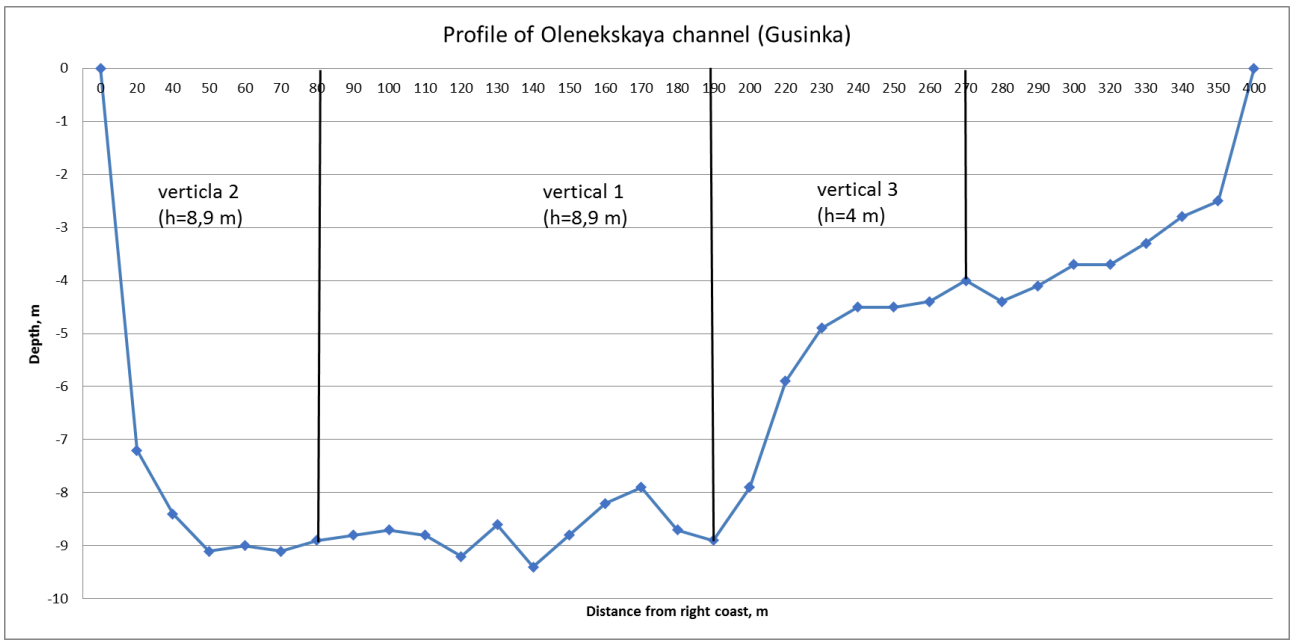

Figure 2.6-7: *Profile of Olenekskaya Channel (Gusinka)*

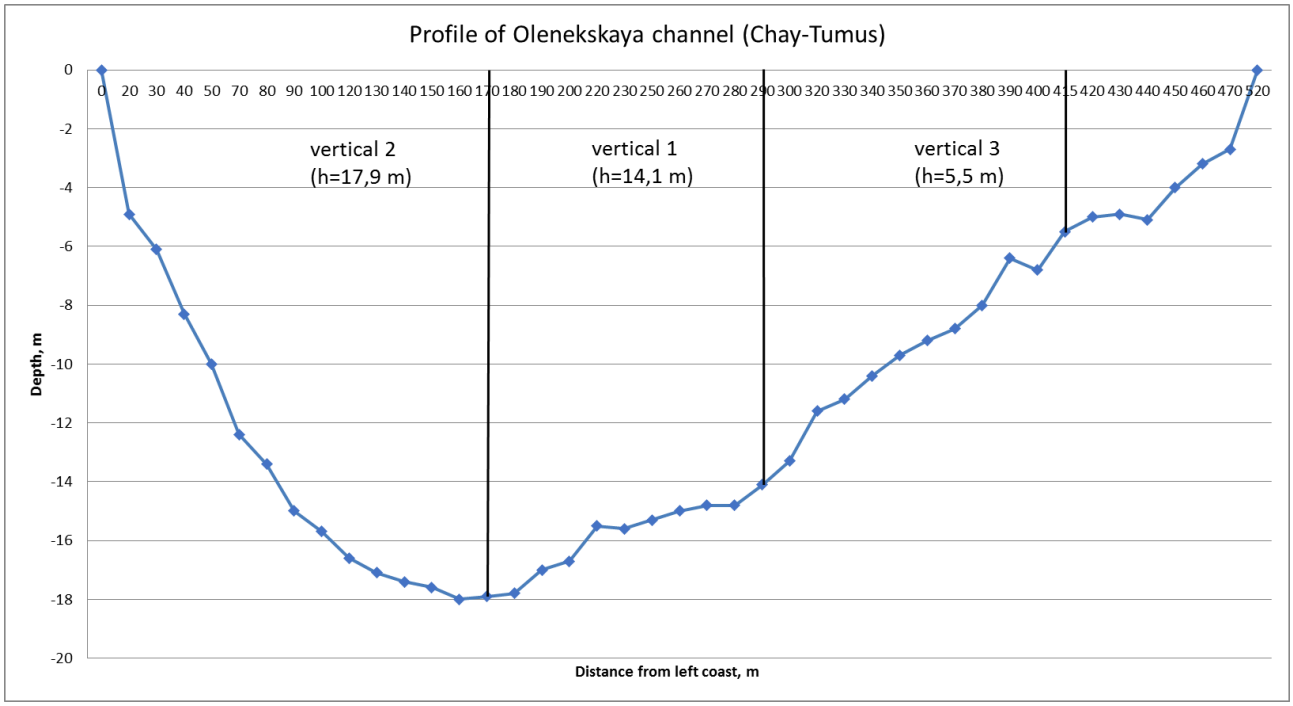

Figure 2.6-8: *Profile of Olenekskaya Channel (Chay-Tumus)*

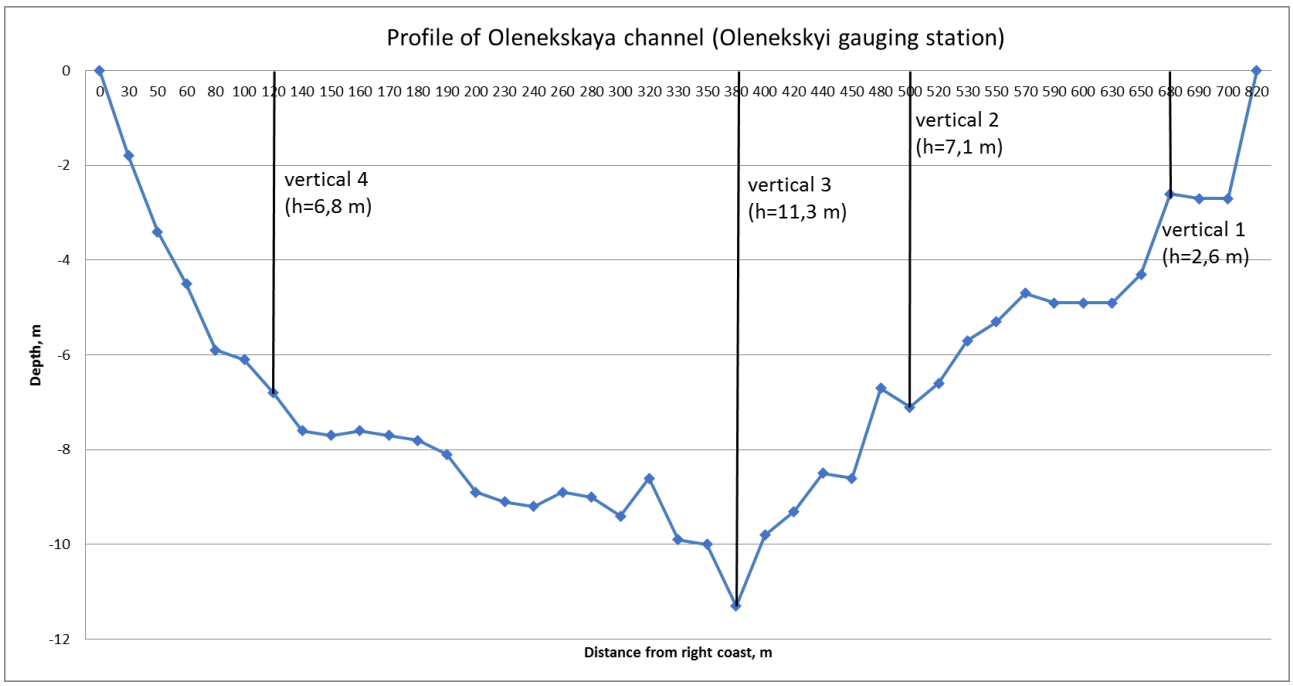

Figure 2.6-9: *Profile of Olenekskaya Channel (Olenekskyi gauging station)*

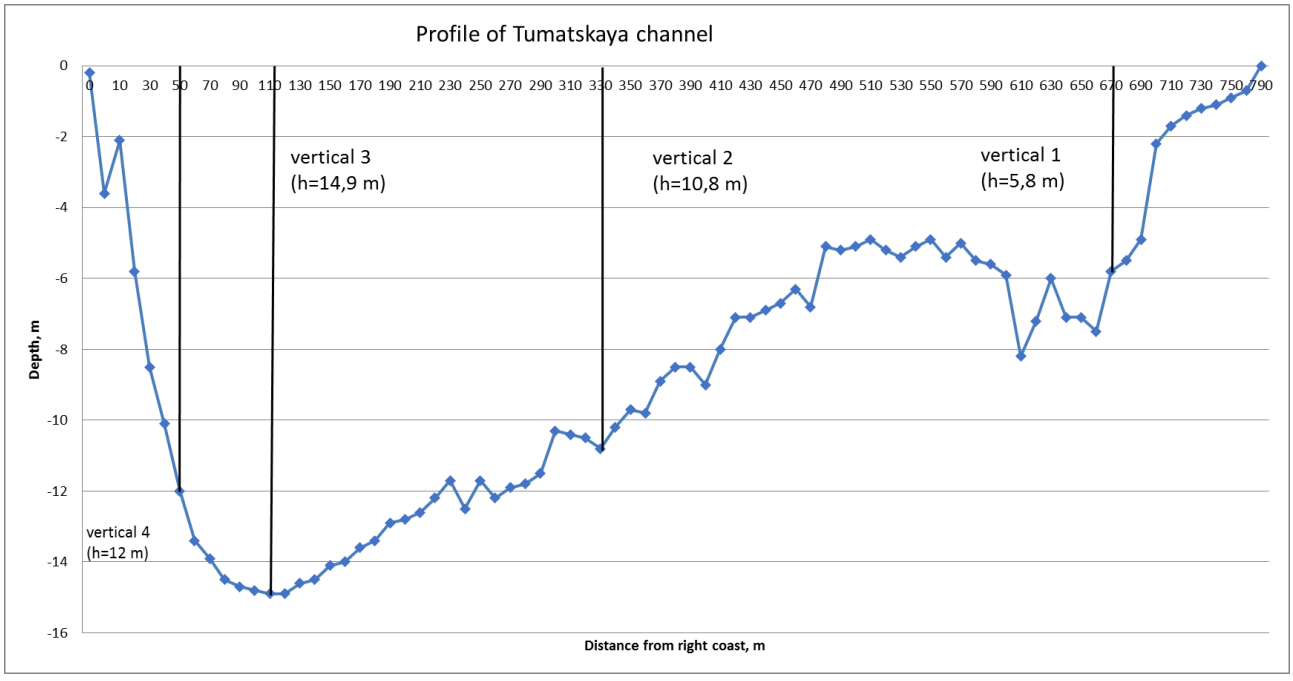

Figure 2.6-10: *Profile of Tumatskaya Channel*

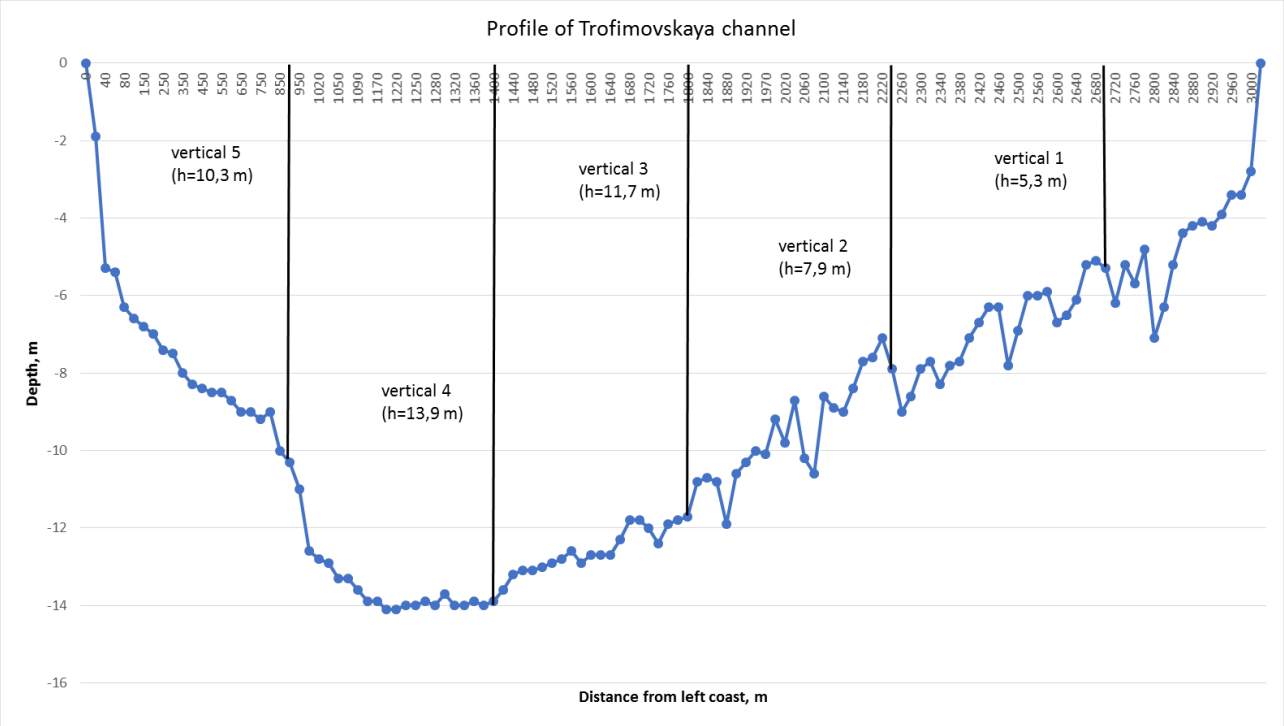

Figure 2.6-11: *Profile of Trofimovskaya Channel*

2.7 Hydrological work in the Lena River Delta in July 2017

Aleksandra Shadrina[1,2], Dmitry Bolshiyanov[2], Irina Fedorova[1], Andrey Alekseev[2], Sergey Pravkin[1,2]

[1] Saint Petersburg State University, St. Petersburg, Russian Federation

[2] Arctic and Antarctic Research Institute, St. Petersburg, Russian Federation

Fieldwork period
July 06th to August 08th, 2017 (in the Lena River and Samoylov Island)

Objectives
The main goal of the field work was a continuation of previous hydrological and hydrochemical investigations of lakes and river channels of the Lena River Delta.
Hydrological measurements were carried out during the expedition to the Lena River Delta in July 2017. These measurements consisted of two parts. First part was from 8. - 21.07.2017 on board of the ”Merzlotoved” of Institute of Permafrost of Siberian Branch of Academia of Sciences along the Lena River from Yakutsk to the Lena Delta. The second part took place on the scientific station “Samoylov Island” in the Lena River Delta.
The following investigations were performed: sampling of water and suspended material at different stations along the river-route ”Yakutsk - Samoylov Island” (Table A.2-13), at the Lena River channels (Table A.2-14) and at Samoylov Island lakes (Table A.2-15), measurements of water discharge in the Main Channels, water sampling for zooplankton and methane (together with colleagues from Kazan and Helgoland respectively). For some water samples analysis was already carried out on Samoylov Station. The study area is presented in Figure 2.7-1 with the river-route ”Yakutsk - Samoylov Island”, Figure 2.7-2 with the Lena channels and Figure 2.7-3 with lakes in the delta.

The studies included the following steps:

- Water sampling from the lakes and river channels (Table A.2-14 and A.2-15).
- Measuring water discharge in the river channels (Tumatskaya, Olenekskaya, Trofimovskaya and Bykovskaya).
- Processing of water samples in the laboratory of the Samoylov Station (conductivity, pH, dissolved oxygen, and turbidity).
- Preparation of water samples for transport and later analysis: main ions, cDOM, DOC, concentrations of nutrients, methane and zooplankton.

Methods
Water sampling in the channels and lakes, laboratory analysis
Water samples from river were taken with an unspecified water sampler. Samples for turbidity were stored in plastic bottles with $>$1 L volume. Water samples for nutrients were taken with a syringe and immediately frozen. Samples for anions and cations were filtered (GF/F, 0.45 μm) into 50-ml plastic bottles. Samples for cations were acid-preserved with 50 - 100 μl of 65 % HCO_3. Water samples for CDOM and DOC were filtered (GF/F, 0.7 μm) into 50- and 100-ml glass bottles. Samples for DOC were preserved by adding 20 - 50 μl of 30 % HCl.
Water conductivity, dissolved oxygen, and pH were measured in laboratory using multiparameter device (WTW 340i). The complete list of samples is shown in (Table A.2-14 and A.2-15).

Measurement of water discharge
Water discharge was measured in four Lena River channels. Cross sections were located in representative parts of the channels (cross sections of Roshydromet) on the Tumatskaya, Olenekskaya, Trofimovskaya, and Bykovskaya branches. Coordinates of the locations were taken by GPS. The main characteristics of the channels are presented in Table A.2-14 Hydrometrical works included determination of water depth and water velocity. Depth measurements were made with an echo-sounder (Fish-Finder Garmin).
At specific sites of the river, depth profiles of water velocity were taken. Depth profiles of water velocity were done at 20 %, 60 % and 80 % of the maximal water depth. There were four depth profiles in Tumatskaya and Olenekskaya Channels, five in Bykovskaya and six in Trofimovskaya Channel.
Measurements of water flow velocity were performed with a Hydrological speed recorder (GR-21). Water samples were filtered in the laboratory through pre-prepared (dried and weighed) filters GF / F (pore size is 0.45 μm). Next, the filters with sediments load were dried and weighed again. Turbidity (S) was calculated according to the difference in the weight of the filters before (m1) and after (m2) filtering the sampled water volume (A) - equation (1).

$$S = (m_1 - m_2)/A \tag{2.2}$$

Sediment load (Qs, g/sec) were calculated by the equation (2), where Qw is the water discharge on a gauge line (m^3/sec), S – turbidity (g/m^3).

$$Qs = Qw * S \tag{2.3}$$

Preliminary results
Data on water discharge and sediment load are presented in Table A.2-14. Water discharge at Tumatskaya Channel (451.4 m^3/sec) was a bit lower than discharge in the other channels, the sediment load was 2.25 kg/sec. The water discharge in Olenekskaya Channel was 757.4 m^3/sec, sediment load was 2.98 kg/sec. In previous years, the discharge in the Olenekskaya Channel was about the same as in the Tumatskaya Channel. However, it was 1.7 times higher in 2017. The water discharge in Bykovskaya Channel was 5,313.4 m^3/sec, sediment load was 17.74 kg/sec. The highest water discharge was observed in Trofimovskaya Channel (11,469 m^3/sec), but with only 64.8 kg/sec – sediment load. Additionally, discharge in the Trofimovskaya Channel was 2.2 times higher than in the Olenekskaya Channel.
Some Preliminary results of water chemistry of the different lakes are shown in Table A.2-15. Conductivity of the lake waters ranged from 48 - 91 μS/cm. The average temperature was 90 °C, pH-value ranged from 7.37 - 8.51. The highest water temperature and conductivity was observed in Banya-2 Lake. Dissolved oxygen concentrations in water were about 11 mg/l which indicates a good water quality.
All turbidity samples were processed in the lab of the “Research Station Samoylov”. The results are presented in Table A.2-14. In the Lena River, turbidity ranged from 2.61 - 15.12 mg/l. Large turbidity values are characteristic for areas with an increased anthropogenic load (near Zhigansk settlement and near the Aldan River estuary).

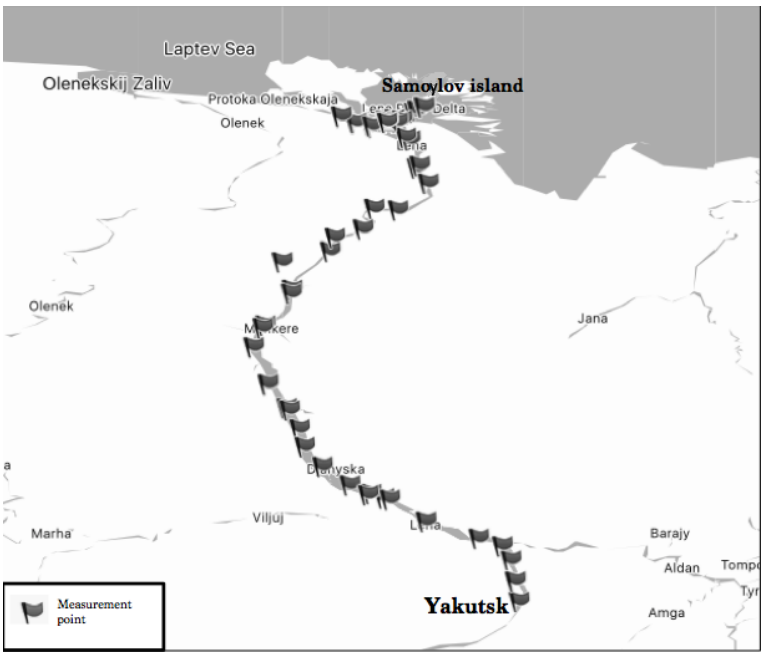

Figure 2.7-1: *The location of water sampling point along the Lena River from Yakutsk to Samoylov Island*

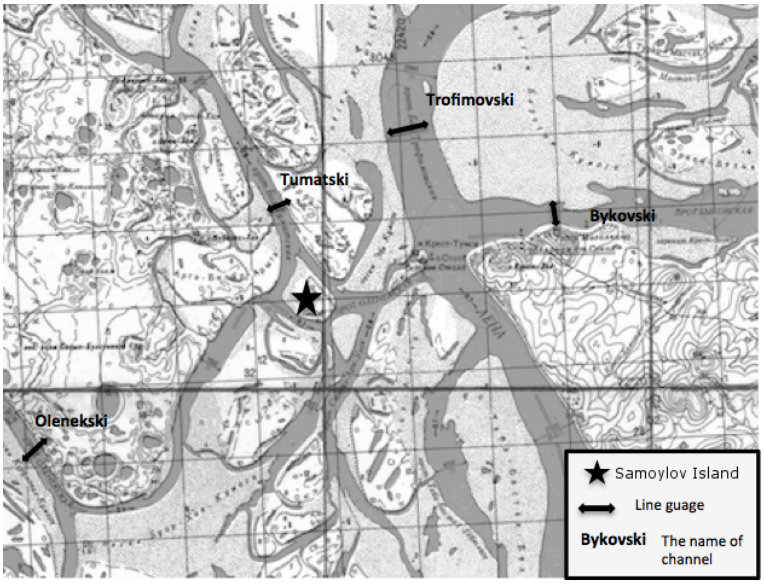

Figure 2.7-2: *Cross profiles for measurements of water discharge*

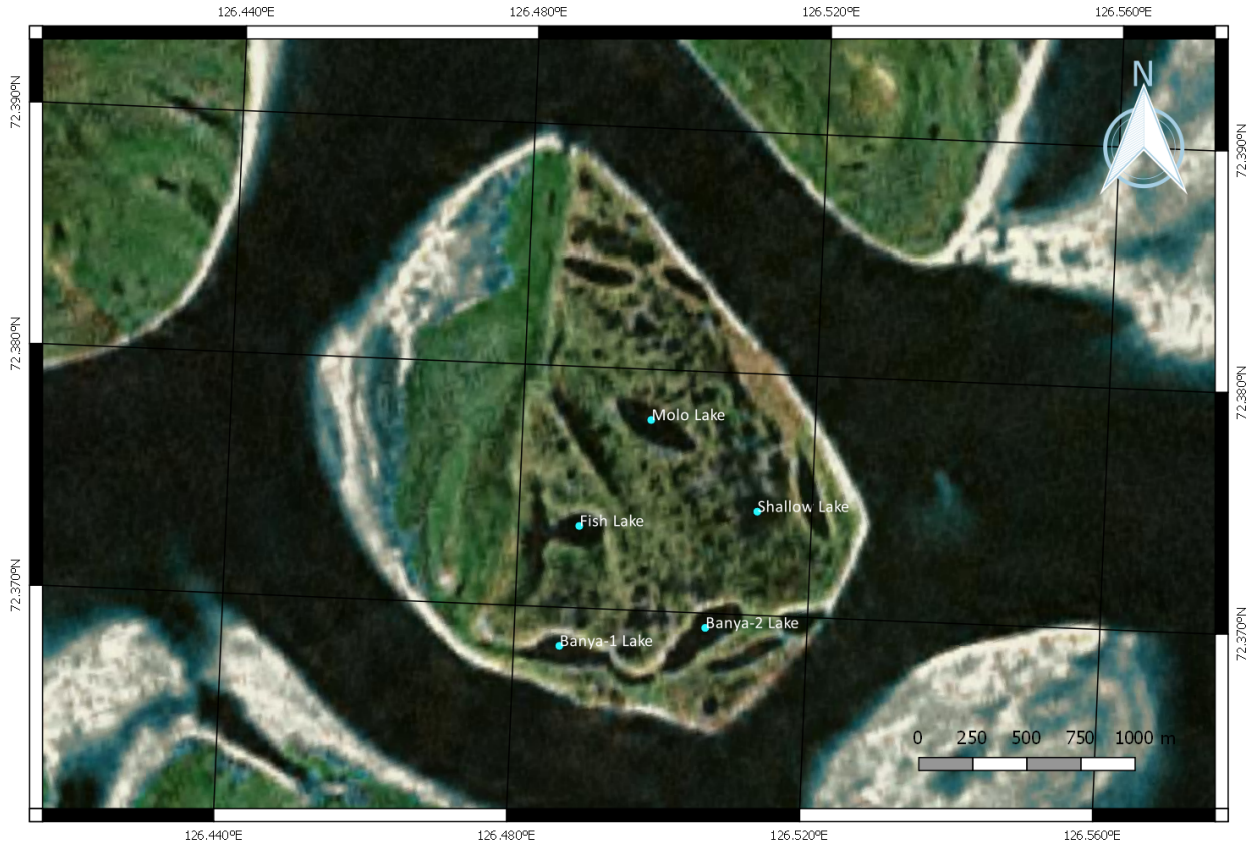

Figure 2.7-3: *Location of sampled lakes on Samoylov Island*

2.8 Water temperature patterns and flow characteristics near the head of the Lena River Delta

Lasse Sander[1], Rune Michaelis[1], Svenja Papenmeier[1], Sergey Pravkin[2], (Vera Fofonova[1]: not in the field)

[1] Alfred Wegener Institute Helmholtz Centre for Polar and Marine Research Sylt, Germany

[2] Arctic and Antarctic Research Institute (AARI), St. Petersburg, Russian Federation

Fieldwork period and location
July 30th to August 13th, 2017 (on Samoylov Island)

Objectives
Large Siberian rivers, such as the Lena, annually discharge large amounts of freshwater into the Arctic Ocean. Their size and orientation determine an effective transfer of heat over large distances and across pronounced seasonal temperature gradients. The volume of river discharge is thus an important parameter affecting water temperature and salinity in arctic deltas, estuaries and in the adjacent shallow shelf seas. Long-term changes in the characteristics of river discharge may consequently have important implications for shelf dynamics and the Arctic Ocean as a whole (Peterson et al., 2002).
At the delta head, the Lena River leaves the confines of the Verkhoyansk Mountain range and is released into a complex pattern of stream channels. With the diversification of the stream network, waters are funneled into beds of different characteristics regarding hydrography, geomorphology and ground temperature. These parameters define the effectivity of cooling at the transition from land to sea.
The aim of the field campaign was to obtain data on channel properties and temperature patterns in the Lena River and in the main Lena Delta branches (Figure 2.8-1). The data further serves to understand temperature anomalies observed in time-series of archived hydrographic data and to improve numerical models of discharge and water temperature (Fofonova et al., 2016).

Methods
Measurements with a CTD probe (Conductivity-Temperature-Depth probe; Sea and Sun Technology) were conducted as depth profiles at regular intervals of between 50 and 200 m (depending on channel widths; see Table 2.18.1) along five cross-river transects. The probe was attached to a rope and manually submerged from the side of *RV Ural*. The boat was drifting during the measurement of each profile. Additional measurements of current velocity and direction were conducted using an Acoustic Doppler Current Profiler (ADCP; WorkHorse Sentinel, RD Instruments) and in the analysis combined with multispectral land-surface information (including thermal bands) obtained from the Landsat program.

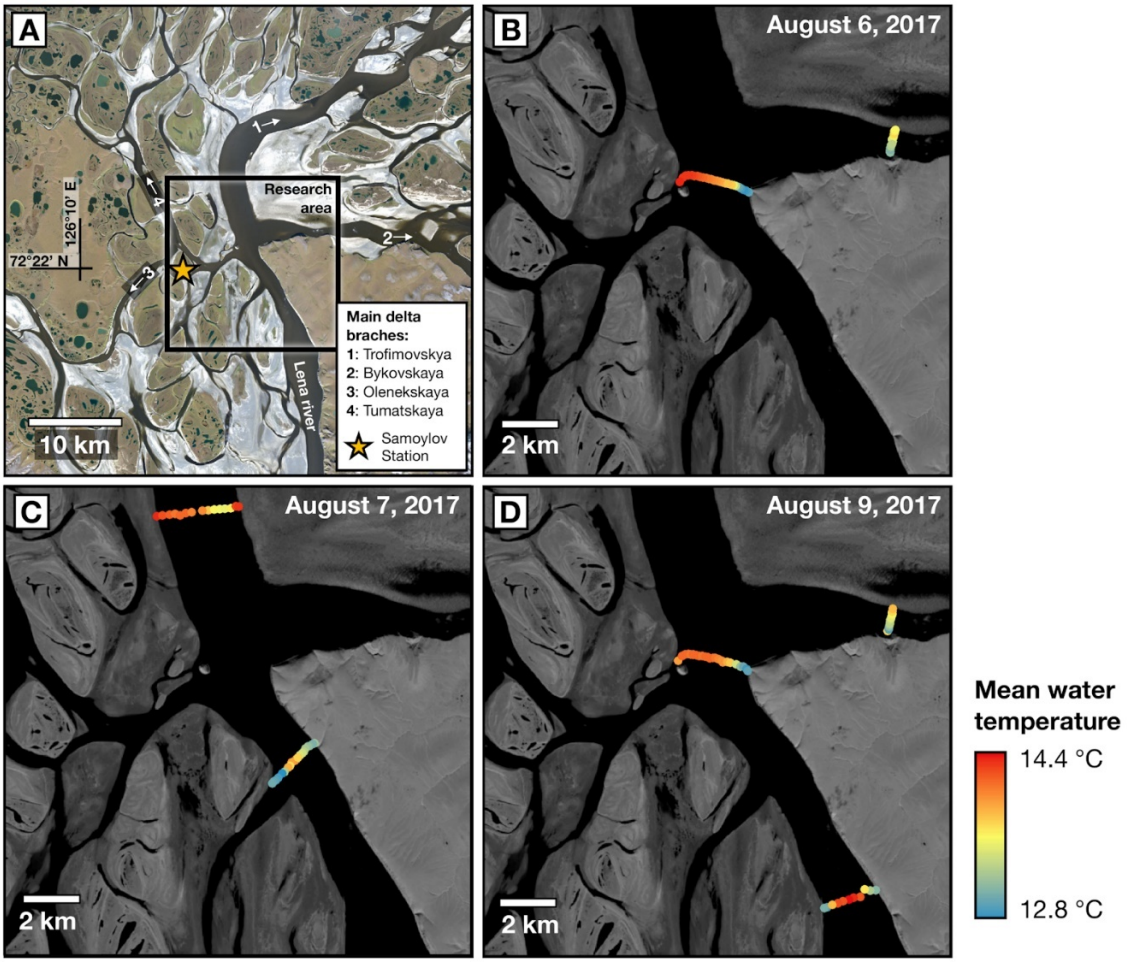

Figure 2.8-1: *(A) Location and basic geomorphology of the field site, (B-D) Mean water temperature values for the CTD profiles obtained at three different days of measurement.*

Preliminary results

For the individual profile measurements, there is virtually no variation in water temperature over depth, which suggests full mixing (i.e. high turbulence) in the water column. Across each transect however, small, but measurable, changes in temperature were observed (in the order of T = 0.2 — 0.8 °C; Figure 2.8-2). The water temperature gradually increases or decreases towards the river banks when compared to the midstream temperature. The temperature pattern in the water appears to be related to spatial differences in land-surface temperature, which determine a local cooling of the flowing water masses. A possible explanation for spatial differences in land-surface temperature is that a large proportion of the delta is flooded during the high summer runoff period. However, during periods of low discharge (between October and April), most river banks, shoals, shallow stream channels and sandbanks are exposed to low air temperatures. While the sand banks in the northern part of the research area appear to be relatively warm (when compared to the river banks in the central part of the area), the right bedrock-bound banks of the Lena River Main Channel and of Bykovskaya branch are relatively cold (cf. Figure 2.8-1 B-D).

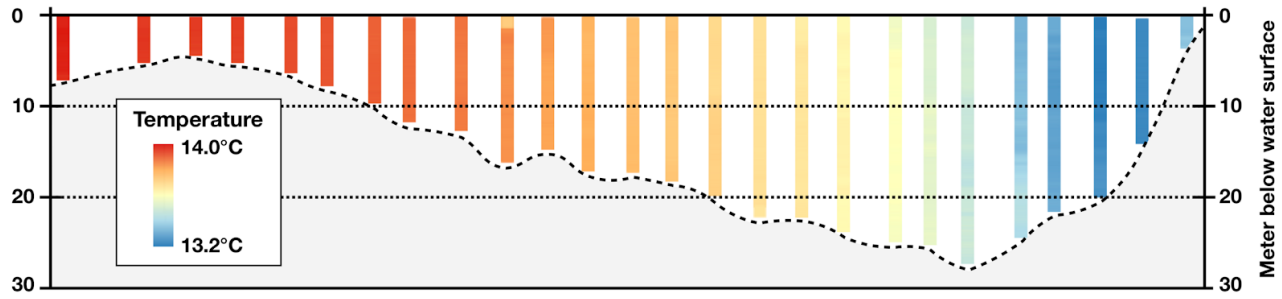

Figure 2.8-2: *Distribution of water temperatures across the approx. 2.6 km long transect B. The dashed line indicates the river bed.*

In addition, our data show a measurable variation of the overall water temperature over short periods of time (several hours to days). The likely reason for this is the passage of warm-water pulses resulting from warm weather conditions in the central Siberian hinterland. This determines that a direct comparison of measured values between the different days is not possible.

Table 2.8.1: Overview of CTD transects

ID	Date [year/ month/ day]	Start coordinate [Deg]	End coordinate [Deg]	Length [meter]	Approx. interval [meter]	Max. Depth [meter]	Number of profiles
A	2017/07/08	72.44315N/ 126.60258E	72.44718N/ 126.68808E	2900	200	15	16
B	2017/08/06 2017/08/09	72.39608N/ 126.72723E	72.39841N/ 126.6540E	2650	100	31	26
C	2017/08/06 2017/08/09	72.41021N/ 126.87353E	72.41736N/ 126.87835E	800	50	17	17
D	2017/07/08	72.37345N/ 126.77686E	72.36033N/ 126.73416E	2050	100	32	20
H	2017/09/08	72.32833N/ 126.86951E	72.32216N/ 126.81663E	1900	200	36	11

2.9 Water ecosystems investigations in polygonal ponds during the expedition Lena 2017

Ekaterina Abramova[1], Victor Alekseev[2], Olga Bolshiyanova[3], Waldemar Schneider[4], Günter Stoof[4]

[1] Lena Delta Nature Reserve, Tiksi, Sakha Republic, Russian Federation

[2] Zoological Institute RAN, St. Petersburg, Russian Federation

[3] Saint Petersburg State Forest Technical, St. Petersburg, Russian Federation

[4] Alfred Wegener Institute Helmholtz Center for Polar and Marine Research, Potsdam, Germany

Fieldwork period and location
April 07th to May 15th and June 23rd to September 01st, 2017 (on Samoylov Island)

Objectives
Wetlands, small lakes and ponds are typical features of circumpolar Arctic regions and in some parts of the Arctic these numerous shallow water bodies can account for up to 90 % of the total land surface area (Pienitz et al., 2008). There has been growing interest from the scientific community in the ecosystem status of Arctic lakes and ponds as possible sensitive indicators of climate change in the high latitude regions (Prowse et al., 2006; Adrian 2009). The small and shallow arctic water bodies can play an important role in capturing and transporting greenhouse gases, primarily CO_2, involving them in the trophic chains by algae communities with their photosynthetic activity. The main tasks of our studies were a) to evaluate Primary Productıon (PP) of Phytoplankton (PhP) and Phytobentic (PhB) algae in arctic polygonal ponds during the whole summer; b) to conduct a comprehensive analysis of these water ecosystems in the Lena Delta (composition, abundance and biomass of winter and summer zooplankton (ZP), composition and abundance of PhP and PhB, chlorophyll concentrations, growth rate and generation number of mass pelagic crustaceans).

Fieldwork summary
We focused on two polygon ponds with different characteristics on Samoylov Island: Pond I had large shallow part (maximum depth 0.5 m) that was either partly or completely covered by macrophytes such as Arctophila, Carex, Eriophorum, etc., while the Pond II had depths of 1-1.5 m with a narrow strip of vegetation offshore. In April 2017, four ice cores were collected from these completely frozen ponds and from five other small water bodies.
Subsections of the ice cores were thawed in boxes at 4 °C. The organisms that appeared after ice melting were collected in Petri dishes and kept in a refrigerator at a temperature of +4 -+9 °C to study their further development (Figure 2.9-1).

In summer (June - August 2017) the measurements of water temperature (T, °C), oxygen concentrations (O_2, mg/l), pH and conductivity (μS/cm) were made in Pond I and Pond II as well the water samples for Chl-a contain and PhP composition and abundance investigations. Additionally, ZP samples were obtained from Pond II in June - August 2017 (Table A.2-16 and Table A.2-17). PhP and ZP samples were collected either by drawing a net vertically from the bottom to the surface in the central part of the pond or by filtering 50 or 100 liters of water through plankton nets with mesh sizes of 20 and 100 μm respectively. Therefore 10 L buckets were used for water collection. Samples were preserved using either 4 % neutral formalin or 70 % alcohol. The processing of the ZP and detailed taxonomic investigations were carried out using Olympus SZX9 and BX60 stereomicroscopes

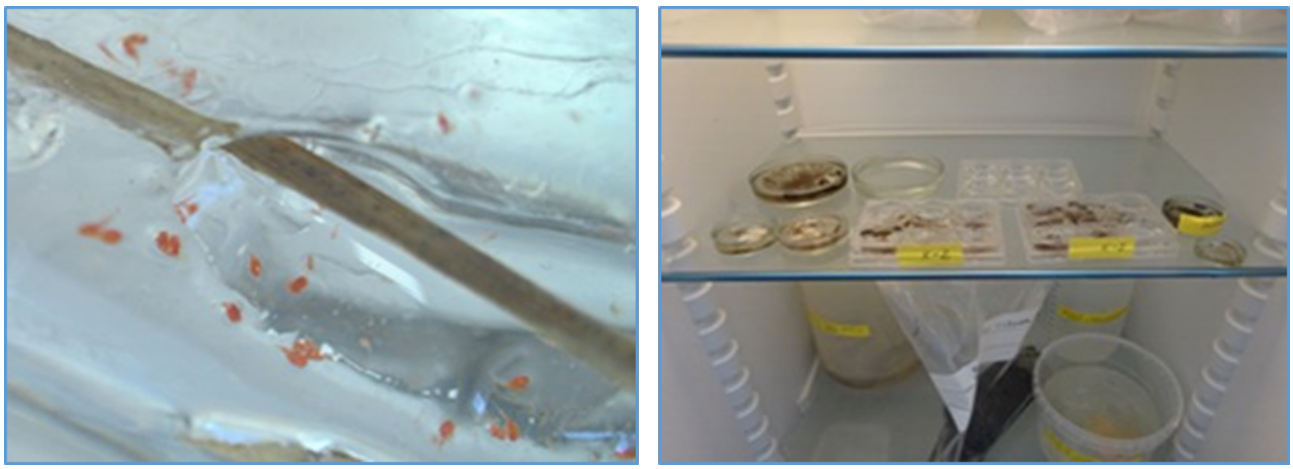

Figure 2.9-1: *Ice - core experiment. Copepods that were frozen in the ice core are shown on the left foto. The right photo shows the thawing of the ice core in plastic containers and finally the petri dishes with living copepods.*

at “Samoylov Island” Station. The individual weights were calculated by using a length-mass relationship (Balushkina and Vinberg, 1979). Therefore, size measurements of key organisms during the entire period of the study were carried out, every 2 to 3 days under the microscope. Only for *Daphnia middendorffiana* Fischer, more than 100 size measurements were done from hatching to adult stages. Primary production was determined through determination of the oxygen production and consumption rates. Therefore the initial O_2 concentration of the samples was determined, as well as the O_2 concentrations after on average of 48 hour incubation at *in situ* conditions under dark and light conditions (Figure 2.9-2). A WTW Multi - 350i instrument was used for determining the O_2 concentrations. For each set up, duplicate 300 ml glass bottles were used. The bottles were incubated at a water depth of 1.4 and 0.5 m. For PhP water sampling we used a 5 L Patalas bathometer (water sampler according to Prof. V. Alekseev), PhB was collected with a stock device that collected sediments with an area of 80 cm^2. Water and sediment samples aliquots were taken for: chlorophyll estimation, algae biomass, species composition identification and initial O_2 concentration.

Figure 2.9-2: *Primary Production experiment*

In order to estimate the chlorophyll-a concentrations, 300 ml of water was filtered through Whatman glass microfiber filters grade (GF/F) and filters were frozen at -20 °C for preservation. These were later analyzed in the Russian-German Otto Schmidt Laboratory for Polar and Marine Research (OSL, AARI, St. Petersburg, Russia).

Preliminary results

Similar to previous years, the most common and numerous copepods in the first half of summer (June - mid July 2017) were representatives of the Cyclops, Acanthocyclops, Eucyclops and Diacyclops genera, while calanoid species such as *Leptodiaptomus angustilobus* (Sars), *Arctodiaptomus novosibiricus* Kiefer, and *Heterocope borealis* (Fischer) dominated the zooplankton communities in the second half of summer (mid July - August 2017), together with two cladocera *Daphnia pulex* De geer and *D. middendorffiana*. The large crustaceans *H. borealis*, *D. middendorffiana* and two Anostraca species (*Polyartemia forcipata* and *Branchinecta paludosa*) were the most important species in the small polygon ponds with respect to zooplankton biomass. Primary Production Data are available upon request. In addition, CO_2 concentrations, solar radiation and water temperature were monitored continuously by the group of Julia Boike (AWI, Potsdam). With this data set, new information of the structure and functioning of polygonal ponds in the Arctic regions will be obtained.

2.10 Hot spots in a cold landscape: Siberian permafrost ponds and carbon dioxide emissions

(Sally Jahn[1]: not in the field), Victor R. Alekseev[2], Lars Kutzbach[5], Elena Chertoprud[3], Ekaterina Abramova[4], Ingeborg Bussmann[1], Paul Overduin[1], Peter Schreiber[1], Lutz Beckebanze[1], Julia Boike[1]

[1] Alfred Wegener Institute Helmholtz Center for Polar and Marine Research, Potsdam, Germany

[2] Zoological Institute of the Russian Academy of Sciences, St. Petersburg, Russian Federation

[3] Dep. of Hydrobiology, Biological faculty, Moscow State University

[4] Lena Delta Reserve, Tiksi, Sakha Republic, Russian Federation

[5] Institute of Soil Science, Universität Hamburg, Germany

Fieldwork period and location
July 10th to September 20th, 2017 (on Samoylov Island)

Objectives
Lakes and ponds are one of the main elements of Arctic permafrost ecosystems and are considered to be an important, fundamental part of the carbon cycle. These waterbodies contribute to a large degree to the carbon dioxide CO_2 and methane CH_4 emissions of the Arctic ecosystem. The strength of the CO_2 and CH_4 emissions is determined by a variety of complex physical and biogeochemical processes. Not only the large thermokarst lakes, but also the smaller ponds, strongly influence the amount of the emitted greenhouse gases (Langer et al., 2015). 25 % of Samoylov Island, the selected study region, located in the Lena River Delta in north-eastern Siberia, is covered with ponds and lakes that strongly influence the delta's ecosystem. These waterbodies contribute highly to the outgassing of CO_2 of this arctic landscape, especially from late summer until autumn, before the ground starts to freeze again. According to the findings of an earlier study with observations in the year 2008, at the end of the vegetation period in September the emissions from lakes and ponds are higher than the observed net CO_2 flux above vegetated tundra surfaces, even about an order of magnitude (Abnizova et al., 2012, GB2041). Therefore, from July to September 2017, *in situ* measurements of CO_2 in three small arctic ponds were conducted to further confirm these observational results and to improve the understanding of the role and the importance of small ponds on CO_2 emission as well as their related physical and biogeochemical processes. For this purpose, Eosense eosGP sensors were deployed from mid-July to mid-September to measure the CO_2 concentrations in three almost adjacent polygonal ponds located close to the Russian-German scientific research station on Samoylov Island. The recorded CO_2 concentrations of these sensors are an important basis to further determine the carbon cycle of these ponds and to help to get better insight into their role as carbon sink or source of CO_2 to the atmosphere (Langer et al., 2015).

Fieldwork
The installed eosGP sensors are compact, up to 3 m waterproof CO_2 concentration probes. The desired gas concentration is measured by a non-dispersive infrared (NDIR) CO_2 sensor that uses the correlation of light source intensity and a specific gas concentration to determine the actual gas concentration. The sensor is exposed to gases through a membrane covering the face of the eosGP acetal housing in which the sensor is embedded. The gas, but no liquid water, can permeate through the material of the membrane. The sensors are used for continuous, accurate, *in situ* measurements

of carbon dioxide concentration in the harsh environment of the Siberian permafrost tundra.
The eosGP sensors offer a measurement accuracy of approx. 1 % of full scale, with a repeatability of 1 % of reading, with CO_2 concentration readings automatically corrected for changes in temperature. The ideal gas law can be used to compensate changes in the atmospheric pressure that influence the recordings of the sensor as well:

$$C^* = C \times (P_{ref}/Pi) \tag{2.4}$$

C is the raw concentration, P_{ref} is the reference pressure (101.35 kPa) and Pi is the pressure measured in the field (in kPa). The sensor concentration and temperature outputs are scaled from 0-5 V. Depending on the sensor calibration, each voltage signal may be correlated with a different concentration and temperature range. The following table (Table 2.10.1) gives an example of typical values and concentration ranges (Eosense, 2016).

Table 2.10.1: From 0-5 V scaled sensor concentration and temperature outputs of the Eosense eosGP sensors. Unlike temperature, concentration analog signals are ranged from zero to calibration range plus 20 % (Eosense, 2016, 6).

Parameter	Voltage Range	Concentration Range
Low-range CO_2 Concentration	0-5 V	0→6,000 ppm
High-range CO_2 Concentration	0-5 V	0→24,000ppm
Temperature	0-5 V	-20°C→50°C

As the NDIR sensors can drift over time due to natural changes in the electrical and mechanical properties of the NDIR components, the sensors should be calibrated from time to time according to the published recommendations of Eosense (Eosense, 2016).
Four eosGP sensors were continuously deployed in two adjacent ponds on Samoylov Island in the period from July 10th to September 20th 2017. Every minute each single sensor records an individual CO_2 measurement, while the datafile is specified to contain averages over an interval of 15 minutes. The fifth sensor was additionally employed to measure temporary the CO_2 concentrations in the two ponds and in a third, neighbouring one. The datafile contains the minute CO_2 concentration measurements. In Pond 1, two eosGP sensors were installed, sensor GP1 close to the water surface, GP2 10 cm above the pond bottom. Two additionally deployed sensors T109 measured the water temperature, LI-COR Li192 PAR sensors the photosynthetically active radiation (pointing up - incoming and pointing down - outgoing). These additional instruments were installed close to the eosGP sensors, attached to a buoy. The eosGP sensors GP3 and GP4 in the slightly deeper Pond 2 were similarly installed and measured the CO_2 concentration at a height of 79 cm and 9 cm above the pond bottom, respectively.
On July 10th, the four sensors, in the following often referred to as GP1, GP2, GP3 and GP4, measured at the beginning of the campaign (10.07.2017, 3:00:00 am UTC) the CO_2 concentrations in the air, 1 m above the ground, for exactly 2 hours. Afterwards, they were installed at the same water level in one pond till 07:20:00 am, before described measurement setup was established. At the end of the measurement campaign, on September 20th, the four sensors and a further, additional, mobile one GP5 were assembled again in the same height, exposed to the arctic air to measure the average airborne CO_2 concentrations.
The four eosGP sensors GP1-4 provided continuously CO_2 concentration measurements in the ponds, with the exception of a short recording gap at the beginning of the study period. This measurement interruption however did not happen due to a sensor failure, but problems with the external power supply. As a result, the minor data gap and possible erroneous data during the initial phase of the measurement campaign were excluded from further analysis, so that the data series of the fixed installed sensors start on July 11th at 02:00:00 am UTC.

Methods

All four eosGP sensors differ widely from one another, also when they were all installed in the same height and were exposed to the same airborne CO_2 concentrations. Also in comparison with the airborne carbon dioxide concentrations measured by the LI-COR Li7000 gas analyzer, the recordings of the eosGP sensors were highly variable and deviant. According to these findings and after consultation with the Eosense-representatives, the measured CO_2 concentrations in the ponds were corrected as follows:

- Pond 2: As the mean of the measured concentrations at the beginning and the end, during the period of atmospheric concentration measurements before the actual experiment began and after it finished, are almost identical. The sensors did not seem to drift from themselves or from each other significantly (GP3 Before and After: 536.3 ppm and 534.7 ppm; GP4 Before and After: 683.2 and 717.8 ppm; Difference GP4-GP3 Before and After: 146.9 and 183.1 ppm). Therefore, the two graphs are both corrected to the atmospheric concentration of the site measured by a Li7000 gas analyzer that is installed close to the study site. A correction term is calculated based on the Li7000 gas analyzer, representing the mean deviation of the calculated average deviations of the respective sensor and gas analyzer recordings at the beginning and the end of the study period.

- Pond 1: After comparing the obtained concentration means of the two sensors as well as their performance at the beginning and the end of the measurement period (GP1 Before and After: 242.4 ppm and 378.5 ppm; GP2 Before and After: 510.8 and 1010.4 ppm; Difference GP1-GP2 Before and After: 264.8 and 631.9 ppm), it can be noted that the sensors not only drift internally, but also drifted strongly from each other. As a result of this first data analysis, a linear drift of the received sensor data is assumed. Therefore, at first a drift correction linear in time (GP1: -0.02 ppm/point and GP2: -0.073 ppm/point, where point is the measurement record number) and afterwards an atmospheric correction like for Pond 2 is conducted.

Preliminary results

As a result of the former described measurements, data preparations and corrections, Figure (2.10-1 a) and b)) depicts the time series of the measured CO_2 concentrations in the ponds can be obtained. In Pond 1, the mean of the measured CO_2 concentrations is lower than in Pond 2, in the upper part of the pond as well as close to the bottom. In Pond 1, at the beginning the CO_2 concentrations in the bottom are slightly higher, at the end of the time series a little bit lower than in the upper zone of the pond. Nevertheless, the data lines of GP1 and GP2 are almost identical during the whole study period. Thus, a sufficient vertical mixing in the pond to compensate concentration differences in the water can be assumed. In Pond 2, the concentration measurements close to the surface and at the bottom of the pond are almost identical, but differ more and more during the course of the measurement period. Furthermore, the CO_2 concentrations depicted by the GP4 sensor are subject to higher fluctuations over time, indicating stronger CO_2 concentration variations in the lower part of the pond.

All in all, a stronger photosynthetic activity lowers the CO_2 concentrations, while a stronger respiration in the pond is indicated by higher CO_2 concentration recordings. Therefore, the CO_2 concentrations measured by the sensors as well as the vertical fluxes and mixing in the pond is influenced by further parameters like e.g. sunshine, light intensity, air pressure, but also wind direction and velocity or temperature. For example, the solubility of CO_2 in water rises with falling water temperatures.

Table 2.10.2 additionally allows an overview of the mean values of the recorded CO_2 concentrations of the extern, mobile sensor GP5 in comparison to the mean concentrations of the fixed installed sensors GP1-4 in the ponds during almost identical time spans, if available. It is clearly obvious that the recorded CO_2 concentration values of GP5 also differ strongly from the concentration means measured by the fixed installed sensors.

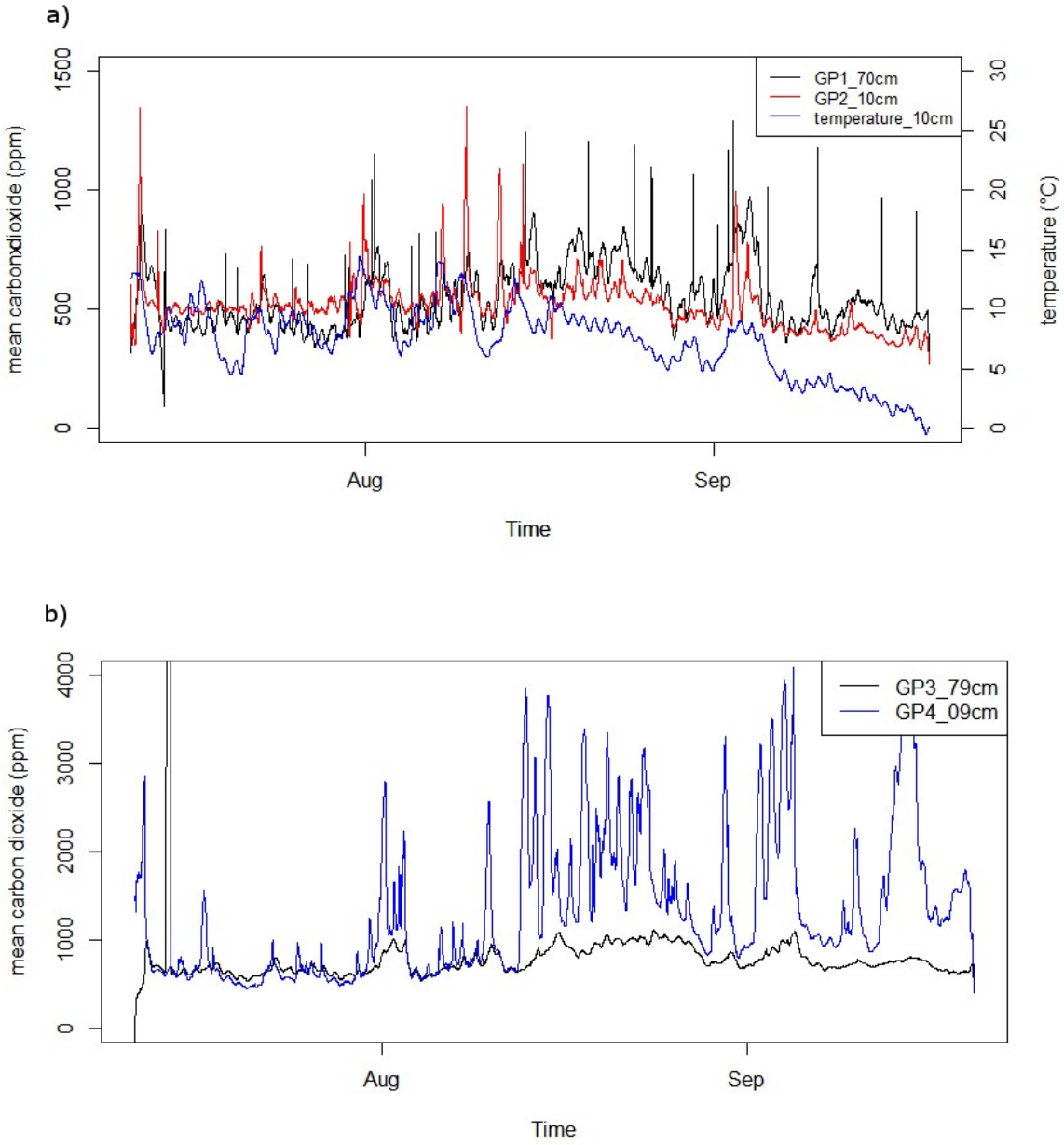

Figure 2.10-1: *a) Corrected mean carbon dioxide concentrations in Pond 1 (plotted together with the measured water temperature of one of the additionally deployed sensors in Pond 1) and b) in Pond 2. The height of the installed sensors above the pond bottom is depicted in the legend for every single sensor.*

Conclusion

In summary, the installation of the eosGP sensors and the generated data records during the study period from mid-July to mid-September give a good insight into the carbon dioxide concentrations and distributions in three different arctic Siberian permafrost ponds. Due to the conducted data corrections and the varying performance of the installed eosGP sensors as well as the fifth, temporary deployed, mobile one, further measurement campaigns in the Siberian polygonal tundra should be conducted to verify the here presented results. As a primary observational result of this study project it should be noted that after the recommended data corrections were implemented, the

mean CO_2 concentration measurements of all long-term installed sensors exceed the carbon dioxide concentrations of the surrounding Siberian arctic air recorded by an extern Li7000 gas analyzer.

Table 2.10.2: Comparison of the mean carbon dioxide concentration measurements of the mobile sensor GP5 and the fixed installed sensors GP1-4 in the same ponds during almost identical time periods.

Pond	**Position**	**cm under water suface**	**Measurement period on September 19th (UTC) - GP5**	**Mean [ppm] - GP5**	**Measurement period on September 19th (UTC) - GP1-4**	**Mean [ppm] - GP1-4**
1		42	01:44 – 02:01	274.82	01:45 – 02:00	GP1: 481.05 GP2: 434.52
2	1	35	02:11 – 02:28	262.28	02:15 – 02:30	GP3: 631.61 GP4: 1552.93
	1	15	02:31 – 02:46	267.33	02:30 – 02:45	GP3: 632.69 GP4: 1558.47
	2	32	02:49 – 02:56	270.87	02:45 – 03:00	GP3: 632.77 GP4: 1564.45
	2	15	02:59 – 03:10	283.79	03:00 – 03:15	GP3: 633.40 GP4: 1571.26
J		39	03:16 – 03:26	303.51		
J		15	03:30 – 03:40	345.63		

2.11 Quantification, isotopic and compositional analysis of dissolved and particulate carbon in the Lena and water bodies of its delta

Maria Winterfeld[1], Hendrik Grotheer[1], (Gesine Mollenhauer[1]: not in the field)

[1] Alfred Wegener Institute Helmholtz Center for Polar and Marine Research, Bremerhaven, Germany

Fieldwork period
July 2nd to July 31st, 2017 (on Samoylov Island, Kurungnakh Island, Lena Main Channel)

Objectives
Understanding carbon cycle in permafrost landscapes is important to assess the climatic relevance of future permafrost thaw. Carbon export from permafrost regions can occur via gas exchange between dissolved inorganic carbon in the water bodies and the atmosphere or by river discharge as dissolved and particulate organic carbon (DOC and POC). Quantification of carbon pools combined with determining their stable isotopic composition (δ^{13}C and δ^{2}H) and radiocarbon dating can be used to estimate the contribution of fossil carbon to total export, organic matter sources and trace organic matter remineralization in the water bodies. It is known that both concentration and radiocarbon composition of DOC and POC vary strongly with season and that their composition reflects the relative contributions from different sources within the Lena watershed. In order to study the sources of carbon and the biogeochemical processes affecting carbon in Siberian rivers and lakes, we collected water samples from thermokarst lakes and ponds on Samoylov and Kurungnakh, and from the Lena River Main Channel. For the expedition “Lena 2017”, the following sampling objectives were constituted:

- Water samples from three depth profiles along a cross section of the Lena Main Channel once a week (4 times in total).
- Water samples from a depth profile from North Lake (on Samoylov Island) and water samples from its outflow stream and ponds downstream of the lake (at least twice during the expedition).
- Water samples from depth profiles of Lucky Lake and Oval Lake (on Kurungnakh Island) and water samples from the outflow streams (at least twice during the expedition).

Methods during field work
a) Lena River - Main Channel
The Lena Main Channel was sampled along a west-east stretching cross-section close to Stolb Island (Figure 2.11-1). Along this transect, three depth profiles were generated, each of them consisting of three sampling depths (near the surface, intermediate depth, close to the ground, see Table A.2-18). Water samples were taken using a 5 L Niskin water sampler (General Oceanics, 1010). The device was equipped with a 30 m long rope, a 1.5 kg iron weight and a 400 g drop messenger. At each sampling depth, the water sampler was deployed three to four times in order to obtain sample volumes of 15 - 20 L. The sampling depth was determined using 1 m marks on the rope. The engine of the boat was switched off during the sampling procedure in order to facilitate a straight vertical immersion of the water sampler. Since it was intended to keep the sampling position rather constant the boat drove a few meters upstream after each deployment of the sampling device in order to correct for drift that had taken place while the engine had been shut down. Water samples for POC and DOC analysis were stored in plastic canisters (15 - 20 L) and were processed in the laboratories on Samoylov Island the same day. Moreover, brown-glass bottles (4 ml and 330 ml) were filled for DIC analysis. Bottles were entirely filled with water in order to avoid entrainment of air

preventing gas exchange with a headspace. Due to bad weather conditions, the Lena transect was sampled just twice in total throughout the expedition period.

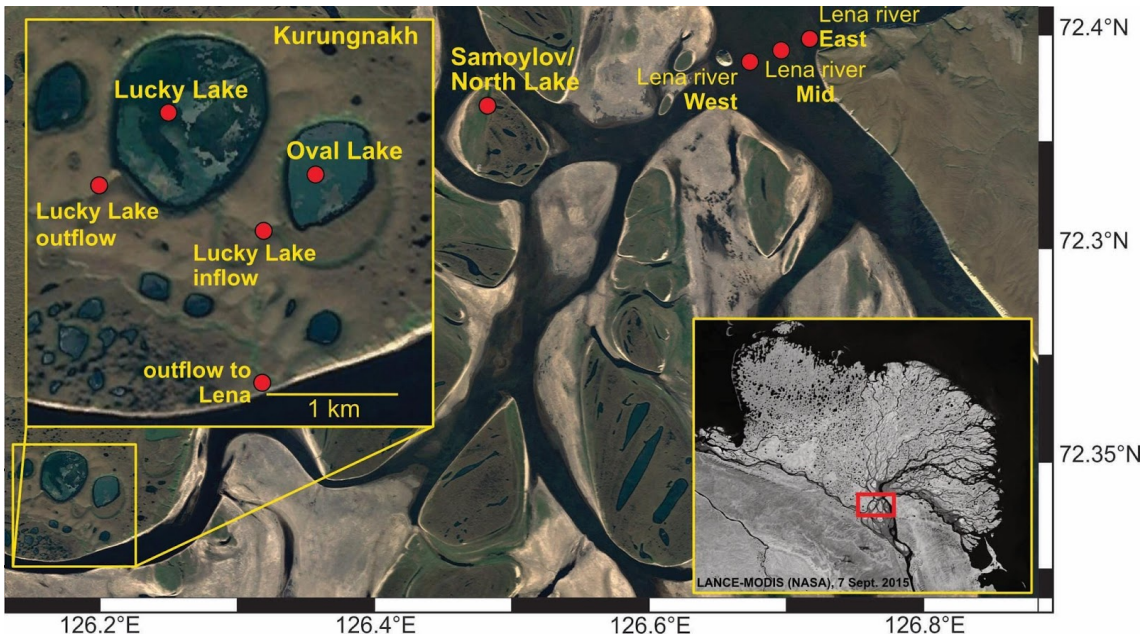

Figure 2.11-1: *Sampling locations in the Lena Delta in 2017*

b) Kurungnakh - Lucky and Oval Lakes

Lucky Lake and Oval Lake are neighboring thermokarst lakes that are connected through a small stream of approx. 1 km in length. The stream serves as an outflow of Oval Lake and discharges into Lucky Lake. The entire lake-system ultimately drains into the Lena River via an outflow stream of Lucky Lake. During the Lena 2017 expedition, water samples were collected from the two stream systems and from depth profiles on Oval Lake and Lucky Lake (Figure 2.11-1). Each profile comprised three sampling depths. Each outflow stream was sampled at one single location where water flow was visible and accessible. Sampling on the lakes was performed using a rubber dinghy deploying the same water sampler as on the Lena River. The water depth was determined with the labeled rope. Both lakes were sampled in the center. In order to prevent drifting during the sampling procedure the boat was anchored with a heavy iron weight (ca. 20 kg). Approx. 20 L (DOC and POC) were collected from each depth and stored in plastic canisters. Brown-glass bottles (4 ml and 330 ml) were filled for DIC analysis at the sampling location. The streams were sampled at the surface by immersing the canisters (20 L) and brown-glass bottles (4 ml and 330 ml) into the water. The sampling program was performed once during the expedition and was completed on two different days. Logistical problems and bad weather conditions circumvented a repetition of the entire procedure.

c) Samoylov - North Lake and adjacent ponds

On North Lake, samples were obtained from one single depth profile consisting of two sampling depths (surface and close to the ground) at the center of the lake. The outflow stream of North Lake was sampled at two locations (in the floodplain near the Lena and in proximity to the lake). Additionally, surface samples were taken from three polygonal ponds (approx. 1 m deep) situated along a north-south transect south of North Lake. Sampling of the lake and its outflow system for POC and DOC (each 20 L) as well as DIC (4 ml and 330 ml brown-glass bottles) was performed according to the sampling protocol at Lucky Lake. Polygonal ponds were sampled at the rim by immersing canisters (sample volume: 20 L) and brown-glass glass bottles (4 ml and 330 ml).

d) Filtration and sample treatment in the laboratories

Large samples (10 - 20 L canisters) were filtered using glass fiber filters (Whatman, GF/F), pore sizes of 0.7 μm) of different diameters (142 mm, 47 mm and 25 mm). In addition, samples were filtered using glass fiber filters (25 mm diameter) with a smaller pore size (ADVANTEC, GB-140, pore size 0.4 μm) in order to assess size fraction dependent isotopic differences in POC and DOC. The filtration volume for the 142 mm filters varied between 6 - 14.5 L per sample, for the 47 mm filter varied between 1 - 2 L, and for the 25 mm filter varied between 200 - 500 mL. The small filters (25 and 47 mm) will be used for δ^{13}C and δ^{14}C analyses of POC as well as the determination of particulate organic carbon concentrations. The large filter (142 mm) will be used to analyze the biomarker composition of the POC. The 142 mm filters were wrapped in pre-combusted aluminum foil, the small filters (47 and 25 mm) were placed in combusted glass petri dishes and all filters were stored frozen. During the filtration, the vacuum pump was set a maximum value of 200 mbar in order to avoid destruction of microorganisms and the release of their particles into the filtrated sample. The filtrate will be used for analyses of organic carbon concentration as well as δ^{13}C and δ^{14}C of DOC. It was filled in 2-3 HDPE bottles (60 ml each) and stored frozen. Samples for DIC concentration δ^{14}C analyses were poisoned with 50 μl (4 ml vial) and 100 μl (330 ml bottles) of a saturated solution of $HgCl_2$ in distilled water and were stored at 4°C. All DOC, DIC, and POC samples were transported to Germany where they were processed in laboratory.

2.12 Meiobenthic and zooplanktonic crustacean faunas (Cladocera, Copepoda) of small water bodies on Samoylov Island

Elena Chertoprud[1] and Ekaterina Abramova[2]

[1] Moscow State University, Moscow, Russian Federation

[2] Lena Delta Reserve, Tiksi, Sakha Republic, Russian Federation

Fieldwork period and location
July 30th to September 01st, 2017 (on Samoylov Island)

Objectives
The main aim of this study was the analysis of the diversity of zooplanktonic and meiobenthic crustaceans (Copepoda and Cladocera) of standing water bodies in the area of Samoylov Island Research Station. Special attention was paid to the species from the meiobenthic order Harpacticoida.

Fieldwork summary
Sampling: 52 quantitative samples of freshwater zooplankton and meiobenthos at 52 stations were collected in the period from 01 to 25 August of 2017. The locations of the stations are marked in Figures 2.12-1, 2.12-2 and 2.12-3, and the general descriptions of the stations are presented in Tables A.2-19 and A.2-20.
Zooplankton: The sampling was performed from the shore using a zooplankton net (10 cm diameter, 50 μm mesh). Samples were preserved with 96 % ethanol. The sampling method was adapted for each locality and the sampling approach depends on both surface area and depth. Samples were taken as vertical and/or horizontal net haul samples by throwing the net into the water. Three replicates were taken at each station and later united in one mixed sample.
Meiobenthos: The samples were collected from the shore with a plastic tube (diameter 2 cm). A column of the upper sediment layer (3 - 4 cm) was pushed out from the tube with a plunger and preserved with 96 % ethanol. Three substrate portions were taken for each mixed sample.
Hydrological characteristics: At each station measurements of Ph, temperature (°C), and mineralization (ppm) were performed. For this purpose, portable equipment of the firm "Hanna Instrument" were used. *Identification of species*: The samples will be processed in laboratory of hydrobiology department of Moscow State University, animals will be identified to species level according to Kotov et al. (2009), Smirnov (1971, 1995, 1996), Lieder (1996), Sinev (1999, 2002, 2009) for Cladocera, Rylov (1948), Borutsky (1952), Dussart and Defaye (1983), Borutsky et al. (1991), Brtek and Mura (2000), Alekseev Tsalolikhin (2010), Fefilova (2015) for Copepoda.

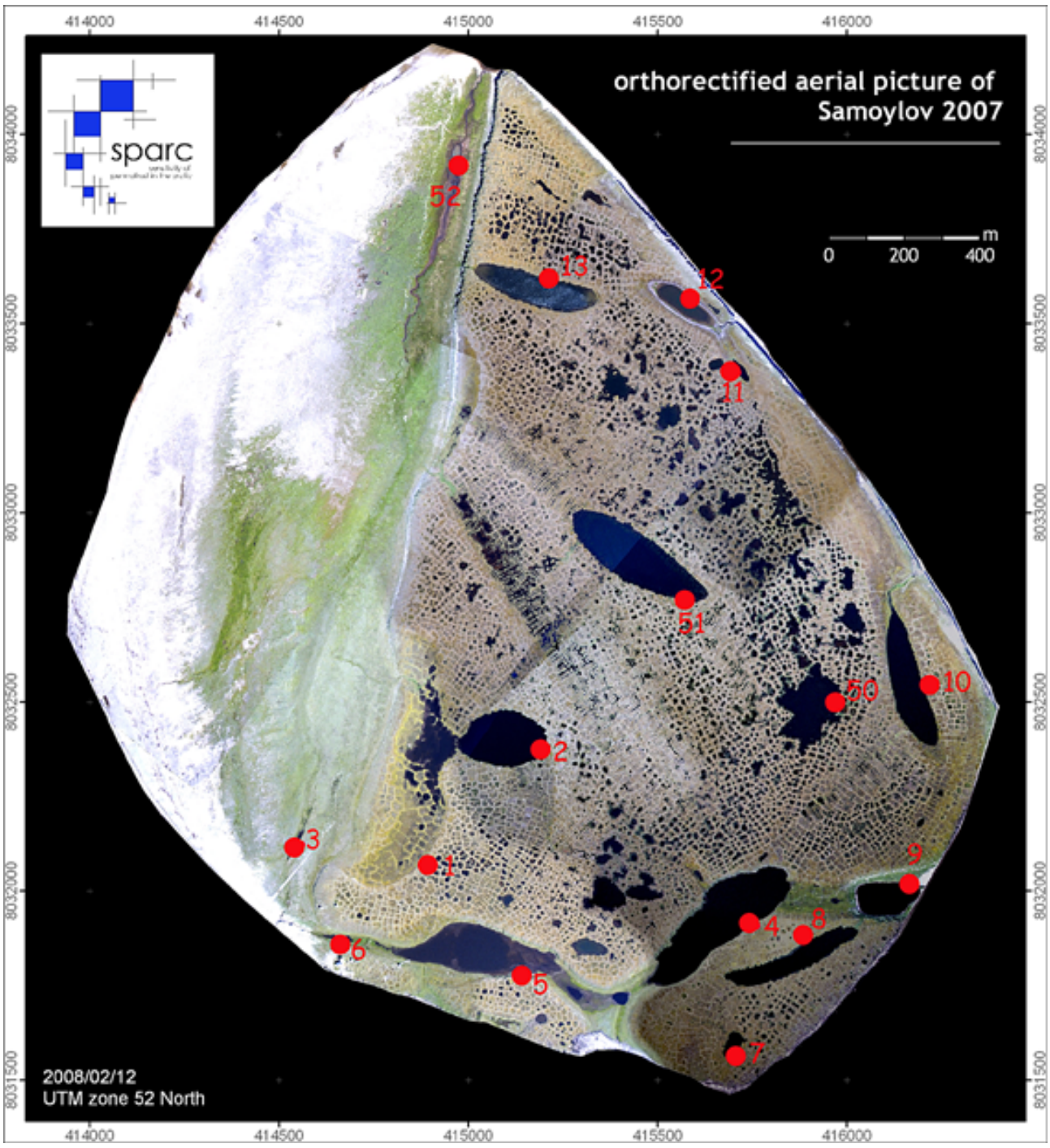

Figure 2.12-1: *Map of the sampling stations locations (red points) in on the Samoylov Island (August 2017)*

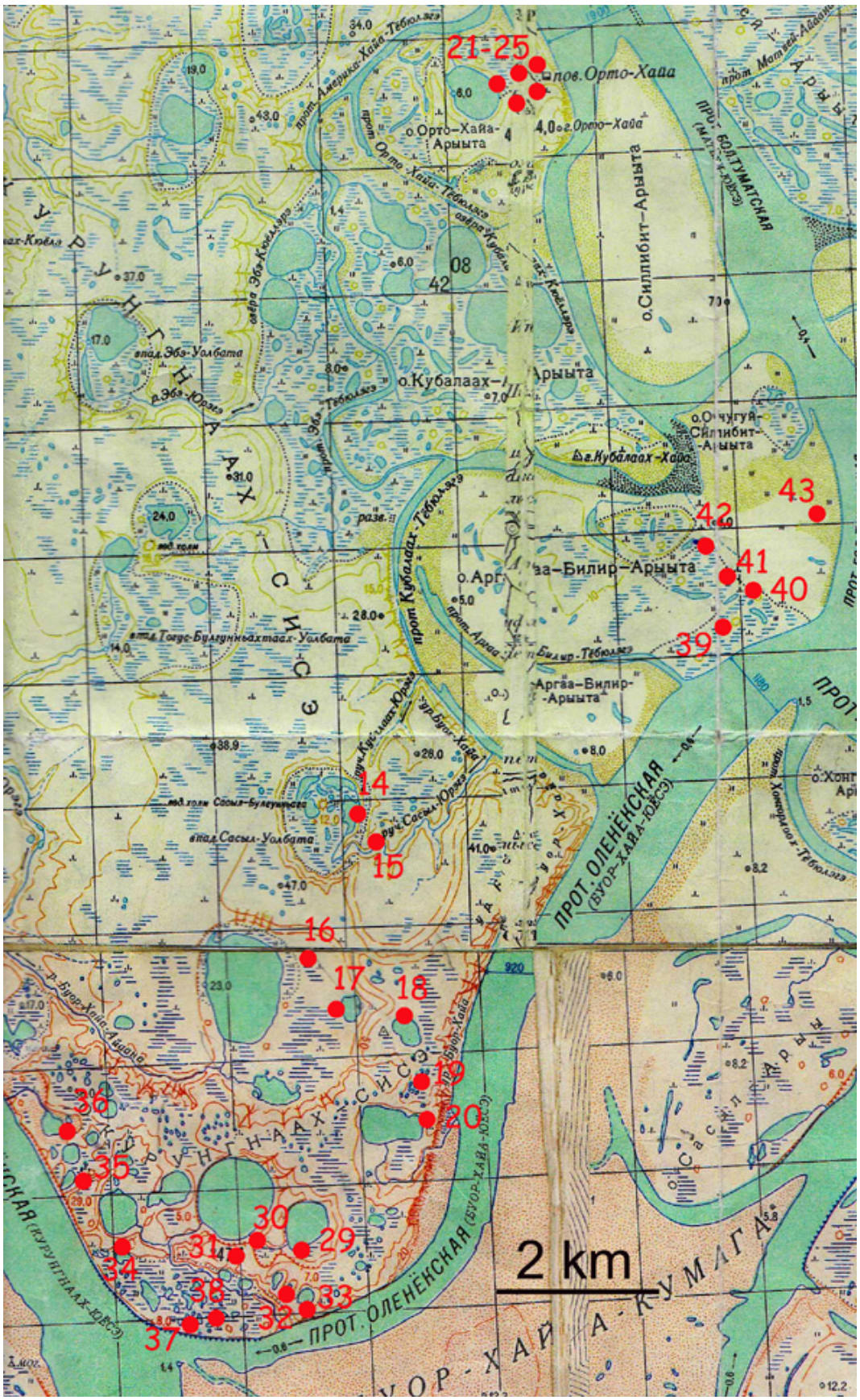

Figure 2.12-2: *Map of the sampling stations locations (red points) in the area close to the Samoylov Island Research Station (August 2017)*

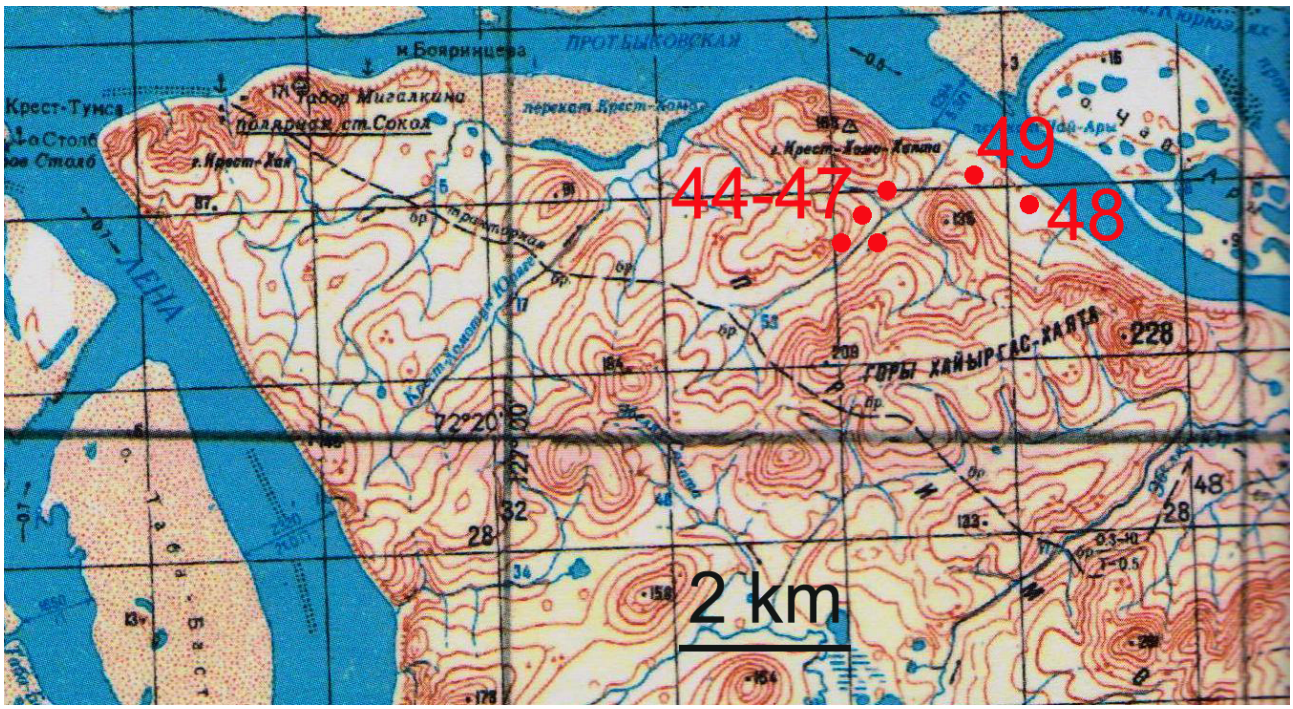

Figure 2.12-3: *Map of the sampling stations locations (red points) close to the Krest-Keydenne River (August 2017)*

Preliminary results

The preliminary species list of Harpacticoida (Copepoda, Crustacea) from the water bodies of Samoylov Island (August 2017) is presented below.

Family Canthocamptidae:

1. *Bryocamptus vejdovskyi* (Mrazek, 1893)
2. *Bryocamptus sp.*
3. *Canthocamptus glacialis* (Lilljeborg, 1902)
4. *Moraria duthiei* (Scott, 1896)
5. *Moraria mrazeki* (Scott, 1903)
6. *Neomrazekiella northumbrica trisetosa* (Chappuis, 1929)
7. *Pesceus schmeili* (Mrazek, 1893)

2.13 Botanical description of the Lena River Delta islands

Olga Bolshiyanova[1]

[1] Arctic and Antarctic Research Institute (AARI), St. Petersburg, Russian Federation

Fieldwork period and location
July 30th to August 28th, 2017 (on Samoylov, Kurungnakh, Amerika Khaya, Arga-Bilir-Aryta, Tit-Ary)

Objectives
Description of tundra vegetation on islands in the Lena River Delta (list of species).

Methods

1. Plant collection
2. Drying in a herbarium press
3. Plant species identification
4. Creation of the herbarium (58 sheets)

Results
During the field season of 2017, plants were collected and identified on Samoylov Island and on the nearby islands Kurungnakh, Amerika Khaya, Arga-Bilir-Aryta, as well as on Tit-Ary (located approx. 50 km south of Samoylov). The collection of samples was conducted in the month of August during the blooming period in the polygonal tundra (Figure 2.13-1). The working method consisted of collecting plants, drying them in a special herbarium press and identification. The most interesting specimen was *Pedicularis sceptrum-carolinum* L. found on Samoylov Island, where it had not been previously reported. It grew on a dry soil hill, which is not typical for this species. The list of species includes the species found on Samoylov Island, and those that were found on the neighboring islands and Tit-Ary Island, but were not noticed on Samoylov Island.
Now, the herbarium is in the collection of the Saint-Petersburg State Forest Technical University.

The species

Samoylov Island

- *Aconogonon ochreatum* (L.) H. Hara
- *Alopecurus sp.* L.
- *Antennaria villifera* Boriss.
- *Armeria maritima* (Mill.) Willd.
- *Astragalus alpinus* L.
- *Betula exilis* Sukaczev
- *Bistorta plumosa* (Small) D. Löve
- *Bistorta vivipara* (L.) Gray

- *Calamagrostis lapponica* (Wahlenb.) Hartman
- *Caltha arctica* R. Br.
- *Campanula rotundifolia* L.
- *Cardamine pratensis* L.
- *Cardaminopsis petraea* (L.) Hiitonen
- *Castilleja caudate* (Pennell) Rebr.
- *Chrysosplenium sibiricum* (Ser. ex DC.) A.P. Khokhr.
- *Delphinium chamissonis* Pritz. ex Walp.
- *Deschampsia borealis* (Trautv.) Roshev.
- *Eleocharis* sp. R.Br.
- *Equisetum arvense* L.
- *Eriophorum scheuchzeri* Hoppe
- *Gastrolychnis taimyrensis* (Tolm.) Czer.
- *Hedysarum arcticum* B. Fedtsch.
- *Orthilia obtusata* (Turcz.) H. Hara
- *Papaver pulvinatum* Tolm. ssp. lenaense Tolm.
- *Parnassia palustris* L.
- *Pedicularis sceptrum-carolinum* L.
- *Polemonium boreale* Adams
- *Polemonium pulcherrimum* Hook.
- *Ranunculus gmelinii* DC.
- *Rumex acetosa* L.
- *Rumex graminifolius* Lamb.
- *Rumex thyrsiflorus* Fingerh.
- *Salix reticulate* L.
- *Sanguisorba officinalis* L.
- *Saussurea tilesii* Ledeb.
- *Saxifraga cernua* L.
- *Saxifraga hirculus* L.
- *Saxifraga nelsoniana* D. Don
- *Saxifraga spinulosa* Adams
- *Silene stenophylla* Ledeb.

- *Stellaria ciliatosepala* Trautv.
- *Tofieldia coccinea* Richards.
- *Valeriana capitate* Pall. ex Link

Kurungnakh Island

- *Artemisia tilesii* Ledeb.
- *Descurainia sophioides* (Fisch. ex Hook.) O.E. Schulz
- *Dryas punctate* Juz.
- *Lagotis minor* (Willd.) Standl.
- *Ledum palustre* L.
- *Minuartia arctica* (Steven ex Ser.) Graebn.
- *Tanacetum bipinnatum* (L.) Sch. Bip.

Tit-Ary Island

- *Cassiope tetragona* (L.) D.Don
- *Empetrum nigrum* L.
- *Parrya nudicaulis* (L.) Regel
- *Petasites frigidus* (L.) Fr.
- *Rubus chamaemorus* L.
- *Vaccinium vitis-idaea* L. ssp. minus (Lodd.) Hultén

Arga-Bilir-Aryta Island

- *Tephroseris palustris* (L.) Rchb.

Amerika Khaya Island

- *Rhodiola rosea* L.

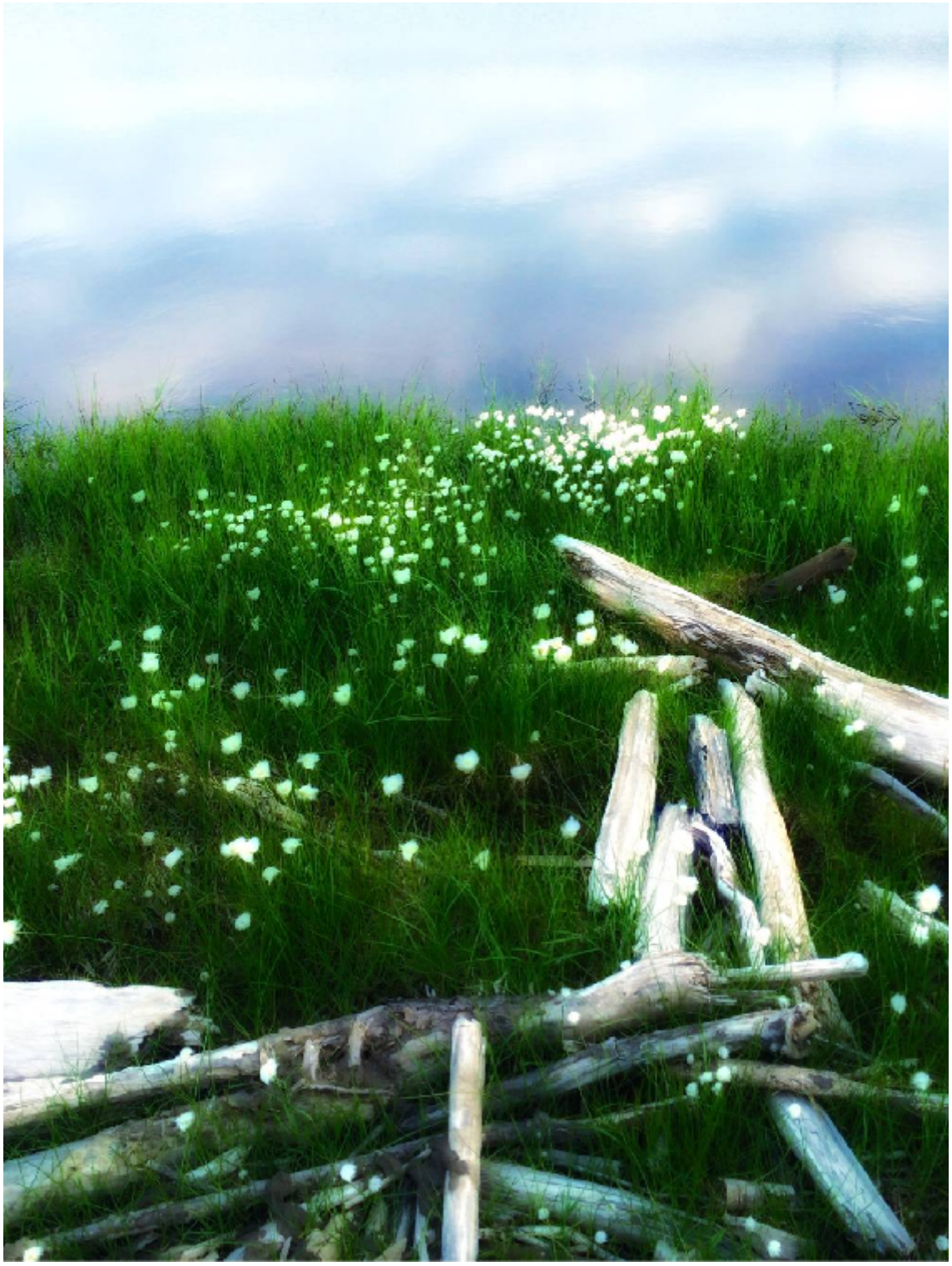

Figure 2.13-1: *Eriophorum scheuchzeri Hoppe (Samoylov Island, bank of the Lena River)*

2.14 Carbon emissions and terrestrial carbon transport

Philipp Wischhoefer[1], Anja Wotte[1], (Janet Rethemeyer[1]: not in the field)

[1] Institute of Geology and Mineralogy, University of Cologne, Cologne, Germany

Fieldwork period and location
July 30th to September 01st, 2017 (on Samoylov and Kurungnakh Island)

Objectives
Increasing thaw in arctic permafrost regions leads to the exposure of previously frozen organic matter to microbial degradation. The subsequent release of the greenhouse gases CO_2 and CH_4 further enhances warming and thawing, causing the so-called permafrost carbon feedback (Schuur et al., 2015). However, dimension and timing of this process are still debated. In the Lena Delta, we therefore investigate a) carbon fluxes from the active layer on Samoylov Island and from ice complex deposits on Kurungnakh Island to the atmosphere, b) their corresponding radiocarbon concentration, and c) the quality of the organic matter, which serves as a substrate for microbial organisms. The radiocarbon content of the respired CO_2 and the organic substrate will help us to identify different carbon sources. This procedure may reveal, which portion of the stored organic carbon is prone to microbial breakdown. At the polygons on Samoylov Island, we sampled respired CO_2 at the surface and at the permafrost table, in order to investigate the change of carbon sources over depth. Furthermore, pore water was sampled for a long-term analysis of dissolved and particulate organic carbon (DOC/POC). On Kurungnakh Island, we extended our investigation of the degradation of freshly eroded “old” (Pleistocene) organic matter in the ice complex deposits (Wotte and Rethemeyer, 2017) and the influence of mixing with younger (Holocene) organic material from the upper terrace.

Fieldwork summary
Water samples of about 600 ml for the analysis of DOC and POC were collected from the base of the active layer at five polygonal sites established in previous years (Table 2.14.1). At the rims, a soil pit was dug down to the permafrost table and pore water was extracted via rhizon samplers (Rhizosphere Research Products, The Netherlands) with 200 ml syringes. From polygon centers, water was extracted via perforated steel tubes and subsequently filtered in the laboratory of Samoylov Research Station to separate POC.
We sampled respired CO_2 on molecular sieve cartridges (Wotte et al., 2017a) at two polygons on Samoylov (actively and passively) and at five sites at the Kurungnakh ice complex deposits and the adjacent terrace (actively), according to the methods described in Wotte et al. (2017b). Passive depth samplers were deployed at Tim’s Polygon and Fish Lake Polygon (see Table 2.14.1 for coordinates) for about 20 days.
For measuring CO_2 fluxes, we used a LICOR 840A (Li-COR Inc., USA) infrared gas analyzer. Single measurements were conducted for less than five minutes in order to not alter the flux by the closed respiration chamber. On Samoylov Island, we collected CO_2 from vegetated and non-vegetated locations to compare flux and radiocarbon concentration of autotrophic and heterotrophic respiration. At the non-vegetated locations, the vegetation was clipped at least one year ago. On Kurungnakh Island, CO_2 (flux) was measured and sampled exclusively at non-vegetated spots. At each sampling location, active layer depth and soil temperatures (up to 45 cm) were measured on the day of CO_2 sampling. Sediment samples were collected from profiles, which were dug down to the permafrost table. If no soil horizons could be distinguished, samples were collected in intervals of 10 cm. Bulk

densities were estimated with soil sample rings. pH values of wet and dry sediments were measured in the station's laboratory with a WTW Multi 340i pH meter (Zeller GmbH, Germany).

Table 2.14.1: Overview of sampling locations and the samples collected during the field campaign in 2017. Coordinates in decimal degrees

Site ID	Name	N [Deg]	E [Deg]	Sample material
Samoylov Island				
FLP	Fish Lake Polygon	72.37278	126.48512	soil DOC. soil POC.
				soil gas. sediment
FLP2	Fish Lake Polygon 2	72.3722	126.4892	soil DOC. soil POC
TiP	Tim's Polygon	72.37407	126.49731	soil DOC. soil POC.
				soil gas. sediment
Kurungnakh Island				
KUP	Kurungnakh Polygon	72.32343	126.22298	soil DOC. soil POC
KUP2	Kurungnakh Polygon 2	72.3252	126.26561	soil DOC. soil POC
KT	Kurungnakh Terrace	72.33914	126.28945	soil gas. sediment
K4	Ice complex. mixed	72.339	126.29207	soil gas. sediment
K14	Ice complex. mixed	72.33939	126.29261	soil gas. sediment
K7	Ice complex. Baidzerakh	72.33923	126.2929	sediment
KX	Ice complex. Baidzerakh	72.3392	126.29199	soil gas. sediment
K15	Ice complex. Baidzerakh	72.33935	126.29201	soil gas. sediment

2.15 Carbon emissions in field-based incubation experiment with buried organic matter on Samoylov Island

Svetlana Evgrafova[1]

[1] V.N. Sukachev Institute of Forest FIC, Siberian Branch, Russian Academy of Sciences, Krasnoyarsk, Russian Federation

Fieldwork period and location
July 30th to September 01st, 2017 (on Samoylov Island)

Objectives
Permafrost thawing may provoke a positive feedback to climate warming by causing increased greenhouse gas emissions. When permafrost soils thaw, ancient organic carbon is made accessible to microbial respiration emitting greenhouse gases (GHG), such as CO_2 and CH_4 (Tarnocai et al., 2009). For example, a positive feedback of methanogenic communities to warmer periods in the Late Pleistocene and Holocene was shown for the Lena River Delta (Bischoff et al., 2013). Current estimates on the degradability of thawing organic matter in permafrost are based on incubation studies, which are highly artificial and probably overestimate the greenhouse gas (GHG) production under *in situ* conditions.
The aim of this study was to identify the microbial response and associated release of CO_2 and CH_4 in/from thawing soil that has previously been permanently frozen. For this purpose, we moved formerly frozen soil to the active layer. This material was either placed partly in the subsoil in order to mimic cryoturbation processes, or was exposed to the soil surface to simulate eroding river banks.

Fieldwork summary
A field-based incubation experiment with buried soil organic matter begun in August, 2015. Frozen buried soil were taken from Holocene permafrost, that has been exposed by river bank erosion of the Lena river. The material was transferred on top of the active layer and partly dug into the subsoil in a rim of an ice-wedge polygon. The principle includes that formerly frozen soil was moved to the active layer, but still residing in the subsoil to mimic cryoturbation processes or exposed to the soil surface to simulate eroded river bank. Plots with buried soil covered by living ground cover of 5 cm thickness has been installed in August, 2015; plots with uncovered buried soil has been installed in August, 2016 on a rim of ice-wedge polygon of Samoylov Island (N 72.37029°, E 126.48223°). The experimental design is described in Figure 2.15-1.
During August 2017, soil respiration (CO_2 and CH_4 fluxes) was measured by a closed chamber technique. Samples of bulk soil as well as formerly buried soil samples were taken to characterize chemical and microbiological properties. Additional gas samples were taken for the measurement of $\delta^{13}C$ in the laboratory at the Institute of Forest, Krasnoyarsk, Russia.
Soil temperature was measured daily at noon using a Campbell data logger (Campbell Scientific, Ltd., USA) that was permanently installed with 5 sensors in different soil depth. Air temperature during gas sampling was recorded by the weather station at Samoylov research station. The active layer thickness was measured manually using a metal probe (Figure 2.15-2).
CO_2 and CH_4 released from the soil was measured by the closed-chamber technique and quantified according to Lal (2016). In the field-based incubation experiment, emission of both GHG (Figure 2.15-3) was much higher in plots with the buried soil covered, as compared to plots with the buried soil exposed. The release of gases from covered plots was mainly responding to soil temperature of the upper layer (0 - 5 cm). Plots, where the buried soil material was placed on the soil surface showed a weak flux of CO_2, despite the fact that the organic matter was in a sufficiently moist state

during the whole measurement period. The one-year cumulative methane efflux from plots with formerly buried soil covered by groundcover was significantly larger than in disturbance control plots.

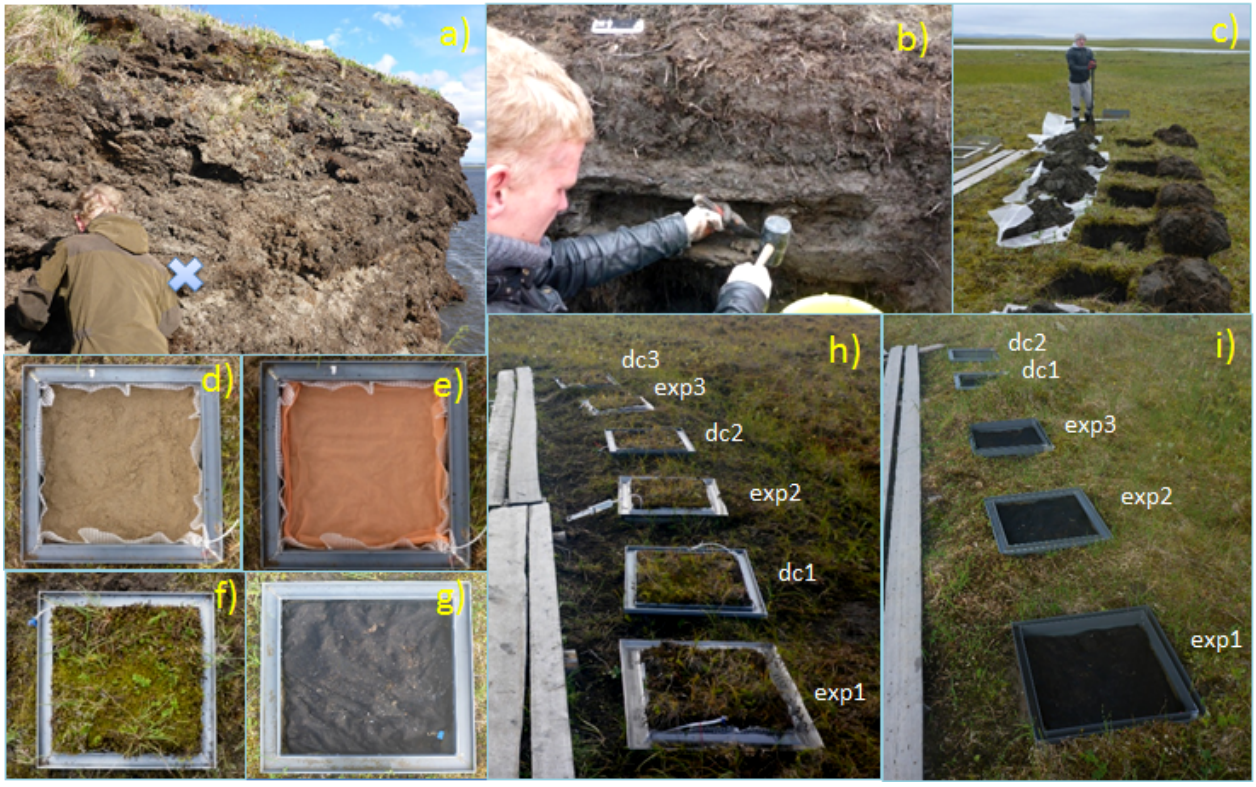

Figure 2.15-1: *Field-based incubation experiment: a) Lena river bank of Samoylov island, x - sampling place; b) sampling of frozen (buried) soil c) experimental site preparation (holes dug up to permafrost table); d) every plot were filled in with carbon-free sand; e) approx. 3.5 - 4.5 kg of buried soil were placed in polyester bags and put on top of sand; f) bags with buried soil covered by groundcover (5 cm thickness) - cryoturbation mimicking experiment; g) bags with buried soil exposing uncovered - eroded river bank simulation experiment; h) artificial cryoturbation experiment, exp1-3: plots with bags filled with buried soil, dc1-3: plots with bags without buried soil, i.e. disturbance control; i) eroded river bank simulation experiment, exp1-3: plots with bags filled with buried soil, dc1-2: plots with bags without buried soil (disturbance control)*

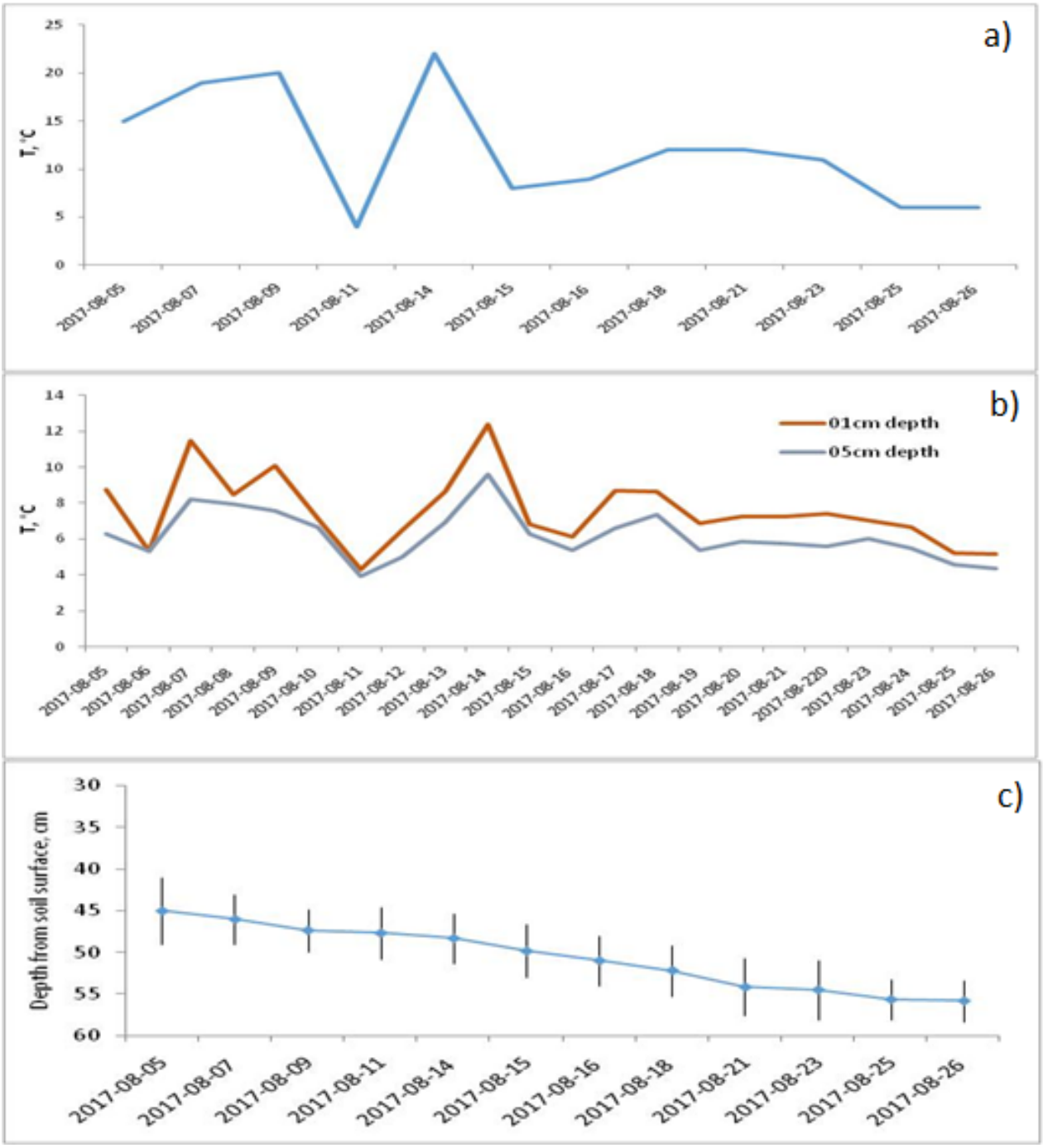

Figure 2.15-2: *Air temperature over the sampling period (a); upper layer soil temperature recorded daily at 12:00 (b); and active layer profile of ice-wedge polygon rim where the field-based experiment was installed (c)*

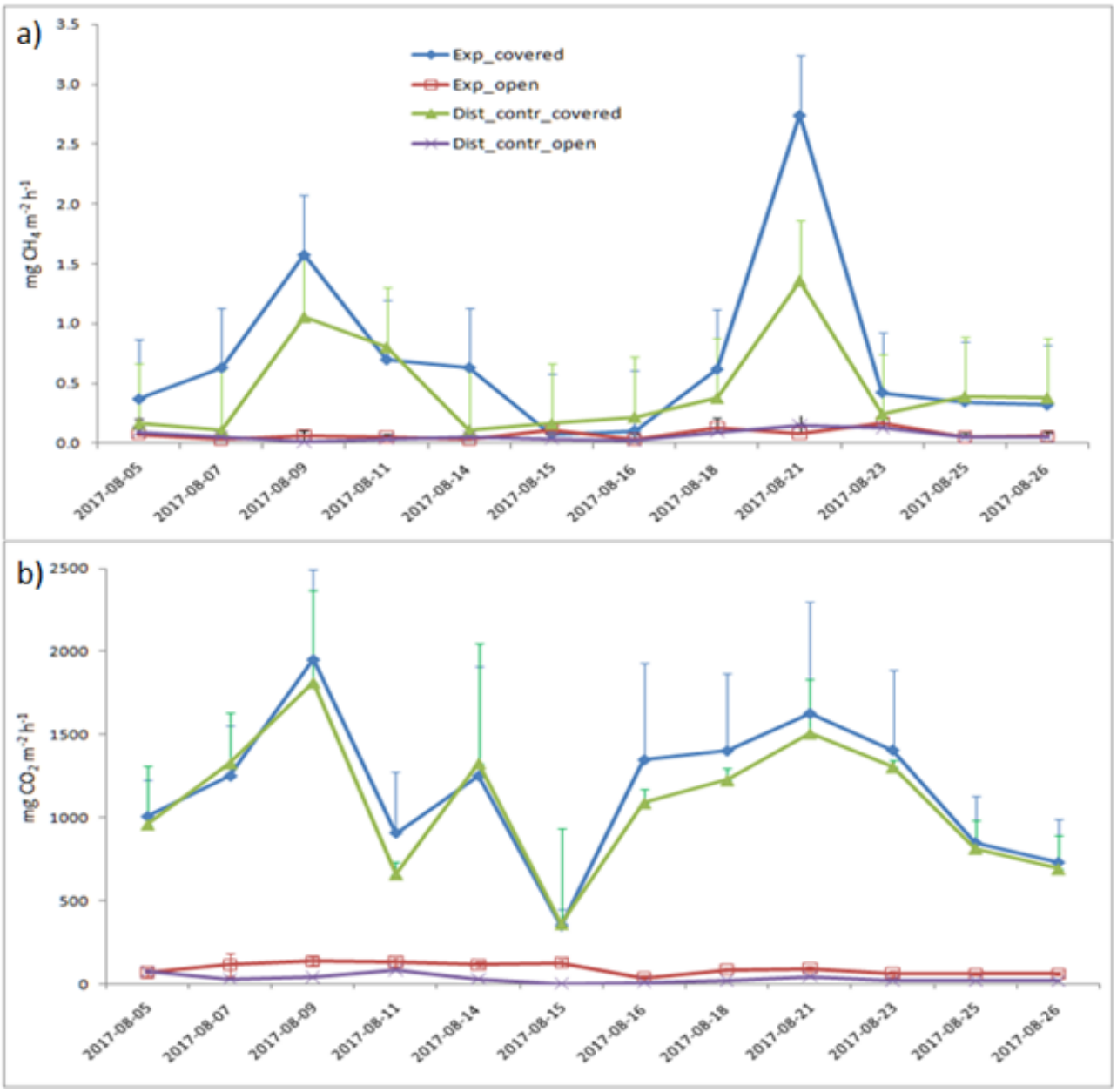

Figure 2.15-3: *Release of CH_4 (a) and CO_2 (b) over time from soil in a field-based experiment. Legend: Exp_covered: mean value between plots with buried soil covered by groundcover (5 cm thickness); Exp_open: mean value between plots with uncovered buried soil; Dist_ contr_covered: mean value between plots without buried soil covered by groundcover (5 cm thickness); Dist_ contr_ open: uncovered plots without buried soil. Bars indicate standard deviations (n=3).*

2.16 Methane distribution and oxidation in ice cores

Ingeborg Bussmann[1], Kirstin Hoffmann[2], (Ellen Damm[3]: not in the field)

[1] Alfred Wegener Institute Helmholtz Center for Polar and Marine Research, Helgoland, Germany

[2] Alfred Wegener Institute Helmholtz Center for Polar and Marine Research, Potsdam, Germany

[3] Alfred Wegener Institute Helmholtz Center for Polar and Marine Research, Bremerhaven, Germany

Fieldwork period
April 14th to April 26th, 2017 (on Samoylov Island)

Objectives
In lakes and coastal seas, the ice formation and the ice cover offer opportunities for the combined use of field studies, remote sensing and modeling, with the goal of identifying methane sources and assessing the relative importance of sea ice as a methane reservoir or buffer and as a habitat for methane-relevant microbial communities. Additionally, the uptake of terrestrial or sedimentary microbial communities into fast ice is an important object of investigation that links the terrestrial/permafrost and marine environments.
Until now, most of our knowledge on the methane cycle in the study area has been obtained in summer. However, as most of the year the study area is ice covered, it is important to assess the methane related process also in the dominant ice-covered season.
During the coring at the Bykovsky Spring expedition, we obtained in total 30 ice cores. The cores delegated for methane analysis were transported from Tiksi to the station. Here they were processed for later analyses. In addition, water samples from the Lena River and some ponds were also analyzed for our methane related research.
We also took snow samples above some ponds to evaluate the input of melting snow on the water chemistry of the ponds below.

Methods
For determining the methane oxidation rates and later methane concentrations and isotopic values, the ice cores were processed at the Samoylov Research Station.
The top 10 cm, a 10 cm mid-section and three 10 cm-sections at the bottom of the core were cut off and transferred to special PVDF gas sampling bags (Keikaventures). The remaining parts of the cores were returned to the thermo boxes. The bags were evacuated and the cores melted within approx. 5 h in a water bath at 8 °C.
Samples for later gas analysis were obtained in three different ways: i) gas of the headspace was taken directly via syringe and transferred into glass bottles filled with saturated NaCl solution; ii) with another syringe 40 ml of water were taken, 20 ml of nitrogen gas added and after vigorously shaking for 2 min the gas phase was transferred into glass bottles filled with saturated NaCl solution. A third glass bottle was completely filled with the sample water and poisoned with 0.3 ml of 25 % H_2SO_4. Gas analysis will be performed later in the home laboratories.
For each depth one subsample (40 ml) was taken for later stable water isotope analysis (δ18O and δD) of the water phase.
To determine the methane oxidation rate, the remaining water was transferred via syringe into further glass bottles, which were closed without headspace. Tritiated methane was added and the samples incubated for 60 h at 1 °C. After stopping the incubation by adding H_2SO_4, the total radioactivity

of the sample and after sparging the radioactivity of only the water was determined. All samples, discarded water and waste are transferred back to the home laboratory.
Additional water samples from below the ice at different locations of the Lena River and samples from ponds on Samoylov Island were also investigated (see Table 2.5.-1). For details of the ice cores see also report Bykovsky Peninsula 2017. The river samples were taken by Irina Fedorova.

Table 2.16.1: Additional sampling

Name	Date	Position	Water depth	Sampling for
Irina I	18.04.2017	N72.37478/ E 126.752	1m/17 m	Methane concentration/Oxidation
Irina II	20.04.2017	N72.37341/ E 126.7458	surface/bottom	Methane concentration/Oxidation
Irina III	22.04.2017	N72.41325/ E126.8672	surface/bottom	Methane concentration/Oxidation
Katja's Pond(II)	20.04.2017		Ice core	Methane concentration/Oxidation
Katja's Pond(II)	16.04.2017		water	Methane concentration/Oxidation
Katja's Pond(II)	23.04.2017		snow	Water Chemistry
Julia's Pond(I)	23.04.2017		snow	Water Chemistry

Preliminary results
The sampling for later gas analysis revealed that the cores contained different amounts of gas (released as gas phase in the sampling bag). We hope to relate the amount of gas to the visual structure of the ice cores.
The fractional turnover rate k' was calculated from the preliminary data, for the final calculation of the methane oxidation rate the methane concentration is necessary, but not yet available. K' is the first-order rate constant calculated as the fraction of $^{3}H\text{-}CH_4$ oxidized per unit time, it can also be seen as an indication of the relative activity. The fractional turnover rates were rather low, and many samples were below the detection limit. For Goltsovoye Lake and the Tiksi Bay, about 88 % and 66 % were below the detection limit respectively (total n = 40, n = 41). For the samples above the detection limit, no spatial trend was obvious i.e. higher activity at top or bottom of the ice cores; also, no difference between the lake and the Bay was obvious. In all samples from the river water, we could detect an activity, within the same range as in the ice samples. Highest activity was recorded in the water of a small pond on Samoylov Island, about 10 times higher as in the other samples (Figure 2.16-1).

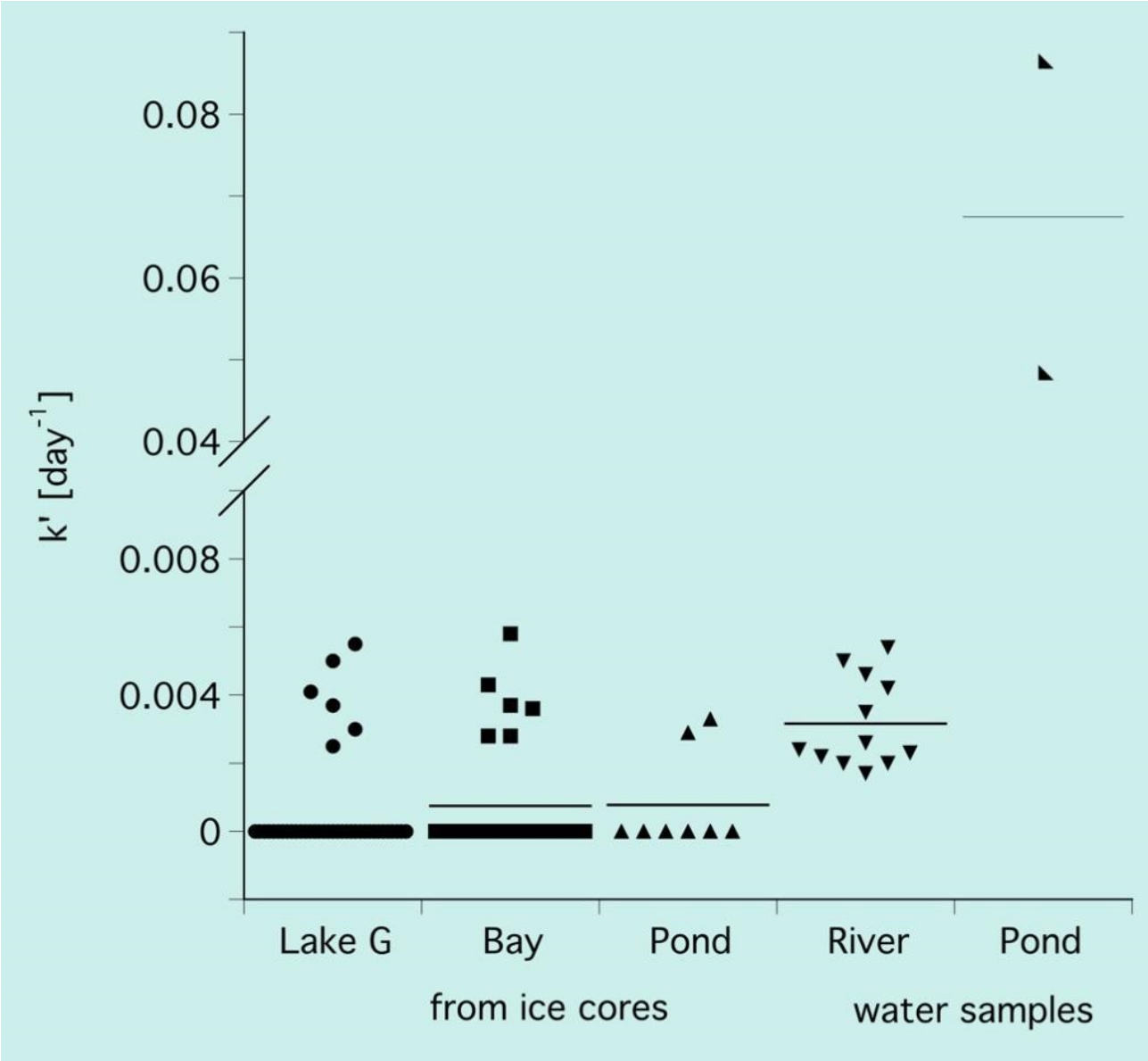

Figure 2.16-1: *Fractional turnover time of methane from ice cores from Goltsovoye Lake, Tiksi Bay, Lena River and a pond on Samoylov Island*

2.17 Geophysical investigations of hydrogenic taliks in the Lena River Delta

Nikita Bobrov[1], Alexey Titov[1]

[1] Saint-Petersburg State University, St. Petersburg, Russian Federation

Fieldwork period and location
July 6th to July 14th, 2017 (on Samoylov Island)

Objectives
Geophysics provides an effective tool to penetrate underground without violation of environment. The objective of the summer campaign in 2017 was to extend the 2016 geophysical works aimed at: i) evaluation of the thickness of sub-river talik under Bolshaya Tumatskaya Channel of the Lena Delta, and ii) determination of the talik thickness under thermokarst lakes at the Samoylov Island. The main instrument used in the spring of 2016 was ground-penetrating radar (GPR). It proved to be inefficient for the study of sub-river talik; in addition, results obtained at the lakes were uncertain (these works were carried out from the ice cover). This summer, another geophysical method - electrical resistivity tomography (ERT) - was applied that allowed to successfully solve the stated tasks.

Methods
ERT is the present-day modification of classical resistivity method, which is based on emitting an electric current in the Earth and measuring the resulting voltage, which depends on the medium's electrical properties. By varying the distance between current and potential electrodes (spacing) we can adjust the depth of investigation, thus performing electrical resistivity sounding. Multi-electrode cables and multi-channel equipment are used for conducting ERT. Each electrode can be used to inject current or measure potential one, electrodes commutation is realized automatically via programmed protocol. As a result of a measurement cycle, a two-dimensional (2D) geoelectrical section is obtained - which means the distribution of conductivity (or inverse value - resistivity) along the profile and in depth. The depth of investigations depends on spacing and can reach several tens of meters when standard cables and power batteries are applied. If a network of parallel profiles is available, one can obtain three-dimensional (3D) image of the medium. The precondition for talik detection and determination of its shape and size with the use of ERT is substantial conductivity difference between thawed and frozen sediments. Besides temperature, the conductivity depends on lithological composition of sediments and porous water mineralization. The application of ERT can give us representation of section structure and the state of frozen materials at a depth inaccessible for drilling with portable facilities.
ERT measurements were carried out with Syscal Pro 48 instrument. Two modes of measurements were used. In studies at lakes, the instrument was placed in the anchored rubber boat at the center of the lake and cables (two, each of 120 m length) were kept at the water surface with the help of equally spaced floats, provided the far ends of cables grounded at the land (Figure 2.17-1a)). Electrodes spacing was equal to 5 meters. In studies at the river, multi(10)-channel measurements in motion were conducted - continuous resistivity profiling (CRP). One towed cable of 240 m long with electrodes spacing equal to 10 meters was used. The equipment was placed in the motorboat, with the help of which the cable was towed (Figure 2.17-1b). At the profile, 3 CRP results were accompanied by on-land ERT sounding at the bank of Samoylov Island.

In the Figure 2.17-2, the locations of geophysical profiles are presented. Additional GPR survey from the water surface allowed us to determine the bottom relief of the lakes along ERT measurements lines (profiles M, B).

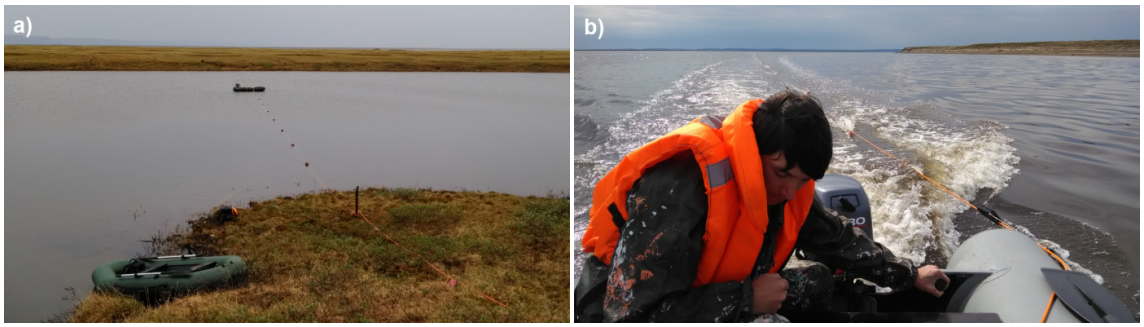

Figure 2.17-1: *ERT survey from the surface of lake (a) and CRP at the river (b)*

Figure 2.17-2: *Location of geophysical profiles (red lines) at the Samoylov Island (M, B) and in the Bolshaya Tumatskaya Channel (1-5)*

Preliminary results

ERT survey has revealed the talik related zones of low resistivity below two lakes at the Samoylov Island and allowed to delineate their shape (Figure 2.17-3). The thickness of these taliks is comparable with the depth of the lakes and is about 10 meters. One should note that thawed sediments below the bottom occured everywhere and turned out to be more conductive than fresh water of the lakes (special thanks to Katya Abramova who has made conductivity measurements at water samples).

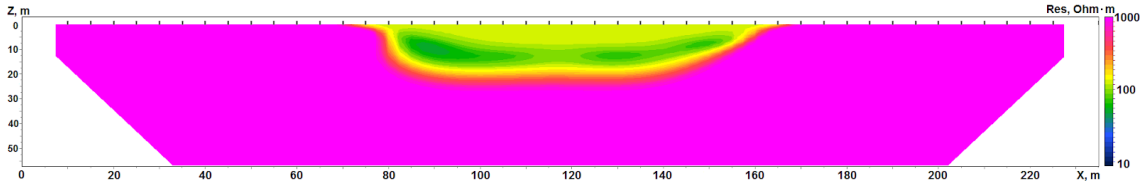

Figure 2.17-3: *Resistivity section obtained as a result of ERT data inversion (Schlumberger array) for the profile B (Bannoye 2 Lake). Horizontal scale – distance along profile, m. Vertical scale – depth, m. Resistivity values (color scale in the right): magenta – more than 1000 Ohm*m (permafrost), green – 50-100 Ohm*m (talik), yellow-green – 120 Ohm*m (water). Depth of water was not recovered but fixed in according with the results of GPR profiling. Water resistivity was fixed in according with direct laboratory measurements.*

CRP in the Bolshaya Tumatskaya Channel has found considerable growth of resistivity values at the depth of 40 - 50 m below the bottom of the river (Figure 2.17-4 and Figure 2.17-5). This confirms the assumption, made in 2016 based on the results of TEM soundings, that permafrost is present under the channels of Lena Delta. The thickness of underbed talik is tens of meters almost everywhere, possibly with the exception of narrow (40 - 60 meters width) apparently thawed deep zones adjacent to permanent frozen sediments under the Samoylov Island (left side of the figures). The nature of these zones is a subject for future investigations.
Obtained estimates of the talik thickness are of great importance for building permafrost energy balance models.

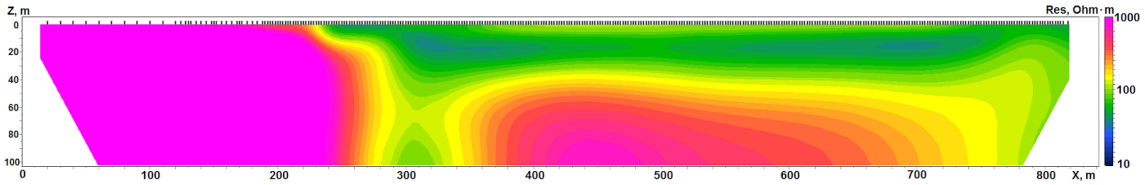

Figure 2.17-4: *Resistivity section obtained as a result of river CRP data inversion (dipole-dipole array), combined with the results of land ERT data inversion (Schlumberger array) for the profile 3. Horizontal scale - distance along profile, m. Vertical scale - depth, m. The color scale of resistivity values is the same as in the Figure 2.17-3.*

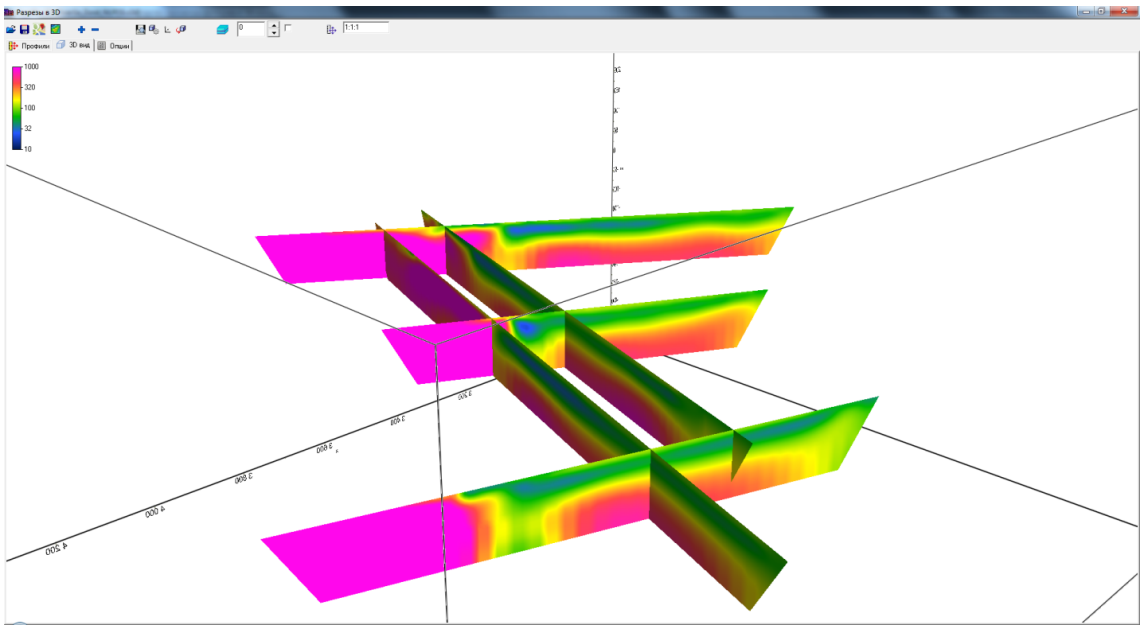

Figure 2.17-5: *Pseudo 3D picture of resistivity under Bolshaya Tumatskaya Channel obtained as a result of CRP data inversion (dipole-dipole array) for the profiles 1-5, combined with the results of land ERT data inversion (Schlumberger array) for the profile 3. View from the north-east to the south-west (Samoylov Island in the left). The color scale of resistivity values is the same as in Figure 2.17-3.*

2.18 Meteorological and permafrost research on Samoylov Island: impact of the soil type on permafrost dynamics and surface to atmosphere energy fluxes as well as characterization of arctic summer precipitation

Maxime Aboukrat[1], Vincent De Staercke[1], Laura Mathieu[1], Léa Pascal[1], Mathieu Schaer[1], Dimitri Zogg[1], Christophe Praz[1], Ksenia Tatarchenko[1]

[1] École Polytechnique Fédérale de Lausanne - Geneva Global, Lausanne, Switzerland

Fieldwork period and location
July 16th to August 14th, 2017 (on Samoylov Island)

Objectives
As a group of students, the main objective of our stay at the Samoylov Research Station has been to get an overall perspective of climate change impacts in an Arctic environment. This was made possible by several pedagogical research activities conducted on Samoylov Island.
The project consisted of several parts: the first part was to collect high quality measurements of atmospheric and ground variables. In a second step, we used these variables together with long time series measurements collected by the AWI Institute (e.g. Boike et al., 2013), to make permafrost simulations based on surface energy balance calculations using the scientific software SNOWPACK (e.g. Bartelt and Lehning, 2002; Gouttevin et al., 2018). Measurements were collected at different locations on the island in order to assess the effect of soil type on permafrost dynamics (polygonal tundra, flood plain, sandy beach).
CO_2 emissions measurements have also been performed in order to evaluate the spatial and temporal variability of greenhouse gases release from different soil types at the scale of the island.

Fieldwork summary and Preliminary results
Three meteorological stations have been used to measure air, surface and subsurface temperature, relative humidity, wind speed and direction, incoming shortwave radiation, and precipitation with a tipping bucket. The stations have been installed in the polygonal tundra (E 126.4807°, N 72.3702°), the floodplain (E 126.4733°, N 72.3716°) and the sandy beach (E 126.4638°, N 72.3718°). The comparison of the results obtained from each station will allow to study the effect of soil type and structure on the energy exchanges between the surface and the atmosphere. Figure 2.18-1 presents a time series of the surface energy balance retrieved from the station installed in the polygonal tundra.
The disdrometer PARSIVEL is a one-dimensional optical disdrometer that can detect the size and velocity of particles between 0.3 and 30 mm. A major advantage of this sensor lies in the direct measurement of the raindrop size distribution (DSD) which is essential to study precipitation processes. The DSD represents the number of falling rain drops per cubic meter of air, for each equivolume diameter class. It can be used to quantify the microstructure of rainfall and all bulk rainfall variables of interest can be derived as weighted moments of the DSD (Raupach and Berne, 2015). The main objectives were to characterize and describe summer rainfall on Samoylov Island, study small scale spatial variability as well as temporal variability of rain characteristics and compare and assess accuracy of measurements from collocated tipping buckets. Two PARSIVEL disdrometers operated for 18 days, one in the polygonal tundra (E 126.4800°, N 72.3704°) and the other one in the floodplain (E 126.4741°, N 72.3713°). Figure 2.18-2 presents a time series of the rain intensity along our stay on Samoylov Island.
A third part of the project consisted in studying CO_2 emissions at the surface. For this purpose, CO_2 concentrations have been measured using a cube size closed chamber made of transparent Plexiglas with a side length of 50 cm. The Hutchinson and Mosier Method (HMR) is used to calculate

the flux of CO_2 emissions with non-linear fitting. Measurements have been done in polygonal ponds (center and rim) (E 126.4886°, N 72.3722°) and over peat (E 126.4767°, N 72.3679°) along with soil temperature measurements in order to assess their influence on CO_2 emissions. Incoming shortwave radiation is also studied to see its correlation with CO_2 emissions. Both measurements with and without coverage of the chamber have been done to evaluate the influence of the photosynthesis on carbon fluxes. Figure 2.18-3 shows the temporal and spatial variability of CO_2 emissions over 24 hours in a polygonal pond with the chamber exposed to sunlight.

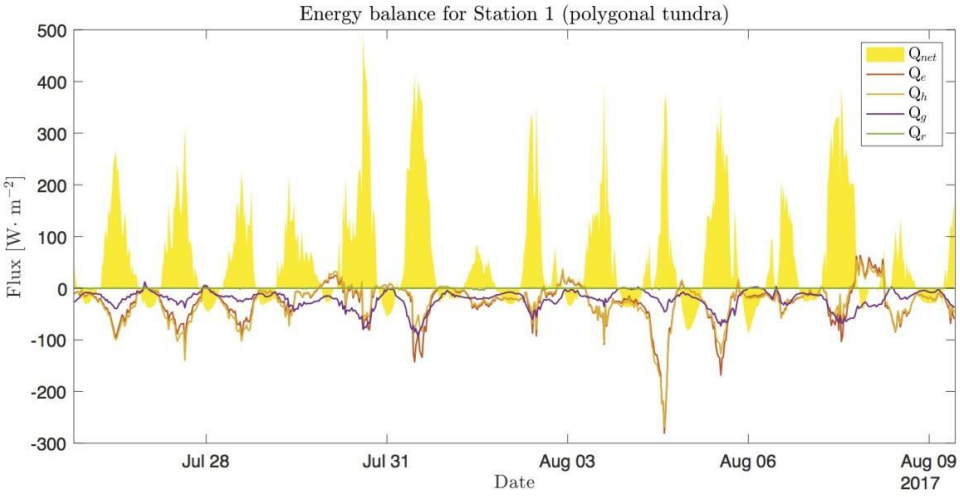

Figure 2.18-1: *Energy balance for station 1 (polygonal tundra)*

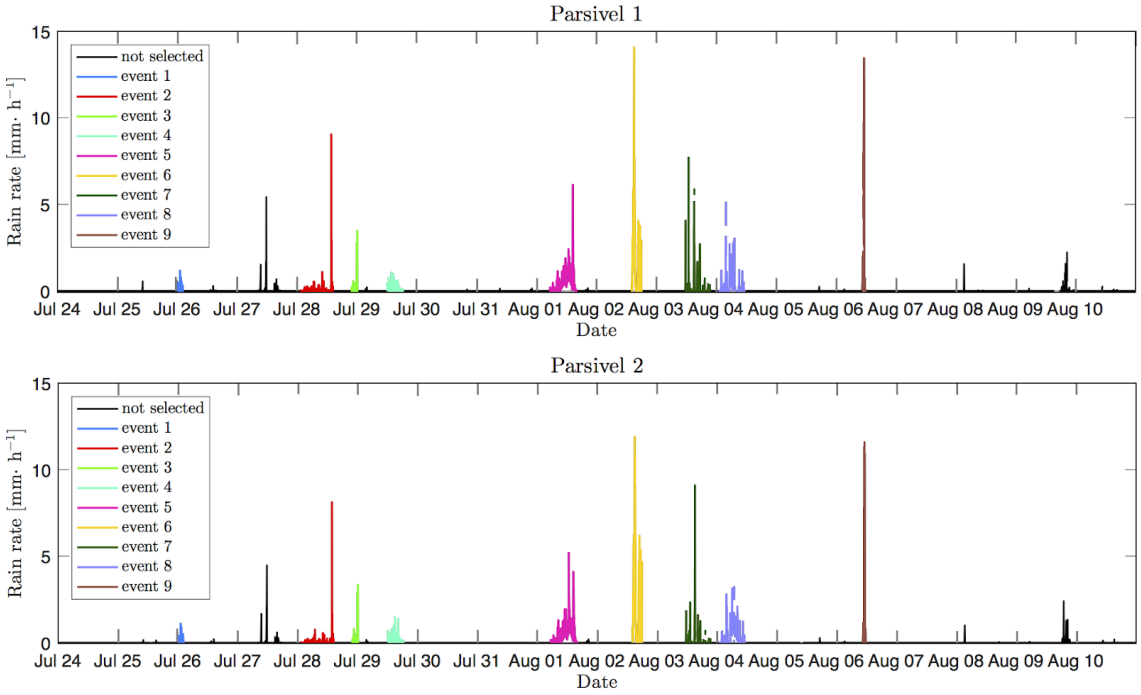

Figure 2.18-2: *Rain rates (Parsivel 1: polygonal tundra - Parsivel 2: floodplain)*

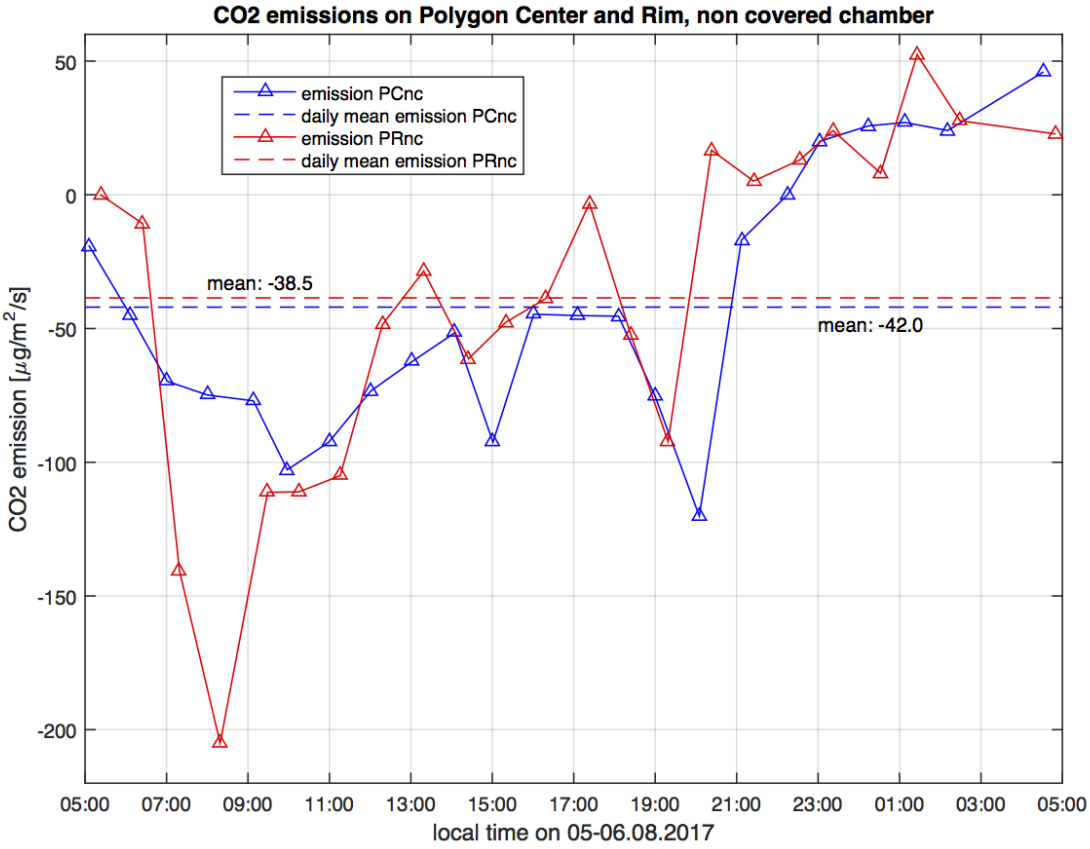

Figure 2.18-3: *24-h measurements of CO_2 emissions over a polygon pond (center and rim)*

Table 2.18.1: Coordinates of the measuring positions

Instrument	Latitude	Longitude
Parsivel 1 - polygonal tundra	72.3704°	126.4800°
Parsivel 2 - floodplain	72.3713°	126.4741°
Weather station 1 - polygonal tundra	72.3702°	126.4807°
Weather station 2 - floodplain	72.3716°	126.4733°
Weather station 3 - sandy beach	72.3718°	126.4638°
CO_2 chamber - polygonal tundra	72.3722°	126.4886°
CO_2 chamber - peat	72.3679°	126.4767°

2.19 Multidisciplinary research of cryolithic zone evolution: selected features of permafrost environment in Lena Delta case study

Leonid Tsibizov[1,2], Aleksey Fage[1,2], Vladimir Olenchenko[1,2], Alina Grigorevskaya[1,2], Konstantin Sosnovtsev[1,2], Egor Esin[1,2], Polina Nikitich[2,3], Andrey Kartozia[2,4], Nikolay Lashchinskiy[2,5], (Vladimir Kashirtsev[1,2], Igor Yeltsov[1,2]: not in the field)

[1] Trofimuk Institute of Petroleum Geology and Geophysics of Siberian Branch, Russian Academy of Sciences (SB RAS), Russian Federation

[2] Novosibirsk State University, Russian Federation

[3] Institute of Soil Science and Agrochemistry of Siberian Branch, Russian Academy of Sciences (SB RAS), Russian Federation

[4] V.S. Sobolev Institute of Geology and Mineralogy of Siberian Branch, Russian Academy of Sciences (SB RAS), Russian Federation

[5] Central Siberian Botanical Garden of Siberian Branch, Russian Academy of Sciences (SB RAS), Russian Federation

Fieldwork period and location
July 5th to August 23rd, 2017 (on Samoylov Island, Kurungnakh Island, Bykovsky Peninsula)

Objectives
The main goal of our research in the Lena River Delta is to construct an integrated picture of cryolithic zone evolution. We develop a multidisciplinary approach to permafrost studies and pay attention to correlation of data from various methods. With this objective, we studied typical objects in the region using a variety of geophysical, geological, geobotanical, and soil methods as well as remote sensing. During the expedition, several aspects were studied on Samoylov and Kurungnakh Islands.

Methods

1. Electrical resistivity tomography (ERT): SibER-48 (http://nemfis.ru) (Figure 2.19-1) at 5 and 10 m step (45 and 90 meters penetration depth respectively).
   Schlumberger and dipole-axis installations were used for taking measurements. The distance between the electrodes was 5 or 10 meters, that chosen based on the expected depth of the anomaly.

2. Ground penetrating radar (GPR): OKO-2 (Figure 2.19-1) with 150 and 700 MHz antennas

3. Magnetic survey: proton magnetometer MMPOS-2 (Figure 2.19-1) and magnetic base station GEM-19T

4. Geological observations in outcrops

5. Soil studies: soil pits were dug to the bottom of the active layer using shovel, afterwards a permafrost core was extracted using a metal tube and sledgehammer. Active layer was sampled according to its genetic soil horizons. Permafrost cores were taken in subsamples of 10 cm to the depth of 100 cm. The meso- and micro-relief, plant community and soils morphology were described visually at every soil sampling location.

Sample analyses:

- measurements in the field: frozen sample volume and weight
- magnetic susceptibility - measured with kappameter KT-5
- laboratory studies (Table A.2-21)

6. Temperature monitoring: autonomous temperature stations ASTM (IPGG SB RAS) with 10 temperature sensors (calibrated DS18B20 with accuracy of 0.06 °C) at 0, 10, 20, 30, 40, 50, 60, 70, 80, 100 cm depth Table 2.19.1
7. Geobotanical studies. Descriptions of plant communities on standard plots 10 by 10 meters in different community types, at least 10 descriptions per each type. Collection of plant specimens (herbarium) for the further determination in laboratory conditions.

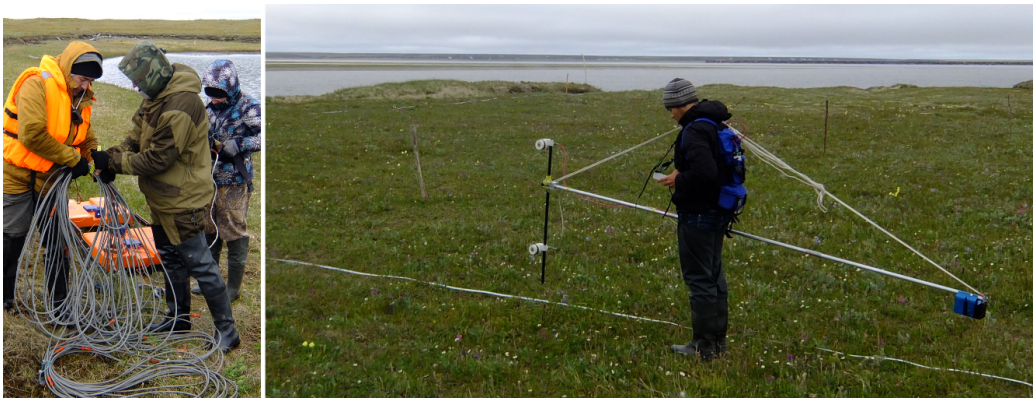

Figure 2.19-1: *Geophysical equipment: wires for ERT station "SibER-48" and GPR "OKO-2" (left); magnetometer MMPOS-2 (right)*

Preliminary results

Fieldwork map is shown on Figure 2.19-2.

Figure 2.19-2: *Fieldwork map: 1 - Northern lakes, 2 - planned borehole area, 3 - recently drained alas, 4 - thermoerosional gully, 5 - ancient time drained alas*

Samoylov Island

A number of studies were conducted in 2017 in addition to earlier results (Tsibizov et al., 2017). The research also develops integrated approach of the island, which was started by Boike at al. (2013). The fieldwork map is shown in Figure 2.19-3.

Based on aerial images (ca. 3 cm/pixel) and digital elevation model (ca. 10 cm relative precision) of the island, a preliminary geobotanical map was produced prior to fieldwork (Figure 2.19-4).

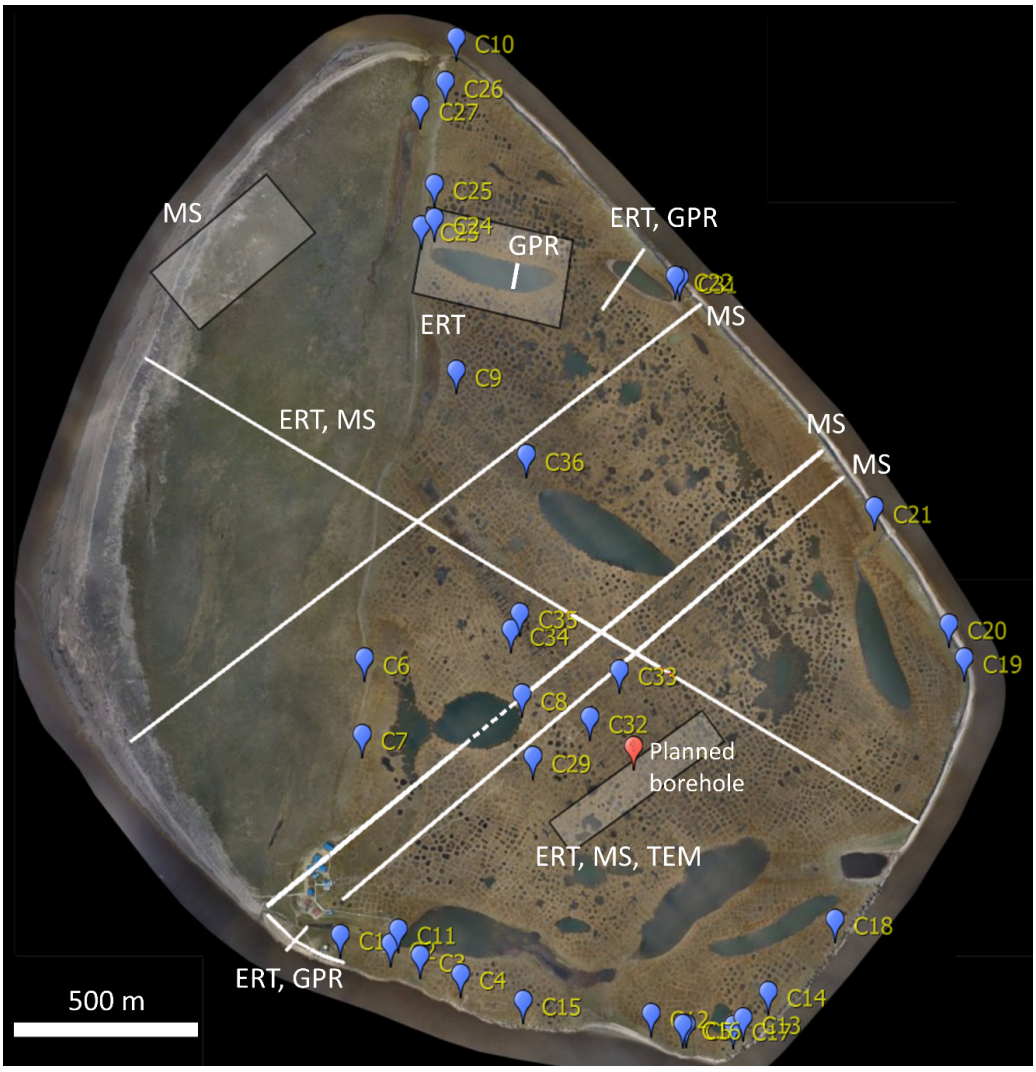

Figure 2.19-3: *Fieldwork map on Samoylov Island (base - aerial photo): ERT – electrical resistivity tomography, GPR – ground penetrating radar, MS – magnetic survey, TEM - transient electromagnetics, blue marks – soil sampling sites; lines – profiling, rectangles – aerial survey or composed parallel profiles covering an area*

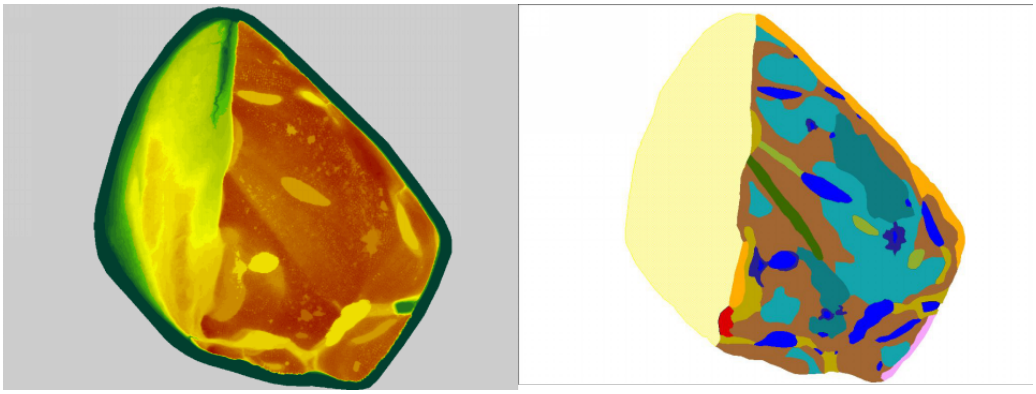

Figure 2.19-4: *Digital elevation model (left) and preliminary geobotanical map of Samoylov Island (right): colors designate different vegetation types*

10 by 10 meter sample plots were established in 5 to 10 replicas in each of the recognized areas in Figure 2.19-4 for a total of 80 plots. Each plot was described with coordinates, species composition (mainly higher vascular plants) and their abundance (coverage). In total, 112 herbarium specimens were collected for the determination.
A detailed geo-geomorphological study of quaternary sediments has been performed on Samoylov Island: near-surface layers of the first upland fringe (mostly seen in the eastern part of the island). Across the southern part of the island, a geological section has been described in the 90 meter long river bank outcropping. Geological cross section uncovered structural nonconformity: a layer of alluvial sediments of the second bottom is overlaid by a layer of the first upland fringe peat. In the course of clearings study we performed a macrovisual description of sediments and built a lithological column of uncovered alluvial structures; hand-drawn a set of texture-structural features of sediments; performed photo shooting of clearings. We also performed a study of a few clearings in the river bank across the northern, north-western, western and south-western parts of the island. Across the western part of the river bank, we observed single geological bodies of alluvial sediments, nonconformly embedded into the first upland fringe. They can be traced both macrovisually (in the course of river bank cross section studies) and in the process of geomorphological inspection of the first upland fringe's micro-relief. Different areas of micro-relief form distribution were allocated, contoured, and described by means of remote sensing (aerial imaging) and field studies. Allocated micro-relief areas differ from one another by a set of morphometric characteristics: ice-wedges polygonal network size, vertical stratification magnitude, average slope angle and micro-relief surface exposition etc., as well as lake abundance (wetness) on the surface. Based on this new knowledge, we plan to refine the genesis of the formation that forms the first upland fringe. We also plan to specify conditions of alluvial sediments formation and their facial attribution.
Soil map of the island will be made on the basis of soil studies. Soil samples were taken with consideration for preliminary geobotanical map and relief pattern distribution. Sampling points and planned analyses are provided in the Table A.2-21.
Talik under "Northern" lakes (site 1 in Figure 2.19-2) was studied using 3-dimensional ERT survey and GPR profiling. These lakes are quite similar but the second one is partially drained, so the case was both to reveal underlake taliks and detect the influence of drainage on their structure. Schlumberger and dipole-dipole array were used to create 3-dimensional model of talik in ERT and also GPR profiling as an auxiliary method. There were 9 profiles crossing North lake and adjoining territory. As well for comparison, one profile (10) crossed Small Lake located to the east of the North Lake (Figure 2.19-5). GPR studies were made with antenna set to 150 MHz central frequency along profile 7 and 10 on the Small Lake.
According to the available data, a zone of lower resistances is clearly visible on geoelectric sections which corresponds to higher temperatures of frozen or thawed rocks. However, it is difficult to determine the exact boundary between them. We also made geoelectric sections at different depths,

according to those, the low resistivity zone can be traced to a depth of approx. 35 m. The resistivity slice at a depth of 12.2 m is depicted in Figure 2.19-7.
GPR cross sections were constructed along profiles 7 and 10 (Figure 2.19-6). They give us detailed information about lake bottom structure. Also on both profiles, the boundary of permittivity change is well traced, but its geological interpretation is yet to be carried out.
GPR data along the profile 7 (Figure 2.19-7) is shown in Figure 2.19-8.

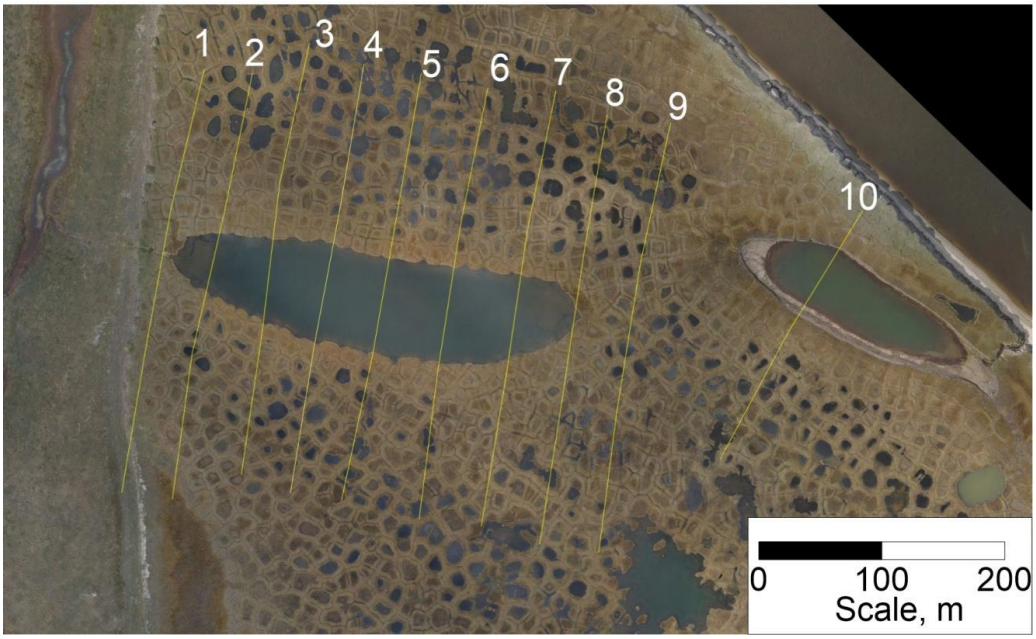

Figure 2.19-5: *The layout of the ERT profiles: the profile numbers are located at the beginning of each profile.*

Figure 2.19-6: *GPR profiling in progress*

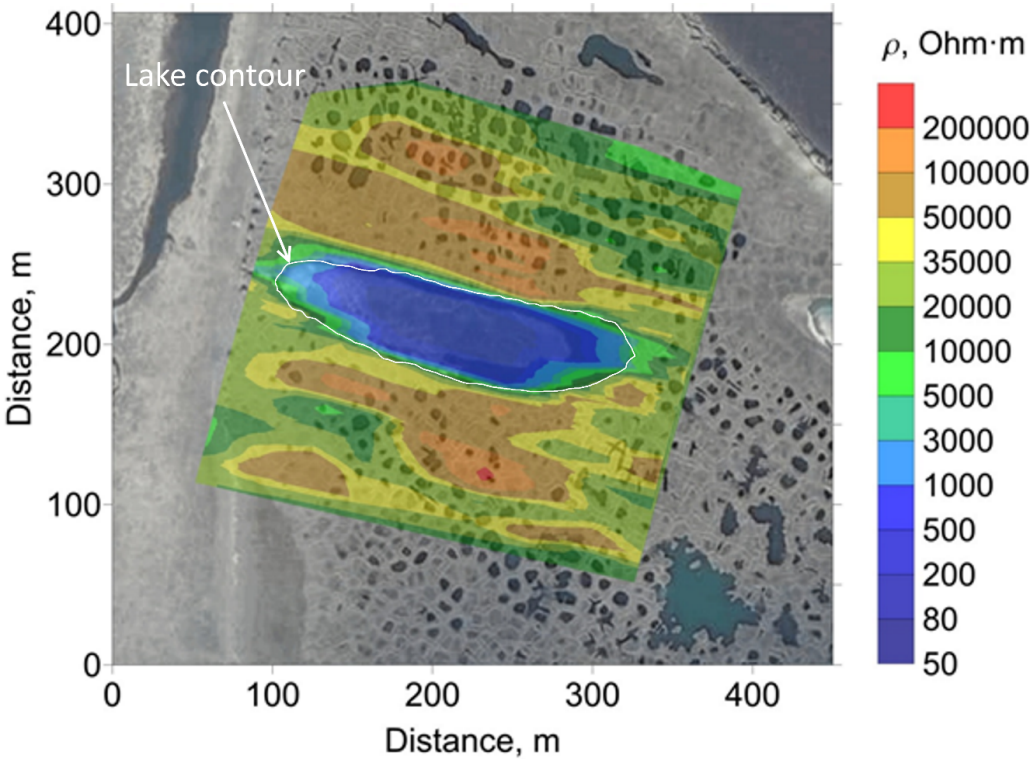

Figure 2.19-7: *Geoelectric section at a depth of 12.2 m*

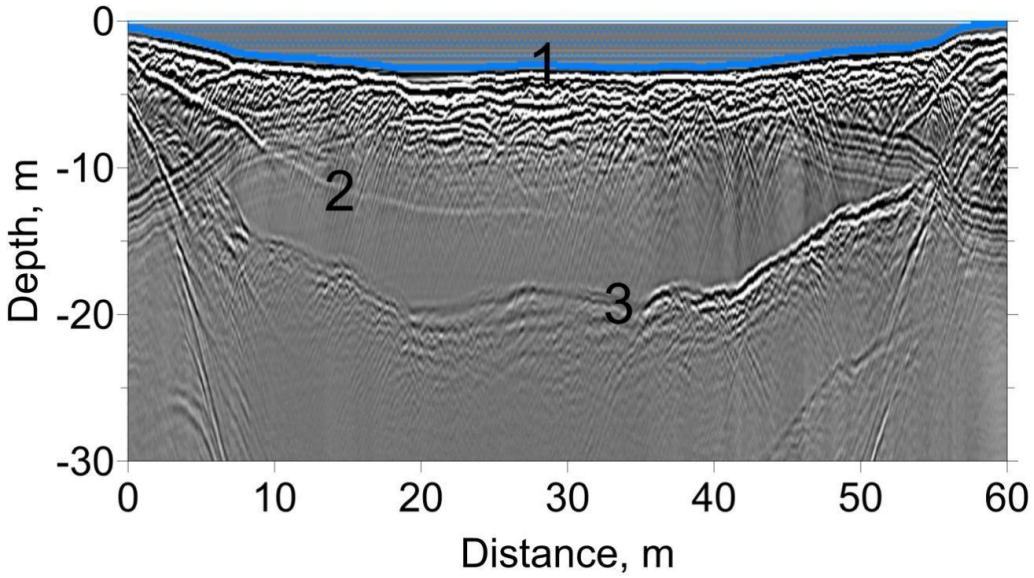

Figure 2.19-8: *GPR cross section along profile 7 (Figure 2.19-7) through the North Lake. 1. – a boundary between lake and bottom sediments, 2 – a boundary which origin has not been established yet, 3 – a boundary caused by multiple reflections.*

Planned temperature borehole area in the center of Samoylov Island (site 2 in Figure 2.19-2). The area is situated on the prolongation of a lineament - linear wet zone crossing the island from the north-west to the south-east (Figure 2.19-9).

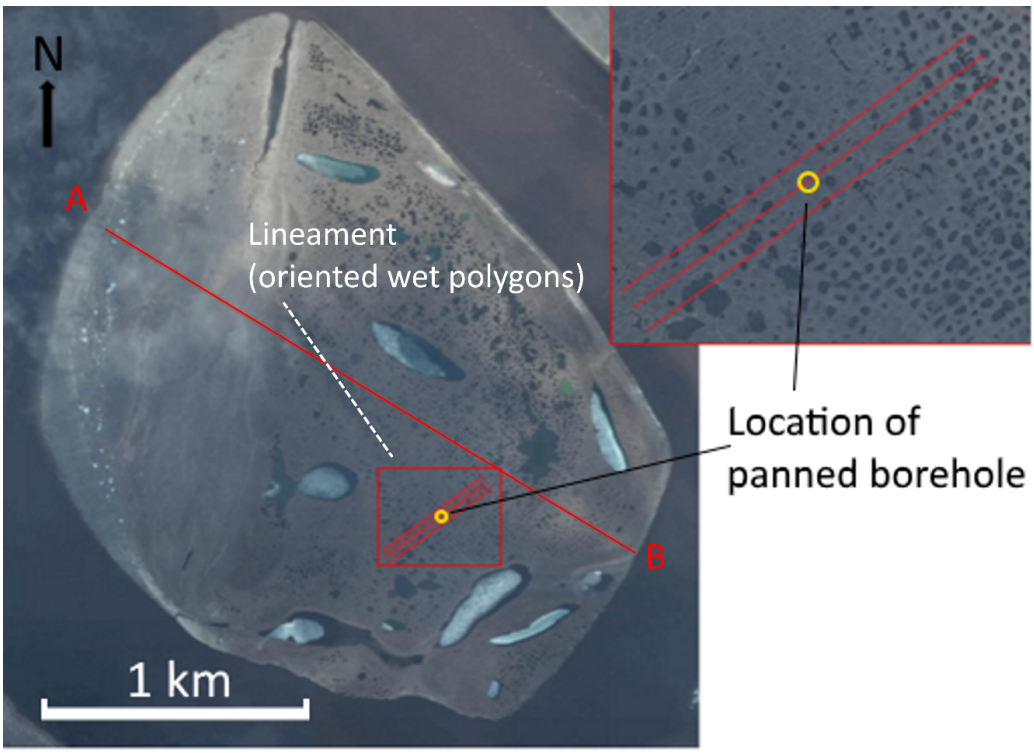

Figure 2.19-9: *Planned borehole area: ERT profiles*

Magnetic and ERT survey results along the profile AB are shown in Figure 2.19-10.

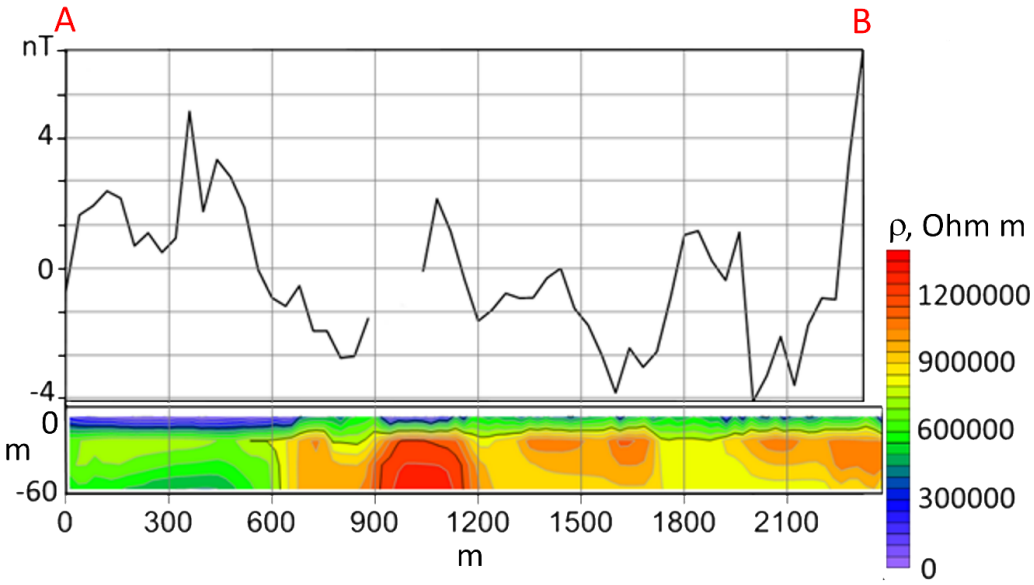

Figure 2.19-10: *Resistivity section and anomalous total magnetic field along the profile AB (Figure 2.19-9)*

Positive magnetic anomaly at the left part of the profile related presumably to the alluvial deposits of the western part of the island. Resistivity is quite high through all the section - lower values are observed in western part on the flood plain. High-resistivity anomaly were revealed under the central lineament of the island (900-1200 m in Figure 2.19-10) and could be probably linked to high ice content.

Two-dimensional and three-dimensional models of resistivity distribution were made as a result of areal ERT surveys. Figure 2.19-11 shows a 3D model of a log. resistivity distribution in the medium and a proposed borehole on Samoylov Island.

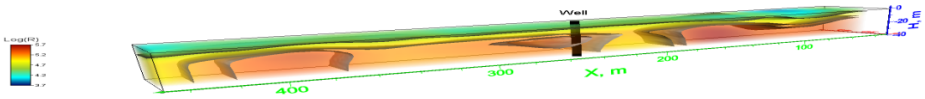

Figure 2.19-11: *3-dimensional resistivity model*

The model in Figure 2.19-11 shows that proposed borehole will go through the localized nonconformity zone of high resistivity, which in its turn is only 20 meters apart from the linear zone of low resistivity (x-coordinate 200 - 230 m). From the cross-section's homogeneity point of view, the best place to make a borehole is the interval 300 - 340 m (x-coordinate). This interval is characterized by vertically non-changing, flat structure of the cross section with no localized nonconformities.
Anomalous total magnetic field within the area is shown on the Figure 2.19-12.

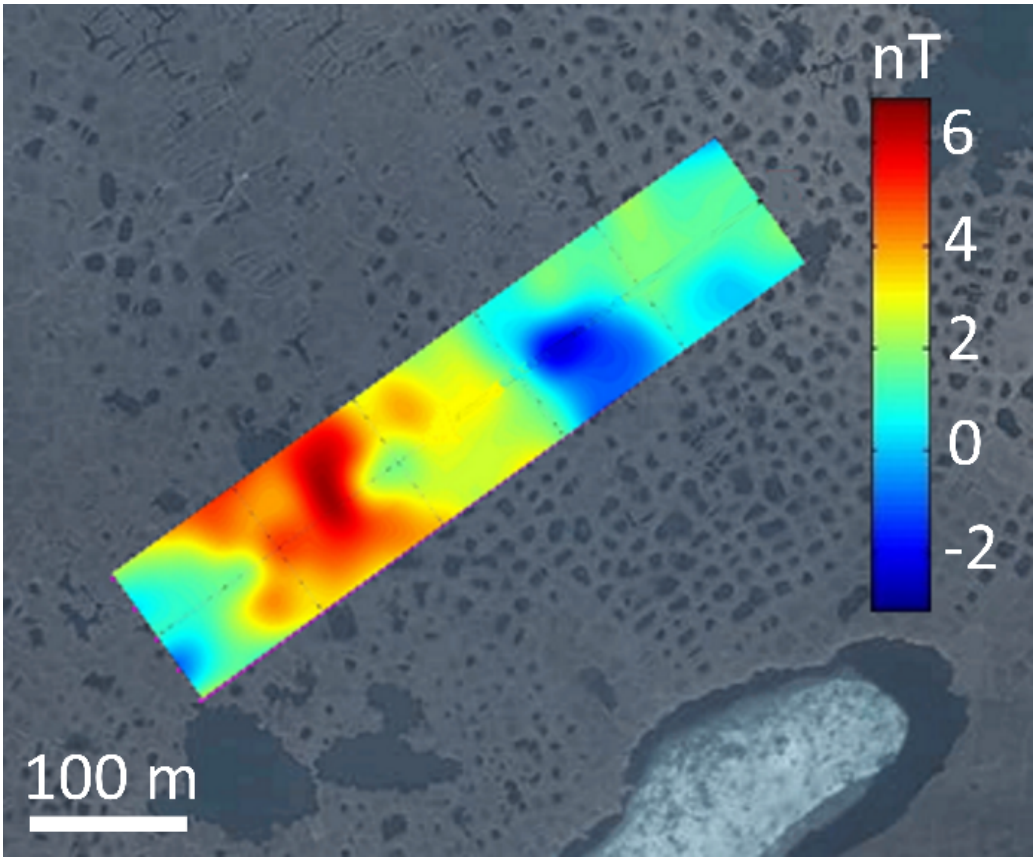

Figure 2.19-12: *Anomalous magnetic field within the planned borehole area*

Negative magnetic anomaly in the central part is situated on the lineament prolongation and could originate from a zone with high ice content or fault structure. One more area was studied with

magnetic survey to reveal whether the presumable fault stretches further to the north-west (Figure 2.19-3), but no similar anomalies were found there.
Experimental work with TEM device showed no convincing results. Due to very high resistivity of the medium and small size of the generating loop, the electromagnetic field is not developing properly and the measured signal is rendered only by the measuring device's inner transient process.

Kurungnakh Island
Three local features were studied during the expedition on Kurungnakh Island: recently and long ago drained alases and erosional gully. Alas which was drained between 1970-1980 years was already the object of research in 2016 (Tsibizov et al., 2017).
The bottom of recently drained lake (site 3 in Figure 2.19-2) has been studied using 3-dimensional ERT survey. Preliminary results are shown in Figure 2.19-13.

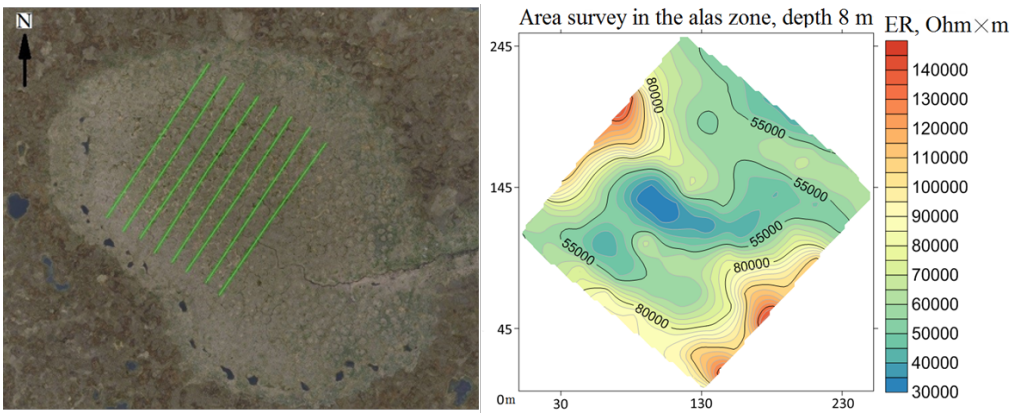

Figure 2.19-13: *Measurement design on aerial photo (left) and horizontal section of 3-dimensional ERT inversion at 8 m depth (right)*

Low resistivity area at the center of the section presumably indicates higher temperature of permafrost. It could be a residual of talik: the lake was drained in the recent past (circa 30-40 years before) and temperature has not still stabilized to the values, which are typical for the region.
Soil sampling was made on sites K1-K5 on the slope of the drained lake (Table A.2-21). Erosional valley and the area of its propagation (site 4 in Figure 2.19-2) were studied using ERT, GPR and magnetic survey.
Measuring scheme is shown in Figure 2.19-15.

Figure 2.19-14: *Erosional gully (left); GPR with 700 MHz antenna (right); studying area is on the background on both photos*

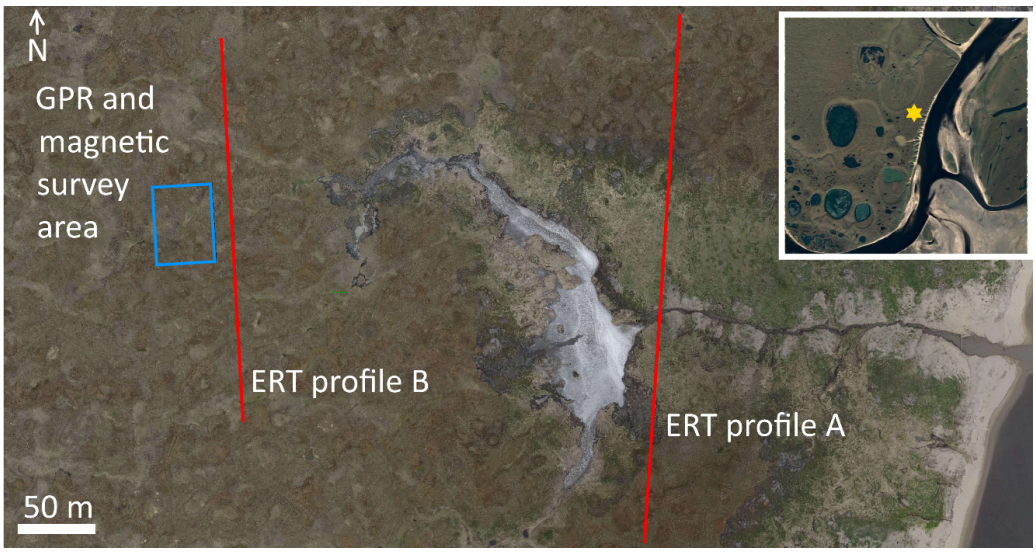

Figure 2.19-15: *Scheme of the measurements on the erosional gully, southern tail of the gully, which is shown on Figure 2.19-14*

High resistivity anomalies probably related to higher ice content areas are on both sides of the gully (Figure 2.19-15, profile A) and on the right part of the section (Figure 2.19-15, profile B).

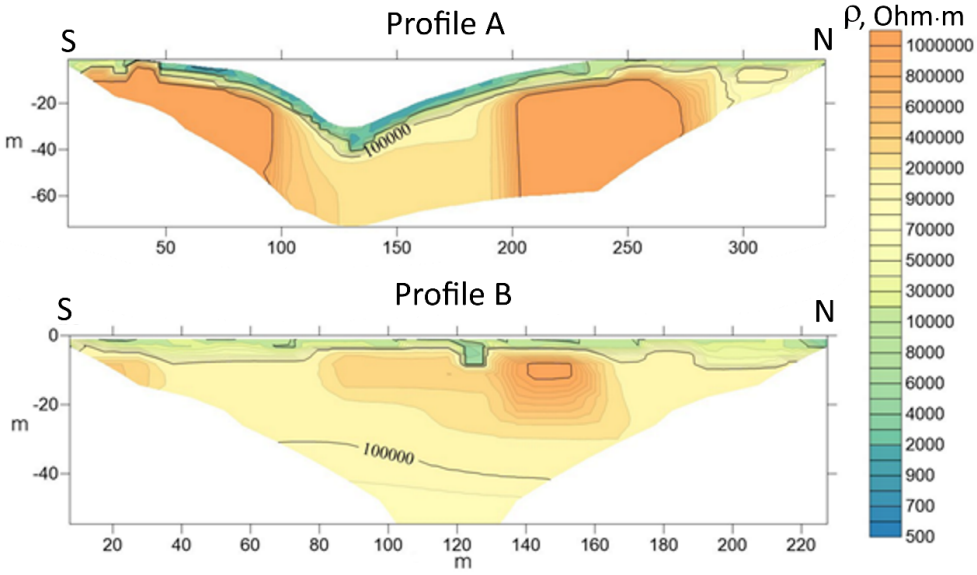

Figure 2.19-16: *ERT profiles (Figure 2.19-15): crossing the gully (upper) and its future propagation area (lower)*

Magnetic survey revealed a polygonal ice-wedge structure of permafrost in the area, where the gully propagates (Figure 2.19-16).

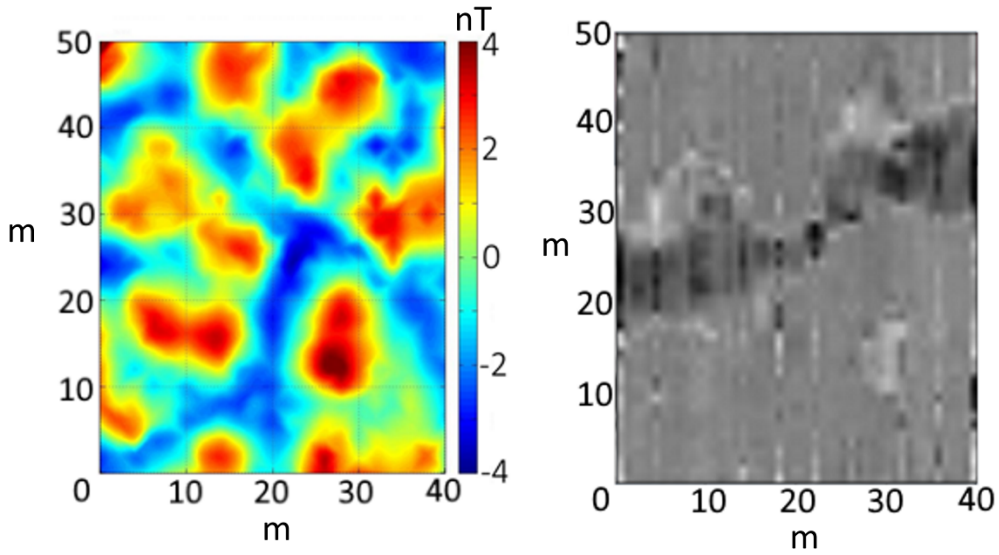

Figure 2.19-17: *Anomalous total magnetic field (left) and GPR data - amplitude slice of reflected energy (right)*

It should be noted that there is a some kind of ranking between magnetic anomalies caused by ice wedges: polygons of big diameter with thick ice wedges on their edges enclose the smaller ones. GPR data (Figure 2.19-17) reveals the area which could be linked with a wet zone. One might assume that thermoerosion follows ice wedge structure, in this case the wet zone is formed initially and indicates the way which the gully propagation will follow.
Alas drained a long time ago (site 5 in Figure 2.19-2) at the southern part of Kurungnakh Island was already the object of research in previous years, published in (Grosse et al., 2017; Tsibizov et al., 2017). A borehole, 17 m deep, was drilled in 2015, where magnetic susceptibility measurements, grain size and palynological analyses were conducted, and a temperature chain was installed. This data is still being processed. Magnetic survey, ERT and soil sampling were conducted, shallow temperature stations (up to 1 m depth) were installed in 2016. A map of the 2017 fieldwork season is shown in Figure 2.19-18.

Table 2.19.1: Temperature measuring sites

Label	Coordinates	Start time	Comments
c1	N 72.28911 E 126.18870	24.07.2016 16:00	outside of alas
c2	N 72.28974 E 126.1868	24.07.2016 20:00	alas slope (k6 sampling point)
c3	N 72.29131 E 126.1864	25.07.2016 16:00	alas bottom (k9 sampling point)
c4	N 72.29058 E 126.18959	26.07.2016 16:00	alas slope
c5	N 72.28960 E 126.18301	26.07.2016 16:00	alas slope

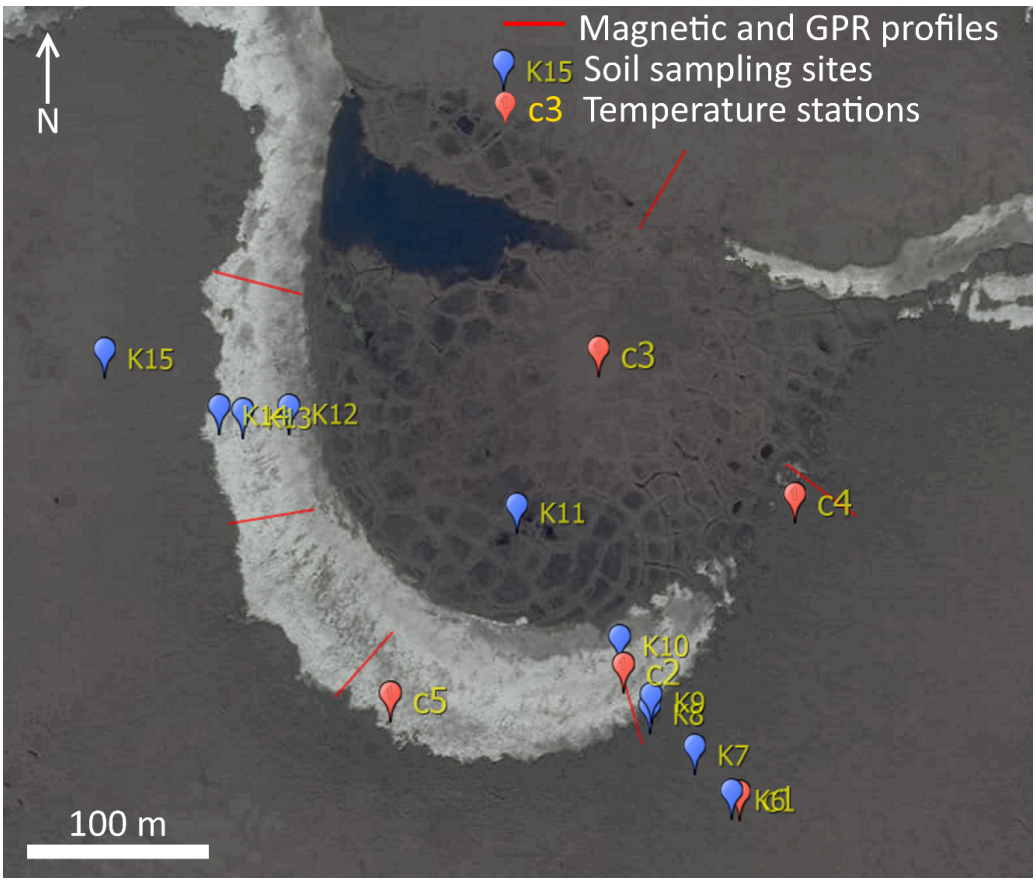

Figure 2.19-18: *Ancient time drained alas: soil sampling sites, GPR and magnetic profiles, temperature stations*

Alas studies are able to help evaluate the potential of northern biological systems, reveal factors that provide their high productivity and better understand how they change with time. The study of basic soil properties will help better understand present mechanisms of ecosystem functioning and predict their behavior in the evolving environment.
It is expected that differences of alas slope structure are going to be found based on magnetic and GPR data along profiles shown in Figure 2.19-18.

Research is funded by:

1. General committee of Russian Academy of Sciences: Project VIII.73.1.7 Geological, geophysical and geochemical studies in Siberian Shelf-Laptev Sea transient zone on a basis of Samoylov Research Station.
2. Novosibirsk State University, Strategic academic unit: Project Geological and Geophysical Investigations in the Arctic and Global Priorities.

2.20 Integrated biostratigraphic and paleomagnetic studies of the Devonian and Carboniferous sedimentary-volcanogenic complexes

Nikolay Mikhaltsov[1,2], Nadezhda Izokh[1], Nikolay Sennikov[1,2], Pavel Pudrikov[1,2], Anastasia Radevitch[1,2], Ivan Alekseev[2], Denis Avdeev[1,2]

[1] Institute of Petroleum Geology and Geophysics, Siberian Branch, Russian Academy of Sciences, Novosibirsk, Russian Federation

[2] Novosibirsk State University, Novosibirsk, Russian Federation

Fieldwork period and location
August 2nd to August 21st, 2017 (near Samoylov Research Station, right banks of the Lena River and of the Bykovsky Channel)

Objectives
Paleomagnetic data provide paleotectonic and paleogeographic reconstructions with a quantitative information. An important criteria is the availability of time-continuous bank of solid paleomagnetic determinations for large crustal blocks. The main goal of Paleomagnetic research in the Lena Delta, together with strong dating provided by biostratigraphic research, is to cover the gap in paleomagnetic data around the Paleozoic period for the Siberian Platform. On the other hand, understanding the distribution of magnetic characteristics of rocks near the global event of Upper Kelwasser has lead to the correlation of the late Devonian abiotic and biotic events. This, in turn, allows us to make the reconstruction of changes in paleoecological conditions in the Upper Devonian sedimentary basins and their correlation with the evolutionary changes of conodonts.

Methods

1. Visual observation and lithological description of the geological section
2. Detailed (layer-to-layer) sampling of rocks for biostratigraphic analysis and also for isotope-geochemical studies
3. Sampling of oriented samples for paleomagnetic study

The most common type of paleomagnetic sampling is using a gasoline-powered portable drilling apparatus with a water-cooled diamond bit (Figure 2.20-1).

Figure 2.20-1: *Portable drill with diamond bit and water cooling system used for paleomagnetic sampling*

The core diameter is usually approx. 2.5 cm. After the coring of the outcrop to a depth of 5 - 12 cm, an orientation stage is slipped over the sample while it is still attached to the outcrop at its base. Orientation stages have an inclinometer for determining inclination (dip) of the core axis and magnetic or sun compass (or both) for determining azimuth of core axis (Figure 2.20-2). The accuracy of orientation by such methods is about +- 2°. After orientation, the core is broken from the outcrop, marked for orientation and identification, and returned to the laboratory (Figure 2.20-3).

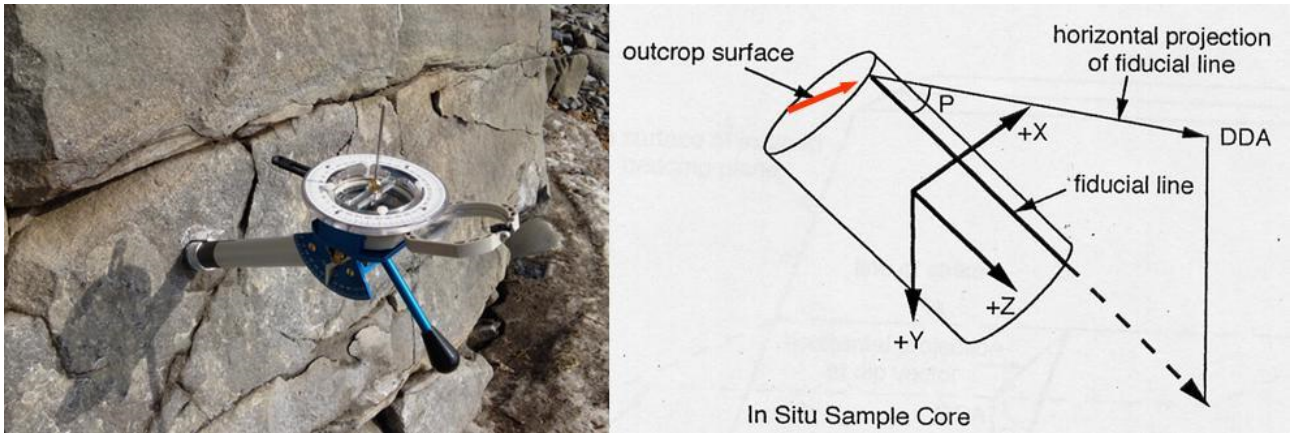

Figure 2.20-2: *Paleomagnetic orientation fixture with inclinometer and magnetic and sun compasses (left); Coordinate system used for core orienting (right). "Dip Direction Azimuth" (DDA) and "Plunge angle" (P) are measured in field.*

Figure 2.20-3: *One of the paleomagnetic sampling sites on Stolb Island. Upper left image presents oriented cores.*

Preliminary results

6 objects were studied during the expedition (Figures 2.20-4 and 2.20-5):

1. Terrigeneous-carbonate section of Stolb Island
2. Devonian limestones and sandstones in the Eastern part of Kurungnakh Island (mts. Orto-Khaya and Kubalaakh-Khaya)
3. Devonian sandstones, limestones and basalts in the Krest-Khomo section
4. Carboniferous sandstones and conglomerates in the Krest-Tumsa section
5. Stratotypic sections of Bastakh (Lower Carboniferous) and Ebelyakh (Upper Devonian) formations on the right bank of the main course of the Lena River.
6. Upper-Cambrian limestones in the Tit-Ary region

Overall, 325 oriented samples in 32 sites were taken for paleomagnetic investigations. More than 150 samples (overall weight about 200 kg) were taken for biostratigraphic analysis on complexes of conodonts and brachiopods, and also for isotope-geochemical studies.

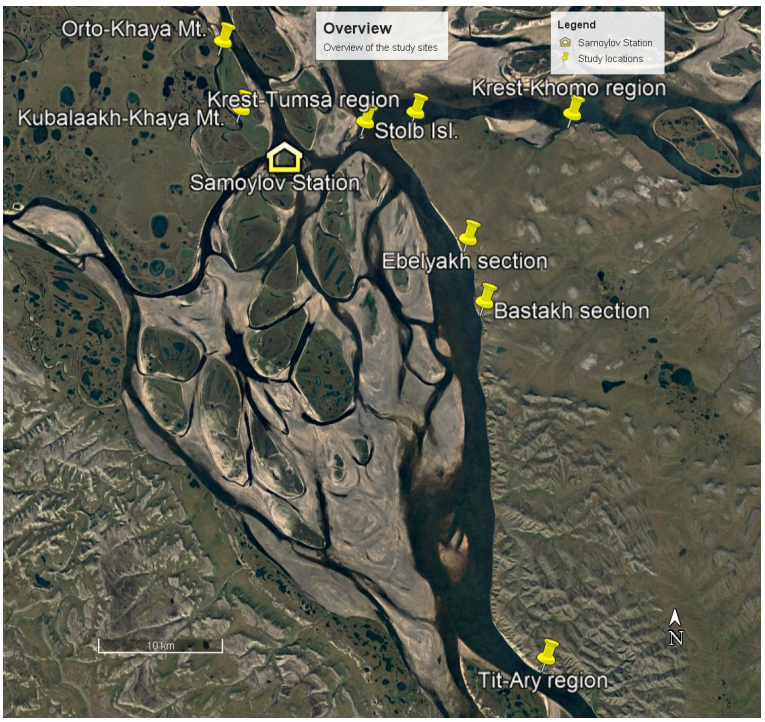

Figure 2.20-4: *Overview of the study locations*

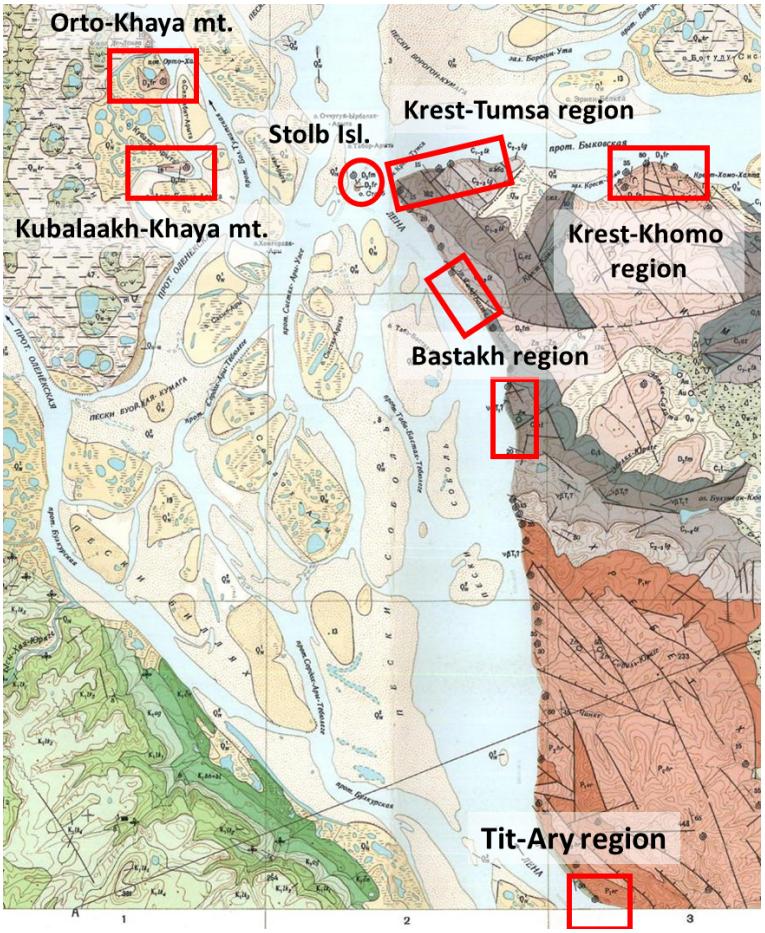

Figure 2.20-5: *Study locations on the geological map*

The Upper Devonian, Carboniferous and Permian (from 385 up to 251 million years ago) sections along the right bank and Delta of the Lena River were studied since 2012. The new paleontological and paleomagnetic collections were collected from studied sections.

Stolb Island

In 2017, new sampling of Upper-Devonian section of Stolb Island (Figure 2.20-6) was performed. Additional samples were taken for microfauna analysis (conodonts), especially for clarification of the age of the lower part of the section (beds 1 - 3) below the Upper Kelwasser global anoxic event (Figure 2.20-7). Paleomagnetic samples were taken from beds 25 - 34.

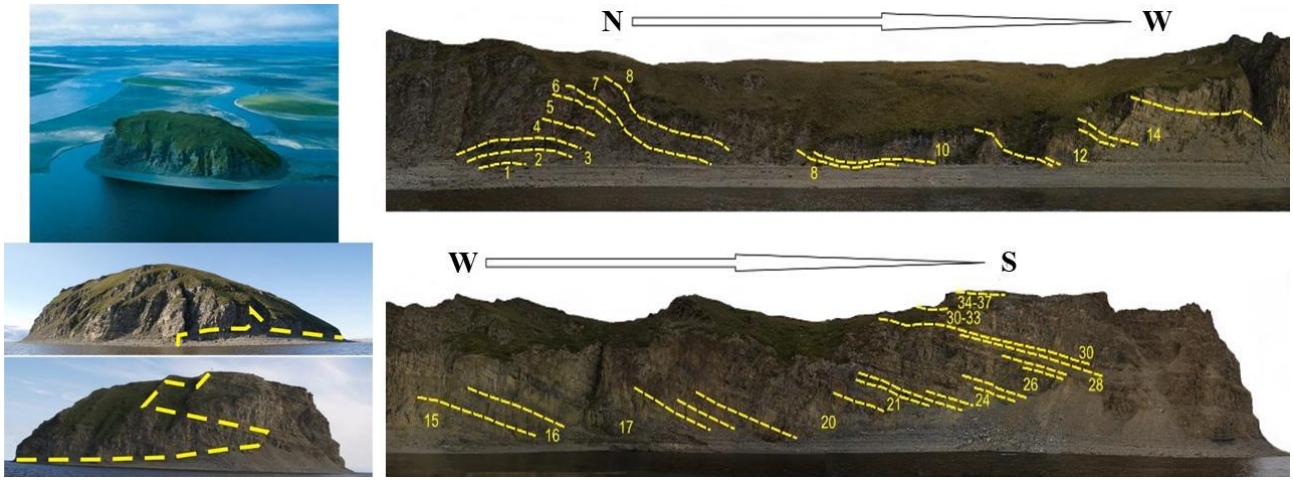

Figure 2.20-6: *Scheme of the geological section of Stolb Island*

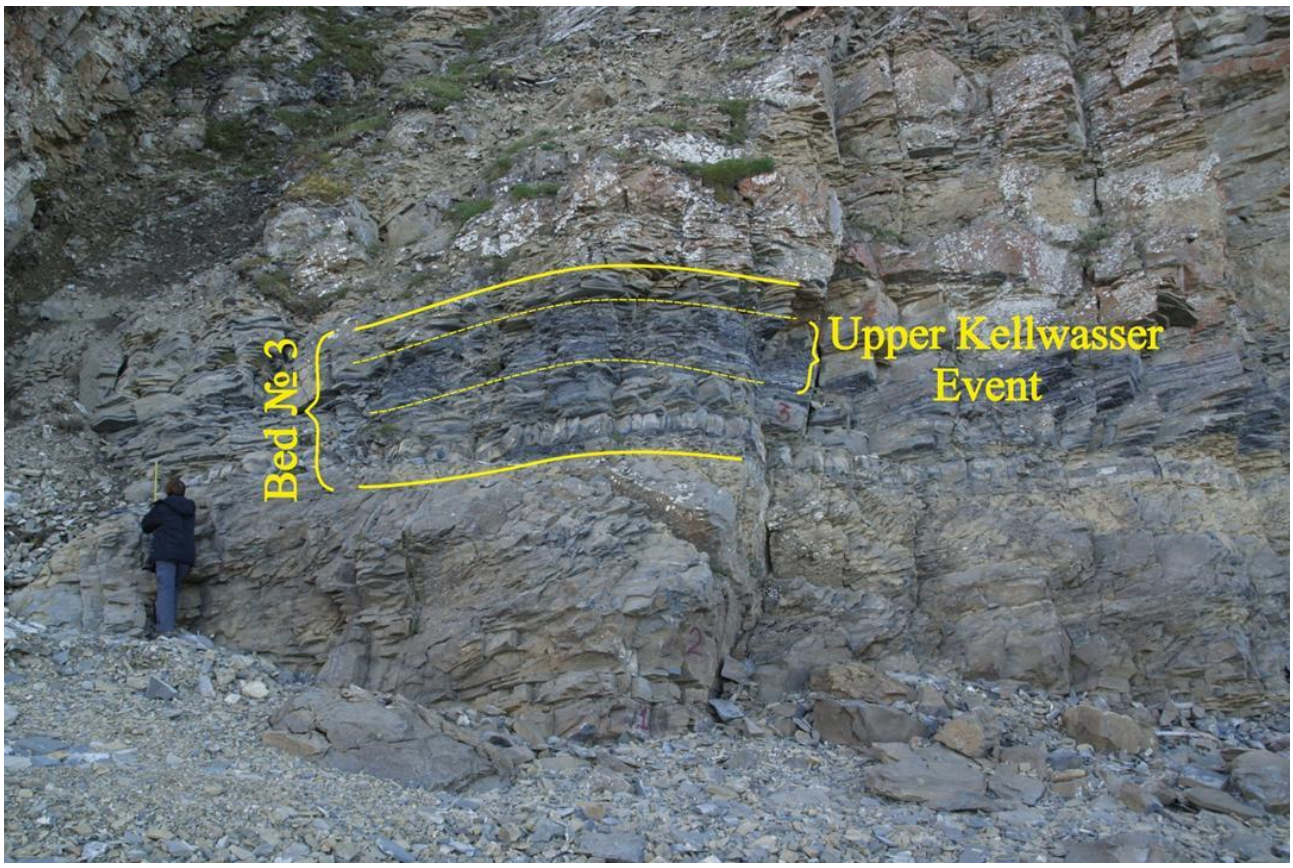

Figure 2.20-7: *Position of Upper Kellwasser Event in the section*

Orto-Khaya and Kubalaakh-Khaya mountains (Figure 2.20-8)
Upper-Devonian section was described “layer by layer” and sampled for microfaunal (conodonts) and macrofaunal (brachiopods) analysis for the purpose of rock age refinement. As this section is assumed to be Stolb’s stratigraphic analogue, detailed paleomagnetic sampling was performed and 11 sites were sampled. All samples for paleomagnetic studies are strongly linked to described layers in the section.

Figure 2.20-8: *Map of sampling sites in Orto-Khaya and Kubalaakh-Khaya Upper-Devonian terrigenous-carbonate section*

Figure 2.20-9: *Fragment of the lower part of Kubalaakh-Khaya section*

Krest-Khomo section

The Upper-Devonian section was described “layer by layer” and sampled for microfaunal (conodonts) and macrofaunal (brachiopods) analysis for the purpose of rock age refinement. In the upper part of the section a bioherm was found (Figure 2.20-10). Samples for paleomagnetic studies were taken from different parts of thick basaltic lava flow and from the baked contact zone of underlying sandstones (Figure 2.20-11).

Figure 2.20-10: *Fragment of the bioherm (its lower part) upon the basalt flow in the Krest-Khomo Upper-Devonian section*

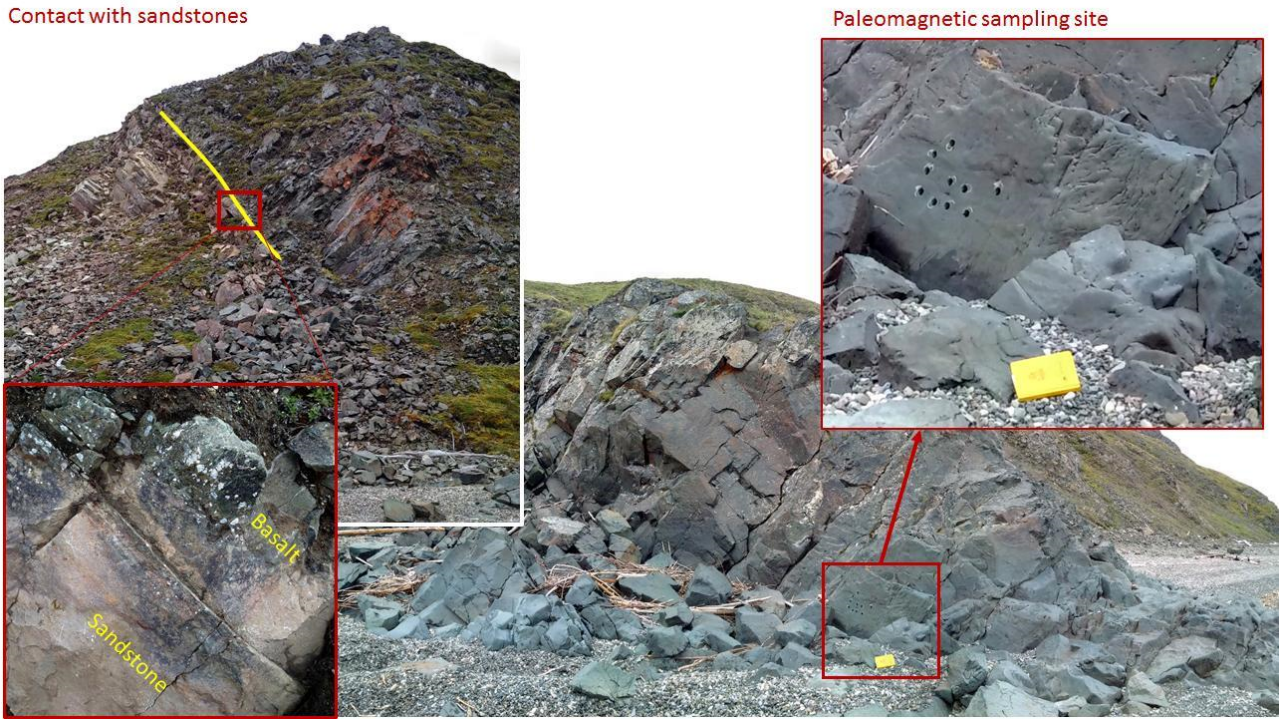

Figure 2.20-11: *Basaltic flow near its lower contact with sandstones*

Krest-Tumsa section

Carboniferous sandstones and conglomerates of Atyrdakh formation (C1-2) near Krest-Tumsa cape were sampled for paleomagnetic study. The rock's lithology is unclear so this is a subject of future investigations.

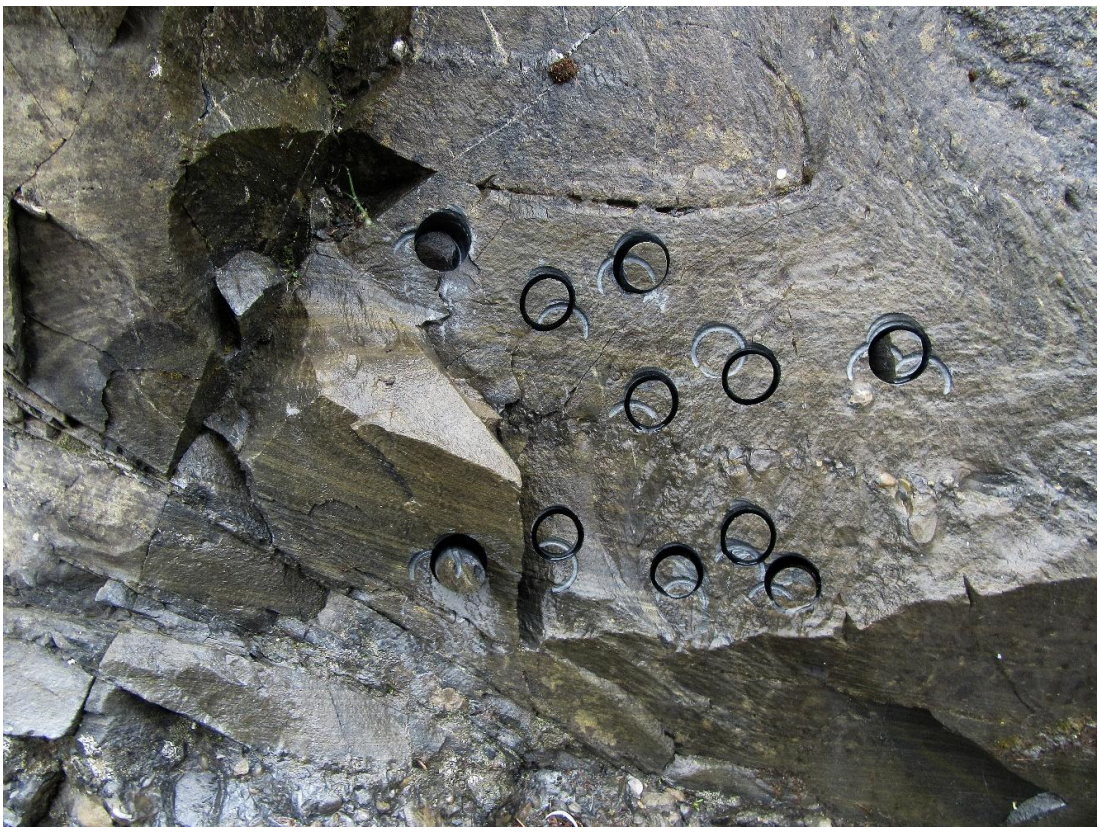

Figure 2.20-12: *View of "Lying overfold" in the sandstones of Atyrdakh formation (C1-2) near Krest-Tumsa cape*

Stratotypic sections of Bastakh (Lower Carboniferous) and Ebelyakh (Upper Devonian) formations on the right bank of the main course of Lena

In 2017, additional samples for macrofaunal analysis were taken from lowermost and uppermost parts of the section (Figure 2.20-13, Figure 2.20-14). Only preliminary paleomagnetic sampling was made in order to verify the compatibility of these rocks for paleomagnetic analysis.

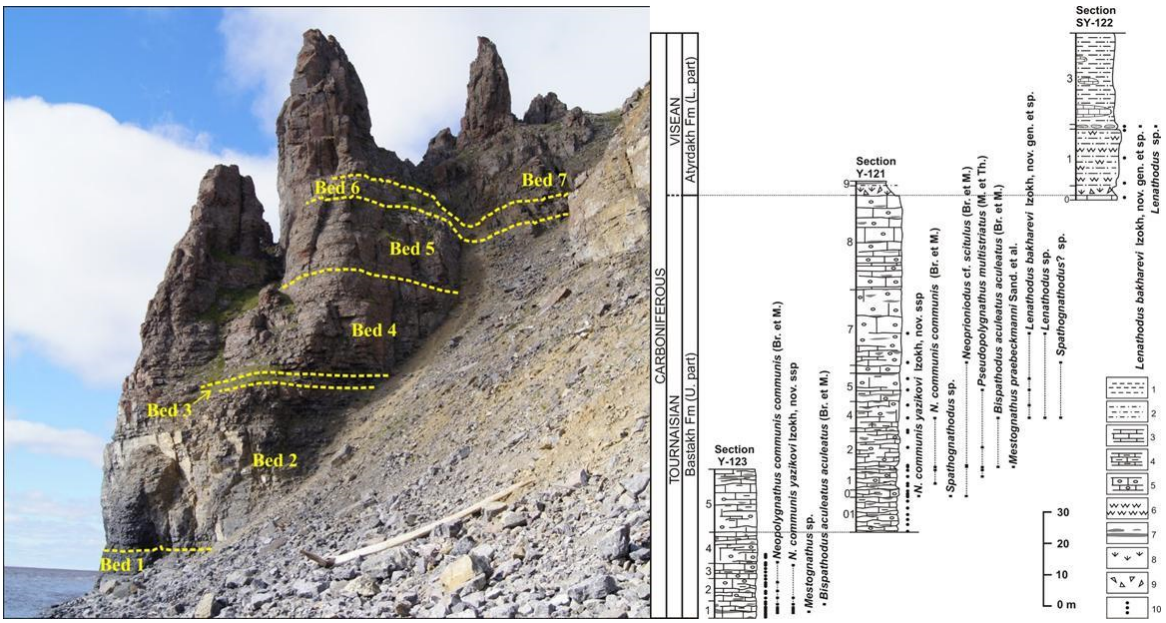

Figure 2.20-13: *Bastakh formation biostratigraphy (Izokh, Yazikov, 2017)*

Figure 2.20-14: *Fragment of the Bastakh formation (Lower Carboniferous)*

Upper Cambrian carbonates near Tit-Ary village
The section was sampled for microfaunal, macrofaunal and isotope-geochemical analysis. Preliminary paleomagnetic sampling was made in order to verify the compatibility of these rocks for paleomagnetic analysis.

2.21 Seismicity of the Laptev Sea Rift

(Wolfram H. Geissler[1], Sergey Shibaev[2], Christian Haberland[3], Daniel Vollmer[4], Boris Baranov[5]: not on board), Jölund Asseng[1], Sergey Petrunin[2], Frank Krueger[4], Nikolay Tsukanov[5], Dmitri Peresypkin[2], Stepan Gukov[2], Rustam Tuktarov[2], Sofia-Katerina Kufner[3]

[1] Alfred Wegener Institute Helmholtz Centre for Polar and Marine Research, Bremerhaven, Germany

[2] Yakutsk Branch Federal Research Center Geophysical Survey Russian Academy of Sciences, Yakutsk, Russian Federation

[3] Helmholtz-Zentrum Potsdam - GFZ German Research Center for Geosciences, Potsdam, Germany

[4] University of Potsdam, Potsdam, Germany

[5] P.P. Shirshov Institute of Oceanology, Russian Academy of Sciences, Moscow, Russian Federation

Fieldwork period and location
July 18th to August 9th, 2017 (Lena River Delta, Tiksi)

Objectives
Extensional tectonics is one of the key players in shaping the Earth's landscape. We want to study one of only very few examples of transition between oceanic and continental rifting. Generally, rifting processes are associated with earthquake and also magmatic activity. In principle, these processes hold risk potential, for instance, earthquakes or fluid escape close to the continental slope of the Laptev Sea might cause major submarine landslides and expulsion of the great amounts of methane influencing on climate change.
The Laptev Sea region is one these very few places on Earth where mid-ocean spreading centres continue into continental rift zones. The Gakkel Ridge, the active spreading centre in the Eurasia Basin of the Arctic Ocean, is characterized by well-defined seismicity close to its axial graben. In contrast below the Laptev Sea Shelf, which consists of a series of sediment filled grabens (500 km wide, 700 km long), only more diffuse seismic activity is observed. The pre-rift basement in the Laptev Sea is most probably formed by Late-Paleozoic and Late-Mesozoic fold belts (Drachev et al., 2010). The Laptev Rift Basin is filled with Upper Cretaceous and Cenozoic sediments of variable thickness (1.5 to 14 km). The westernmost limit of seismicity is located close to edge of thick lithosphere of the Siberian Shield (Sloan et al., 2011), which indicates some structural control on the recent tectonic activity. Focal depths are mainly $<$25 km (continent) and $<$10 km (ocean) (Franke et al., 2000; Fujita et al., 2009). Sparse observations of upper mantle earthquakes (Avetisov, 1999; Kovachev et al., 1994) are under debate. The pole of rotation is very close to the study area, most probably to the south of Lena Delta (e.g. Gaina et al., 2002). Existing data indicate changes between compressional and extensional tectonic phases over short distances. This might be a consequence of the fact that the pole of rotation is close to our study area. The Khatanga-Lomonosov Shear Zone marks the border between the Gakkel Ridge and Laptev Sea Rift System, but its nature and extent is debated (e.g. Jokat et al., 2013; Laverov et al., 2013).
According to Franke et al. (2000), crustal extension is concentrated in the eastern Laptev Sea area. Fault plane solutions are sparse and mostly not well determined to describe the movements in greater detail. Thus, with this project we intend to investigate details on tectonic movements in the Laptev Sea to better describe this amagmatic rifting and its consequences in an Arctic and global context. In

general, we intend to increase the number of seismological stations for monitoring local earthquakes in the Laptev Sea/Lena Delta to fulfill the following objectives:

1. Location of microseismicity and its relationship with active faults: We want to identify seismologically active faults zones. In a first step, we like to deploy instruments in earthquake areas, which are already identified by the global seismological network, though with low spatial resolution.

2. Focal mechanisms: What is the present geodynamic setting, where is extension and where is compression in the Laptev Sea and in the Lena delta region, where is the exact pole of rotation? What is the relation of the recent seismicity to pre-existing crustal and lithosphere structures (e.g. western Verkhoyansk Fold-and-Thrust Belt/Olenek Zone or South Anyui Suture)?

3. Lithosphere structure. It is interesting to note that despite the Cenozoic continental rifting in the Laptev Sea little volcanism is known. Thus, we like to compare the deep crustal and upper mantle structure with other continental rift systems (e.g. Afar) to enhance our understanding on the driving forces.

Methods and field work

In a first step, we want to study the local and regional seismicity and lithospheric structure by means of a network of seismological stations and a seismological array. During the 2016 fieldwork (Geissler et al., 2017), we had installed 12 seismological stations in the Lena Delta to study the local seismicity along the southern part of the Olenek Fault Zone and 13 stations in an array SE of Tiksi to study the regional seismicity of the Laptev Sea. Instrumentation of the stations includes Cube data loggers and Mark-1Hz Seismometers. The stations run autonomously with batteries. This first installation was dedicated to test the station configuration under the extremely harsh environmental conditions in northern Siberia and to gain a first set of data.

In summer 2017, we maintained all array stations and partly dismantled the Lena delta network stations (Figure 2.21-1, Table 2.21.1, Table 2.21.2). The data recovery from 25 stations was, surprisingly, almost completed 9 months at 23 stations (Table 2.21.3). In the array one vertical component did not work. One of the array stations stopped operating in December 2016; a second one stopped in late February 2017. This happened most probably due to water leakage into connectors or CUBE data loggers. Logged temperatures at selected array stations went down to -26 °C, however, seemingly did not cause technical problems (Figure 2.21-2). Data acquisition stopped at most stations in late April/early May due to the 32-Gbyte limitation of the CUBE data loggers. Batteries could be reloaded (all were at or above 11.5 V capacity). Network stations were partly dismantled to reduce logistical efforts and costs (vessel and helicopter) for 2018 field season. Also, we did not expect that almost all recorders and batteries were still intact. Only four of the Lena Delta network stations were kept in operation, because these can be easily maintained by the boat of the nearby Samoylov Island Station. Additionally, three former network stations were deployed as a small array around permanent station STOLB (Figure 2.21-3).

Data are shared among the partners (Yakutsk, Moscow, Potsdam/Bremerhaven), where it has to be mentioned that the German side only has allowance to export resampled 40 Hz data (original sample rate is 100 Hz) to Germany.

Table 2.21.1: Station list Lena Delta

Name	Locality	Latitude [°N]	Longitude [°E]	Elevation [m]	Begin date*	End date of operation*	s/n seismometer	s/n recorder
LD004	DeLong-Chalta	72.654	124.347	12	27072016	24072017	1006	DC-620
LD007	Mountains	72.184	124.889	264	25072016	17072017	1007	DC-621
LD008	Tchaika	72.442	125.313	12	25072016	27072017	1009	DC-622
LD010	Tchai-Tumus	72.326	125.76	34	26072016	25072017	1015	DC-623
LD011	Amerika-Chaja	72.476	126.275	73	31072016	-	1170	DC-624/DC-620**
LD012	Pik Stalin	72.174	126.107	30	27072016	25072017	1178	DC-625
LD014	Mountains	71.888	126.036	241	25072016	27072017	1190	DC-626
LD015(B)	GeoCamp	72.117	126.982	54	30072016	-	1331a	DC-627/DC-622**
LD016(C)	By Stolb	72.4	127.147	71	1082016	-	1335	DC-628/DC-624**
LD018	White Mountains	71.929	127.313	23	28072016	28072017	1336	DC-629
LD019(D)	Nordenshield	72.075	128.325	35	3082016	-	1342a	DC-630/DC-629**
LD021	Lena Castle/Tigie	71.399	127.247	111	29072016	27072017	1348a	DC-631
LD031	Stolb - Red Hut	72.405	126.822	15	31072017	-	1348a	DC-631
LD032	Stolb - Hill	72.398	126.807	71	1082017	-	1015	DC-632
LD033	Stolb - Cliff	72.403	126.797	57	2082017	-	1178	DC-625

** all times are local Tiksi time*

*** device changed 2017*

Table 2.21.2: Station list Tiksi array

Name	Locality	Lat-itude [°N]	Long-itude [°E]	Ele-vation [m]	Begin date*	s/n seis-mome-ter	s/n recorder
TIK01	central station	71.574	129.073	135	23072016 1500	1831	DC-632
TIK02	inner circle	71.576	129.068	139	23072016 1800	1889	DC-633
TIK03	inner circle	71.576	129.078	131	24072016 1200	1895	DC-634
TIK04	inner circle	71.574	129.081	136	24072016 1500	2828	DC-636
TIK05	inner circle	71.572	129.078	140	26072016 1300	2829	DC-637
TIK06	inner circle	71.572	129.069	121	26072016 1600	2860	DC-638
TIK07	inner circle	71.574	129.065	119	26072016 1800	4191	DC-640
TIK08	outer circle	71.584	129.069	85	27072016 1300	4192	DC-641
TIK09	outer circle	71.579	129.099	98	27072016 1600	2830	DC-301
TIK10	outer circle	71.569	129.097	120	28072016 1200	2858	DC-302
TIK11	outer circle	71.563	129.075	146	28072016 1700	2859	DC-303
TIK12	outer circle	71.572	129.043	50	29072016 1200	3045/1007**	DC-304
TIK13	outer circle	71.582	129.049	109	29072016 1600	3052	DC-305

** all times are local Tiksi time*

*** device changed 2017*

Table 2.21.3: Data recording status 2016/2017

Site name	Start	End	Data Volume[GB]
TIK01	23.7.16 06:31:14.7	22.4.17 18:40:53.7	30.9
TIK02	23.7.16 09:02:44.8	1.5.17 19:04:40.0	31.9
TIK03	24.7.16 03:21:14.7	2.5.17 13:18:52.4	31.9
TIK04	24.7.16 05:51:14.7	2.5.17 16:07:12.8	31.9
TIK05	26.7.16 03:57:32.7	4.5.17 13:53:46.3	31.9
TIK06	26.7.16 06:44:13.7	4.5.17 16:40:44.2	31.9
TIK07	26.7.16 09:17:14.7	4.5.17 19:20:45.2	31.9
TIK08	27.7.16 03:58:44.7	26.4.17 16:10:09.1	30.9
TIK09	27.7.16 06:32:42.7	16.2.17 23:39:23.1	23.6
TIK10	28.7.16 03:31:12.7	6.5.17 12:30:37.7	31.9
TIK11	28.7.16 07:26:12.7	6.5.17 16:45:43.1	31.9
TIK12	29.7.16 03:10:42.7	3.12.16 17:08:37.7	14.4
TIK13	29.7.16 06:47:12.7	7.5.17 16:00:10.1	31.9
LD004	25.7.16 031206.4	24.4.17 21:21:14.2	30.9
LD007	25.7.2016 04:19:45	3.5.17 14:18:53	31.9
LD008	25.7.16 12:14:16.7	25.4.17 05:05:43.4	30.9
LD010	26.7.16 08:16:15.9	25.4.17 20:40:18.8	30.9
LD011	31.7.16 07:54:06.7	9.5.17 18:16:17.9	31.9
LD012	27.7.16 05:06:40.8	5.5.17 15:06:09.1	31.9
LD014	25.7.16 07:03:15.7	24.4.17 19:20:02.9	30.9
LD015(B)	30.7.16 04:21:03.7	29.4.17 17:17:05.9	30.9
LD016(C)	1.8.16 05:08:42.7	10.5.17 16:57:33.5	31.9
LD018	28.7.16 08:04:14.8	2.5.17 13:18:52.4	31.9
LD019(D)	3.8.16 01:58:43.7	3.5.17 14:16:55.4	30.9
LD021	29.7.16 02:37:15.8	28.4.17 15:44:28.8	30.9

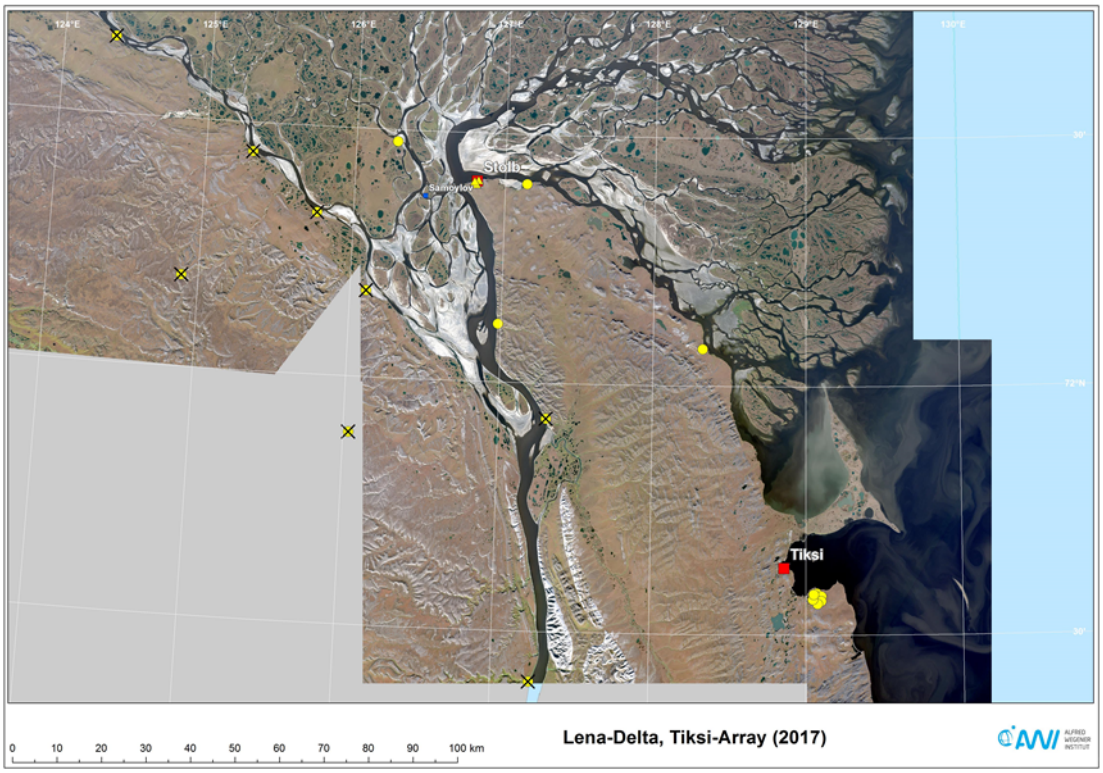

Figure 2.21-1: *Map of the study area showing the temporary station distribution for 2017/18 (yellow dots). Crosses mark stations that were dismantled in 2017. Red squares mark positions of permanent observatories Tiksi and Stolb.*

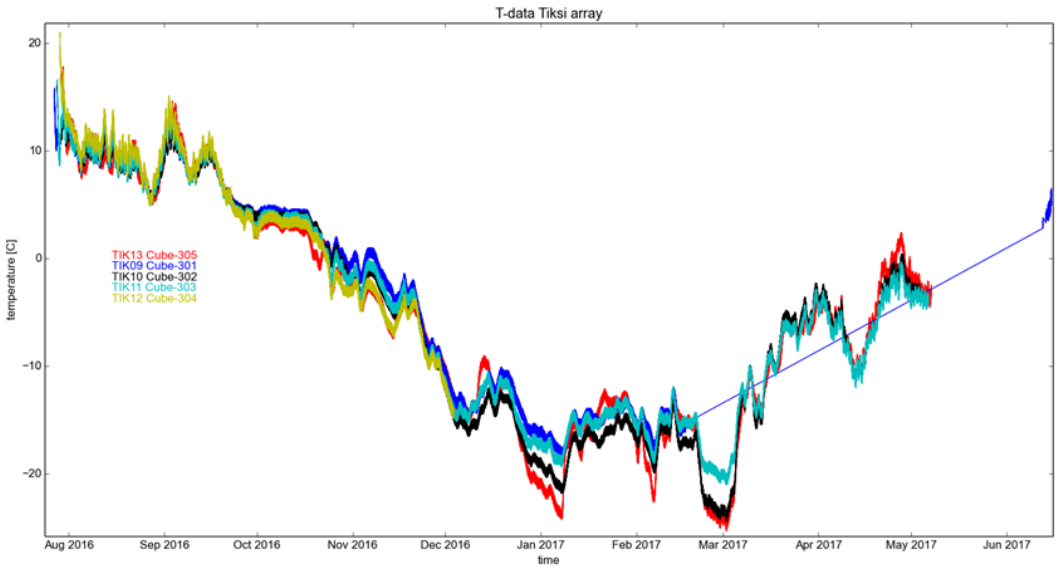

Figure 2.21-2: *Temperature data at selected sites of the Tiksi array*

Figure 2.21-3: *Photograph illustrating the configuration of the Stolb array*

Acknowledgments
We are grateful to our Russian and German colleagues who helped to start the experiment. Instruments were provided by Geophysical Instrument Pool Potsdam (GIPP). We appreciate also the support of the Melnikov Permafrost Institute Yakutsk, which made their vessel available to us. We thank the captain and crew of the vessel Merslotoved as well as all people of the Samoylov Island Station.

2.22 Characteristics of wave-built sedimentary archives in Buor Khaya Bay

Lasse Sander[1], Rune Michaelis[1], Svenja Papenmeier[1], Sergey Pravkin[2], Karen H. Wiltshire[1]

[1] Alfred Wegener Institute Helmholtz Centre for Polar and Marine Research, Sylt, Germany

[2] Arctic and Antarctic Research Institute (AARI), St. Petersburg, Russian Federation

Fieldwork period and location
August 15th to August 20th, 2017 (Buor Khaya Bay, southern Laptev Sea)

Objectives
Sequences of prograded beach deposits (so-called beach-ridge systems) are a wave-built coastal geomorphological feature of global occurrence. The deposits may preserve information on the environmental conditions during their formation and have been used as archives for the reconstruction of parameters such as relative sea-level, wave climate, extreme events, sediment supply or sea-ice extent (see e.g. Funder et al., 2011; Tamura, 2012; Sander et al., 2016). Buor Khaya Bay is one of the few places along the Russian arctic coast, where wide beach-ridge systems exist. The area was visited during an expedition in August 2017 in order to obtain baseline information on the morphology, lithology and surface properties at the different field sites (Figure 2.22-1). The overarching aim of the field campaign was to establish the potential of the beach-ridge systems for paleoenvironmental reconstructions of Holocene sea level and past sea-ice extent. A couple of other sedimentary systems (spits, barriers and coastal lagoons), which may serve as complementary archives for long-term coastal change, were likewise visited.

Methods
Basic field surveys of beach geomorphology, grain-size distribution, cross-ridge elevation and vegetation were conducted. Data collection was supplemented by GPS-RTK (Global Positioning System-Real Time Kinematic) measurements and Kite Aerial Photography (KAP) surveys. The analysis of Landsat satellite images provided background data for the assessment of the spatial arrangement of landforms and basic environmental properties at the field sites. The area was accessed by boat.

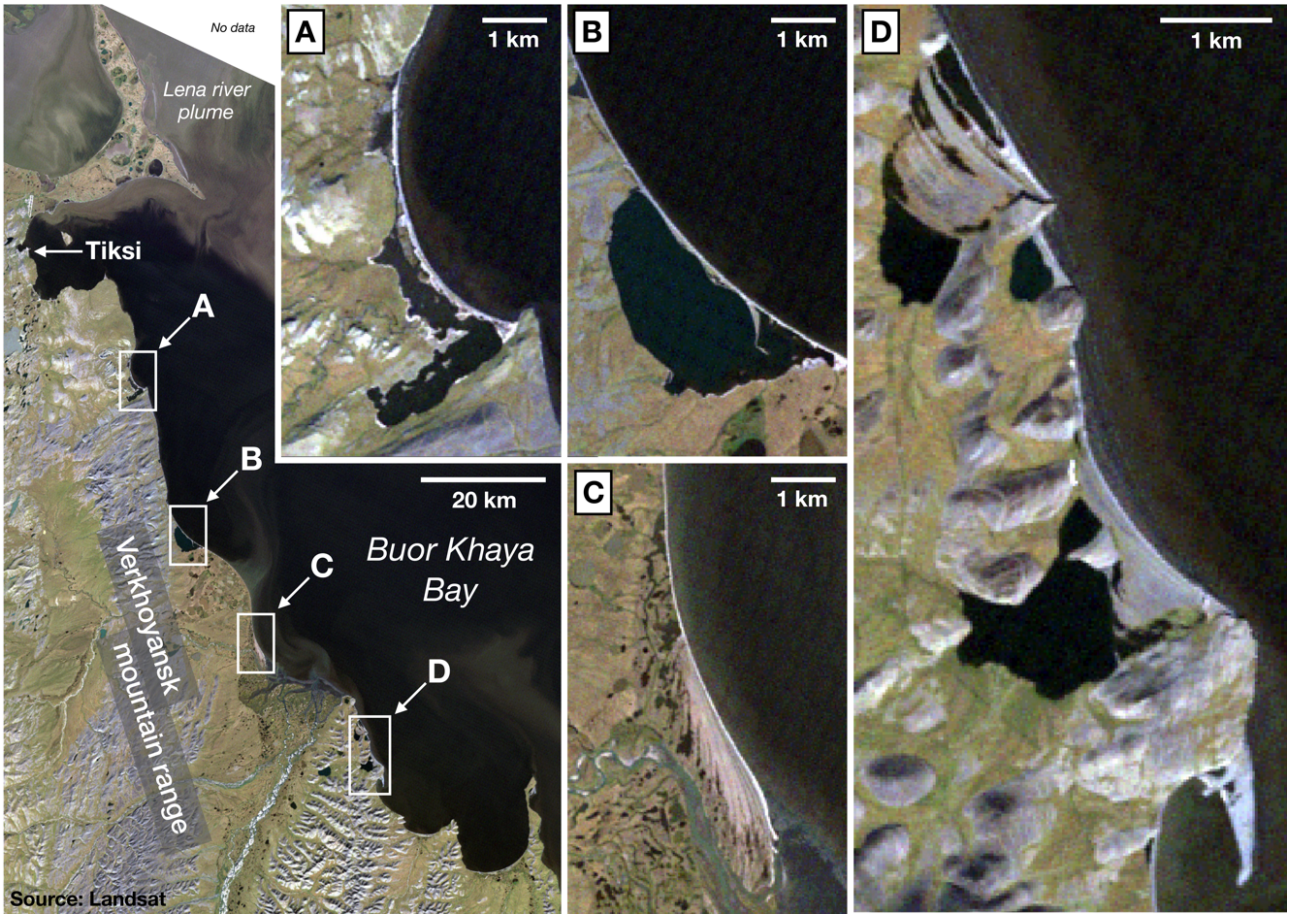

Figure 2.22-1: *The southwestern shoreline of Buor Khaya Bay is located at the transition of the Verkhoyansk mountain range and the southern Laptev Sea. Several lagoons (A, B, D), barriers (A, B, C), spits (B, C, D) and beach-ridge systems (C, D) formed in topographic depressions within the denudated mountain relief. Weathering products from protruding headlands and cliffs are the most important source of sediment for the formation of wave-built deposits. Image source: Landsat OLI color composite*

Preliminary results

The modern shoreline at both beach-ridge sites (Figure 2.22-1 D) is composed of a low gradient upper shoreface with longshore bars primarily composed of sands and gravels, and a steeply inclined beachface characterized by pebble to cobble sized material and the presence of ample amounts of debris (driftwood, anthropogenic debris). The headlands show clear indication of wave erosion (in the form of active and palaeocliffs) and thick layers of regolith cover the slopes. The minerogenic beach deposits are composed of shales and are probably of local origin, given their high degree of similarity (color, lithology) with the weathering products from the bedrock cliffs. No aeolian deposits were observed. The elevation and composition of the beach deposits suggests a construction during energetic (storm-) wave conditions. Both systems can be divided into distinct sets of ridges, suggesting (1) continuous progradation under conditions of high sediment availability, and (2) unconformities evidencing periods with an increase in allogenic perturbation or reduced sediment supply. The beach ridges lie at elevations of between 2 and 5 m above mean sea level and are separated by swales (Figure 2.22-2). Material for the establishment of age control was sampled in the field.

The slim barriers at the lagoon sites A and B are much lower and indication of recent barrier breaching and overwashing have been observed. Patterns of resilience and disturbance are reflected in the species distribution within the sparse vegetation cover.

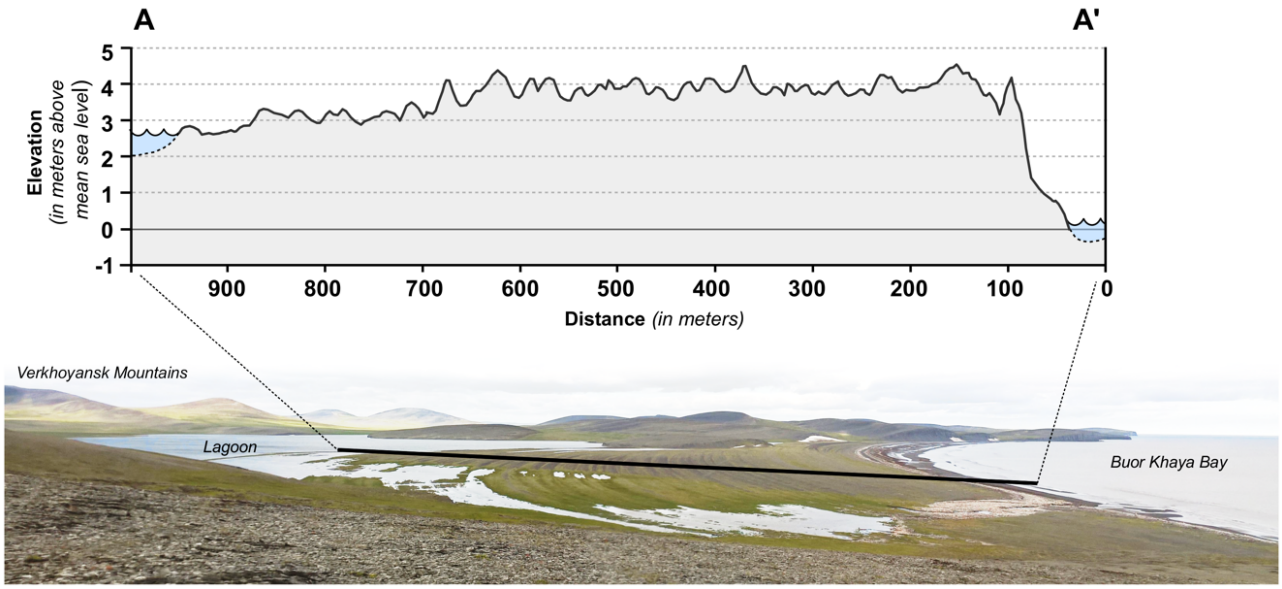

Figure 2.22-2: *Elevation transect and panoramic overview of the southern beach-ridge system (see Figure 2.22-1 D for location)*

The observations made during this first expedition to southwestern Buor Khaya Bay have shown that all visited field sites have a great potential for further investigation and the information obtained will be used to plan and design more directed and comprehensive field investigations in the near future.

2.23 Investigation of thermal erosion of Yedoma Ice Complex deposits on Kurungnakh Island and characterization of land surface types for thermal and hydrological modeling of thermo-erosional valleys

Jan Nitzbon[1], Anne Morgenstern[1], Katharina Anders[2], Oliver Kaufmann[3], Stephan Lange[1], Julia Boike[1], Sebastian Laboor[1]

[1] Alfred Wegener Institute Helmholtz Centre for Polar and Marine Research, Potsdam, Germany

[2] University of Heidelberg, Heidelberg, Germany

[3] University of Hamburg, Hamburg, Germany

Fieldwork period and location
August 20th to September 23rd, 2017 (on Kurungnakh Island)

Objectives
During this field campaign, two main project goals were mostly pursued. The first major goal of the project aimed at improving the understanding of how thermal erosion develops, changes ice-rich permafrost landscapes and impacts their hydrological regime and carbon budget by the investigation of several thermo-erosional valleys in the Lena River Delta. The Yedoma Ice Complex deposits of the third geomorphological main terrace of the Lena Delta are prone to degradation by thermal erosion and features numerous thermo-erosional valleys and gullies that have developed during the Holocene. On Kurungnakh Island, short thermo-erosional ravines are actively developing along the eastern cliff of the island that is being eroded by the Olenekskaya Channel. More inner parts of the island are affected by longer and mostly stabilized thermo-erosional valley networks. Thus, the objectives of the field campaign were to quantify the morphometry of thermo-erosional valleys and ravines by measuring longitudinal and transverse profiles as well as the spatial extent of current thermo-erosional activity and the impact of current thermo-erosional activity on the hydrochemical composition of associated stream waters. Embedded in and closely connected with these first major study objectives was the second goal of the campaign with the aim to characterize different types of landscape covers within the catchment of one of these thermo-erosional valleys on Kurungnakh Island to enable the representation of the thermal and hydrological dynamics of these landforms within process-based land surface models. The collected data are used on the one hand to better constrain model input parameters and on the other hand for validation of novel model features. Besides this the characterization of the catchment also contributes to a better understanding of thermokarst and thermal erosion processes of the Yedoma Ice Complex on Kurungnakh Island.

Methods
For three thermo-erosional ravines and valleys longitudinal and transverse profiles were measured using a Leica Viva GNSS. Active layer measurements were conducted at all profile measurement points using a standard active layer measurement rod. Surface water samples were collected from the valley streams at strategically relevant points like source areas from upstream water tracks, junctions of stream branches, after strongly eroding valley parts. At the sampling sites, water temperatures were measured and overall conditions of the water, weather, and time of the day were noted. Where possible, discharge was estimated by filling a bucket with milliliter scale and stopping the time. Additionally, samples from snow patches were taken and melted in the lab.
In one of these valleys further methods have been applied to characterize the surface and subsurface physical parameters to later implement these data in process-based land surface models. Therefore,

four distinct sites within a catchment of this thermo-erosional valley on Kurungnakh were selected and investigated (Figure 2.23-2). At each site, a detailed set of field parameters has been determined at a central location, in addition spatially distributed measurements have been performed. All in this specific valley conducted measurements are completely listed again in the following:

- Spatially distributed measurements of active layer thickness (ALT), water tables (WT) soil stratigraphies, soil temperatures, soil moistures, soil thermal properties at each site
- Determination of density, porosity, water/ice content and soil thermal properties using soil specimens from different soil layers of each site
- Drilling of sediment cores at each site to analyze grain size distributions, ice contents, total organic carbon content and stable isotopes
- Terrestrial laser scanning (TLS) of the surface microtopography and vegetation cover at each site
- Differential GPS (DGPS) measurements of the longitudinal and cross profile of the investigated valley

Preliminary results

All water samples were measured in the lab of the Research Station Samoylov Island for pH and electrical conductivity using a WTW Multilab 540. Subsequently, they were divided into subsamples for hydrogeochemical analyses in the labs of AWI Potsdam (stable water isotopes, dissolved organic carbon (DOC)) as well as a backup sample. The subsample for DOC analyses were filtered and acidified in order to conserve them until final lab analyses. An overview of the water sampling sites and planned analyses is given in Figure 2.23-1 and Table A.2-22. For a better overview, further samples (17 - 47) taken in the Lena River Delta were additionally added to the list in Table A.2-22.

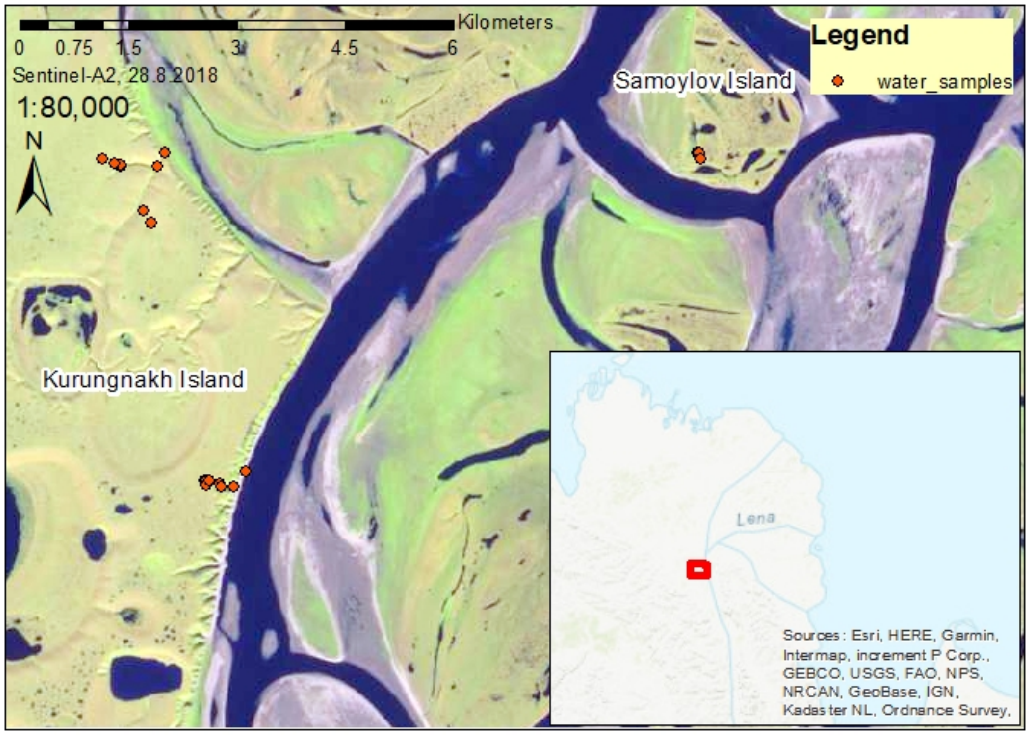

Figure 2.23-1: *Location of water sampling sites*

At the four specific investigated sites A-D (Figure 2.23-2) in one of the valleys, the desired parameters could be sampled. Each of these sites is representative for a specific land surface type in the catchment of the valley: intact ice complex plateau (site C), water track network at the upper part of the valley (site D), slopes (site A), valley floor (site B). First results show that the magnitude and variance of crucial parameters such as ALT differ significantly between the different sites (Figure 2.23-3). The soil specimens of the active layer and frozen ground have been analyzed in the laboratory on Samoylov and the determined properties are in line with previous findings for Kurungnakh. The 1 - 2 m sediment cores have been roughly characterized based on visual inspection, while a more detailed analysis is going to be undertaken in the scope of a Bachelor's thesis. The complementary DGPS and TLS data are going to be used in combination with digital elevation models (e.g., Arctic DEM) for a detailed characterization of the meso- and microtopography of the investigated catchment. First results prove the high quality of the acquired data (Figure 2.23-4). An overview of all geodetic survey data taken during the expedition is given in Table A.2-23 and Table A.2-24.

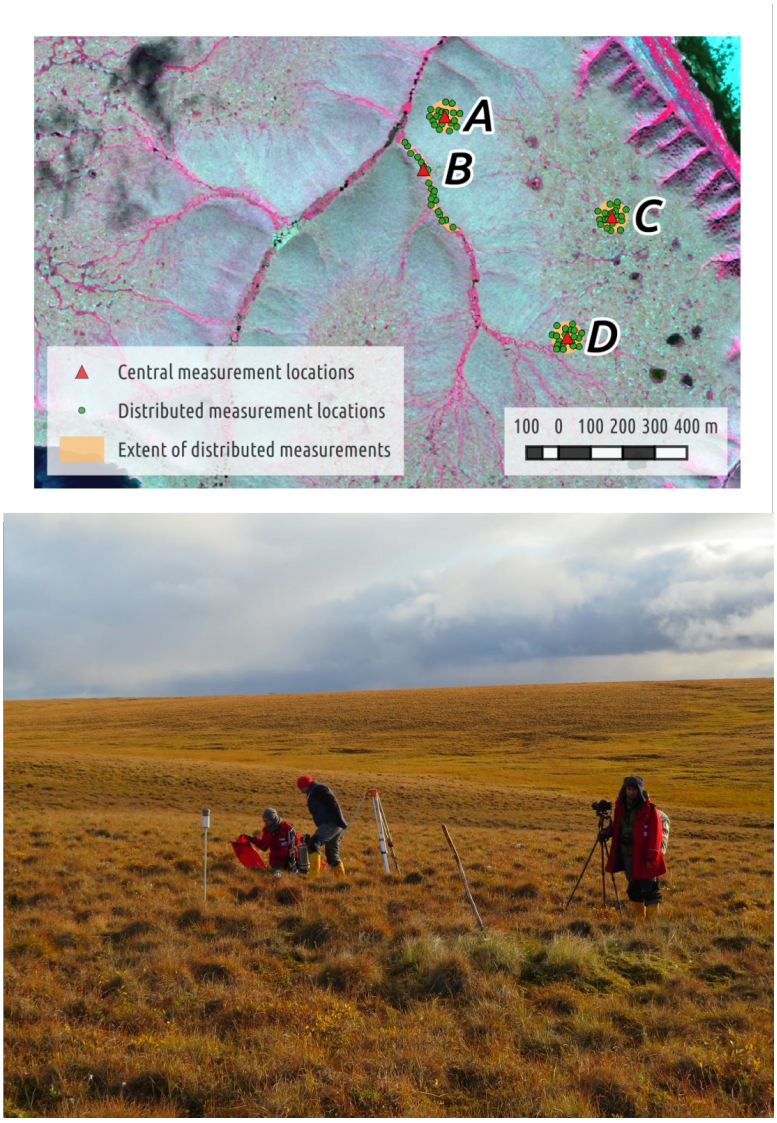

Figure 2.23-2: *Top: False-color satellite image of the investigated catchment on Kurungnakh with the four measurement sites indicated which represent different parts of the land surface (A: slope, B: valley floor, C: upper plateau, D: water tracks). Bottom: Photo showing the investigated valley.*

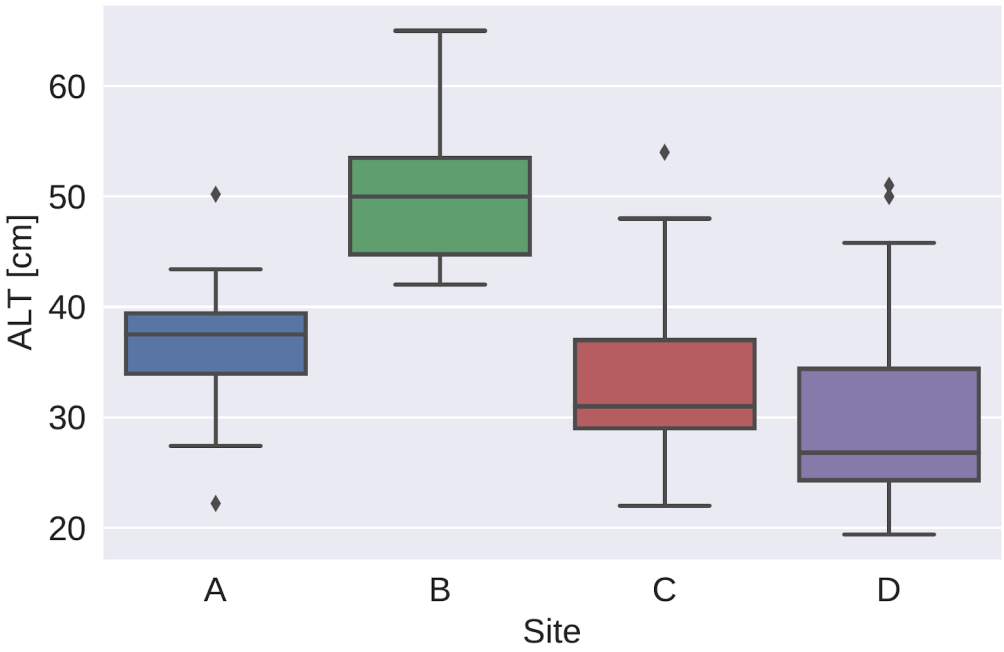

Figure 2.23-3: *Boxplots of the distributions of active layer thicknesses for the different sites*

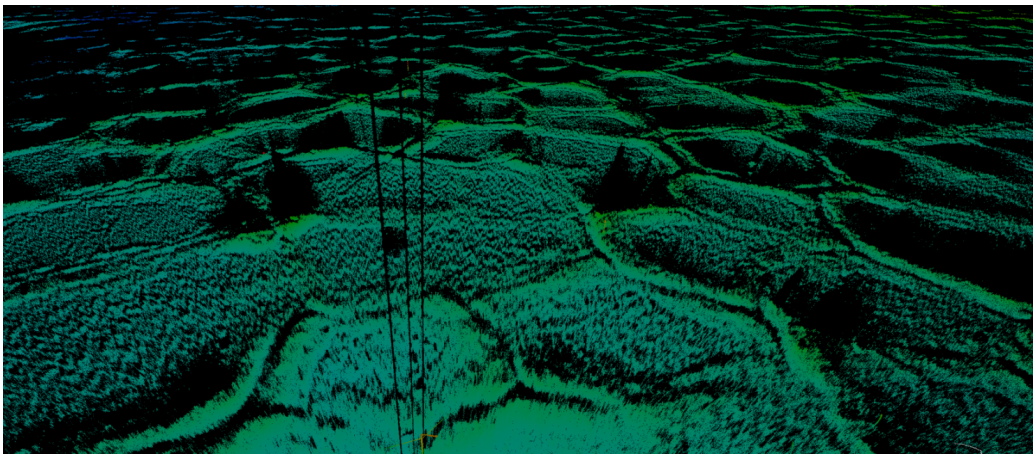

Figure 2.23-4: *Point cloud generated from a laser scan position within the polygonal tundra of Samoylov. Comparable scans have been conducted in the vicinity of the measurement sites A-D on Kurungnakh.*

2.24 Geomorphological investigations in the Lena River Valley: Lena Delta as a result of the river and the sea interaction

Dmitry Bolshiyanov[1], Sergey Pravkin[1]

[1] Arctic and Antarctic Research Institute (AARI), St. Petersburg, Russian Federation

Fieldwork period
June 30th to July 30th, 2017 (on the banks of the Lena River from Yakutsk to Lena Delta, Samoylov Island and the banks of Aldan River)

Objectives
Geomorphological and geological structure of the Lena River valley and Low Aldan River valley for paleogeographical reconstructions. An attempt to determine the role of the main river valley in the formation of the Lena River Delta.

Methods

- Geomorphological investigations (mapping)
- ^{14}C Dating
- OSL Dating
- Quaternary sediments studying
- Spore and pollen analyses
- Diatom analysis

Preliminary results
The Lena River, the longest and full-flowing river in Eastern Siberia, became an object of investigation at the 20th annual 1998 Russian-German expedition to the shores of the Laptev Sea. Since then, the structure and development of the Lena River Delta is the main target of research. Within this framework, the marine factors affecting the delta were widely investigated and published by Bolshiyanov et al. (2013). However, there is still a lack of understanding of the interaction between the river (Lena River) and the sea (Laptev Sea) during the different stages of delta evolution.
In 2014, within the framework of the Russian-German expedition, the research was focused on the lower part of the river, stretching from the delta to the village of Kyusyur. In 2016, a voyage from Yakutsk to the mouth of the Vilyui River (approx. 400 km) was undertaken on a rubber boat. The journey was then continued on the ”Merzlotoved” vessel from the Permafrost Institute (additional approx. 1,150 km). During this period, more than 1000 km of the banks were described, of which more than 20 sites were studied in detail, several dozen samples were selected for their dating and study by spore-pollen and diatom analysis.
In 2017, only the ”Merzlotoved” vessel was used to study the banks of the Lena River (Table A.2-25, Figure 2.24-1).
But first we took a trip to the banks of the Aldan River, the main tributary of the Lena. Several outcrops in the area of the village of the Ust’-Tatta (Bulun) were studied there, include the ”Mammoth Mountain”, well-known in geomorphological literature. The main purpose was to date the sediments composing the 60 meter and 100 meter high terraces of the Aldan River, and to clarify the data available in the literature.

In the quarry, a section of ancient sand deposits was studied in the vicinity of the Yakutsk, near the Big Chabada Lake, at an altitude of 160-165 m above the Lena River. We assume that these deposits date to the pre-Quaternary age and, possibly, are marine sediments.
The next stage of the voyage was along the Lena River on the ”Merzlotoved”. One of the objectives was to update the last year’s data, e.g. the dating of a wooden sample recovered from 9 - 10 m high terrace deposits at the mouth of the Vilyuy River. Downstream, there is an interesting area where the Lena River splits into numerous branches, which in turn divides the land into thousands of islands, of which the Ulahan-Kistiah Island was studied. Samples were taken for spore-pollen analysis and radiocarbon dating. In the same area, the right bank of the Lena was also explored, which is a 12-13-meter rock-defended terrace.
The following significant points (3 outcrops) were studied downstream from the village of Zhigansk, from the river Menkere to Natara. Next to the mouth of the Menkere River In a steep cliff of 60 - 65 meters of sandstone terrace there are several small paleovalleys, filled with deposits of sand and silt. Their bottom is much higher than the modern water level in Lena.
The Duoldanga-Aryita Island is located between the mouths of the Menkere and Natara Rivers, 550 km away from the Lena River Delta. This island is characterized by the fact that its lower region is partly composed of a ”sloenka”, which is an undecomposed moss-vegetable remain. ”Sloenka” is widespread in the Lena Delta, where it features on Samoylov Island. It can be concluded that this part of the river valley should have some resemblance to the delta in its structure and age of formation.

Figure 2.24-1: *Map showing the location of sampling points*

2.25 Bibliography

Abnizova A., Siemens J., Langer M., Boike J. (2012): Small ponds with major impact: The relevance of ponds and lakes in permafrost landscapes to carbon dioxide emissions. Global Biogeochem. Cycles 26. doi:10.1029/2011GB004237

Adrian R., O'Reilly C.M., Zagarese H., Baines S.B., Hessen D.O., Keller W., Livingstone D.M., Sommaruga R., Straile D., Donk E.V., Weyhenmeyer G.A., Winder M. (2009): Lakes as sentinels of climate change. Limnol Oceanogr 54 (6, 2), pp. 2283–2297.

Alekseev V.R., Tsalolikhin S.Y., editors (2010): Guide of freshwater zooplankton and zoobenthos of European Russia. Zooplankton, vol 1. Moscow: KMK Press. [In Russian]

Ask J., Karlsson J., Persson L., Ask P., Byström P., Jansson M. (2009): Terrestrial organic matter and light penetration: Effects on bacterial and primary production in lakes. Limnol. Oceanogr. 54, pp. 2034–2040. doi: 10.4319/

Avetisov G.P. (1999): Geodynamics of the zone of continental continuation of Mid-Arctic earthquakes belt (Laptev Sea). Phys. Earth Planet. Inter. 114, pp. 59–70.

Bailey A., Noone D., Berkelhammer M., Steen-Larsen H. C., Sato P. (2015): The stability and calibration of water vapor isotope ratio measurements during long-term deployments. Atmos. Meas. Tech. 8, pp. 4521-4538. doi:10.5194/amt-8-4521-2015

Balushkina E.V. , Winberg G.G. (1979): The relationship between weight and body length in planktonic animals. General principles of the study of aquatic ecosystems. L. Nauka, pp. 169 - 172 (in Russian).

Bartelt P., Lehning M. (2002): A physical SNOWPACK model for the Swiss avalanche warning: Part I: numerical model. Cold Regions Science and Technology 35 (3), pp. 123-145.

Bischoff J., Mangelsdorf K., Gattinger A., Schloter M., Kurchatova A., Herzschuh U., Wagner D. (2013): Response of methanogenic Archae to Late Pleistocene and Holocene climate changes in the Siberian Arctic. Global Biogeochemical Cycles 27 (2), pp. 305-317.

Bobrova O., Fedorova I. , Chetverova A., Potapova T., Dmitriev V., Runkle B., Morgenstern A., Eulenburg A. (2014): Current dissolved organic carbon content in the Lena delta in comparison with historical data for East Siberian Arctic Rivers. Proceedings of International conference THAW 2014 - Thermokarst Aquatic ecosystems Workshop. 12-15 March 2014, Quebec City, Canada. http://www.cen.ulaval.ca/thaw2014/document/THAW_2014_full_programme.pdf

Boike J., Kattenstroth B., Abramova K., Bornemann N., Chetverova A., Fedorova I., Fröb K., Grigoriev M., Grüber M., Kutzbach L., Langer M., Minke M., Muster S., Piel K., Pfeiffer E. M., Stoof G., Westermann S., Wischnewski K., Wille C., Hubberten H. W. (2013): Baseline characteristics of climate, permafrost and land cover from a new permafrost observatory in the Lena River Delta, Siberia (1998-2011). Biogeosciences 10, pp. 2105-2128.

Bolshiyanov D.Yu., Makarov A.S., Schneider W., Stoof G (2013): Origin and development of the Lena River Delta. SPb: AARI, p. 267.

Borutsky E.V, Stepanova L.A., Kos M.S. (1991): Key to identification of Calanoida from fresh waters. St-Petersburg: Nauka [In Russian].

Borutsky E.V. (1952): Crustaceans Freshwater Harpacticoids. Fauna of USSR Crustacea. Vol. 3. Moscow-Leningrad: AN USSR Publ [In Russian].

Brtek J., Mura G. (2000): Revised key to families and genera of the Anostraca with notes on their geographical distribution. Crustaceana 73, pp. 1037–1088.

Drachev S.S., Malyshev N.A., Nikishin A.M., (2010): Tectonic history and petroleum geology of the Russian Arctic Shelves: an overview. Petroleum Geology Conference series 7, pp. 591-619. doi: 10.1144/0070591.

Dussart B.H., Defaye D. (1983): Répertoire mondial des Crustacés Copépodes des eaux intérieures. Calanoïdes. Paris: CNRS Bordeaux.

Eosense (ed.) (2016): eosGPCO_2. eosGP Gas Probe and Software. User Manual. Dartmouth, Nova Scotia, Canada.

Fefilova E.B. (2015): Copepods (Copepoda). Fauna of the European North-East of Russia. Moscow: KMK Scientific Press.

Fofonova V., Zhilyaev I., Krayneva M., Yakshina D., Tananaev N., Volkova N., Wiltshire K.H. (2016): The water temperature characteristics of the Lena River at basin outlet in the summer period. Hydrology and Earth System Science Discussions. doi:10.5194/hess-2016-254.

Franke D., Hinz K., Oncken O. (2001): The Laptev Sea Rift. Mar. Petrol.Geol. 18, pp. 1083-1127.

Franke D., Krüger F., Klinge K. (2000): Tectonics of the Laptev Sea – Moma 'Rift' Region: Investigation with Seismologic Broadband Data. J. Seismology 4, pp. 99–116.

Fujita K., Koz'min B.M., Mackey K.G., Riegel S.A., McLean M.S., Imaev V.S. (2009): Seismotectonics of the Chersky Seismic Belt, eastern Sakha Republic (Yakutia) and Magadan District, Russia. Stephan Mueller Spec. Publ. Ser. 4, pp.117–145.

Funder S., Goosse H., Jepsen H., Kaas E., Kjær K.H., Korsgaard N.J., Larsen N.K., Linderson H., Lysså A., Möller P., Olsen J., Willerslev E. (2011): A 10,000-Year Record of Arctic Ocean Sea-Ice Variability—View from the Beach. Science 333, pp. 747-750. Doi: 10.1126/science.1202760.

Gaina C., Roest W.R., Müller R.D. (2002): Late Cretaceous-Cenozoic deformation of northeast Asia. Earth Planet. Sci. Lett. 197, pp. 273-286.

Geissler W.H., Shibaev S., Haberland C., Petrunin S., Krueger F., Peresypkin D., Vollmer D., Gukov S., Tuktarov R., Baranov B. (2017): Seismicity of the Laptev Sea Rift. In: Overduin P.P., Blender F., Bolshiyanov D.Y., Grigoriev M.N., Morgenstern A., Meyer H. Russian-German Cooperation: Expeditions to Sibiria in 2016. Berichte zur Polar- und Meeresforschung 709, pp. 103-107.

Gouttevin I., Langer M., Löwe H., Boike J., Proksch M., Schneebeli, M. (2018): Observation and modelling of snow at a polygonal tundra permafrost site: spatial variability and thermal implications. The Cryosphere Discuss., in review.

Grosse G., Morgenstern A., Ramage J. (2017): Sampling of Thermokarst and Thermoerosion Features to Characterize Soil Carbon Stocks, Ground Ice, and Surface Waters. In: Overduin P.P., Blender F., Bolshiyanov D.Y., Grigoriev M.N., Morgenstern A., Meyer H. Russian-German Cooperation: Expeditions to Siberia in 2016, Berichte zur Polar- und Meeresforschung 709 , pp. 51-55.

Jokat W., Ickrath M., O'Connor J. (2013): Seismic transect across the Lomonosov and Mendeleev Ridges: Constraints on the geological evolution of the Amerasia Basin, Arctic Ocean. Geophysical Research Letters 40 (19), pp. 5047-5051.

Kotov A.A, Ishida S, Taylor D.J. (2009): Revision of the genus Bosmina Baird, 1845 (Cladocera: Bosminidae), based on evidence from male morphological characters and molecular phylogenies. Zool J Linn Soc. 156, pp. 1–51.

Kovachev S.A., Kuzin I.P., and Soloviev S.L., (1994- engl. 1995): Short-term study of microseismicity in the GubaBuorkhaya, Laptev Sea, using ocean bottom Seismographs. Physics of the Solid Earth 30 (7/8), pp. 647-658.

Lal, R. (2016): Encyclopedia of Soil Science, Third Edition. Boca Raton: CRC Press.

Langer M., Westermann S., Walter Anthony K., Wischnewski K., Boike J. (2015): Frozen ponds: production and storage of methane during the Arctic winter in a lowland tundra landscape in northern Siberia, Lena River Delta. Biogeosciences 12, pp. 977-990.

Laverov N.P., Lobkovsky L.I., Kononov M.V., Dobretsov N.L., Vernikovsky V.A., Sokolov S.D., Shipilov E.V. (2013): A geodynamic model of the evolution of the Arctic basin and adjacent territories in the Mesozoic and Cenozoic and the outer limit of the Russian Continental Shelf. Geotectonics 47 (1), pp. 1-30.

Lieder U. (1996): Crustacea: Cladocera/Bosminidae. Süsswasserfauna von Mitteleuropa. Stuttgart: Fischer Verlag.lo.2009.54.6.203

Overduin P., Blender F., Bolshiyanov D.Y., Grigoriev M.N., Morgenstern A., Meyer H. (2017): Russian-German Cooperation: Expeditions to Siberia in 2016, Berichte zur Polar- und Meeresforschung = Reports on polar and marine research. Bremerhaven: Alfred Wegener Institute for Polar and Marine Research 709, p. 295.

Peterson B.J., Holmes R.M., McClelland J.W., Vörösmarty C.J., Lammers R.B., Shiklomanov A.I., Shiklomanov I.A., Rahmstorf S. (2002): Increasing River Discharge to the Arctic Ocean. Science 298, pp. 2171-2173. Doi: 10.1126/science.1077445.

Pienitz R., Doran P.T., Lamoureux S.F. (2008): Origin and geomorphology of lakes in the polar regions. In: Vincent W.F., Laybourn-Parry J.: Polar Lakes and Rivers. Limnology of Arctic and Antarctic Aquatic Ecosystems. Oxford: Oxford University Press, pp. 25–41.

Prowse T.D., Wrona F.J., Reist J.D., Gibson J.J., Hobbie J.E., Lévesque L.W.J., Vincent W.F. (2006): Climate Change Effects on Hydroecology of Arctic Freshwater Ecosystems. Ambio 35 (7), pp. 347-358.

Raupach T. H., Berne A. (2015): Correction of raindrop size distributions measured by Parsivel disdrometers, using a two-dimensional video disdrometer as a reference. Atmospheric Measurement

Techniques 8 (1), pp. 343-365.

Rylov V.M. (1948): Cyclopoida of the fresh-water. Fauna of USSR. Crustacea, 2. Moscow-Leningrad: AN USSR Publ. [In Russian].

Sander L., Hede M.U., Fruergaard M., Nielsen L., Clemmensen L.B., Kroon A., Johannessen P.N., Nielsen L.H., Pejrup M. (2016): Coastal lagoons and beach ridges as complementary sedimentary archives for the reconstruction of Holocene relative sea-level changes. Terra Nova 28 (1), pp. 43-49. Doi: 10.1111/ter.12187.

Schuur E. a. G., McGuire A.D., Schädel C., Grosse G., Harden J.W., Hayes D.J., Hugelius G., Koven C.D., Kuhry P., Lawrence D.M., et al. (2015).: Climate change and the permafrost carbon feedback. Nature 520, pp. 171–179.

Seekell D.A., Lapierre J.F., Ask J., Bergstrom A.K., Deininger A., Rodrıguez P., Karlsson J. (2015): The influence of dissolved organic carbon on primary production in northern lakes. Limnol. Oceanogr. 60, pp. 1276-1285. DOI: 10.1002/lno.10096

Sinev A.Y. (1999): Alona werestschagini sp. n., new species of genus Alona Baird, 1843, related to A. guttata Sars, 1862 (Anomopoda, Chydoridae): Arthropoda Sel. 8, pp. 23–30.

Sinev A.Y. (2002): A key to identifying cladocerans of the genus Alona (Anomopoda, Chydoridae) from the Russian European part and Siberia. Zool Zhurnal. 81, pp. 926–939.

Sinev A.Y. (2009): Notes on morphology and taxonomic status of some North American species of the genus Alona Baird, 1843 (Cladocera: Anomopoda: Chydoridae). Hydrobiologia 175, pp. 59–77.

Smirnov N.N. (1971): Chydoridae of the world fauna. Fauna SSSR, Rakoobraznye (Crustacea), 1. Leningrad: Nauka. [In Russian].

Smirnov N.N. (1995): Check-list of the Australian Cladocera (Crustacea). Arthropoda Sel. 4, pp. 3–6.

Smirnov NN. (1996): Cladocera: the Chydorinae and Sayciinae (Chydoridae) of the world. Guides to the identification of the microivertebrates of the continental waters of the world 11. Amsterdam: SPB Academically Publ.

Tamura T. (2012): Beach ridges and prograded beach deposits as palaeoenvironment records. Earth-Science Reviews 114 (3), pp. 279-297.

Tarnocai C., Canadell J.G., Schuur E.A.G., Kuhry P., Mazhitova G., Zimov S. (2009): Soil organic carbon pools in the northern circumpolar permafrost region. Global Biogeochemical Cycles 23 (2): GB2023.

Tsibizov L., Fage A., Rusalimova O., Fadeev D., Olenchenko V., Yeltsov I., Kashirtsev V. (2017): Integrated non-invasive geophysical-soil studies of permafrost upper layer and aerial high-resolution photography. In: Overduin P., Blender F., Bolshiyanov D.Y., Grigoriev M.N., Morgenstern A., Meyer H.: Russian-German Cooperation: Expeditions to Siberia in 2016, Berichte zur Polar- und Meeresforschung 709, pp. 56-69.

Tsibizov L., Rusalimova O. (2017): Magnetic imaging of the Kurungnakh Island ice complex upper layer structure, Lena Delta, Russia. Near Surface Geophysics 15 (5), pp. 527-532.

Wotte A., Rethemeyer J. (2017): Carbon export from Siberian permafrost soils. In: Overduin P., Blender F., Bolshiyanov D. Y., Grigoriev M. N., Morgenstern A, Meyer H.: Russian-German Cooperation: Expeditions to Siberia in 2016. Reports on polar and marine research 709, p. 295.

Wotte A., Wischhöfer P., Wacker L., Rethemeyer J. (2017b): $^{14}CO_2$ analysis of soil gas: Evaluation of sample size limits and sampling devices. Nucl. Instrum. Methods Phys. Res. Sect. B Beam Interact. Mater. At. 413, pp. 51–56.

Wotte A., Wordell-Dietrich P., Wacker L., Don A., Rethemeyer J. (2017a): $^{14}CO_2$ processing using an improved and robust molecular sieve cartridge. Nucl. Instrum. Methods Phys. Res. Sect. B Beam Interact. Mater. At. 400, pp. 65–73.

Chapter 3

Drilling Campaign on Bykovsky Peninsula: Spring 2017

Edited by: Jens Strauss, Mikhail Grigoriev, Susanne Liebner, Dirk Wagner and Guido Grosse

3.1 Introduction

Jens Strauss[1], Mikhail Grigoriev[2,3]

[1] Alfred Wegener Institute Helmholtz Center for Polar and Marine Research, Potsdam, Germany

[2] Melnikov Permafrost Institute, Yakutsk, Russian Federation

[3] Trofimuk Institute of Petroleum Geology and Geophysics, Novosibirsk, Russian Federation

General scientific rationale and objectives
Permafrost thaw is associated with impacts on climate, land surface and coastal structures. Thermokarst and thermoerosion, for example, lead to ground subsidence and the development of thermoerosional valleys and thermokarst depressions which gradually transform into lakes and lagoons. Thereby, subaquatic permafrost exists underneath layers of taberite (*in situ* thawed, but not relocated deposits), lacustrine and potentially marine sediments. Periods of freeze-back may have led to even more complex stratigraphy and multiple talik generations.

Exposed to subaquatic conditions, permafrost thaw occurs exponentially and the associated extent of taliks and alterations of biogeochemical gradients are difficult to predict. Taliks are suggested to function as nutritious tanks for microbial activity and hence promote the production and release of methane and carbon dioxide.
This drilling campaign aimed to retrieve frozen and unfrozen sediment cores, ice cores as well as geophysical data from Bykovsky Peninsula (Figure 3.1-5) to cover several scientific disciplines including geomicrobiology, geocryology, geophysics and geochemistry. Thus, this project consists of several work packages (WP) (Figure 3.1-1):

- WP 1: Microbial processes and communities in thawing subaquatic permafrost
- WP 2: Organic matter and sediment composition of thawing permafrost
- WP 3: Holocene environmental variability
- WP 4: Ice-rich permafrost thaw under sub-aquatic conditions
- WP 5: Methane distribution and oxidation in ice cores
- WP 6: Ice core and sediment sampling for ice algae genetics

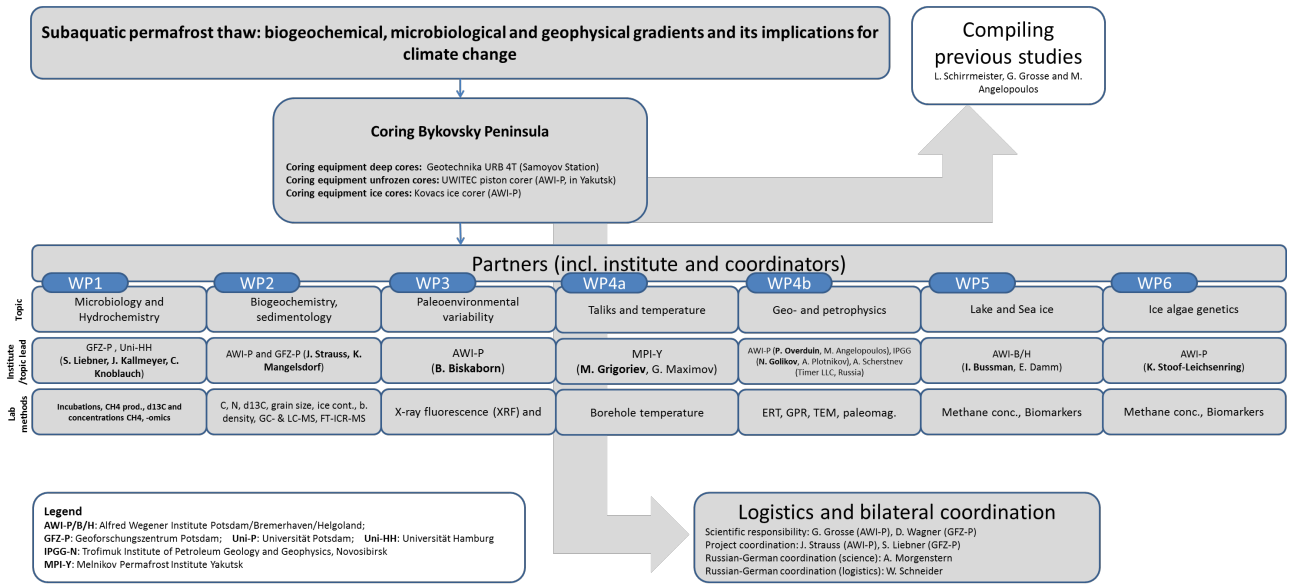

Figure 3.1-1: *Flow chart and work packages of the drilling project*

Expedition Itinerary and general logistics The fieldwork was separated into two expedition legs. In total 26 participants were part of the expedition with a maximum number of 22 at the same time (Figure 1-9 and 1-10). Six scientific institutions and three private companies (Figure 3.1-4) were involved in the joint fieldwork and logistic preparation. The camp (Figure 3.1-2 and 3.1-6) was moved between 3 priority locations.

Figure 3.1-2: *Vehicles during expedition. A: Camp consist of two cabins on sledges (balok) for accommodation, eating and generator sledge; B: Buran (snowmobile) for external sampling sites; c: two tractors for pulling the sledges and vezdekhod (caterpillar all-terrain vehicle) for field sites external of campsites*

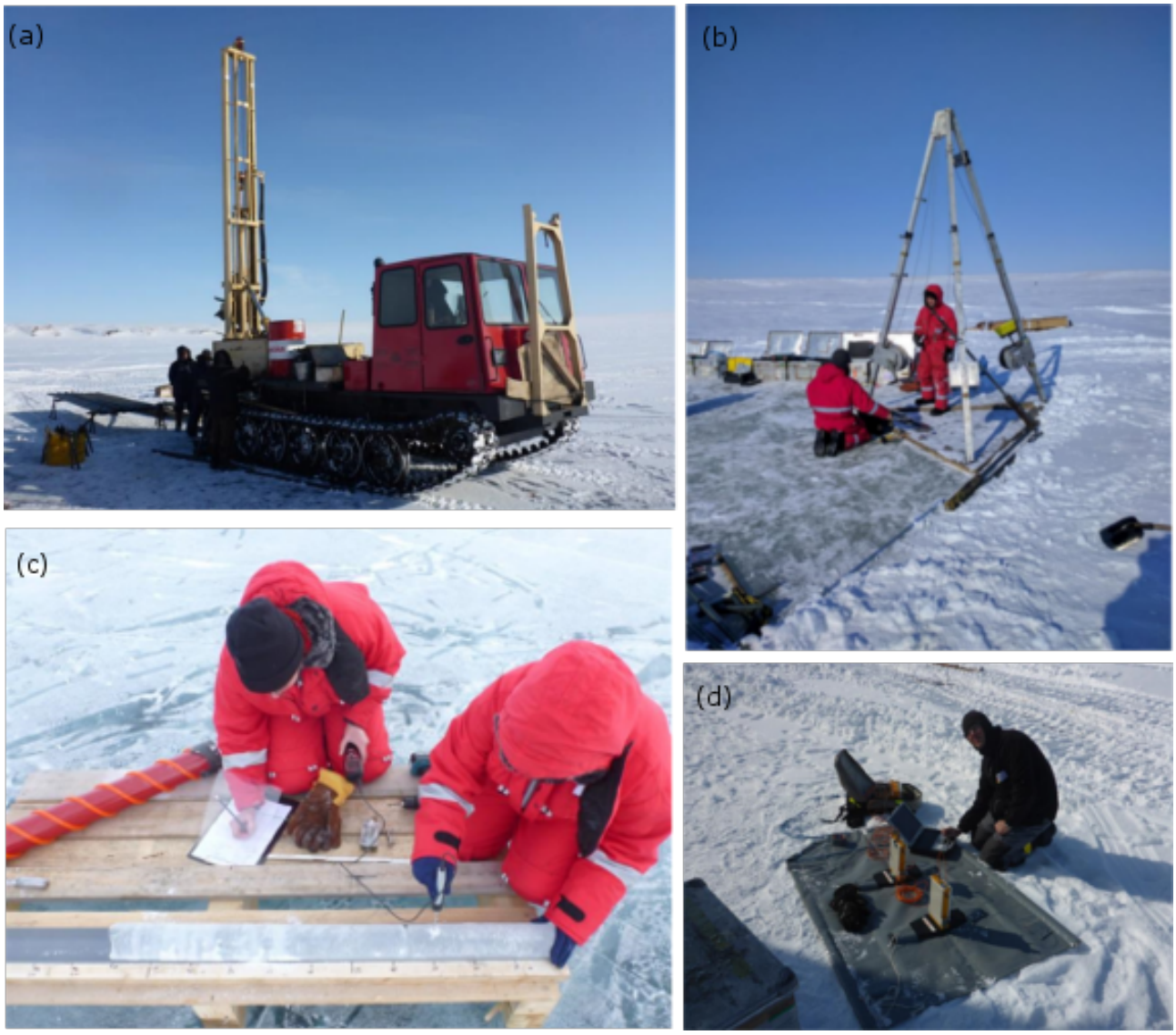

Figure 3.1-3: *Used coring and measuring equipment. a: URB2-4T drilling rig for deep cores >10m; b: Kovacs Mark II ice corer; c: UWITEC™ piston corer; d: Ground penetrating radar*

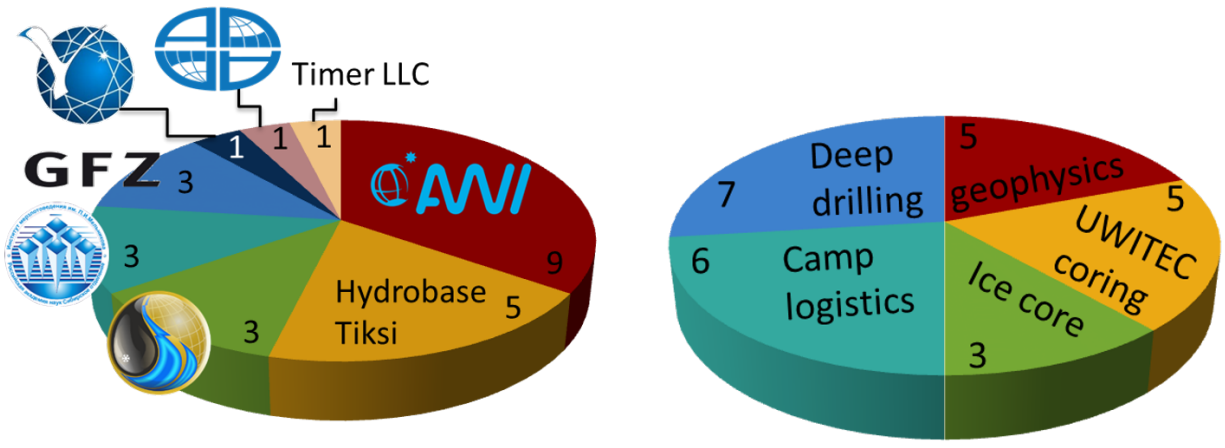

Figure 3.1-4: *Number of participants per (a) involved institute and (b) working group*

Itinerary

06.04.2017 Transfer Tiksi Uomullyakh-Kyuel Lagoon, beginning of fieldwork
07.04.2017 - 11.04.2017 Uomullyakh-Kyuel Lagoon
12.04.2017 Uomullyakh-Kyuel Lagoon, end of period 1 (ice coring group leave field site)
13.04.2017 Transfer Uomullyakh-Kyuel Lagoon to Polar Fox Lagoon, start of field period 2
13.04.2017 - 17.04.2017 Polar Fox Lagoon
18.04.2017 Transfer Polar Fox Lagoon to Goltsovoye Lake
19.04.2017 - 23.04.2017 Goltsovoye Lake
24.04.2017 Transfer Goltsovoye Lake to Tiksi, end of fieldwork

Bykovsky Peninsula

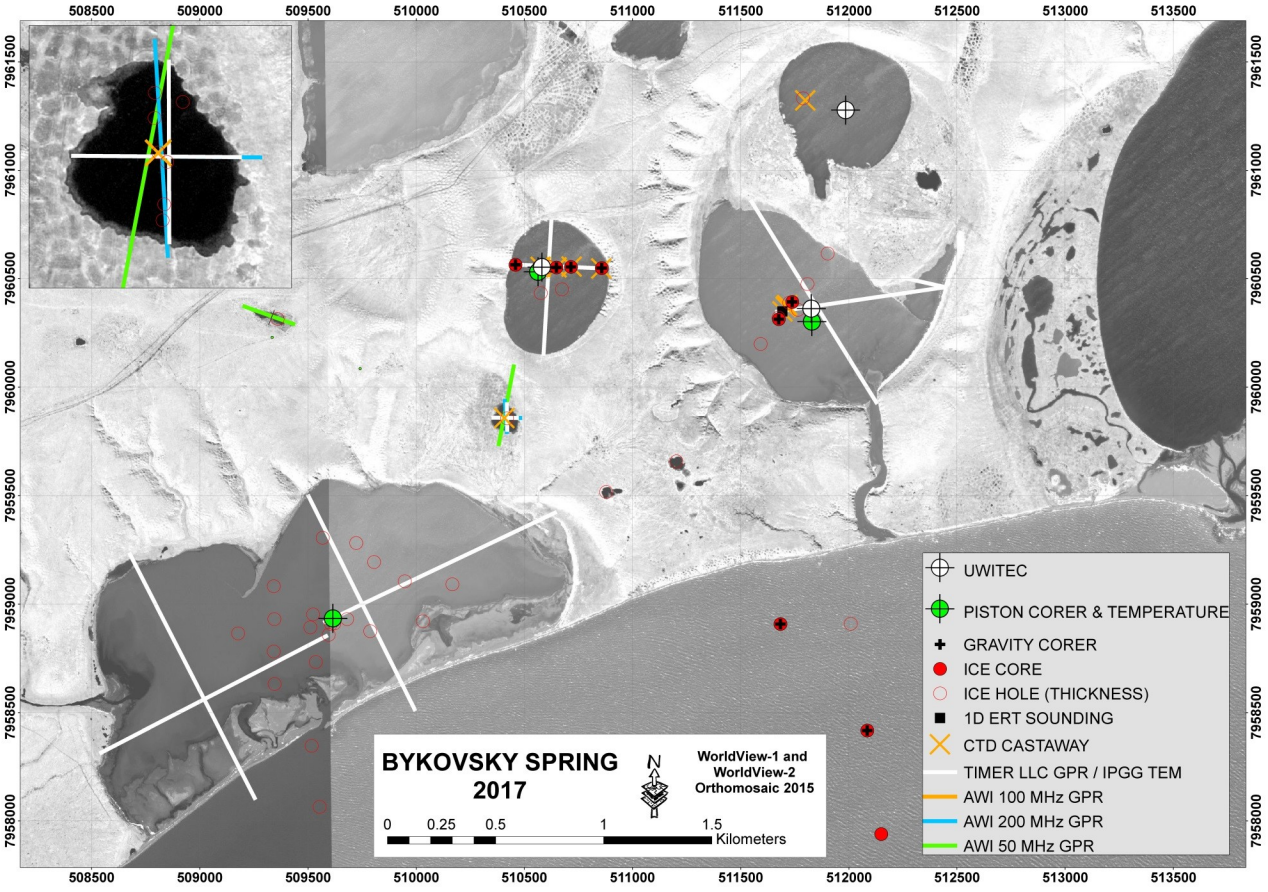

Figure 3.1-5: *Location of the drilling sites: Satellite image of the study area. The enlarged lake on the upper left side is the lake at the centre of the map. Map compiled by M. Angelopoulos.*

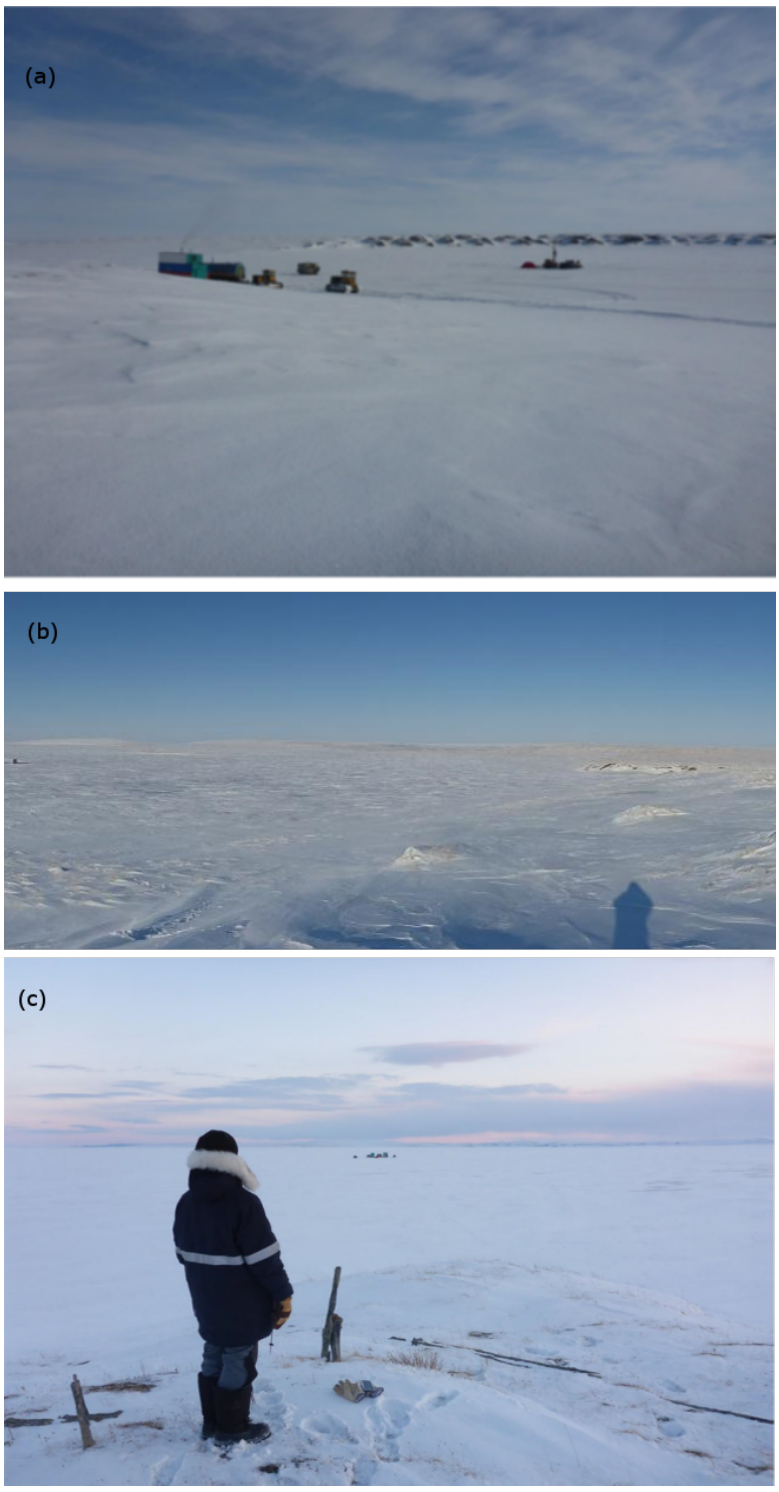

Figure 3.1-6: *Camp locations at the priority sites; a: Uomullyakh-Kyuel Lagoon, b: Polar Fox Lagoon, and c: Goltsovoye Lake*

The Bykovsky Peninsula is one of the oldest study sites of permafrost paleoenvironmental archives. In 1804 Michael Adams conducted the first scientific description of a mammoth cadaver detected at the east coast of Bykovsky Peninsula in 1796 (Adams, 1808). During the first International Polar Year (1881-84), Alexander Bunge conducted research excursions to the ice coast of Bykovsky Peninsula from the Russian polar station at Sagastyr Island in the Lena Delta (Bunge, 1895). It was also an important location for permafrost research at the end of the last century (Tomirdiaro and Chernenky, 1987; Kunitsky, 1989; Slagoda, 1991, 1993, 2004; Grigoryev, 1993, Fukuda 1994; Nagaoka, 1994).

During former Russian expeditions numerous exposures were studied along the Bykovsky Peninsula coasts and permafrost drilling transects were conducted in front of the coasts.

Geological background

Intensive vertical block tectonics and strong seismic activity characterize this terrain due to the position in the western margin of the Ust-Lena Rift (Grigoryev et al., 1996; Drachev et al., 1998). The position of the Bykovsky Peninsula in a zone of subsidence explains the large thickness of the Ice Complex in these locations (Ivanov and Katasonova, 1978). In general, the larger study region consists of two major geological segments. The Kharaulakh Range with heights up to 500 m a.s.l. represents the northern foothills of the Verkhoyansk Mountains. Farther east, the Bykovsky Peninsula represents remains of a former accumulation plain with elevations of up to 45 m a.s.l. The stratigraphic map of Sergienko et al. (2004) distinguishes two structural regions: The "Kharaulakhsky Rayon" (including the Khorogor Valley) with a general uplift tendency during the Pleistocene and Holocene, and the "Buorkhainsky Rayon" (including the Bykovsky Peninsula) with a general subsidence tendency.

The Kharaulakh Range consists mainly of permo-carboniferous sandstones and slates, which are characterized by strong dissection due to tectonic activity during the Cenozoic. In addition, neotectonic activity in the wider region is proven by seismic studies (Grigoriev et al., 1996; Drachev et al., 1998; Imaev et al., 2000; Franke et al., 2001). In 1998, 1999, 2000, and 2002 Russian-German teams studied this area several times (Andreev et al., 2002; Bobrov et al., 2004; Kienast et al., 2005; Siegert et al., 1999; 2002; Sher et al., 2000, 2005; Schirrmeister et al., 2001, 2002a/b, 2003; Wetterich et al., 2005). In addition, the area of the southern Bykovsky Peninsula was research object of Russian teams studying permafrost temperatures, organic carbon characteristics and thermokarst processes (Tumskoy 2001; Kholodov et al. 2003).

The modern morphology of the Bykovsky Peninsula results mainly from thermokarst and thermal erosion as well as from thermoabrasion of the coast. A well subdivided landscape with Yedoma hills (47 %) and numerous lakes within thermokarst depressions (46 %), and with thermo-erosional valleys (6 %) characterize this area (Grosse et al., 2005, 2007). Several pingos are located within thermokarst depression. Ice wedge polygon systems cover the bottom of this depression. Yedoma hills reach altitudes of up to 40 m a.s.l. Its surface is dissected by numerous thermo-erosional valleys and in places takes the form of small young thermokarst lakes.

On the western Bykovsky Peninsula boreholes cover sediment sequences from 25 m b.s.l. to 32.5 m a.s.l. (Grosse et al., 2007). According to Grigoriev (1993) and Slagoda (1993, 2004), the lowermost 25 m consists of early Quaternary fluvial coarse-grained sands and gravels with plant remains and a massive cryostructure. They are followed by 32 m of Ice Complex deposits, first by 5 m of early Weichselian alluvial interbeddings of silty sands, gravels, and silts with banded cryostructure and second by 27 m of middle and late Weichselian proluvial, silty fine sand deposits. The sequence is completed by 0.5 m of unfrozen Holocene soil on top. The slopes of Yedoma hills are often covered by about 1 m thick peaty deposits the middle Holocene age.

Recent research activities on the peninsula

A sediment core was also drilled in the Ivashkina Lagoon in spring 1999 (Schirrmeister et al, 2018). Several stages of landscape dynamics were reconstructed, starting with an initial Yedoma Ice Complex, locally thawed by thermokarst during the Late Glacial with subsequent lacustrine sedimentation. A final stage completed the landscape dynamics during the last few hundreds of years that characterized by lake drainage and lagoon development. Extrapolation the organic carbon inventory to the lagoons of the Bykovsky Peninsula we found 1.68 +- 0.04 million ton in the first 6 m of the lagoon sediments. In spring 2004, a second core was drilled by a Russian expedition to the Ivashkina Lagoon. Their results on grain-size analyses, mineral analyses, and thermophysial properties were published by Cheverev et al. (2007). Later in 2013 and 2014, in the frame of a Russian-American expedition two other cores were drilled in center and at the northern rim of

Ivashkina Lagoon (Ulyantsev et al., 2016a, b). Further results from these cores were presented by Ulyantsev et al. (2016c, 2017a, b), Drozdova et al. (2016), and Romankevich et al (2017). The major focuses of this project were methane and subsea permafrost studies in the East Siberian Arctic Shelf (Shakhova et al., 2015, 2017).

Field methods and sampling strategy

To give a broad overview, the following sampling and analyses were in the focus of the drilling campaign: Recovered sediment (unfrozen and permafrost) were packed and sealed in the field. Unfrozen core sections were partially subsampled in the field. E.g. sampling for gas concentration was performed immediately after core sections are sealed. Frozen and unfrozen sections of the cores were transported back to Potsdam, Germany. Descriptions of sediment recovery and of the sediment for the frozen sections were done in the field.

Complete sediment cores taken with an UWITEC^{TM} system were sampled and stored unfrozen in thermoboxes until they were transported to AWI and GFZ laboratories. The material of sediment cores will be used for sedimentological, geochemical, paleoecological, and paleogenetic analyses. Ice cores were taken close to sediment coring locations. Additionally, transects of ice cores from the coast into the marine realm were obtained by using the ice coring system. Ice cores were subsampled and/or processed or stored frozen in the field until further laboratory analyses. The ice cores will be used to investigate methane distribution and oxidation in ice and for the exploration of community changes in freshwater and marine ice algae.

The sample name code for the majority of the sediment samples is composed of the AWI standard general nomenclature. For the periglacial section we used the abbreviation PG, and the number are in the range of 2410 to 2426. One example of a sample name is PG2412.

3.2 Work package 1: Microbial processes and communities in thawing subaquatic permafrost

Susanne Liebner[1], Jens Kallmeyer[1], Axel Kitte[1], (Dirk Wagner[1], Christian Knoblauch, [2]: not in field)

[1] Helmholtz Center Potsdam – GFZ German Research Center for Geosciences, Potsdam Germany

[2] Universität Hamburg, Institute for Soil Science, Hamburg, Germany

Fieldwork period and location
From April 05th to April 24th, 2017 (on Bykovsky Peninsula)

Background and objectives
Currently 20 % of the northern permafrost region is covered by thermokarst lakes (Olefeldt et al., 2016). Their sediments are dominated by anaerobic conditions and provide excellent natural laboratories to study the response of the inherent microbial community to permafrost thaw spanning decades to millennia. Studies on anaerobic greenhouse gas (GHG) formation in permafrost landscapes are based on few incubation studies that revealed highly variable rates. Microbial GHG formation in Siberian thermokarst lake sediments are overall lacking. Also, anaerobic methane oxidation associated with permafrost thaw is proposed (Overduin et al., 2015, Winkel et al., 2018) but remains to be studied in detail. The working hypotheses of this WP are that 1) the quantification of microbial carbon decomposition as well as GHG production and consumption in thermokarst lake sediments will reduce uncertainties associated with the implementation of anaerobic carbon turnover processes in permafrost carbon feedback models, 2) microbial functions and community composition change in response to permafrost thaw, and 3) understanding timing and extent of these changes enables us to forecast the long-term response of microbial communities to permafrost thaw. The objectives of this WP are to integrate molecular biological and biogeochemical approaches for projecting the net GHG production in thermokarst landscapes of the Bykovsky Peninsula. We will assess the community response of microorganisms to long-term permafrost thaw and quantify microbial carbon decomposition, GHG production and the mitigation of GHG release.

Sampling and methods
This WP uses thawed, cryotic and ice-bonded sediments for molecular microbiological and biogeochemical analysis as well as for the quantification of carbon turnover processes including methanogenesis, anaerobic methane oxidation (AOM), and sulfate reduction. Up to 6 m long cores of the unfrozen thermokarst sediment column were recovered with a hammer-driven piston corer (UWITEC^{TM}) in overlapping 3 m sections as described in section 1.5. One UWITEC^{TM} core per site was subsampled in the field in 10 cm whole round cores. Sediment plugs for molecular analysis and for CO_2 and CH_4 concentrations as well as isotopes (δ 13C and δD) were retrieved with a sterile syringe and transferred to 15 ml Falcon tubes and serum bottles containing saturated NaCl-solution, respectively. The molecular samples were preserved with either RNA-later or through immediate freezing. Subsequently all whole-round cores were packed in N2-flushed bags on which a vacuum was applied and were stored at approx.4 °C. The deeper unfrozen and frozen sediments were recovered with a Geotechnika URB-4T rotary corer as described in section 3.3., Figure 3.1-5 and Table 3.2.1 illustrate sampling sites and methods of this WP, respectively.

Table 3.2.1: Overview of methods and approaches of work package 1 Microbial processes and communities in thawing subaquatic permafrost

Approach	Lab methods
Molecular analysis, -omics	Total nucleic acid extraction, metagenomics, amplicon sequencing, bioinformatics
Pore-water chemistry	Pore water extraction via hydraulic squeezing, analysis via Ion chromatography, photometry and titration
Turnover rates/radiotracer (AOM, methanogenesis)	Incubation experiments with radio-isotopes; GHG production through headspace measurements
CH_4 and CO_2 concentrations and isotopes (δ^{13}C-CH_4, δ_{13}DIC, and δD-CH_4)	GC-MS (Universität Hamburg)

Using molecular DNA- and RNA- based techniques functional, short-term modulations (transcriptional changes) will be distinguished from long-term, whole community responses to permafrost thaw. Total nucleic acids (-omics), and specific phylogenetic and functional marker genes (e.g. 16S rRNA, mcrA) will be assessed in initial thermokarst lake and ice-bonded sediments and at the beginning and end of temperature mesocosm experiments (see below). Aseptic permafrost sediment sampling, isolation of total nucleic acids and cDNA synthesis will be done as described previously (Liebner and Svenning, 2013; Tveit et al., 2012). Deep, next generation Illumina paired end sequencing and quantitative PCR will be done as described before (Liebner et al., 2015, Mitzscherling et al., 2017).
Interstitial pore water will be extracted from representative subsamples of all types of samples by hydraulic squeezing. The pore water samples are analyzed by ion chromatography for all major cat-and anions as well as volatile fatty acids. Additionally, other parameters like alkalinity and iron speciation will be measured via titration or photometry, respectively.
Using mesocosms GHG production and ratios of CO_2:CH_4 and Q10 values as a function of time since thaw will be determined. Sediment slurries will be incubated stepwise at different temperatures between 0 and 12 °C. The increase in headspace CH_4 and CO_2 concentrations will be determined via Gas Chromatography as described previously (Liebner et al., 2015). Also, isotopic signatures of $\delta^{13}CH_4$, δD and δ^{13}DIC indicative for microbial pathways of GHG formation will be analyzed on the same samples at the Universität Hamburg in collaboration with Christian Knoblauch (Knoblauch et al., 2015). The initial sediment samples as well as slurries after each temperate increment will be analyzed for microbial community functions and composition, potential microbial carbon sources like volatile fatty acids (VFA), total cell counts as a measure of biomass and major anions, and cations. Further, rates of anaerobic methane oxidation (AOM) will be determined using radioisotopes. Mesocosm experiments will be set up spiking the headspace with ^{14}C radiolabeled methane. AOM rates will be quantified using well-established analytical protocols (Treude et al., 2003).

Preliminary results
Pore water and DNA were extracted from all UWITEC^{TM} cores. DNA content, bacterial, archaeal, and methanogenic abundance was quantified using qPCR as mentioned above. Concentrations of sulfate, chloride, bromide, iron2+, iron3+, acetate, and formate as well as conductivity, alkalinity and pH were measured. Preliminary data for conductivity, alkalinity and DNA content are illustrated in Figure 3.2-1.

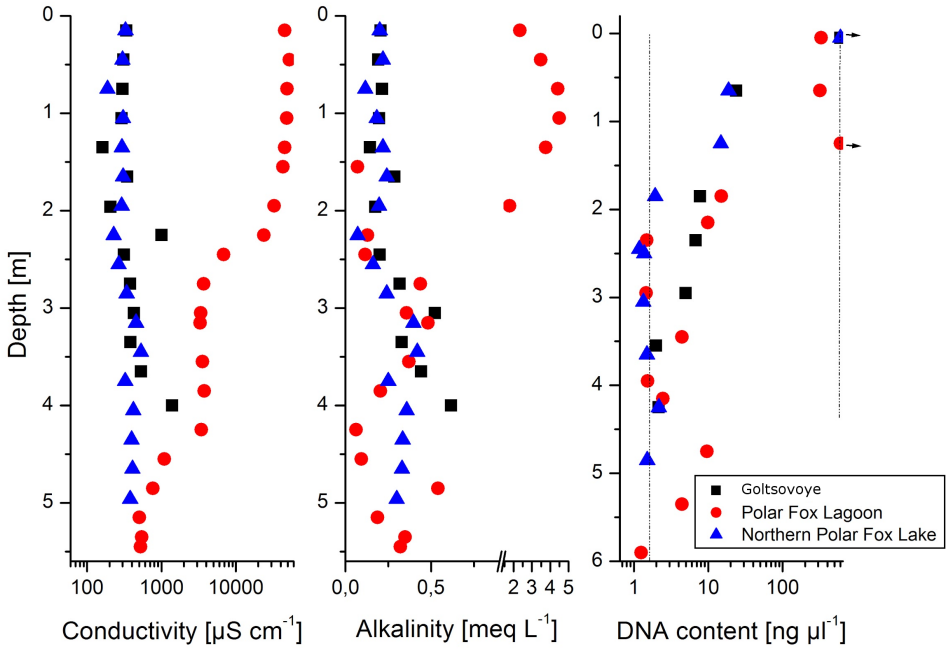

Figure 3.2-1: *Preliminary pore water conductivity and alkalinity values as well as DNA content of the two thermokarst lakes (Goltsovoye and Northern Polar Fox lakes) and a thermokarst lagoon (Polar Fox Lagoon) of the Bykovsky Peninsula. Dashed line indicates upper detection limit.*

3.3 Work package 2: Organic matter and sediment composition of thawing permafrost

Jens Strauss[1], Mikhail Grigoriev[2,3], Georgii Maximov[2,3], Sergeii Pravkin[4], Lutz Schirrmeister[1]

[1] Alfred Wegener Institute Helmholtz Center for Polar and Marine Research, Potsdam, Germany

[2] Melnikov Permafrost Institute, Siberian Branch, Russian Academy of Sciences, Yakutsk, Russian Federation

[3] Trofimuk Institute for Petroleum Geology and Geophysics, Siberian Branch, Russian Academy of Sciences, Russian Federation

[4] Arctic and Antarctic Research Institute, St. Petersburg, Russian Federation

Fieldwork period and location
From April 05th to April 24th, 2017 (on Bykovsky Peninsula)

Objectives
Permafrost sequences with frozen and unfrozen intervals, especially if deposited during the same time period (similar organic matter source), provide the opportunity to investigate changes in the organic matter composition caused by microbial alteration in the thawed interval.
The research hypothesis for the sediments is that there have been repeating cycles with land-ocean interactions including flooding, draining and permafrost degradation and aggregation. Besides recovering and interpretation of the facies changes into a paleoenvironmental reconstruction of the landscape, this sub-project aims to quantify and qualify the sequestered organic matter including its transformation and conservation during and after thaw (lake and lagoon facies) as well as in the permafrost below the taliks.

Methods
We used a Geotechnika URB 4T for coring the sediment. This drill is owned by the research station Samoylov.
After cleaning the cores, they were all described (sedimentology, cryolithology, organic carbon characteristics) and photographed in the field. Afterwards all cores were frozen, labelled and packed in thermoboxes.

Preliminary results
In total, 3 locations were cored. In total, we drilled 100.75 m below water surface, which included 93.8 m below sediment surface. The core recovery was 85 %, which is 79.60 m of core material.

Core PG 2410
The first core PG 2410 (Figure 3.3-1, Table A.3-1, Table A.3-4) was drilled from 08. to 11. April in the Uomullyakh-Kyuel Lagoon. After a drilling survey for finding water in this lagoon, where we did not find any water, the deep drilling campaign started. In the meantime, the UWITEC™ drilling team changed their plans and moved to the next site as water is needed for this coring technique. During the first two days, there were some problems with the hydraulic equipment of the drilling machine, which was solved by getting spare parts from Tiksi.
The ice thickness at the first drilling site was 120 cm, after which 240 cm of partly frozen fine-grained sediments was drilled. Further below, the material was unfrozen, a black to dark grey clayish silt with parallel sediment structures were found up to 480 cm deep. From 480 to 625 cm deep, the

material was alternating between silty fine sandy and medium to coarse grained (Figure 3.3-1). From 655 to 865 cm, a clayish fine sand material with parallel sediment structures was drilled. Following that, the core material changed several times in form of alternated bedding from silty fine sand to coarse-grained sand with pebbles down to the core end at 3350 cm depth. The thickness of these layers changed between a few decimeters and about one meter. The lower part in between single core segments were frozen but mostly the core was already thawed. This could be caused by repeated drilling in the same depth in order to get the core material. In the depths of 3050 cm and 3330 cm, water came out and was sampled.

Core PG 2411

The second core PG 2411 (Figure 3.3-2, Table A.3-2, Table A.3-5) was drilled from 14. to 17. April in the Polar Fox Lagoon. The ice thickness was 155 cm and the water depth was 175 cm. The first 35 cm of sediment core were salty, but from 365 to 630 cm the fine grained and layered material with shell remains contain freshwater. Core material in 720 to 750 m depth tasted salty again. Down to 920 cm, the sediment core contains silty to silty sandy material with gradually increased grain sizes. Between 1120 and 1210 cm depth sediment was partly frozen. It is not clear if unfrozen sediment was thawed during the drill process or if frozen and unfrozen sediment parts vary originally. The deeper core consists of alternate bedded fine, medium and coarse sand with low cohesiveness down to the end of the core at 3105 cm depth. The coarse sand often contained rounded pebbles of 1-3 cm in diameter. These core segments look like fluviatile deposits. Frozen segments occurred again at 1815-1855, 2040-2050 and 2970-2985 cm depth. Organic remains were visible at 720-750, 1460-1500, and 2735 cm depth. At 1810-1815, 2105-2115, 2235-2245 woody horizons from branch fragments exist. The core was repeatedly interrupted by core loss sections.

Core PG 2412

The third core PG 2412 (Figure 3.3-3, Table A.3-3, Table A.3-6) was drilled between 18. and 20. of April into the thermokarst Goltsovoye Lake. The ice cover at the drilling site was 160 cm thick and the water depth was 350 cm. The lake bottom, where the sediment core started, was at 510 cm depth. From 510 to 724 cm unfrozen dark grey clayish, silty and fine sandy unfrozen sediment with plant remains and shells were drilled. This continues until 930 cm depth. Deeper the material changed to medium, coarse and, and partly fine sand. The coarse sand layers often contained pebbles up to 2 cm in diameter. The fine sand and silty fine sand parts are mostly layered. At 1905 cm and 2035 - 2050 cm depth, the fine sand layers contained big wooden remains. Similar wood fragments were found at depths of 2670, 2715, 2875 and 2910 cm. At 2985 cm a wood horizon was observed. In addition, large wood fragments occurred repeatedly in deeper core segments (3120 - 3130, 3395 - 3510, 3550 - 3570 cm). Core loss occurred only twice, at 2050 - 2135 cm and 3510 - 3550 cm depth in PG 2412. From 3425 cm down to the core end at 3650 cm the core was frozen. In the lowermost core segment at 3570 - 3650 cm no plant remains were visible.

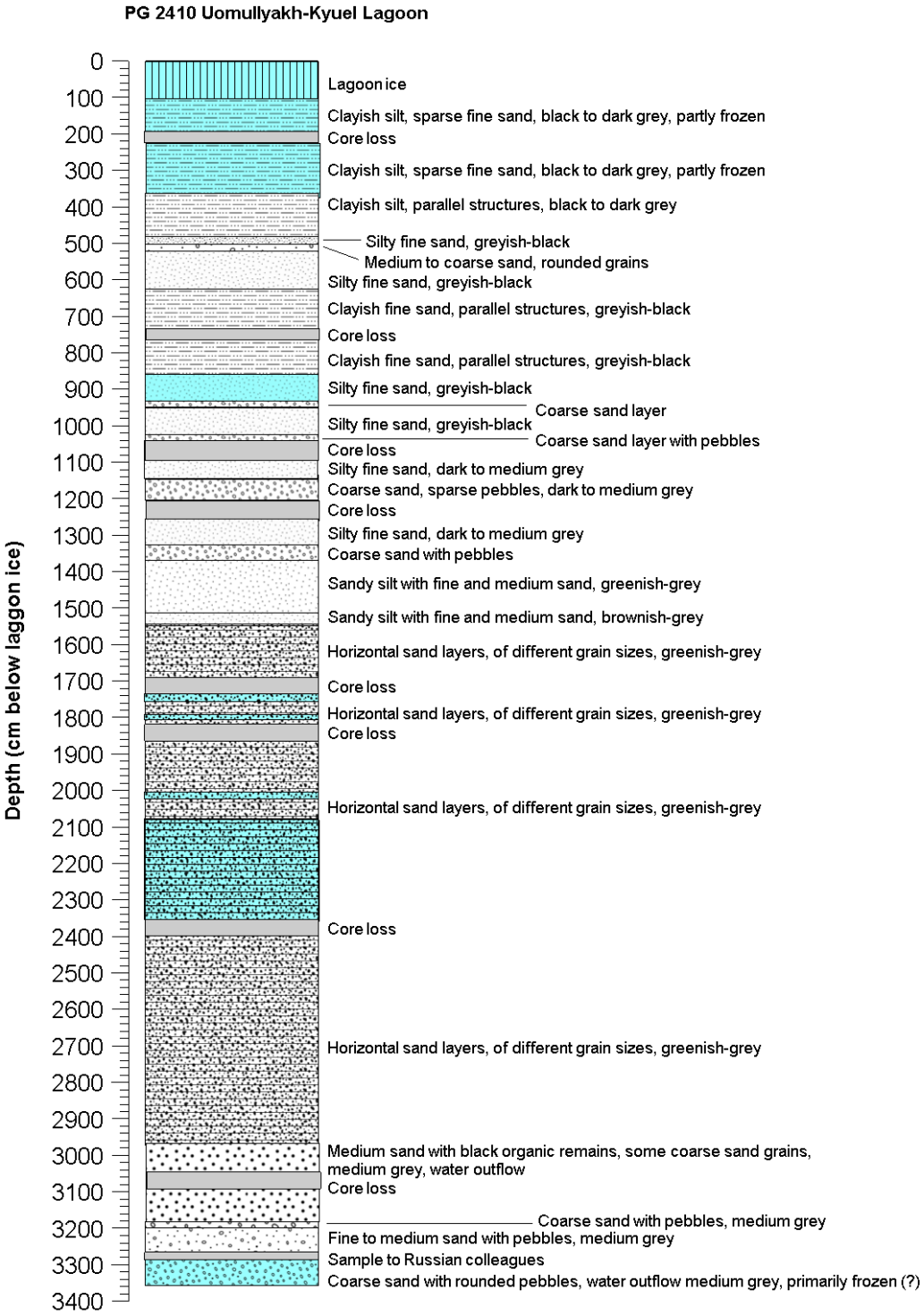

Figure 3.3-1: *Core lithology of PG 2410 (Uomullyakh-Kyuel), blue – frozen segments, grey - core loss*

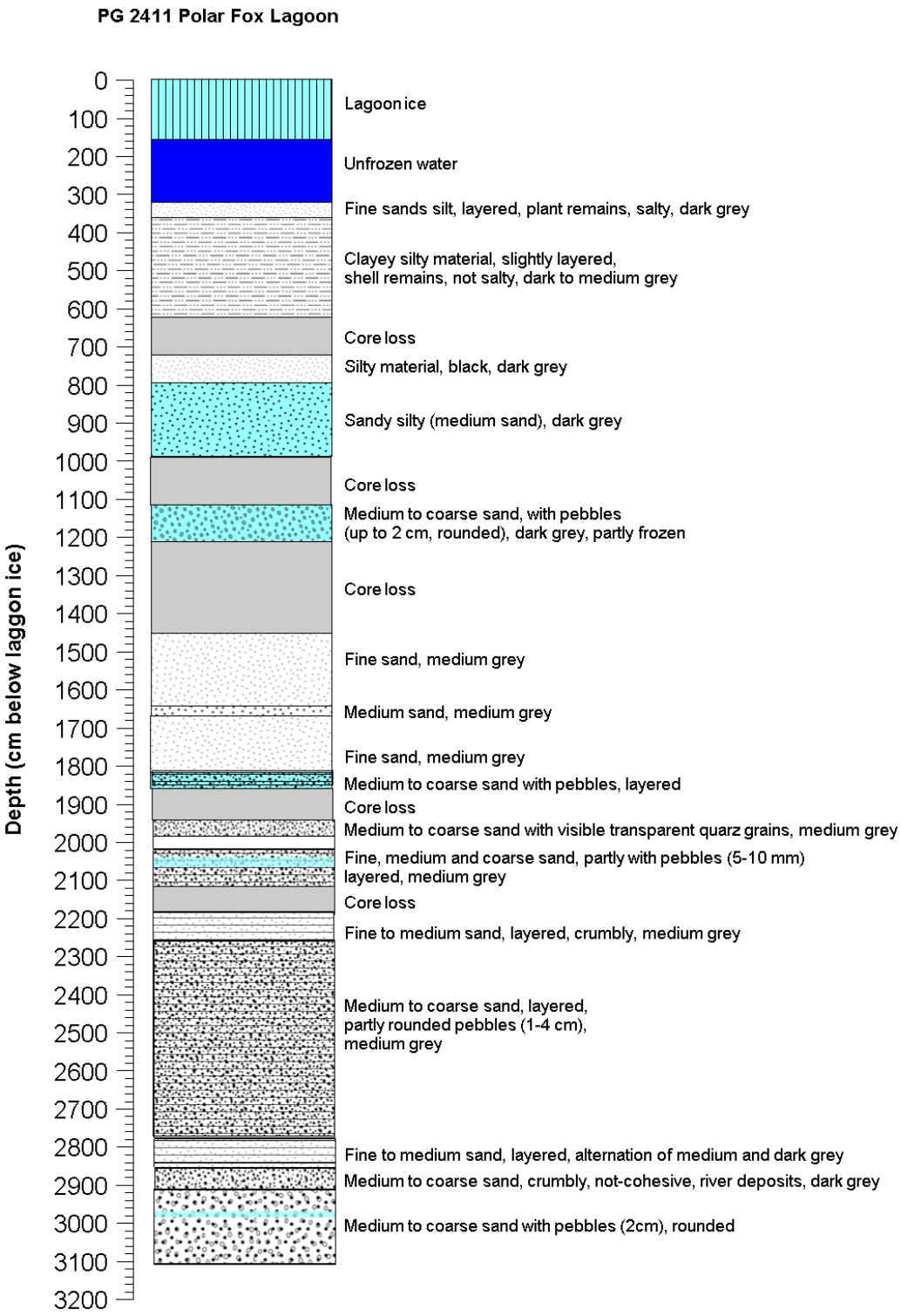

Figure 3.3-2: *Core lithology of PG 2411 (Polar Fox Lagoon) blue – frozen segments, grey - core loss*

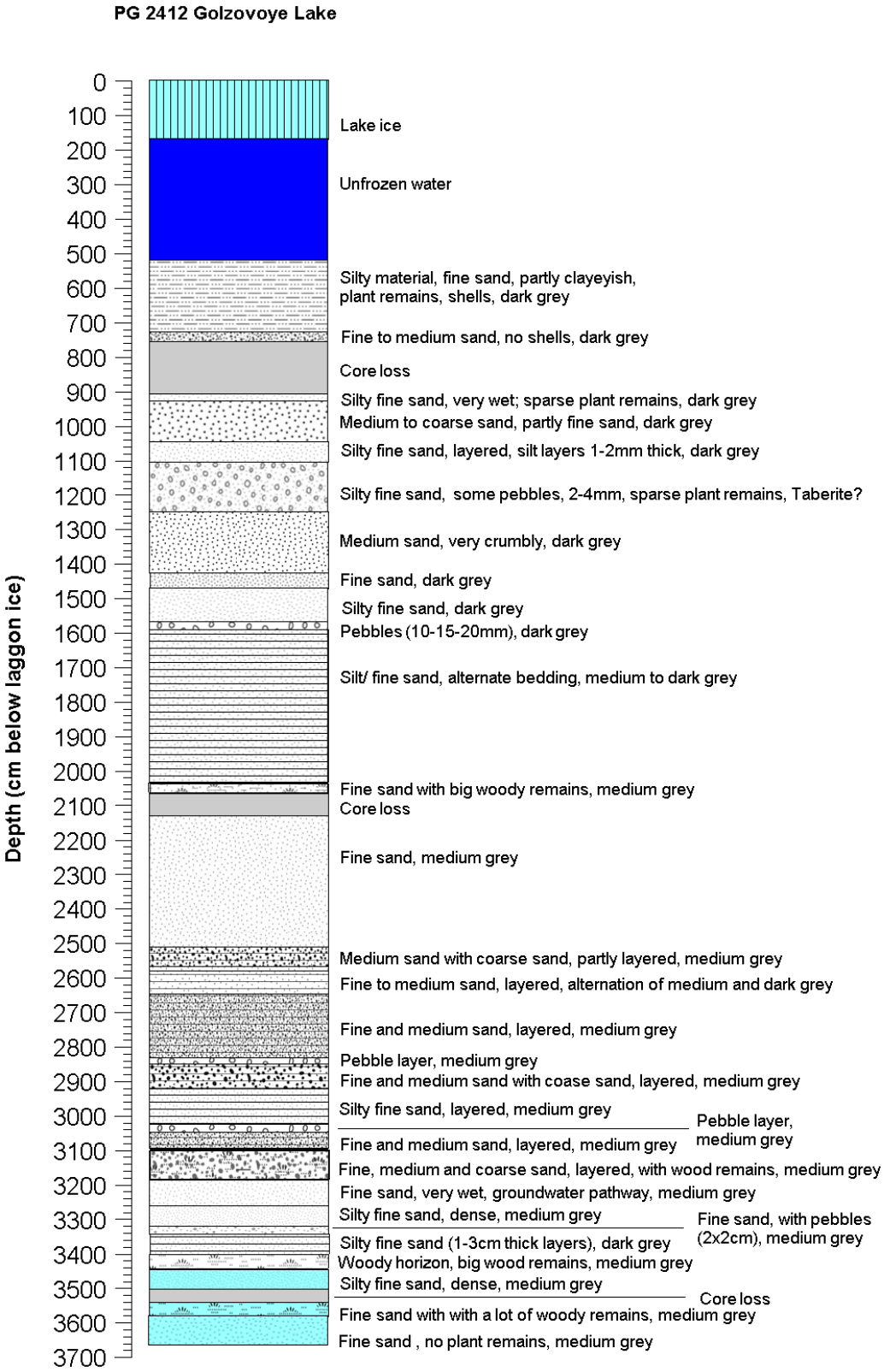

Figure 3.3-3: *Core lithology of PG 2412 (Goltsovoye Lake), blue – frozen segments, grey - core loss*

3.4 Work package 3: Holocene environmental variability

Boris K. Biskaborn[1], Jan Kahl[1], (Bernhard Diekmann[1]: not in field)

[1] Alfred Wegener Institute Helmholtz Center for Polar and Marine Research, Potsdam, Germany

Fieldwork period and location
From April 05th to April 24th, 2017 (on Bykovsky Peninsula)

Objectives
Knowledge of the biotic and abiotic development of the basin systems is essential for sound interpretation of biogeochemical, microbiological and geophysical gradients. The ecosystem and sedimentological changes that are expected in the lagoon setting are of special interest to understand transitions between marine and freshwater environments. Another aspect is to gain insights in causal relationships between external environmental variability and internal sediment-geochemical variations over time in different basin systems (Diekmann et al., 2017).
The objective of WP 3 are the reconstruction of the past environmental variability and climate changes in the late Quaternary Lena Delta region. WP 3 also provided the opportunity to retrieve sediment material that can be analyzed with the goal to answer the overarching question related to the SIBLAKE project (Figure 3.4-1): how do aquatic systems in the Russian Arctic respond to both external climate forcing and internal limnologic/brackish system development: “lake/lagoon ontogeny”.

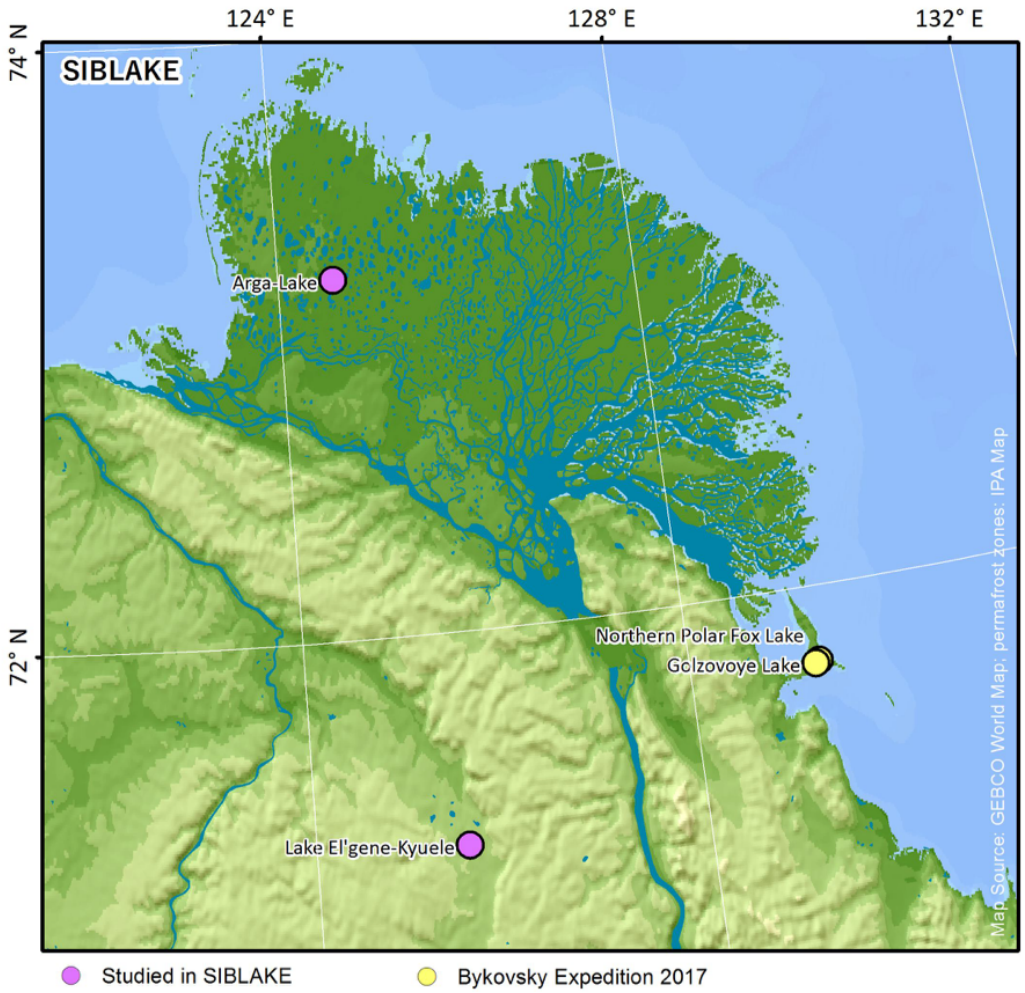

Figure 3.4-1: *Bykovsky in context of previously published sediment core archives from thermokarst lake settings in the Arga region (Biskaborn et al., 2013a) and at Lake El'gene Kyuele (Biskaborn et al., 2013b; Schleusner et al., 2014)*

Methods

We used a piston coring UWITEC^{TM} system with a tripod system operated from the ice cover of the water bodies to recover unfrozen sediment cores. We retrieved every sediment core twice in parallel at 2 m distance on the ice surface. The first one was processed directly in-field (see WP 1, cut in 10 cm sections) and the second one was cut in 1 m sections for transportation in thermoboxes to AWI, Germany. To retrieve undisturbed surface sediments in short cores up to 60 cm, we applied an UWITEC^{TM} gravity corer. All core material was stored in PVC tubes.

The UWITEC^{TM} cores will be opened and logged in the AWI laboratories, applying Avaatech XRF Core Scanner on "archive-half" for elemental composition and line scanning (core pictures and RGB values). Correlated core sections will be radiocarbon-dated to create a consistent age-depth model. Subsampling of the "work-half" for diatom, pollen and sediment-geochemical analyses (TOC/TN ratios, δ13C, grain-size, XRD for mineral composition) will be performed with the help of PhD and Master student projects.

Preliminary results

All technical aims during fieldwork were reached. On site, WP 3 and WP 1 performed well as a team for core-retrieval (Table 3.4.1) and in-field subsampling (Figure 3.4-2). We retrieved 3 m of sediment core material by UWITEC^{TM} technique at 10 different locations. At each long core site, we penetrated through the Holocene layers. Additionally, we cleared areas on the ice of Goltsovoye

Lake and the Northern Polar Fox Lake (1.5 x 70 m) and documented the methane bubbles visible (Figure 3.4-3) within different depths the lake ice cover, which varied between 1.5 - 2.0 m thickness in total (Table 3.4.1).

Table 3.4.1: Metadata list of most important retrieved long cores using UWITEC piston coring system during expedition Bykovsky 2017 spring)

Location	**Date of sampling**	**Core ID**	**N [DecDeg]**	**E [DecDeg]**	**Water Depth [m]**	**Ice Thick-ness [m]**	**Driling Depth**
Lake Golzovoye	2017-04-09	PG2420	71.74530	129.30243	5.1	1.93	520
Polar Fox Lagoon	2017-04-15	PG2423	71.74356	129.33824	3.1	1.52	610
Northern Polar Fox Lagoon	2017-04-19	PG2426	71.75176	129.34251	5.6	1.68	540

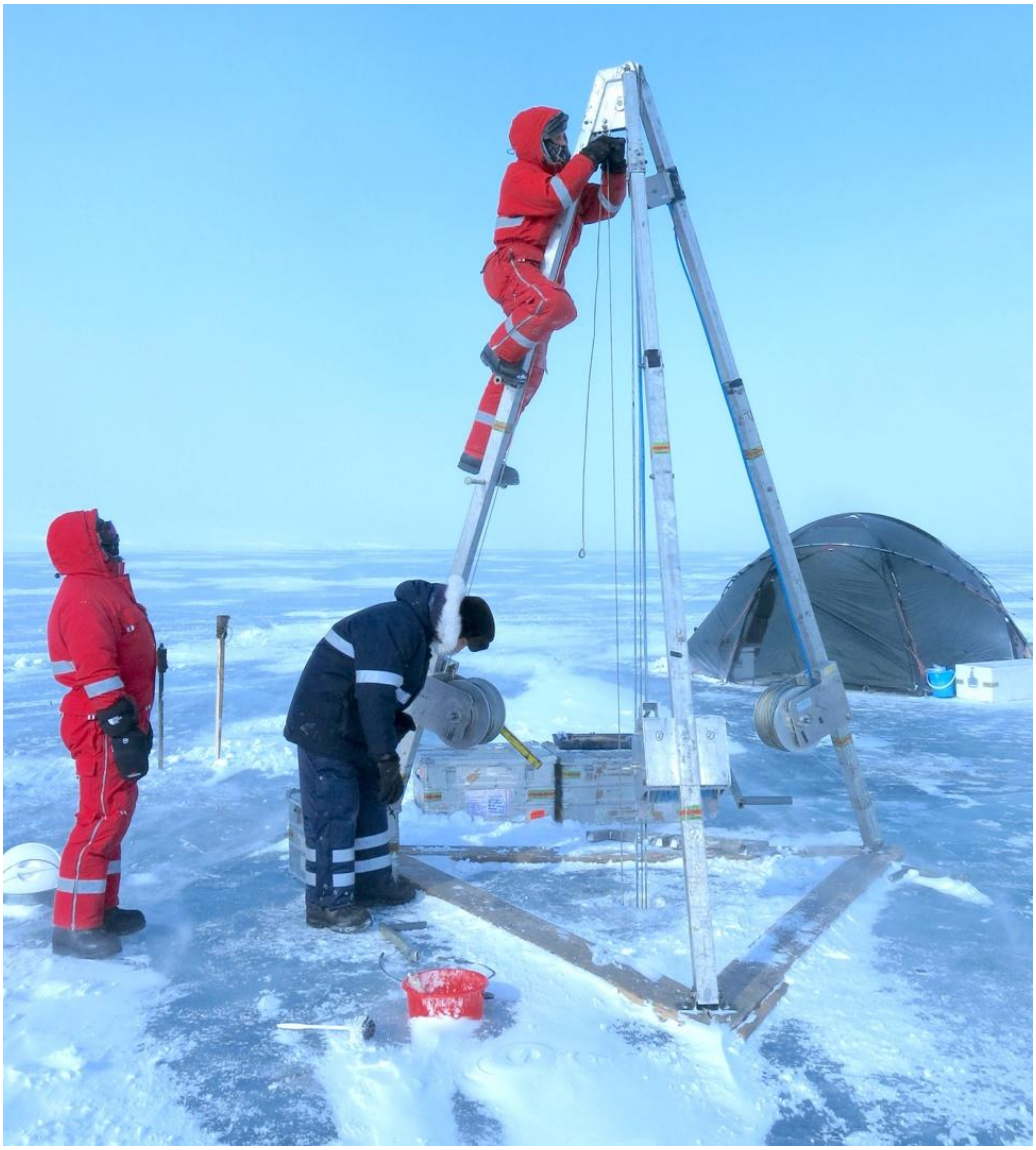

Figure 3.4-2: *UWITEC tripod fixed on ice cover of Goltsovoye Lake, using the piston coring technique. Cores were subsampled by WP 1 directly after core retrieval in the tent next to the drilling station.*

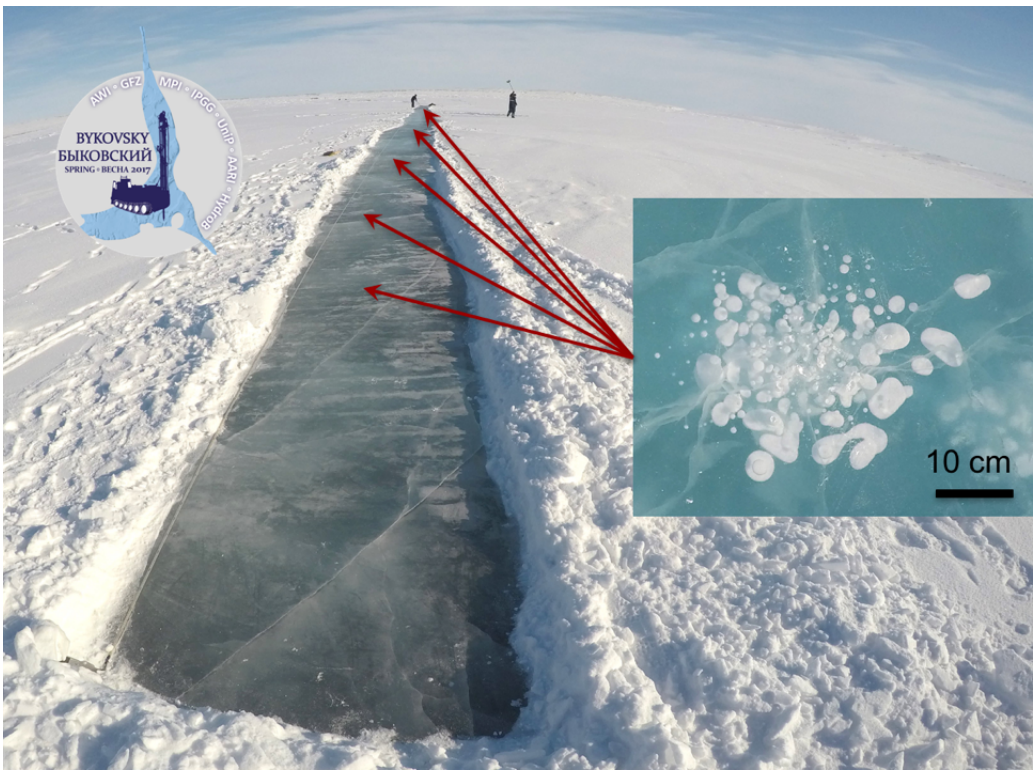

Figure 3.4-3: *Profiles on lake ice for methane bubble analyses*

3.5 Work package 4: Ice-rich permafrost thaw under sub-aquatic conditions

Michael Angelopoulos[1], Nikita Golikov[2], Mikhail Grigoriev[2,3], Georgii Maximov[2,3], Pier Paul Overduin[1], Andrey Plotnikov[2], and Alexey Scherstnev[4]

[1] Alfred Wegener Institute Helmholtz Center for Polar and Marine Research, Potsdam, Germany

[2] Melnikov Permafrost Institute, Siberian Branch, Russian Academy of Sciences, Yakutsk, Russian Federation

[3] Trofimuk Institute for Petroleum Geology and Geophysics, Siberian Branch, Russian Academy of Sciences, Novosibirsk, Russian Federation

[4] Timer LLC, Moscow, Russian Federation

3.5.1 Part 1: Geophysical and thermal characterization of subaquatic permafrost for multiple cryostratigraphic settings in freshwater and saltwater environments

Michael Angelopoulos[1], Pier Paul Overduin[1]

[1] Alfred Wegener Institute Helmholtz Center for Polar and Marine Research, Potsdam, Germany

Fieldwork period and location
From April 05th to April 24th, 2017 (on Bykovsky Peninsula)

Abstract
Degradation of sub-aquatic permafrost can, impact offshore infrastructure, affect coastal erosion and release large quantities of methane, which may reach the atmosphere and function as a positive feedback to climate warming. The degradation rate depends on the duration of inundation, warming rate, sediment characteristics, the coupling of the bottom to the atmosphere through bottom-fast ice, and brine injections into the sediment (Overduin et al., 2012). The relative importance of these controls on the rate of sub-aquatic permafrost degradation, however, remains poorly understood. Therefore, the overarching science goal for the 2017 Bykovsky Spring Expedition was to evaluate the nature and distribution of subaquatic permafrost and taliks in multiple cryostratigraphic settings with near-surface geophysics and temperature sensors. At some sites, shallow coring and surface water analyses were performed to gather additional data. To monitor fieldwork conditions, a meteorological station was set up at each base camp. The primary sites included a large freshwater body (Goltsovoye Lake), a small freshwater lake within alas terrain (Small Alas Lake), a shallow salty lagoon eroding into both Yedoma and Alas permafrost (Uomullyakh-Kyuel Lagoon), as well as a saltwater body within a partially drained Alas (Polar Fox Lagoon). This research was coordinated with the deep drilling and UWITEC™ coring teams, because stratigraphic data is paramount to geophysical and thermal data interpretation. Future laboratory analyses on core samples will ultimately be used to further interpret the data.

Fieldwork summary

The study sites are shown in Figure 3.1-5 and individual fieldwork maps are provided for Goltsovoye Lake (Figure 3.5-1), Small Alas Lake (Figure 3.5-2), Uomullyakh-Kyuel Lagoon (Figure3.5-3), and Polar Fox Lagoon (Figure 3.5-4). In addition, detailed lists of field data are shown in Table 3.5.1, Table 3.5.2, Table 3.5.3, and Table 3.5.4. The following is a short description of the central science activities performed.

1. Ground-penetrating radar: Alfred Wegener Institute (AWI)-led ground-penetrating radar (GPR) surveys were carried out at Goltsovoye Lake (50 Megahertz (MHz)) and the Small Alas Lake (50, 100, and 200 MHz). Since saltwater and salty permafrost strongly attenuate GPR signals, no AWI surveys were carried out at Uomullyakh-Kyuel Lagoon and Polar Fox Lagoon. However, Russian collaborators from Timer LLC, Moscow, performed low frequency surveys (15 MHz and 75 MHz) at the freshwater lakes, as well as 15 MHz surveys at the saltwater lagoons. The Timer LLC GPR had a much higher power (9 - 15 kilovolts) compared to AWI's equipment and was therefore attempted on the saltwater lagoons. For the AWI surveys, a MALA Geoscience RAMAC GPR system was employed.

2. Electrical resistivity: One-dimensional (1D) electrical resistivity soundings with multiple electrode array configurations and transmitter voltages were performed at Polar Fox Lagoon close to the deep borehole and UWITEC coring locations. An IRIS Syscal Pro Deep Marine system was used for all surveys. Several holes were drilled through the lagoon's ice cover in order to place electrodes directly on the sediment surface and establish good contact. The goal of the 1D soundings was mainly to evaluate the resistivity system's ability to detect the top and potentially the base of ice-bearing permafrost in a subaquatic environment in which salt diffusion is a factor. The motivation behind these surveys was to help optimize survey design for three-dimensional marine electrical resistivity mapping in summer.

3. Temperature chains: At Goltsovoye Lake, Uomullyakh-Kyuel Lagoon, and Polar Fox Lagoon, one or two thermistor cables were installed following the completion of each deep rotary drilling borehole. The temperature sensors remained in the borehole until within two days of the end of the expedition. At Goltsovoye Lake, an RBR Concerto temperature chain that had been already calibrated by the manufacturer was used. The RBR cable was optimal for Goltsovoye Lake, because the thermistor spacing decreased with increasing depth, providing highest spatial resolution around the permafrost table at the bottom of the borehole. The latter setup is particularly valuable for delineating the talik to permafrost transition. At the lagoons, GeoPrecision temperature chains were used in parallel with temperature cables from Russian colleagues based at the Melnikov Permafrost Institute (MPI) in Yakutsk. The MPI data is not discussed in this report. A summary of the temperature chains deployed by AWI and preliminary results are shown in Figure 3.5-5.

4. Surface water analyses: Conductivity, temperature, and depth (CTD) measurements were taken using a SonTek Castaway instrument at the center of the Small Alas Lake and the 1D electrical resistivity sounding location at Polar Fox Lagoon. At the Small Alas Lake, the CTD data were used to validate the freshwater condition of the lake, as well as to acquire lakebed temperatures essential for thermal modelling. At Polar Fox Lagoon, the CTD was instrumental in confirming the high salinity of the water as further demonstrated by the existence of liquid water at sub-zero temperatures.

5. Shallow coring: At the Small Alas Lake, several ice holes were drilled to measure ice thickness, water depth, and occasionally talik thickness. This data is crucial to generate accurate time to depth conversions for GPR profiles, particularly for bathymetry.

6. Meteorological station: A Davis Vantage Vue wireless weather station was used at each station to monitor indoor/outdoor temperature, indoor/outdoor relative humidity, barometric pressure, wind speed, wind direction, as well as wind chill temperature.

Table 3.5.1: Ground-penetrating radar surveys performed by AWI at Goltsovoye Lake and the Small Alas Lake

Site	Date	Frequency [MHz]	Survey Direction	Start [Decimal Degrees]		End [Decimal Degrees]	
				Latitude [N]	Longitude [E]	Latitude [N]	Longitude [E]
Goltsovoye Lake	08.04.2017	50	North-South	71.74729	129.30395	71.74168	129.30279
	08.04.2017	50	East-West	71.74527	129.31075	71.74545	129.2991
Small Alas Lake	12.04.2017	50	North-South	71.74132	129.29889	71.73795	129.29677
	14.04.2017	100	North-South	71.73976	129.29795	71.73853	129.29794
	14.04.2017	100	South-North	71.73853	129.29794	71.73976	129.29795
	14.04.2017	100	East-West	71.73911	129.29948	71.73912	129.29587
	14.04.2017	100	West-East	71.73912	129.29587	71.73911	129.29948
	19.04.2017	200	North-South	71.73989	129.29766	71.73845	129.29791
	19.04.2017	200	South-North	71.73845	129.29791	71.73989	129.29766
	19.04.2017	200	East-West	71.73911	129.29991	71.73912	129.29587
	19.04.2017	200	West-East	71.73912	129.29587	71.73911	129.29991

Table 3.5.2: Electrical Resistivity Surveys at Polar Fox Lagoon

Site and Coordinates	Date	Electrode Spacing [meters]	Array Type	Transmitter Voltage [volts]
Polar Fox Lagoon (Multipoint of arrays at approx. 71.74345 °N, 129.334394 °E)	10.04.2017	10	Wenner-Schlumberger	12
	10.04.2017	10	Wenner-Schlumberger	24
	10.04.2017	10	Wenner-Schlumberger	36
	10.04.2017	10	Wenner-Schlumberger	48
	21.04.2017	5	Reciprocal Wenner-Schlumberger	12
	21.04.2017	5	Reciprocal Wenner-Schlumberger	24
	21.04.2017	5	Reciprocal Wenner-Schlumberger	36
	21.04.2017	5	Reciprocal Wenner-Schlumberger	48

Table 3.5.3: Temperature Cable Installations at Deep Borehole Drilling Locations

Site	Installation Date	Decimal Degrees	
		Latitude [N]	Longitude [E]
Goltsovoye Lake	21.04.2017	71.74515	129.30217
Uomullyakh-Kyuel Lagoon	12.04.2017	71.73087	129.27483
Polar Fox Lagoon	17.04.2017	71.74303	129.3383

Table 3.5.4: CTD Castaway Measurements at Mike's Lake and Polar Fox Lagoon

Site	Date	Decimal Degrees	
		Latitude [N]	Longitude [E]
Small Alas Lake	22.04.2017	71.73914	129.29772
Uomullyakh-Kyuel Lagoon	20.04.2017	71.74335	129.33439

Table 3.5.5: Shallow Coring to Measure the Thickness of Different Layers at the Small Alas Lake

Site	Hole	Date	Decimal Degrees		Thickness of Different Laysers [meters]			
			Latitude [N]	Longitude [E]	Snow	Ice	Water	Unfrozen Sedi-ment
Amall Alas Lake	X6	17.04.17	71.73948	129.29824	0.4	1.25	1.18	>0.67
	X5	17.04.17	71.73954	129.29765	0.4	1.24	0.33	0.85
	X4	17.04.17	71.73937	129.29764	0.23	1.58	0.78	Unknown
	X1	15.04.17	71.73914	129.29772	0.45	1.4	1.45	Unknown
	PAUL	17.04.17	71.73908	129.2979	0.36	1.31	1.43	Unknown
	X2	15.04.17	71.7388	129.29783	0.35	1.3	0.93	>0.77
	X3	15.04.17	71.73869	129.29779	0.37	0.9	0	Grounded ice

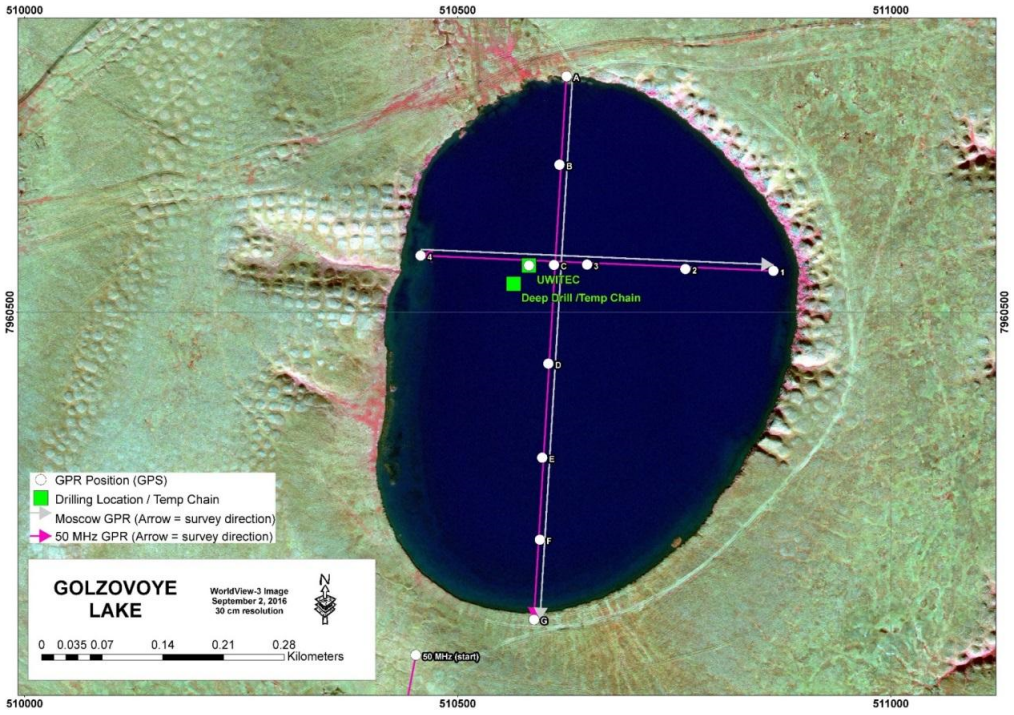

Figure 3.5-1: *Goltsovoye Lake study site*

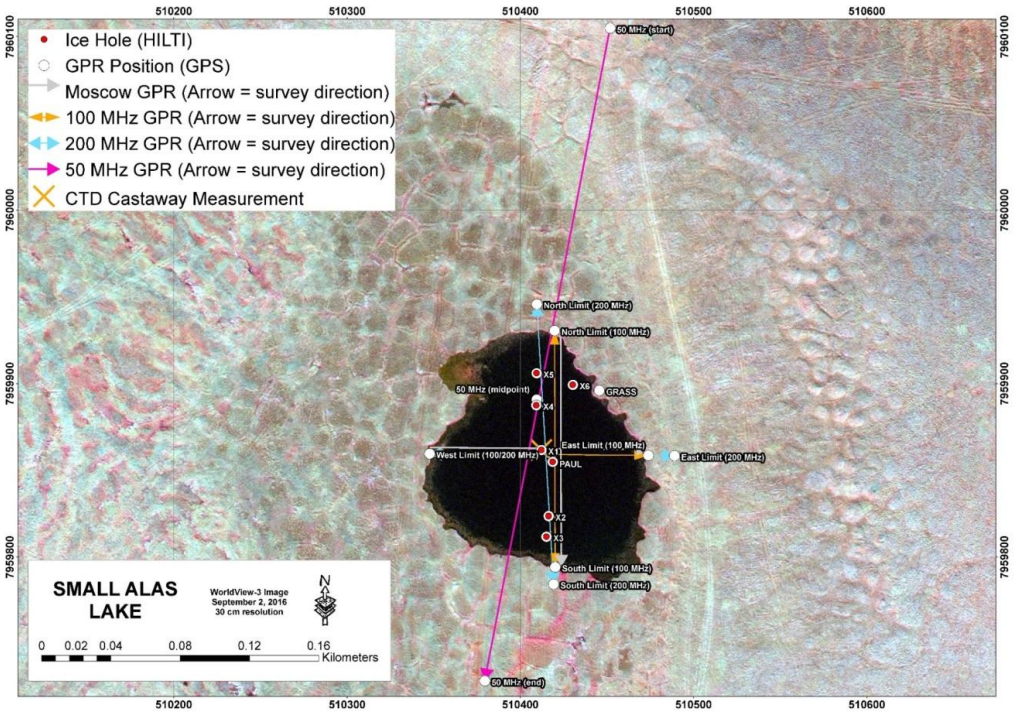

Figure 3.5-2: *Small Alas Lake study site*

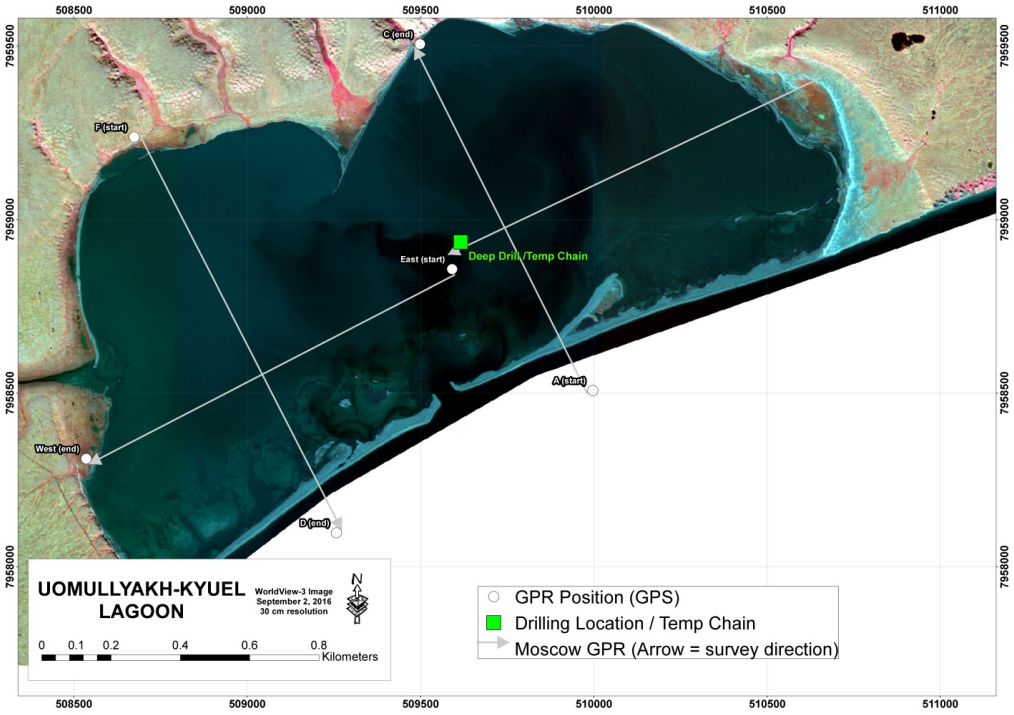

Figure 3.5-3: *Uomullyakh-Kyuel Lagoon study site*

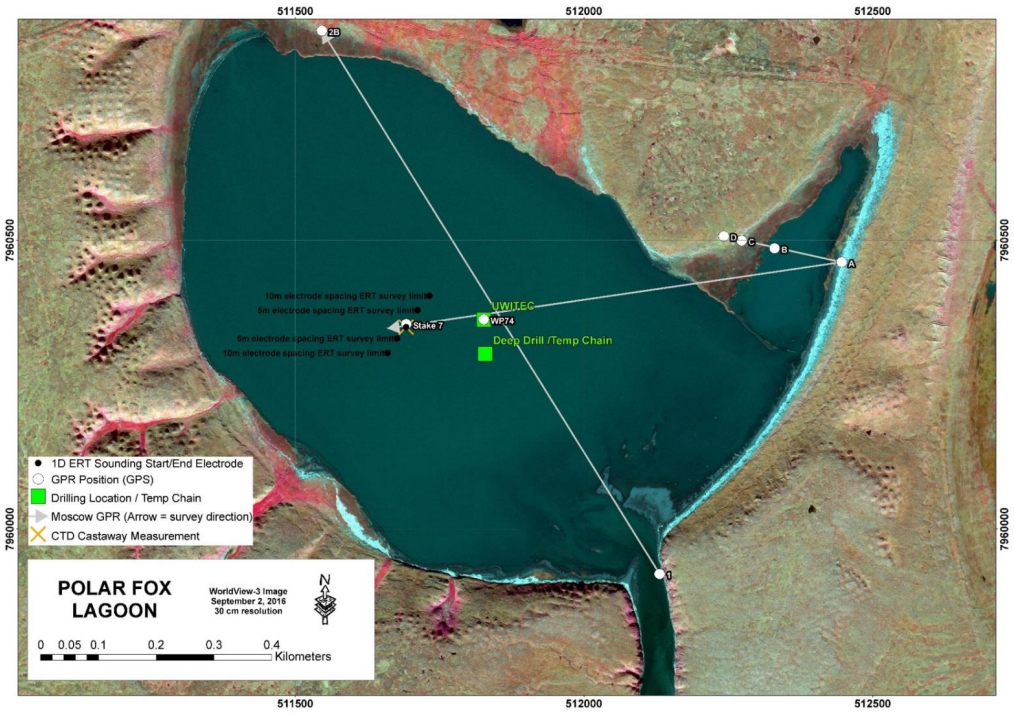

Figure 3.5-4: *Polar Fox Lagoon study site*

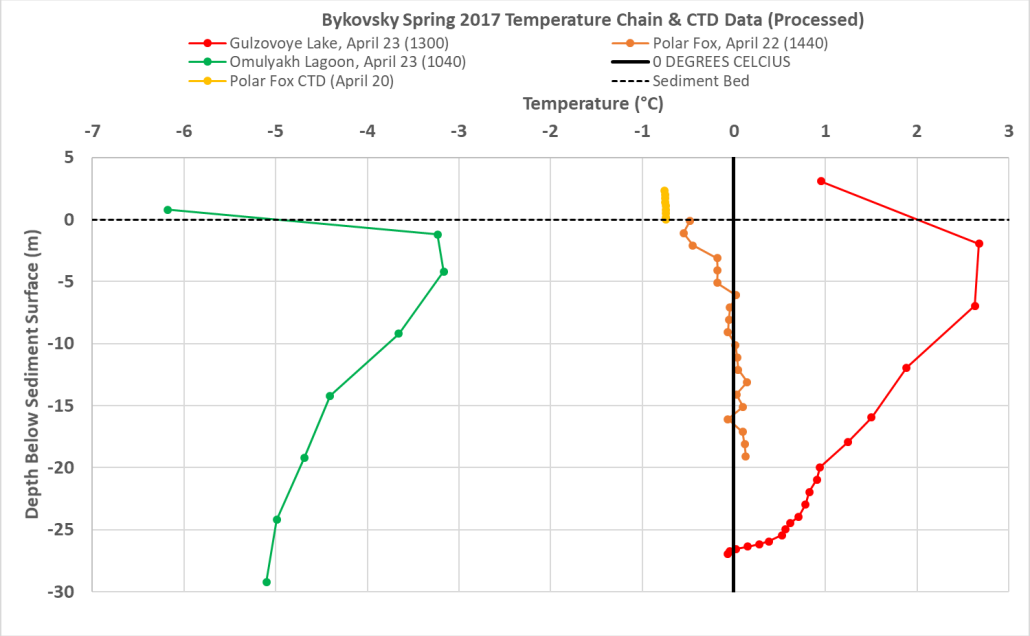

Figure 3.5-5: *Temperature node locations and thermal regimes at Goltsovoye Lake, Uomullyakh-Kyuel Lagoon, and Polar Fox Lagoon. The results have been corrected for drilling heat and sensor calibration effects.*

3.5.2 Part 2: Transient electromagnetic sounding (TEM) and deep ground-penetrating radar (GPR)

Andrey Plotnikov[1], Nikita Golikov[1], (Alexey Sherstnev[2], Vladimir Kashirtsev[1], Igor Yeltsov[1], Vladimir Olenchenko[1]: not in the field)

[1] Trofimuk Institute for Petroleum Geology and Geophysics, Siberian Branch, Russian Academy of Sciences, Novosibirsk, Russian Federation

[2] Timer LLC, Moscow, Russian Federation

Fieldwork period and location
From April 13th to April 24th, 2017 (on Bykovsky Peninsula)

Objectives
Geophysical datasets, thermal modelling, and drilling data suggest that most Arctic shelves are underlain by submarine permafrost due to their exposure during the glacial low water stands (Romanovskii et al., 2004). The degradation of submarine permafrost could release large quantities of methane into the atmosphere, impact offshore drilling activities, and affect coastal erosion. The degradation of subsea permafrost itself depends on the duration of inundation, warming rate, the coupling of the seabed to the atmosphere from bottom-fast ice, and brine injections into the seabed (Overduin et al., 2012). The impact of brine injections on permafrost degradation is dependent on seawater salinity, which changes seasonally in response to salt rejection from sea ice formation and terrestrial freshwater inflows. The rate of submarine permafrost evolution and the relative importance of the many controls responsible for degradation, however, remain poorly understood. This work will evaluate submarine permafrost degradation rates on the Bykovsky Peninsula (north Siberia) using a combination of geophysical, sampling, and remote sensing methods. In addition, the work will study submarine permafrost thaw mechanisms and an approach to their representation using thermal modelling.

Methods

1. Transient electromagnetic sounding (TEM) was conducted with aligning arrangement, transmitting loop had the size of 50 x 50 m, receiving loop - 18 x 18 m.
2. Ground-penetrating radar (GPR) surveys were conducted with equipment GROHT 12H central frequency 15 MHz (15 kV transmitter with 10 m antennas).

Preliminary results
Measuring scheme of TEM survey is shown in figure 3.5-6.

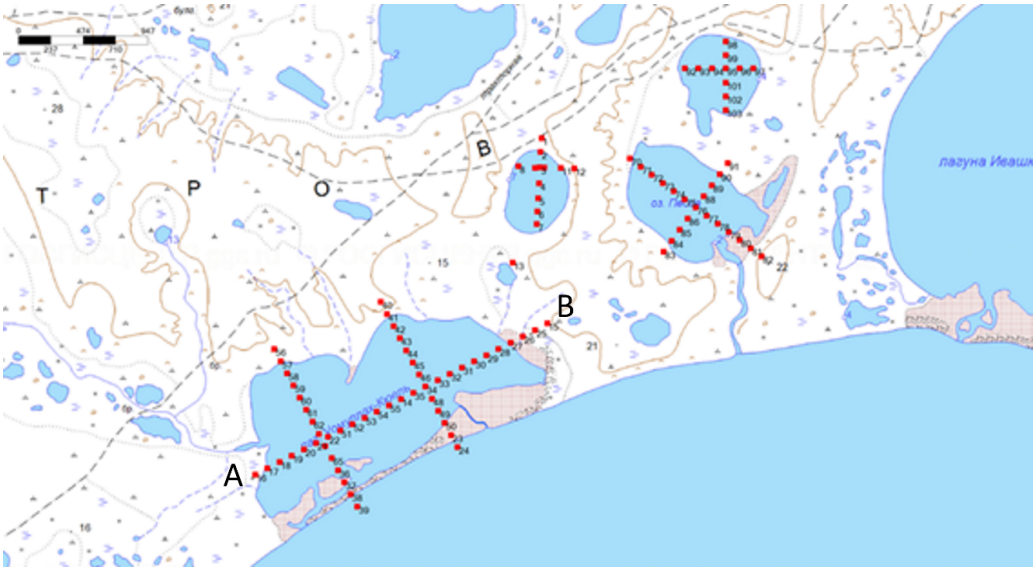

Figure 3.5-6: *Profiles of TEM measurements*

The most representative results are obtained on the Uomullyakh-Kyuel Lagoon. The geoelectrical cross-section is based on the 1D inversion of the TEM data is shown in figure 3.5-7.

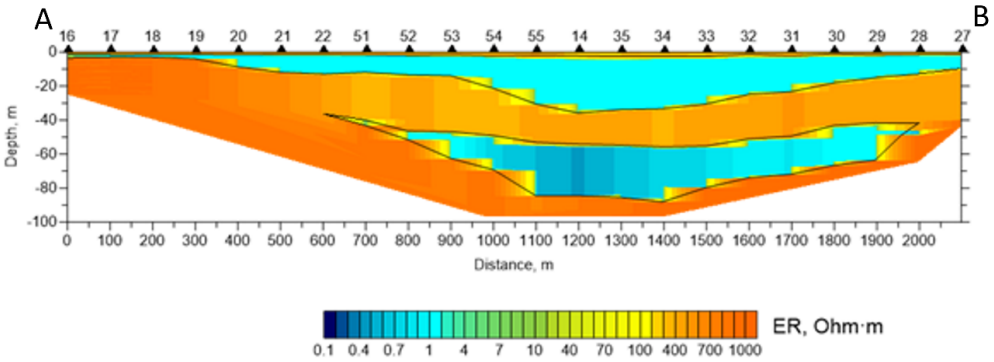

Figure 3.5-7: *Geoelectrical cross-section based on 1D inversion of TEM data*

The low resistivity area (about 1 ω·m) in the upper part of the section (up to the depth of 33 m) presumably corresponds to a talik. The high-resistivity (more than 400 ω·m) deposits are frozen. The extremely low resistivity area is revealed in the central part of the profile at the depths of 50 - 80 m. That area is interpreted as saline supercooled thawed rocks. Figure 3.5-8 shows the GPR data along the same profile.

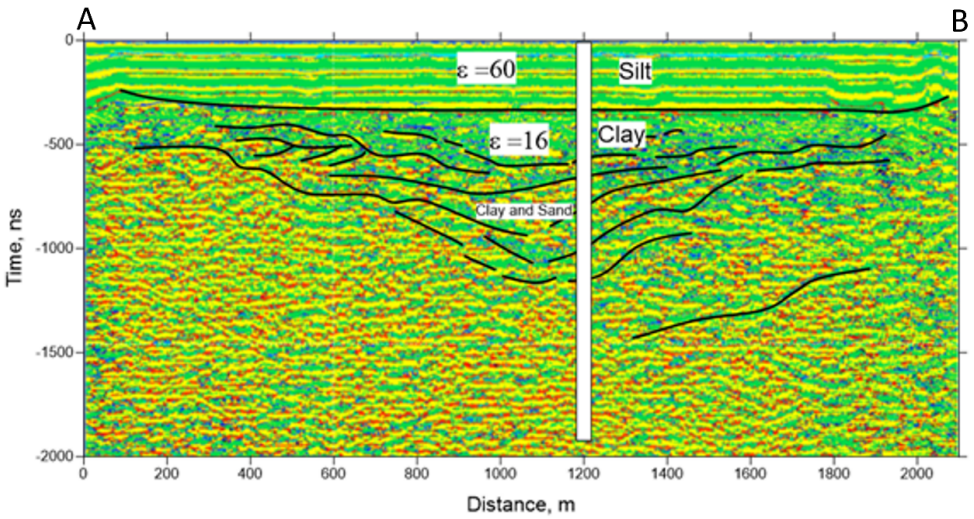

Figure 3.5-8: *Radargram along the profile AB (Fig 3.5-6) crossing the Uomullyakh-Kyuel lagoon; borehole position is shown by the white vertical column.*

It is difficult to interpret GPR data unambiguously. The talik contours can be marked where the wave pattern changes, but clear boundaries are not displayed on the radargram. This indicates the complex structure of the talik, associated with the difference in thawing over time in different materials, as well as possible erosion. For a clearer interpretation, GPR data is now processed (calibration of speed and attenuation of the signal in different layers with comparison of the temperature data). The GPR data at other sites (Polar Fox Lagoon, etc.) are also processed to calibrate the velocities in comparison with the temperature data. The TEM data on these lakes are not representative because of their shallow depth, which leads to a short duration of the transient process.

The research is funded by:

1. General committee of Russian Academy of Sciences: Project VIII.73.1.7 Geological, geophysical and geochemical studies in Siberian shelf-Laptev sea transient zone on a basis of Samoylov research station.

2. Novosibirsk State University, Strategic academic unit: Project Geological and Geophysical Investigations in the Arctic and Global Priorities.

3.6 Work package 5 and 6: Coring of lake, lagoon, and sea ice

Ingeborg Bussmann[1], Guido Grosse[2], Heike Zimmermann[2]

[1] Alfred Wegener Institute Helmholtz Centre for Polar- and Marine Research, Helgoland, Germany

[2] Alfred Wegener Institute Helmholtz Centre for Polar- and Marine Research, Potsdam, Germany

Fieldwork period and location
From April 05th to April 12th, 2017 (on Bykovsky Peninsula)

Objectives
Ice cores were obtained for later analysis of the methane cycle (WP 5) and molecular analysis for community changes in freshwater and marine ice algae (WP 6).

Methods
For each station three ice cores were drilled with a Kovacs Mark II ice coring system (9 cm diameter), one to measure the in-situ temperature and as back-up core (labelled with "T"), one core was for methane analysis ("M") and the third for DNA-extraction ("G").
The ice temperature was measured immediately after retrieval with a temperature probe (Testo 720) in predrilled holes every 10 cm. The ice cores for temperature and methane measurements were packed in PE tubings and stored in thermo boxes continuously frozen. For DNA ice cores all handling was performed with nitrile gloves, which were changed between the different samples.
Water samples below the ice and above the bottom were taken from stations 20, 23, 24 as well as 31 and 32. Subsamples were taken for later gas analysis. Additionally, the water was filtered through 0.2 μm filters (Millipore GTTP), which were frozen for later DNA-analysis and the filtrate subsampled for WP 1 for nutrient analysis.

Preliminary results
On Goltsovoye Lake we laid a west east transect across the lake (cores BYK17-ICE 20 - 24). In the cores # 20 – 24 the ice was cold (-6 °C) at the surface, with an almost linear temperature increase towards 0 °C at 1 m depth until the water interface (Figure 3.6-1). The cores # 21 and # 23 were only around -4 °C at the surface, with a linear temperature increase toward -1 °C towards the water interface (Figure 3.6-1).

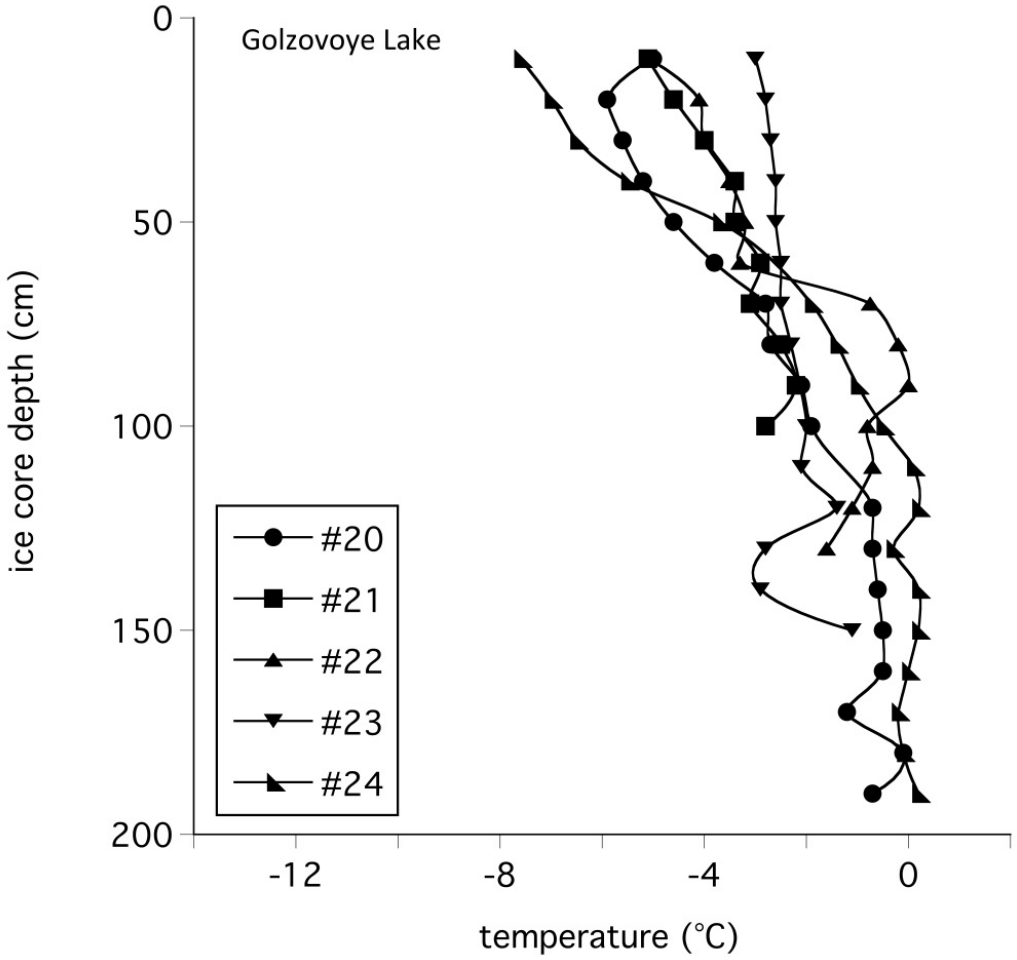

Figure 3.6-1: *Temperature profiles of ice cores from Goltsovoye Lake*

The cores 27 – 30 were positioned as a transect from the outlet of Polar Fox Lagoon towards the outer Tiksi Bay. The ice was not as thick as in Goltsovoye Lake and the water below slightly brackish. The temperature of the four ice cores was very similar: very cold at the surface (-7 °C), followed by a linear increase with depth towards -0.3 °C the water interface (Figure 3.6-2).

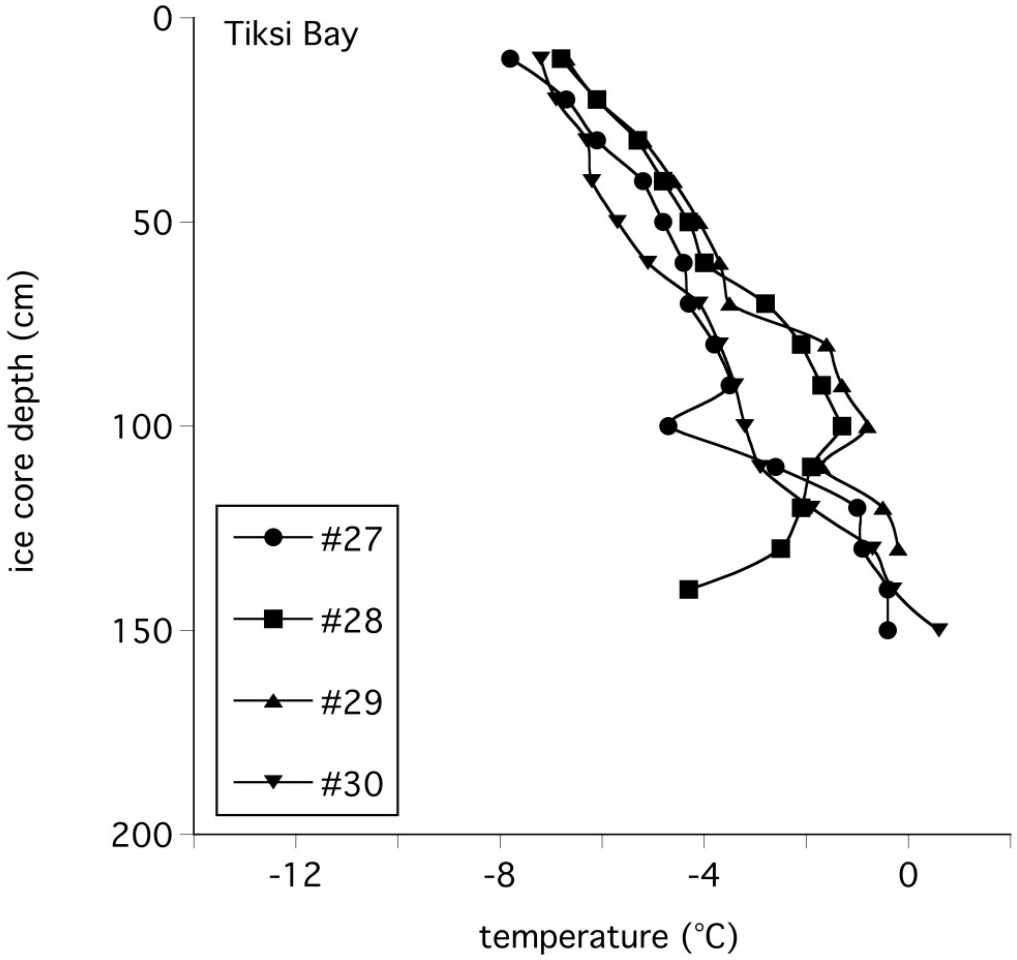

Figure 3.6-2: *Temperature profiles of ice cores from Tiksi Bay*

The temperature profiles of the two ice cores from Polar Fox Lagoon were also very similar with -12 °C at the surface and -0.5 °C at the bottom (Figure 3.6-3).

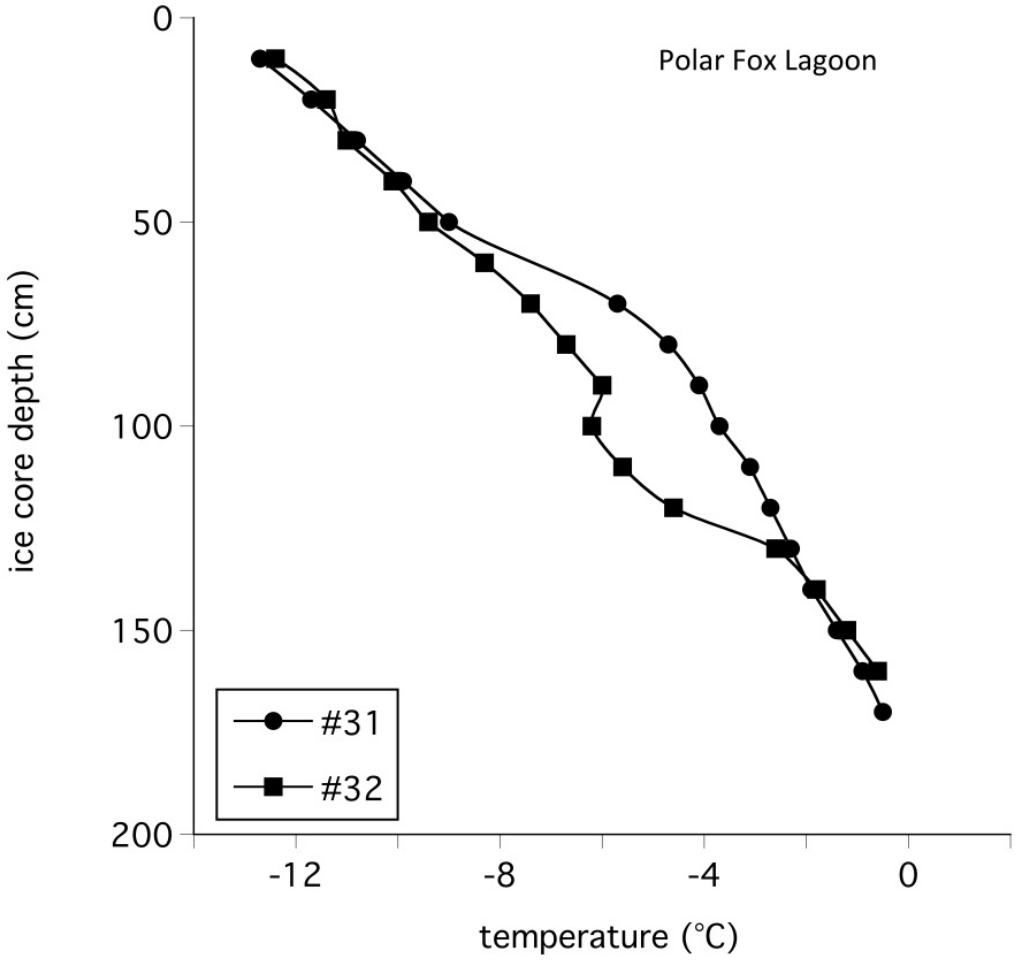

Figure 3.6-3: *Temperature profiles of ice cores from Polar Fox Lagoon*

Site and ice core descriptions

BYK17-ICE 20 (07.04.2017)
The coring site was snow free. The ice was 190 cm thick, transparent-white, and no algae inclusions were visible (Table 3.6.1, Figure 3.6-4).

BYK17-ICE 21 (08.04.2017)
The drilling took place at the lake shore, where the ice was frozen to the ground (Table 3.6.1, Figure 3.6-4). The snow cover was 23 cm thick, hard and characterized by melt form conformation. The ice thickness was estimated to be 110 cm. To avoid contamination of the ice with sediments, the coring was stopped at 100 cm depth. The upper 5 cm of the cores are made up of snow ice. The ice included small, elongated air bubbles. No algae inclusions were visible. The lowest 2 cm of the DNA ice core were lost, because the coring dogs were frozen.

BYK17-ICE 22 (08.04.2017)
The snow cover was 14 - 15 cm thick, very hard and characterized by melt form conformation (Table 3.6.1, Figure 3.6-4). At 111 cm depth and downwards the ice appeared whiter. No algae inclusions were visible. A short core (PG2421) was taken to retrieve surface sediments (0 - 2 cm depth).

BYK17-ICE 23 (08.04.2017)
The snow cover was 92 cm thick, hard and characterized by melt form conformation (Table 3.6.1, Figure 3.6-4). A temperature profile along the snow depth was taken every 10 cm. After collecting

the first core, methane bubbles ascended. From the surface until about 112 - 114 cm depth, the ice is milky, white and below the ice is clear. No algae inclusions were visible. A short core (PG2422) was taken to retrieve surface sediments (0 - 2 cm depth).

BYK17-ICE 24 (08.04.2017)
The coring site was snow free. The ice thickness was 197 cm (Table 3.6.1, Figure 3.6-4). The ice core for methane analyses included methane bubbles. No algae inclusions were visible. A short core was taken to retrieve surface sediments (0 - 2 cm depth).

BYK17-ICE 27 (10.04.2017, marine)
The snow cover was 11 cm thick. The ice thickness was 149 cm. The uppermost 3 cm of the ices core are composed of snow ice (Table 3.6.1, Figure 3.6-4). The ice is not clear and has a very high concentration of air bubbles. No algae inclusions were visible.

BYK17-ICE 28 (10.04.2017, marine)
The snow cover was between 25 and 32 cm thick. The ice thickness was 150 cm (Table 3.6.1, Figure 3.6-4). The uppermost 6 cm of the ice cores appear milky. The ice is not clear and has a very high concentration of air bubbles. No algae inclusions were visible.

BYK17-ICE 29 (11.04.2017, marine)
The snow cover was 32 cm thick. The ice thickness was 131 cm (Table 3.6.1, Figure 3.6-4). The uppermost 7 to 10 cm of the ice cores are made up of snow ice. The ice is not clear and has a very high concentration of air bubbles. No algae inclusions were visible.

BYK17-ICE 30 (11.04.2017, marine)
The snow cover was 14 cm thick. The ice thickness was 144 cm. The ice is not clear and has a very high concentration of air bubbles (Table 3.6.1, Figure 3.6-4). No algae inclusions were visible. After drilling the deepest part (114 - 143 cm depth) of the second ice core (methane ice core) at this site, the core was frozen in the corer, which prevented the collection of a third ice core (DNA ice core).

BYK17-ICE 31 (11.04.2017)
The snow cover was 8 cm thick. The ice was 167 cm thick. The ice was clear and contained inclusions of elongated air bubbles. No algae inclusions were visible (Table 3.6.1, Figure 3.6-4).

BYK17-ICE 32 (11.04.2017)
The snow cover was 20 cm thick. The ice thickness was 165 cm. The uppermost 3 cm of the ice cores are milky-white. The deepest part of the ice was salty. The ice was clear and contained inclusions of elongated air bubbles. No algae inclusions were visible (Table 3.6.1, Figure 3.6-4).

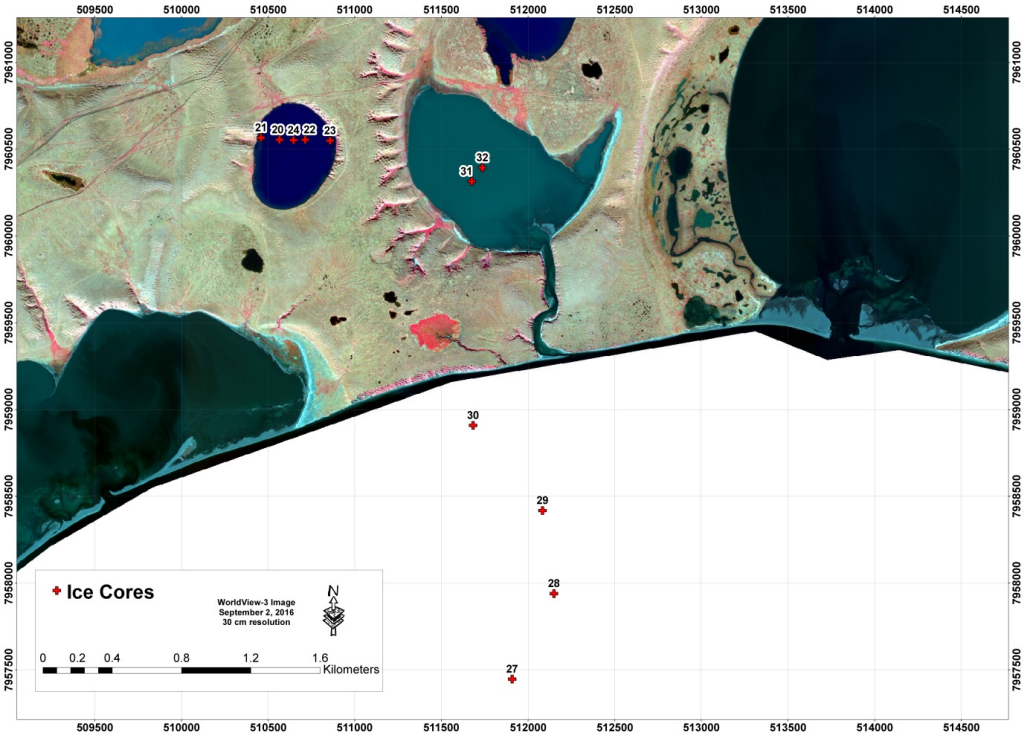

Figure 3.6-4: *Position of the different ice cores in the lakes and Tiksi Bay*

Table 3.6.1: Position of the ice cores, as well as information on ice thickness, water depths and snow cover

Station	Position [Latitude N / Longitude E]	Ice thick-ness [m]	Water depth [m]	Snow cover	Remark
Goltsovoye Lake					
BYK17- ICE 20	71.74534 / 129.30222	1.9	5	0.01	Additional water sampling
BYK17- ICE 21	71.74544 / 129.29916	1.1	0	0.23	Top 5 cm snow ice
BYK17- ICE 22	71.74533 / 129.30647	1.33	8.48	0.15	
BYK17- ICE 23	71.74528 / 129.31055	1.68	6.2	0.92	After coring water was streaming out of the borehole, additional water sampling
BYK17- ICE 24	71.74531 / 129.30455	1.97	5.7	0.01	Additional water sampling
Tiksi Bay					
BYK17- ICE 27	71.71741 / 129.3401	1.49	4.21	0.11	
BYK17- ICE 28	71.72182 / 129.34707	1.5	3.3	0.28	
BYK17- ICE 29	71.72611 / 129.34528	1.31	3.87	0.32	
BYK17- ICE 30	71.73053 / 129.33391	1.44	2.84	0.14	
Polar Fox Lagoon					
BYK17- ICE 31	71.74313 / 129.33391	1.67	2.81	0.08	Additional water sampling
BYK17- ICE 32	71.74384 / 129.33569	1.65	2.62	0.2	Additional water sampling

3.6.1 Work package 5: Methane distribution and oxidation in ice cores

Ingeborg Bussmann[1] and (Ellen Damm[2]: not in the field)

[1] Alfred Wegener Institute Helmholtz Centre for Polar and Marine Research, Helgoland, Germany

[2] Alfred Wegener Institute Helmholtz Centre for Polar and Marine Research, Bremerhaven and Potsdam, Germany

Fieldwork period and location
From April 05th to April 24th, 2017 (on Bykovsky Peninsula)

Objectives
In lakes and coastal seas, the ice formation and the ice cover offer opportunities for the combined use of field studies, remote sensing and modelling, with the goal of identifying methane sources and assessing the relative importance of sea ice as a methane reservoir or buffer and as a habitat for methane-relevant microbial communities. Additionally, the uptake of terrestrial or sedimentary microbial communities into fast ice is an important object of investigation that links the terrestrial/permafrost and marine environments.
Until now most of our knowledge on the methane cycle in the study area has been obtained in summer. However, as most of the year the study area is ice covered it is important to assess the methane related process also in the dominant ice-covered season.

Methods
For determining the methane oxidation rates and later methane concentrations and isotopic values the ice cores were processed at the Research Station “Samoylov Island”.
The top 10 cm, a 10 cm mid-section and three 10 cm-sections at the bottom of the core were cut off and transferred to special PVDF gas sampling bags (Keikaventures). The remaining parts of the cores were returned to the thermo boxes. The bags were evacuated and the cores melted within approx. 5 h in a water bath at 8 °C.
Samples for later gas analysis were obtained in three different ways: i) gas of the headspace was taken directly via syringe and transferred into glass bottles filled with saturated NaCl solution; ii) with another syringe 40 ml of water were taken, 20 ml of nitrogen gas added and after vigorously shaking for 2 min the gas phase was transferred into glass bottles filled with saturated NaCl solution (Pohlman et al., 2017). A third glass bottle was completely filled with the sample water and poisoned with 0.3 ml of 25 % H_2SO_4. Gas analysis will be performed later in the home laboratories. For each depth one subsample (40 ml) was taken for later isotope analysis of the water phase. To determine the methane oxidation rate, the remaining water was transferred via syringe into further glass bottles, which were closed without headspace. Tritiated methane was added and the samples incubated for 60 h at 1 °C. After stopping the incubation by adding H_2SO_4, the total radioactivity of the sample and after sparging the radioactivity of only the water was determined (Bussmann et al., 2015). All samples, discarded water and waste are transferred back to the home laboratory. Additional water samples from below the ice at different locations of the Lena River and samples from a small pond on Samyolov Island were also investigated.

Preliminary results
The sampling for later gas analysis revealed that the cores contained different amounts of gas (revealed as gas phase in the sampling bag). We hope to relate the amount of gas to the visual structure of the ice cores.

The fractional turnover rate k' was calculated from the preliminary data, for the final calculation of the methane oxidation rate the methane concentration is necessary, but not yet available. K' is the first-order rate constant calculated as the fraction of ^{3}H-CH_4 oxidized per unit time, it can also be seen as an indication of the relative activity. The fractional turnover rates were rather low, and many samples were below the detection limit. For Goltsovoye Lake. and Tiksi Bay about 88 % and 66 % were below the detection limit respectively (total n = 40, n = 41). For the samples above the detection limit no spatial trend was obvious i.e. higher activity at top or bottom of the ice cores; also, no difference between the lake and the Bay was obvious. In all the samples from the river water, we could detect an activity, within the same range as in the ice samples. The highest activity was recorded in the water of a small pond on Samoylov island, about 10 times higher as in the other samples.

3.6.2 Work package 6: Paleoenvironment and paleogenetics on ice algae

Heike Zimmermann[1], Ulrike Herzschuh[1] and Kathleen Stoof-Leichsenring[1]

[1] Alfred Wegener Institute Helmholtz Centre for Polar and Marine Research, Potsdam, Germany

Fieldwork period and location
From April 05th to April 12th, 2017 (on Bykovsky Peninsula)

Objectives
The seasonal extent and properties of arctic ice and snow cover on land and ocean determine the efficacy of the albedo feedback mechanism causing arctic climate amplification. The various ice types are inhabited by specific ice algae communities that across taxonomic boundaries share the habitability of these extreme arctic environments. The community composition (taxonomic diversity) will be studied in ice samples, in the water column and surface sediments (marine and lake sediments). This application aims at the understanding of the long-term development of arctic ice cover representing a key environmental variable. It combines ancient DNA and modern genomic analyses and integrates the survey of taxonomic and also functional diversity.

Methods
Ice cores, snow samples and surface sediments were taken according to the sampling scheme (Figure 3.6-5) from three different sampling locations: (1) Goltsovoye Lake, (2) Polar Fox Lagoon and (3) a marine transect in the Tiksi Bay. In the field we sampled the upper part of the ice core (40 cm), the middle part (40 cm) and the lower part (20 cm). These sections were stored and transported to Potsdam while continuously frozen. In the new Potsdam diatom laboratory, the ice samples will be thawed and filtered through a sterile cellulose nitrate filter. The DNA will then be extracted from these filters and state-of-the-art genetic methodologies (high-throughput amplicon sequencing, shotgun sequencing) will be used to analyze the algae diversity and community composition.
At the same localities short sediment cores were taken using a UWITEC™ gravity corer. From the short gravity cores, the surface sediments (upper 2 cm of the core) were sub-sampled for genetic analyses in the camp at room temperature to avoid freezing of the samples. Additionally, a 2 cm thick slice at the depth from 8 to 10 cm was sub-sampled. Cores from unfrozen sediments, which were taken by WP3 will be analyzed for long-term environmental and community changes of algae.

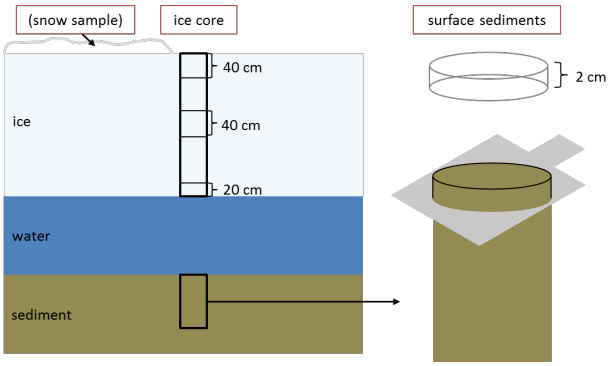

Figure 3.6-5: *Schematic overview for the sampling of snow, ice core sections and short gravity sediment cores for molecular genetics analyses*

3.7 Bibliography

Adams M. (1808): Some Account of a Journey to the Frozen-Sea, and of the Discovery of the Remains of a Mammoth. The Philadelphia Medical and Physical Journal, Part 1 Vol. 3, pp. 120-137.

Andreev A.A., Schirrmeister L., Siegert C., Bobrov A.A., Demske D., Seiffert M., Hubberten H.-W. (2002): Paleoenvironmental changes in Northeastern Siberia during the Late Quaternary - evidence from pollen records of the Bykovsky Peninsula. Polarforschung 70, pp. 13-25.

Biskaborn et al (2013a): Late Holocene thermokarst variability inferred from diatoms in a lake sediment record from the Lena Delta, Siberian Arctic. JOPL

Biskaborn et al (2013b): Thermokarst processes and depositional events in a tundra lake, north-eastern Siberia. PPP

Bobrov A.A., Andreev A.A., Schirrmeister L., Siegert Ch. (2004): Testate amoebae (Protozoa: Testacea) as bioindicators in the Late Quaternary deposits of the Bykovsky Peninsula, Laptev Sea, Russia. Palaeogeography palaeoclimatology palaeoecology 209, pp. 165-181.

Bunge A. (1895): Die Lena Expedition 1881-1884. In: Tillo A.: Beobachtungen der russischen Polarstation an der Lenamündung. Expedition der Kaiserl. Russischen Geographischen Gesellschaft, St. Petersburg, pp 1-96.

Bussmann I., Matousu A., Osudar R., Mau S. (2002): Assessment of the radio ^{3}H-CH_4 tracer technique to measure aerobic methane oxidation in the water column. Limnol. Oceanogr. Methods 13, pp. 312-327. doi:10.1002/lom3.10027.

Cheverev V.G., Vidyapin I.Y., Tumskoy V.E. (2007): Composition and characteristics of the thermokarst lagoon deposits, Bykovsky Peninsula. Kriosfera Zemli 11 (3), pp. 44–50 (in Russian).

Diekmann B., Pestryakova L., Nazarova L., Subetto D., Tarasov P.E., Stauch G., Thiemann A., Lehmkuhl F., Biskaborn B.K., Kuhn G., Henning D., Müller S. (2017): Late Quaternary Lake Dynamics in the Verkhoyansk Mountains of Eastern Siberia: Implications for Climate and Glaciation History. Polarforschung 86, pp. 97-110. doi: 10.2312/polarforschung.86.2.97.

Drachev S.S., Savostin L.A., Groshev V.G., Bruni I.E. (1998): Structure and geology of the continental shelf of the Laptev Sea, Eastern Russian Arctic. Tectonophysics 298, pp. 357-393.

Drozdova A.N., Vetrov A.A., Romankevich E.A., Prokuda N.A., Sukhoverkhov S.V., Bratskaya S.Yu., Sergienko V.I., Semiletov I.P., Ulyantsev A.S. (2016): Polycyclic aromatic hydrocarbons in Holocene–Pleistocene sediments of the Laptev Sea. Doklady Earth Sciences 468, pp.496–499. doi: 10.1134/S1028334X16050123.

Franke F., Hinz K., Oncken O. (2001): The Laptev Sea rift. Marine and Petroleum Geology 18, pp. 1083-1127.

Fukuda M. (1994): Occurrence of Ice-complex (Edoma) in Lena River Delta Region and Big Lhyakovsky Island, High Arctic Eastern Siberia. In: Inoue G.: Proceedings 2nd Symposium on the Joint Siberian Permafrost Studies between Japan and Russia. pp 5-13.

Grigoriev M. N., Imaev V. S., Koz'min B. M., Kunitski V. V., Larionov A. G., Mikulenko K. I., Skryabin R. M., Timirshin K. V. (1996): Geology, seismicity and cryogenic processes in the arctic areas of western Yakutia. 80. Scientific Center SD RAS, Yakutsk (in Russian).

Grigoryev M.N. (1993): Cryomorphogenesis of the Lena Delta mouth area. Yakutsk: Permafrost Inst Academy of Science USSR, Siberian Dep., pp 1-176 (in Russian).

Grosse G., Schirrmeister L., Kunitsky V.V., Hubberten H.-W. (2005): The use of CORONA images in remote sensing of periglacial geomorphology: an illustration from the NE Siberian coast. Permafrost and periglacial processes 16, pp. 163-172.

Grosse G., Schirrmeister L., Siegert Ch., Kunitsky V.V., Slagoda E.A., Andreev A.A., Dereviagyn A.Y. (2007): Geological and geomorphological evolution of a sedimentary periglacial landscape in Northeast Siberia during the Late Quaternary. Geomorphology 86 (1/2), pp. 25-51.

Imaev V.S., Imaeva L.P., Kozmin B.M. (2000): Seismotektonika Yakutii [Seismo-tectonics of Yakutia]. Moscow: GEOS (in Russian).

Ivanov M.S., Katasonova E.G. (1978): Pecularities of cryolithogenic deposits of the Muostakh Island. In: Anisimova N.P., Katasonova E.G.: Geokriologicheskie i gidrogeologicheskie issledovaniya in Yakutia (Geocryologic and hydrogeologic research in Yakutia). Yatutsk: Permafrost Institute, SO AN SSSR, pp. 12-25 (in Russian).

Kholodov A.L., Rivkina E.M., Gilichinsky D.A., Fedorov-Davydov D.G., Gubin S.V., Sorokovikov V.A., Ostroumov V.E., Maksimovich S.V. (2003): Estimation of the organic carbon input into Arctic Ocean due to erosion of Laptev and East-Siberian seashore. Kriosfera Zemli (Earth' Cryosphere) 7, pp. 3–12.

Kienast F., Schirrmeister L., Siegert C., Tarasov P. (2005): Palaeobotanical evidence for warm summers in the East Siberian Arctic during the last cold stage. Quaternary Research: 63 (3), pp. 283-300.

Knoblauch C., Spott O., Evgrafova S., Kutzbach L., Pfeiffer E.-M. (2015): Regulation of methane production, oxidation, and emission by vascular plants and bryophytes in ponds of the northeast Siberian polygonal tundra. Journal of Geophysical Research: Biogeosciences 120, pp. 2525-2541.

Kunitsky V.B. (1989): Cryolithogenesis of the lower Lena Permafrost. Yatutsk: Inst Acad of Sci USSR, Siberian Dep, pp. 1-162 (in Russian).

Liebner S., Ganzert L., Kiss A., Yang S., Wagner D., Svenning M.M. (2015): Shifts in methanogenic community composition and methane fluxes along the degradation of discontinuous permafrost. Frontiers in Microbiology 6, pp. 1-10. doi: 10.3389/fmicb.2015.00356

Liebner S., Svenning M.M. (2013): Environmental transcription of mmoX by methane oxidizing Proteobacteria in a Sub-Arctic palsa peatland. Applied and Environmental Microbiology 79, pp. 701-706.

Mitzscherling J., Winkel M., Winterfeld M. et al. (2017): The development of permafrost bacterial communities under submarine conditions. Journal of Geophysical Research: Biogeosciences 122, pp. 1689-1704.

Nagaoka D. (1994): Properties of Ice Complex deposits in eastern Siberia. Proceedings of the 2nd Symposium on the Joint Siberian Permafrost Studies between Japan and Russia, pp 14-18.

Olefeldt D., Goswami S., Grosse G. et al. (2016): Circumpolar distribution and carbon storage of thermokarst landscapes. Nature Communications 7, pp. 1-11 13043.

Overduin P.P., Liebner S., Knoblauch C. et al. (2015): Methane oxidation following submarine permafrost degradation: Measurements from a central Laptev Sea shelf borehole. Journal of Geophysical Research: Biogeosciences 120, pp. 965-978.

Overduin P.P., Westermann S., Yoshikawa K., Haberlau T., Romanovsky V., Wetterich S. (2012): Geoelectric observations of the degradation of nearshore submarine permafrost at Barrow (Alaskan Beaufort Sea). Journal of Geophysical Research 117, pp. 1-9. F02004, doi:10.1029/2011JF002088.

Pohlman J.W., Greinert J., Ruppel C., Silyakova A., Vielstädte L., Casso M., Mienert J., Bünz S. (2017): Enhanced CO_2 uptake at a shallow Arctic Ocean seep field overwhelms the positive warming potential of emitted methane. Proceedings of the National Academy of Sciences 114, pp. 5355-5360.

Romankevich E.A., Vetrov A.A., Belyaev N.A., Ulyantsev A.S., Sergienko V.I., Sukhoverkhov S.V., Bratskaya S.Y., Prokuda N.A., Semiletov I.P. (2017): Alkanes in quaternary deposits of the Laptev Sea. Doklady Earth Sciences 472 (1), pp. 36-39. doi: 10.1134/S1028334X17010093.

Romanovskii N.N., Hubberten H.W., Gavrilov A.V., Tumskoy V.E., Kholodov A.L. (2004): Permafrost of the east Siberian Arctic shelf and coastal lowlands. Quaternary Science Reviews 23 (11), pp. 1359-1369.

Schirrmeister L., Grigoriev M.N., Strauss J., Grosse G., Overduin P.P., Kholodov A., Guenther F., Hubberten, H.-W. (2018): Sediment characteristics of a thermokarst lagoon in the northeastern Siberian Arctic (Ivashkina Lagoon, Bykovsky Peninsula). arktos 4 (13). doi:10.1007/s41063-018-0049-8.

Schirrmeister L., Kunitsky V., Grosse G., Kuznetsova T., Kuzmina S., Bolshianov D. (2001): Late Quaternary and recent environmental situation around the Olenyok Channel (western Lena Delta) and on Bykovsky Peninsula, Berichte zur Polar- und Meeresforschung 388, pp. 85-135.

Schirrmeister L., Siegert C., Kunitzky V.V., Grootes P.M., Erlenkeuser H. (2002a): Late Quaternary ice-rich permafrost sequences as an paleoenvironmental archive for the Laptev Sea Region in northern Siberia. International journal of earth sciences 91, pp. 154-167. DOI 10.1007/s005310100205.

Schirrmeister L., Siegert C., Kuznetsova T., Kuzmina S., Andreev A.A., Kienast F., Meyer H., Bobrov A.A. (2002b): Paleoenvironmental and paleoclimatic records from permafrost deposits in the Arctic region of Northern Siberia. Quaternary International 89, pp. 97-118.

Schleusner et al. (2014): Basin evolution and palaeoenvironmental variability of the thermokarst lake El'gene-Kyuele, Arctic Siberia, Boreas

Sergienko A.I., Belolyubsky I.N., Grinenko O.V. (2004): Stratigraphic scheme of Quaternary deposits of the northern Verkhoyan (Eastern Yakutia). Otechestvennaya Geologiya 4, pp. 88–92 (in Russian).

Shakhova N., Semiletov I., Gustafsson O., Sergienko V., Lobkovsky L., Dudarev O., Tumskoy V., Grigoriev M., Mazurov A., Salyuk A., Ananiev R., Koshurnikov A., Kosmach D., Charkin A.,

Dmitrevsky N., Karnaukh V., Gunar A., Meluzov A., Chernykh D. (2017): Current rates and mechanisms of subsea permafrost degradation in the East Siberian Arctic Shelf. Nature Communications 8, pp. 1-13. 15872, doi: 10.1038/ncomms15872.

Shakhova N., Semiletov I., Sergienko V., Lobkovsky L., Yusupov V., Salyuk A., Salomatin A., Chernykh D., Kosmach D., Panteleev G., Nicolsky D., Samarkin V., Joye S., Charkin A., Dudarev O., Meluzov A., Gustafsson O. (2015): The East Siberian Arctic Shelf: towards further assessment of permafrost-related methane fluxes and role of sea ice. Philosophical Transactions A 373, pp. 1-13. 20140451, doi.org/10.1098/rsta.2014.0451.

Sher A., Parmuzin I., Bortsov A. (2000): Ice Complex on the Bykovsky Peninsula. In: Rachold V., Grigoriev M.N.: Russian-German Cooperation System Laptev Sea 2000: The Expedition LENA 1999. Reports on Polar Research 354, pp. 169-182.

Sher A.V., Kuzmina S.A., Kuznetsova T.V., Sulerzhinsky L.D. (2005): New insights into the Weichselian environment and climate of the East Siberian Arctic, derived from fossil insects, plants, and mammals. Quaternary Science Reviews 24, pp.533–569.

Siegert C., Kunitzky V.V., Schirrmeister L., Meyer H., Derevyagin A., Tumskoy V., Kuznetsova T., Kuzmina S., Sher A. (1999): Paleoclimate signals of ice-rich permafrost. Berichte zur Polar- und Meeresforschung 315, pp. 145-259.

Siegert C., Schirrmeister L., Babiy O. (2002): The sedimentological, mineralogical and geochemical composition of late Pleistocene deposits from the ice complex on the Bykovsky peninsula, northern Siberia. Polarforschung 70 (2000), pp. 3-11.

Slagoda E.A. (1991): Microstructure features of the deposits of ice complexes in northern Yakutia by the example of Bykov Peninsula). In: Gilichinskiy D.A.: Kriologiya pochv. Pushchino, IPFS PNTs AN SSSR, pp. 38-47 (in Russian).

Slagoda E. A. (1993): Genesis and microstructure of cryolithogenic deposits at the Bykovsky Peninsula and the Muostakh Island. Dissertation, RAS Sibirian Section, Permafrost Institute, Yakutsk, pp. 1-218 (in Russian).

Slagoda E.A. (2004): Cryolithogenic deposits of the Laptev Sea coastal plain: lithology and micromorphology. Publishing and Printing Centre Express, Tyumen, p. 119 (in Russian).

Tomirdiaro S.V., Chernenky B.I. (1987): Cryogenic deposits of East Arctic and Subarctic. AN SSSR Far-East-Science Center, pp. 1-196 (in Russian).

Treude T., Boetius A., Knittel K., Wallmann K., Jörgensen B.B. (2003): Anaerobic oxidation of methane above gas hydrates at Hydrate Ridge, NE Pacific Ocean. Marine Ecology Progress Series 264, pp. 1-14.

Tumskoy V.V. (2001): Thermokarst and its role for the development of the Laptev Sea region during the late Pleistocene and Holocene. Moscow State University: PhD Thesis, author referat, pp. 109.

Tveit A., Schwacke R., Svenning M.M., Urich T. (2012): Organic carbon transformations in high-Arctic peat soils: key functions and microorganisms. ISME J 7, pp. 299-311. doi: 10.1038/ismej.2012.99

Ulyantsev A.S., Bratskaya S.Yu., Romankevich I.P., Semiletov E.A., Avramenko V.A. (2016a): Particle size composition of Holocene–Pleistocene deposits of the Laptev Sea (BuorKhaya Bay). Doklady Earth Sciences 467 (1), pp. 241–245. doi:10.1134/S1028334X16030168.

Ulyantsev A.S., Polyakova N.V., Romankevich E.A., Semiletov I.P., Sergienko V.I. (2016c): Ionic composition of pore water in shallow shelf deposits of the Laptev Sea. Doklady Earth Sciences 467 (1), pp.308–313. doi: 10.1134/S1028334X16030211.

Ulyantsev A.S., Romankevich E.A., Bratskaya S.Yu., Prokuda N.A., Sukhoverkhov S.V., Semiletov I.P., Sergienko V.I. (2017a): Characteristics of the Quaternary sedimentation at the Laptev Sea Shelf based on molecular composition of n-Alkanes. Doklady Earth Sciences 473 (2), pp. 449-453. doi: 10.1134/S1028334X17040158

Ulyantsev A.S., Romankevich E.A., Bratskaya S.Yu., Semiletov I.P., Avramenko V.A. (2017b): Organic and Inorganic carbon in permafrost and thawed deposits from Buor-Khaya Bay (Laptev Sea). Doklady Earth Sciences 473 (2), pp. 467-471. doi: 10.1134/S1028334X17040237.

Ulyantsev A.S., Romankevich E.A., Peresypkin V.I., Belyaev N.A., Vetrov A.A., Semiletov I.P., Bratskaya S.Y., Sergienko V.I. (2016b): Lignin as an indicator of the sedimentation conditions of the Arctic Shelf. Doklady Earth Sciences 467 (1), pp. 264–269. doi: 10.1134/S1028334X16030089.

Wetterich S., Schirrmeister L., Pietrzeniuk E. (2005): Freshwater ostracodes in Quaternary permafrost deposits from the Siberian Arctic. Journal of Paleolimnology 34, pp. 363-376. doi:10.1007/s10933-005-5801-y.

Winkel M., Mitzscherling J., Overduin P.P. et al. (2018): Anaerobic methanotrophic communities thrive in deep submarine permafrost. Scientific Reports 8, pp. 1-13. doi: 10.1038/s41598-018-19505-9

Chapter 4

Summer campaign on Bykovsky Peninsula

Edited by: Michael Angelopoulos, Katharina Jentzsch, Bennet Juhls, Georgii Maximov, Pier Paul Overduin

4.1 Expedition Report – Bykovsky Peninsula Summer Expedition 2017

Michael Angelopoulos[1], Georgy Maximov[2], Bennet Juhls[3], Mikhail Grigoriev[2], Pier Paul Overduin[1], Aleksey Fage[4,5], Vladimir Olenchenko[4], Konstantin Sosnovtsev[5], Egor Esin[5], Polina Nikitich, [5,6], Andrey Kartozia[5], Vladimir Kashirtsev[4], Igor Yeltsov[4]

[1] Alfred Wegener Institute Helmholtz Centre for Polar and Marine Research, Potsdam, Germany

[2] Melnikov Permafrost Institute, Siberian Branch, Russian Academy of Sciences, Yakutsk, Russian Federation

[3] Institute of Space Sciences, Freie Universität Berlin, Berlin, Germany

[4] Trofimuk Institute of Petroleum Geology and Geophysics of Siberian Branch Russian Academy of Sciences, Novosibirsk, Russian Federation

[5] Novosibirsk State University, Novosibirsk, Russian Federation

[6] Institute of Soil Science and Agrochemistry, Siberian Branch, Russian Academy of Sciences, Novosibirsk, Russian Federation

[7] V.S. Sobolev Institute of Geology and Mineralogy of Siberian Branch, Russian Academy of Sciences, Novosibirsk, Russian Federation

Fieldwork period and location
July 09th to August 09th, 2017 (Bykovsky Peninsula)

Itinerary

Jul. 9: German participants travel to Tiksi

Jul. 11: Transfer to and establishment of basecamp at Uomullyakh-Kyuel Lagoon on the Bykovsky Peninsula

Aug. 1-6: Work aboard the Yacht Nicole in Tiksi Bay, Buor Khaya Bay and the Lena Delta

Aug. 5: Decamping from Uomullyakh-Kyuel Lagoon

Aug. 8: Travel from Tiksi to Yakutsk

Aug. 9: German participants return to Germany

Background and objectives
This expedition focused on interactions between water bodies and permafrost along the coast of the central Laptev Sea. This region is currently undergoing rapid environmental changes that include longer open water season, increasing snow depth, warming air and shelf sea temperatures, increasing river discharge, and freshening of shelf surface water. The consequences of these changes for the shelf ecosystem are likely to be severe, but it is not clear where the trajectory of change leads. Process studies and large-scale monitoring activities are necessary to understand the current state of the system and to be able to detect ongoing and future changes.
In April 2017, four sites were drilled on the Bykovsky Peninsula (Strauss et al., this volume). By connecting observations from the boreholes into geophysical surveys, the spatial distribution of permafrost beneath an incipient thermokarst lake, a thermokarst lake (Goltsovoye Lake), a saltwater lake within a drained freshwater lake basin (Polar Fox Lagoon), a coastal lagoon (Uomullyakh-Kyuel Lagoon) and in front of the coast can be analysed. Analysis of multi-temporal remote sensing data

provides a temporal context for the expansion of thermokarst water bodies, the progress of coastal erosion and sediment transport and the rates of permafrost aggradation and degradation.

Geophysical datasets, thermal modelling, and drilling data suggest that most Arctic shelves are underlain by submarine permafrost due to their exposure during the glacial low water stands (Romanovskii et al., 2004). The degradation of submarine permafrost could release large quantities of methane into the atmosphere, impact offshore drilling activities, and affect coastal erosion. The degradation of subsea permafrost itself depends on the duration of inundation, warming rate, the coupling of the seabed to the atmosphere from bottom-fast ice, and brine injections into the seabed (Overduin et al., 2012). The impact of brine injections on permafrost degradation is dependent on seawater salinity, which changes seasonally in response to salt rejection from sea ice formation and terrestrial freshwater inflows. The rate of submarine permafrost evolution and the relative importance of the many controls responsible for degradation, however, remain poorly understood. This work will evaluate submarine permafrost degradation rates on the Bykovsky Peninsula (north Siberia) using a combination of geophysical, sampling, and remote sensing methods. In addition, the work will study submarine permafrost thaw mechanisms and an approach to their representation using thermal modeling.
Sediment dynamics on the Siberian Shelf are changing but poorly constrained, especially coastal regions which are too shallow for research requiring larger marine vessels and year-round moorings. Nonetheless, the current dramatic reduction of sea ice thickness, extent and duration and rapidly changing land-to-ocean fluxes are impacting the ecosystem and oceanography of the shelf. The transition of the shelf ecosystem is due in particular to changing surface water dynamics, tied to ice thawing and freezing, river discharge, and the influx of nutrients, carbon, freshwater from coastal erosion. Monitoring and understanding the trajectory of these impacts requires remote sensing techniques. The observation of ocean colour with multi-spectral sensors permits estimation of changing shelf sediment dynamics and productivity. Furthermore, we target the unexplored but critical connection of submarine permafrost to sediment dynamics. Recent evidence, such as the disappearance of Ice Complex islands on the shelf (Romanovskii et al., 2004), the appearance of new shoals, and the migration of barriers and spits, suggest that sediment dynamics are changing, perhaps before we have a chance to establish an observational baseline for antecedent conditions. The use of ocean colour remote sensing data in arctic coastal waters is critical due to the optically complex properties (very turbid and cDOM rich waters) and the size and remoteness of the study area. The paucity of data from the region makes simultaneous measurement of optical properties and surface water chemistry necessary for the interpretation and application of ocean colour data.
Our objectives are to i) measure the distribution of permafrost-relevant geophysical parameters beneath water bodies representing various stages in the transition of terrestrial to submarine permafrost, which will allow us to quantify rates of permafrost degradation and ii) measure and apply above-water and water column radiometric measurements for the evaluation of satellite ocean colour products. The latter, combined with analyses of surface water for its constituents, will help us to understand how the optical properties of different water masses are tied to processes integral to shelf ecosystem and oceanography. *In situ* concentrations of different biogeochemical water constituents alongside with above-water and in-water reflectance measurements will be used within radiative transfer simulations to improve a better retrieval of the optical water properties via remote sensing data.

Site description

The Bykovsky Peninsula is located east of the Lena Delta in the western part of the Buor-Khaya Gulf of the Laptev Sea in northeastern Siberia, Russia (Figure 4.1-1). Cape Moustakh, the southeastern limit of the peninsula, is located approx. 20 km east-northeast of Tiksi, a harbour town and the closest urban settlement. The peninsula is an erosional remnant of an accumulation plain on the foreland of the Kharaulakh Ridge that started to form in the Late Pleistocene. The erosion of the Kharaulakh Ridge through nival and seasonal hydrological processes was the main sediment supply for the accumulation of medium to fine-grained ice-rich deposits known as the Yedoma Ice Complex. During the late stage of the Weichselian glaciation, increased meltwater resulted in higher erosion rates of the Kharaulakh Ridge's valley deposits, which ultimately disconnected the accumulation plain from its sediment source. In the early Holocene, a warming climate resulted in intense thermokarst development. Following deglaciation, marine transgression and ingression, as well as mechanical and thermal erosional processes, produced the landscape of the Bykovsky Peninsula seen today. The Yedoma Ice Complex can extend from the top of the peninsula's highlands (up to 45 m above sea level) to 10 m below sea level. However, the base of the Yedoma Ice Complex can be as high as 1 m below sea level in the Western Bykovsky Peninsula and 10 m below sea level in the Eastern Bykovsky Peninsula. Moustakh Island, also an erosional remnant, is located 15 km southeast of the Bykovsky Peninsula and also shows that the Yedoma Ice Complex can reach 10 m below sea level. Furthermore, the total ice content (wedge ice and intrasedimentary ice) can be up to 87 % by volume. Sediments within the Yedoma Ice Complex at or below sea level on the Bykovsky Peninsula mainly range from silt to fine sand. The depth to coarse-grained sandy gravel was reported to be as high as 9 m below sea level on the Western Bykovsky Peninsula and up to 29 m below sea level on the Eastern Bykovsky Peninsula. In between the Yedoma Ice Complex and the coarse-grained deposits, the soil type ranges from silty sand to sand and may contain massive cryostructures. Offshore of the Bykovsky Peninsula, part of the Yedoma Ice Complex is submerged and subsea permafrost is currently degrading. The thickness of subsea permafrost on the Laptev Sea shelf can be hundreds of metres thick and its presence can possibly extend up to 350 km offshore. Offshore of Moustakh Island, repeated borehole measurements separated by 31 - 32 years show an ice-bearing subsea permafrost degradation rate of 0.14 m per year. Furthermore, geoelectric observations offshore of Moustakh Island show that the degradation rate of ice-bearing subsea permafrost decreased from 0.4 m per year after inundation to 0.1 m per year 60 - 110 years after submergence. They also demonstrated that the depth to ice-bearing subsea permafrost at a given distance perpendicular to shore is inversely correlated with the coastal erosion rate. On the Bykovsky Peninsula, the coastal erosion rate is related to the orientation of the shoreline. From 1951-2006, the mean erosion rate was as high as 1.05 m per year for north-facing shores and as low as 0.42 and 0.27 m per year for south-facing and southeast-facing shorelines, respectively. The southern shoreline of the Bykovsky Peninsula lies in Tiksi Bay, which is a marine environment affected by the outflow of the Lena River. Due to its isolation behind Moustakh Island and Cape Moustakh, sea ice tends to be preserved longer than in the Central Laptev Sea. Northeast of Muostakh Island in 7.2 m water depth, recorded hourly benthic temperature and electrical conductivity data from 01.09.2008 to 31.08.2009. The mean annual seabed temperature was 0.5 °C, but seabed temperatures reached values lower than -1 °C below the ice in winter and spring. The mean annual electrical conductivity of the water was 7.1 mS/cm, but values can be as high as 35 mS/cm underneath the ice in winter. Following ice break-up, the influence of the Lena River discharge results in an electrical conductivity less than 0.3 mS/cm. The sea ice season in Tiksi Bay and the Buor-Khaya Gulf typically starts in late September/early October and ends in June. The mean annual air temperature in Tiksi between 1932 and 2016 was -12.8 °C (World Meteorological Organization station in Tiksi) and the average day for which air temperatures started to dip below 0 °C was September 25^{th}.

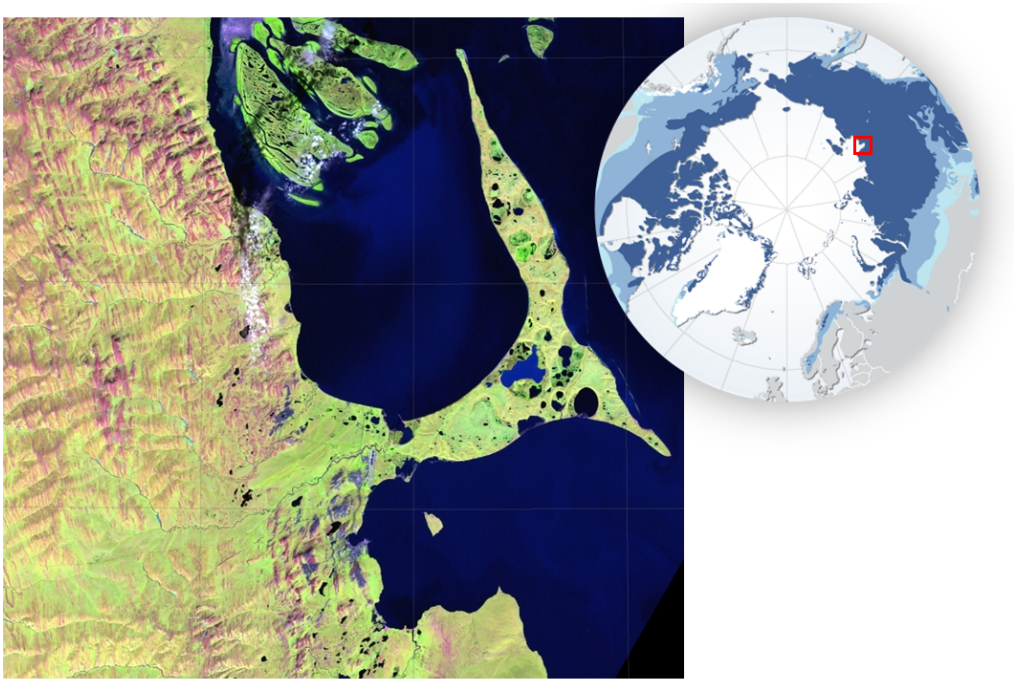

Figure 4.1-1: *Location of Bykovsky Peninsula*

Methods

Meteorological observations

A Davis Vantage Vue wireless weather station was employed at the Uomullyakh-Kyuel Lagoon to measure camp air temperature, precipitation, relative humidity, barometric pressure, wind speed and wind direction. The station was installed on a hilltop behind the camp, at location 71.73592 N, 129.29983 E. The data were recorded hourly for the period from 13.07.2017 10:00 to 04.08.2017 20:00.

- The instrument was mounted 1.7 m above the ground surface on a tripod at an elevation of 7.7 m above sea level. The tripod was secured in place with three ropes tied to tent pegs in the ground (Figure 4.1-2).
- The elevation value was extracted from a 2015 one-meter resolution digital elevation model. This value was passed to the Vantage Vue console to calibrate the barometric pressure reading.
- The instrument's wind speed detection limit was 0.83 m/s (3 km/hour).
- The instrument's rain collector measured precipitation in 0.2 mm increments.

Figure 4.1-2: *The Davis Vantage Vue meteorological station setup at Uomullyakh-Kyuel Lagoon camp on 2017-07-23*

Active layer survey

Three north to south active layer surveys were carried out, each traversing Yedoma upland permafrost, a beach terrace, and the floodplain (Figure 4.1-6). In general, the deepest active layers were recorded on the terrace. More specifically, the average active layer thickness values were 0.43, 0.54, and 0.44 m for the upland permafrost, beach terrace, and floodplain respectively. The deepest active layer thickness (0.88 m) was measured on the terrace of Profile 2 on July 18th, 2017 (Figure 4.1-4). The thinnest active layer (0.23 m) was measured on the upland of Profile 1 on July 13th, 2017. (Figure 4.1-3). The deeper active layers on the terrace are likely due to the absence of a dense insulating vegetation layer, as well as separation from the occasionally submerged tidal floodplain. Hence, the scarcely vegetated terrace likely has the greatest exposure to warm summer air temperatures.

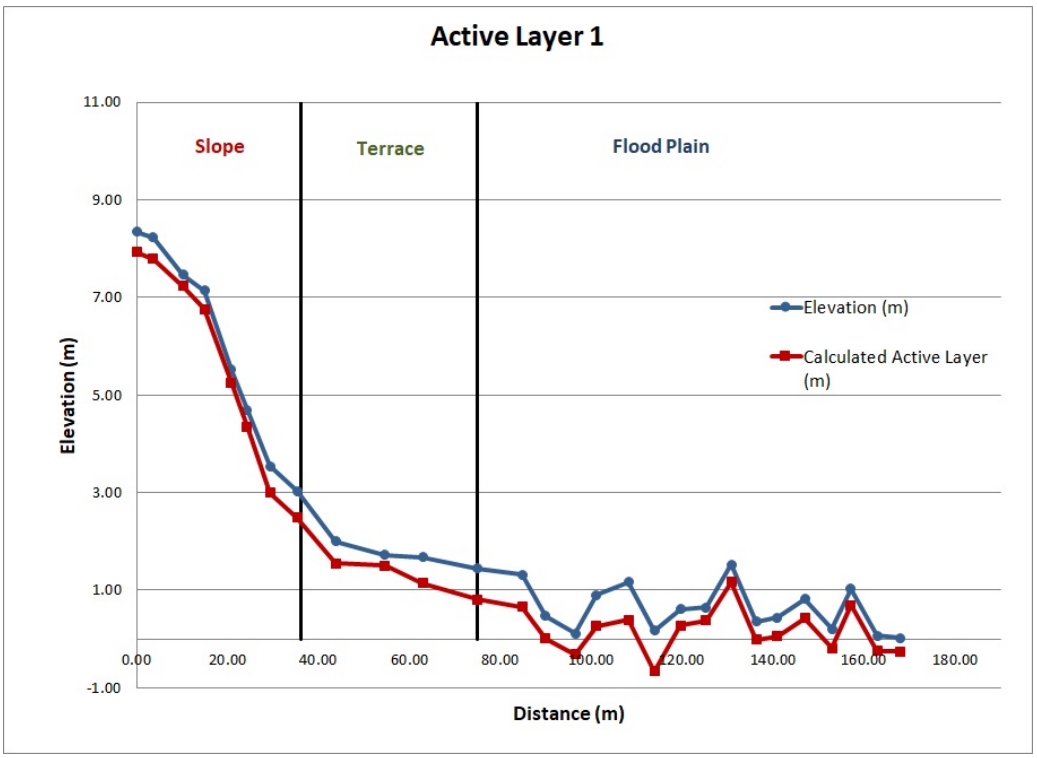

Figure 4.1-3: *North to South active layer survey in order to find out depth and thickness. Results for active layer 1*

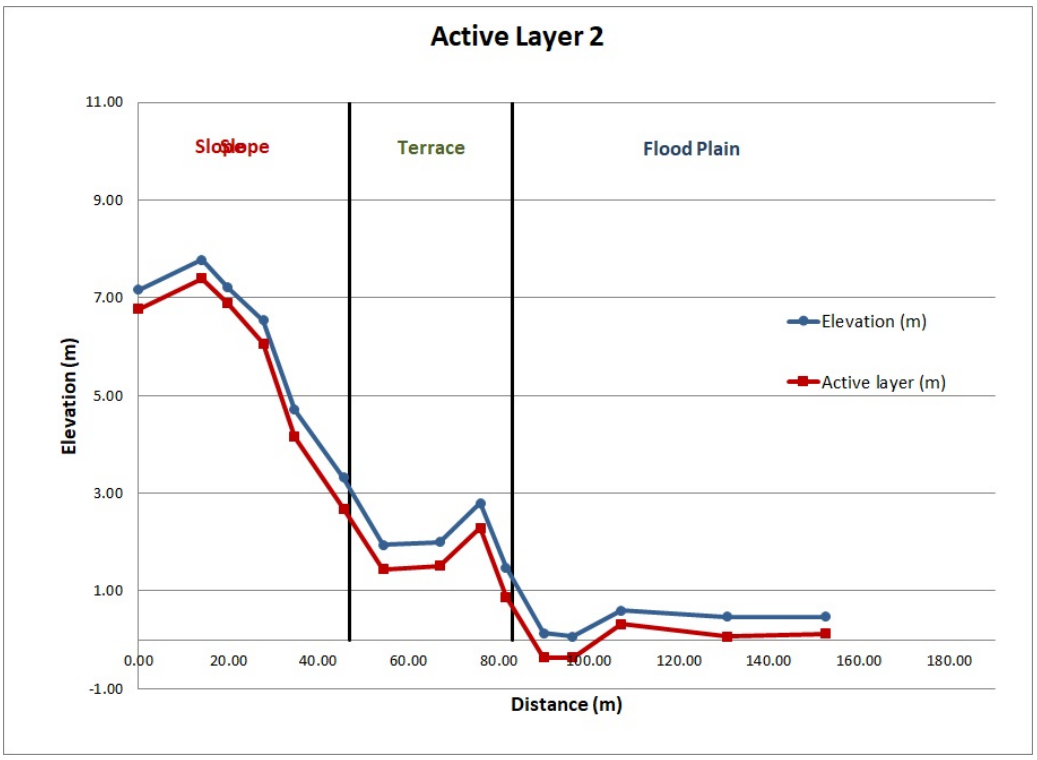

Figure 4.1-4: *North to South active layer survey in order to find out depth and thickness. Results for active layer 2*

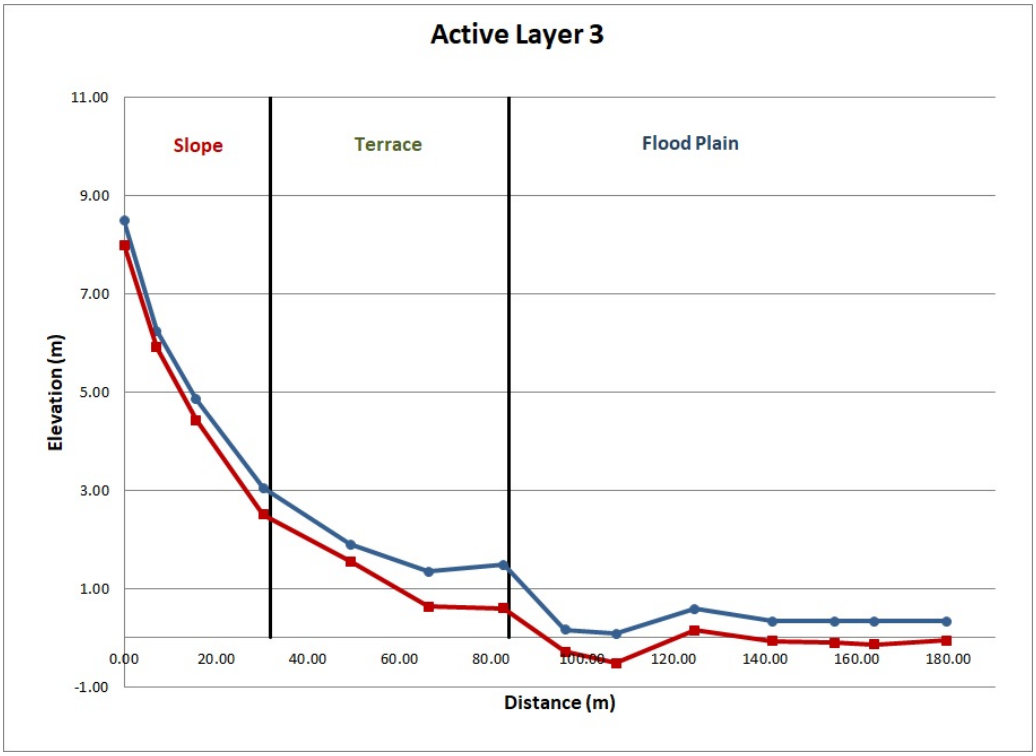

Figure 4.1-5: *North to South active layer survey in order to find out depth and thickness. Results for active layer 3*

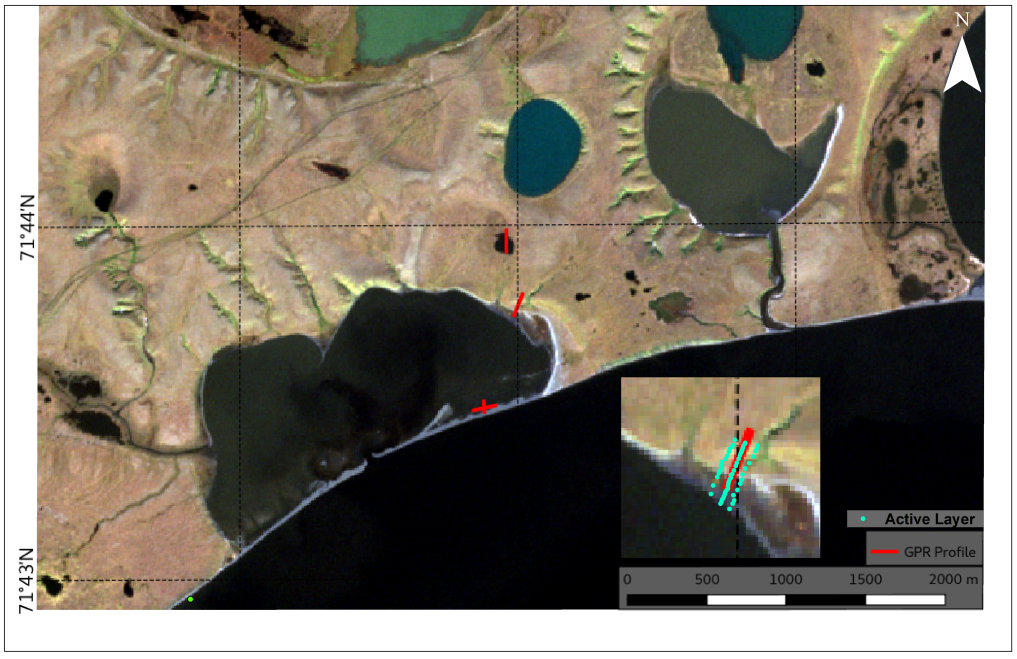

Figure 4.1-6: *Active Layer Map*

Electrical resistivity

The main goal of electrical resistivity tomography (ERT) surveying was to map unfrozen and frozen sub-aquatic sediments at Goltsovoye Lake, Polar Fox Lagoon, Uomullyakh-Kyuel Lagoon, and the nearshore coastal zone just offshore of Uomullyakh-Kyuel Lagoon. Terrestrial permafrost surveys were performed at Uomullyakh-Kyuel and Polar Fox Lagoons to relate thawing sub-aquatic

permafrost with undisturbed terrestrial permafrost. Offshore work also included surveys of the Lena River Delta Channel. The ERT method is effective at delineating unfrozen and frozen sediment, because there is an increase in electrical resistivity as water freezes to form ice (e.g. Kneisel et al., 2008). However, this increase in resistivity is mainly due to the decrease in unfrozen water content. Therefore, the resistivity of sub-aquatic permafrost soils is highly dependent on porosity, grain size, temperature, and the quantity of total dissolved solids in the porewater, all of which affect unfrozen water content. As a result, the transition from relatively low to high resistivity could be sharp or gradual depending on the nature of sub-aquatic conditions and stratigraphy. In addition, the order of magnitude for what constitutes a frozen sub-aquatic soil in terms of electrical resistivity is site-specific.

Not including surveys offshore of the Bykovsky Peninsula, three sites characterized by unique boundary conditions in early spring were investigated: 1) a deep freshwater lake with no ice grounding in the centre of the lake (Goltsovoye Lake), 2) a saltwater lake with no ice grounding in the centre of the lake (Polar Fox Lagoon), and 3) a shallow saltwater lagoon with ubiquitous ice grounding (Uomullyakh-Kyuel Lagoon). The boundary conditions are summarized in Figure 4.1-9. Due to the saltwater at Polar Fox Lagoon, the near-surface sediments below the lakebed were also suspected to be salty. In October 2017, the German Research Centre for Geosciences (GFZ) performed porewater chemistry analyses of samples collected by the UWITEC^{TM} coring team during the April 2017 expedition. In the uppermost metre of sediment, the maximum electrical conductivity of the porewater was 52,300 μS/cm, which translates to a freezing point of approx. –2.2 $^{\circ}$C. At Uomullyakh-Kyuel Lagoon, grounded ice conditions were encountered at all ice auger locations in April 2017 and therefore the salt concentrations in the sediment are suspected to be even higher compared to Polar Fox Lagoon.

At the saltwater sites, an IRIS Syscal Pro Deep Marine (ISPDM) system was used for all resistivity surveys. For freshwater lakes and channels, as well as terrestrial permafrost settings, the standard IRIS Syscal Pro (ISP) system was used. The ISPDM produces a higher maximum current output (50 amperes) compared to the ISP, which produces a maximum current output of 2.5 amperes. However, the ISPDM has a lower transmitter output voltage (200 volts) compared to the ISP (2000 volts). In very conductive environments like saltwater lagoons, the ISPDM is well-suited to produce the high current intensity forced by the low resistivity water layer in contact with the electrodes, whereas in more resistive environments like freshwater lakes and terrestrial permafrost, a higher transmitter voltage is needed to generate sufficient current intensity.

For all surveys on water, a 120 m or 60 m geoelectric cable with floating electrodes was towed behind a small inflatable boat with a 5 horse-power outboard motor (Figure 4.1-10). Both the ISPDM and ISP were equipped with a GPS and an echo sounder to record the position and water depth at the boat locations. The 120 m and 60 m cables had electrode separations of 10 m and 5 m, respectively. In total, two current electrodes and 11 potential electrodes were used. Both the ISPDM and the ISP have 10 channels and can thus measure 10 voltages with different combinations of the current electrodes and two potential electrodes simultaneously. The only array type used for the sub-aquatic surveys was the Reciprocal Wenner-Schlumberger array as shown in Figure 4.1-11(a). For nearly all water surveys, measurements were taken every 5 m of trip distance. However, in areas with rapidly changing bathymetry like the baydjarakh structures beneath Goltsovoye Lake, a 1 m measurement interval was occasionally used. An overview of geoelectric surveys is presented in Figure 4.1-7 for Uomullyakh-Kyuel Lagoon, Polar Fox Lagoon, and Goltsovoye Lake, as well as in Figure 4.1-8 for the Byskovskaya outflow channel of the Lena Delta. A detailed summary of profile settings and start/end coordinates are shown in Table A.4-1 for water surveys and Table A.4-2 for terrestrial surveys.

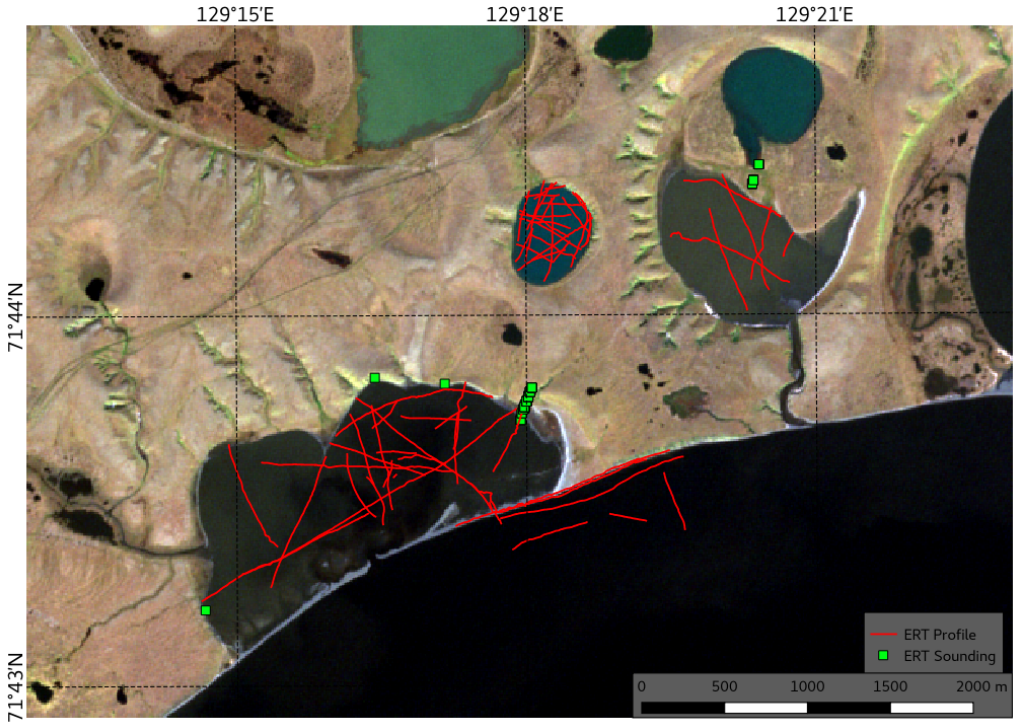

Figure 4.1-7: *ERT Soundings and Profiles in Uomollyakh-Kyuel Lagoon*

Figure 4.1-8: *ERT Profiles in the Bykovskaya outflow channel*

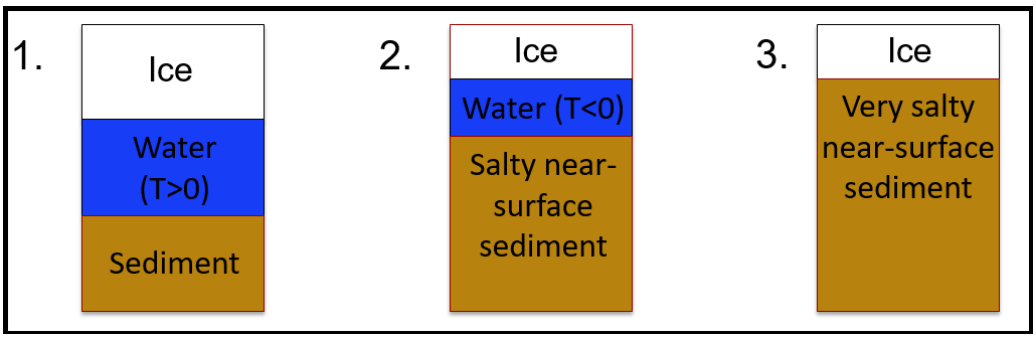

Figure 4.1-9: *Boundary conditions at borehole locations in April 2017 at Goltsovoye Lake (1), Polar Fox Lagoon (2), and Uomullyakh-Kyuel Lagoon (3) and the suspected sediment characteristics*

Water surveys

Uomullyakh-Kyuel Lagoon and Offshore

In total, 37 surveys were collected in Uomullyakh-Kyuel Lagoon and offshore of the lagoon in the nearshore coastal zone with a 10 m electrode spacing to maximize penetration depth. In addition, 6 surveys were taken in the freshwater Bykovskyaya channel of the Lena Delta. The first priority in Uomullyakh-Kyuel Lagoon was to collect west to east, as well as north to south profiles intersecting the deep borehole location from the April 2017 expedition. The temperature and stratigraphic information available from the borehole is critical for geophysical interpretation. The second priority was to collect resistivity data across the west to east, as well as the two north to south transient electromagnetic survey lines carried out by the Institute of Petroleum Geology and Geophysics (IPGG) in April 2017. The IPGG profiles were taken along the same lines as the ground-penetrating radar surveys performed by Timer LLC (Figure 3.5-6). The next goal was to collect a series of ERT profiles perpendicular to Uomullyakh-Kyuel Lagoon and offshore shorelines characteristic of both Alas and Yedoma permafrost terrain. The rationale for these surveys is to plot the position of the ice-bearing permafrost table with the ERT as a function of distance away from the shoreline. When tied in with shoreline erosion rates inferred from historical remote sensing imagery, an ice-rich permafrost degradation rate can be calculated. Of particular interest is investigating how the ice-rich permafrost table slopes differ between Alas and Yedoma permafrost. Having already undergone a thermokarst and refreezing cycle, it is speculated that the Alas terrain could have less ice content and a warmer initial ground thermal regime upon inundation compared to the Yedoma. Hence, the ice-rich permafrost table degradation rate is potentially faster for eroding Alas shorelines. Perhaps even more curious were the surveys crossing the lagoon's southern sand bar adjacent to the sea. The results to date suggest permafrost is aggrading beneath the center of the sand bar, but since the spit is a very dynamic feature, this newly formed permafrost will soon be inundated with seawater as the spit retreats further north. Therefore, it is also speculated that a "permafrost tail" exists south of the spit where recently formed permafrost (i.e. decadal time-scale) is currently degrading due to inundation. In an effort to map near-surface frozen soils below and south of the spit, higher resolution surveys with a 5 m electrode spacing were carried out in the addition to the standard 10 m electrode spacing. Critical to all the aforementioned science questions is knowing the resistivity signatures of undisturbed permafrost, as well as inundated permafrost right at the shoreline. Knowing full well the pitfalls of three-dimensional geology and how they pertain to electrical current propagation, three one-dimensional soundings with the 120 m cable parallel to the shoreline were taken along Uomullyakh-Kyuel Lagoon's western and northern shorelines. Furthermore, considerable effort was invested to acquiring a water survey that overlaps the terrestrial active layer and resistivity transects described in Section *Terrestrial Survery, Uomullyakh-Kyuel Lagoon*.

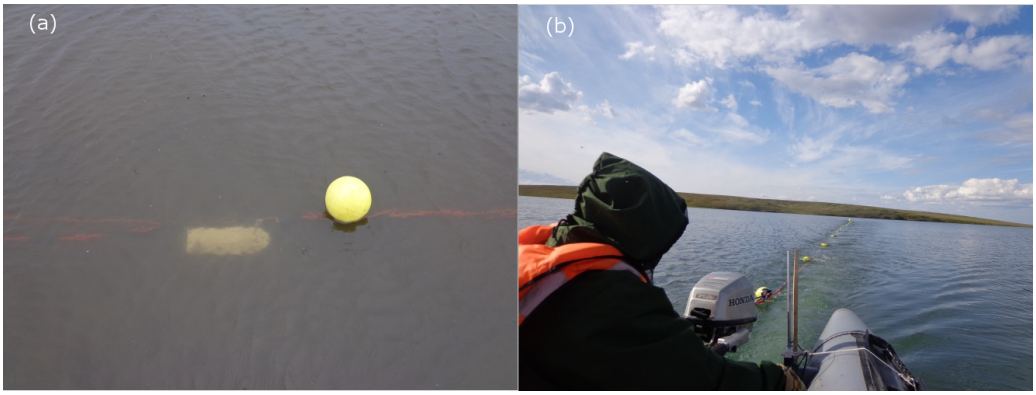

Figure 4.1-10: *(a) For water surveys, thin metal plates were used as electrodes and hung approx. 10 cm below the top of the water surface by attaching buoys to the cable. (b) The geoelectric cables were towed behind a small inflatable motor boat.*

Polar Fox Lagoon

In total, 6 surveys were collected at Polar Fox Lagoon with a 10 m electrode spacing to maximize penetration depth. Similar to Uomullyakh-Kyuel Lagoon, the first priority was to collect west to east, as well as north to south profiles intersecting the deep borehole and UWITEC^{TM} coring locations from the April 2017 expedition. The second objective was to intersect the April 2017 one-dimensional ERT sounding location. This is exciting, because the seasonal comparison could show transient resistivity changes in the near-surface due to warming sub-aquatic soil temperatures from April to July. Since the temperature chain data exists only for April 2017, the multi-season ERT data could shed light on the depth of zero annual amplitude. The latter is particularly important to grasp at Polar Fox Lagoon, because the soil temperatures were very close to 0 °C at all depths in April 2017. Thus, small seasonal changes in temperature could have profound impacts on unfrozen water content, as well as the frozen/unfrozen state of the soil. To acquire an electrical resistivity signature of the permafrost just above the shoreline, a mixed terrestrial and floating electrode survey was carried out. More specifically, the centre of the Reciprocal-Schlumberger array was placed at the shoreline, such that 7 floating electrodes were placed in the water, and 6 electrode nails were inserted into the tundra. Once a measurement was taken, the boat moved 10 m further offshore as the entire array was moved 10 m towards the lake. This process continued until all floating electrodes were in the water. At this point, the measurements continued as a water survey with resistivity values recorded every 5 m of trip distance.

Goltsovoye Lake

At Goltsovoye Lake, 23 surveys were carried out. The 5 m electrode spacing was used for all surveys because: 1) Due to the lake's relatively small size, greater mobility with the motor boat and the cable was desired, 2) High resolution data below baydjarakh structures was optimal to identify potentially submerged ice wedges, and 3) The talik thickness at the April 2017 deep borehole location was already known (31 m below the top of the water surface) and thought to be beyond the maximum depth of investigation for surveys with a 10 m electrode spacing. Note that the 60 m cable used for these surveys has fixed positions for the current electrodes and thus the Reciprocal Schlumberger Array configuration (Figure 4.1-11(b)) was slightly different than Uomullyakh-Kyuel Lagoon and Polar Fox Lagoon. In addition to intersecting the deep borehole and UWITEC^{TM} drilling locations from April 2017, one of the science goals was to conduct ERT surveys over the methane bubble photo lines from the spring expedition. The photo profile showed bubbles trapped in the lake ice, which were interpreted as methane gas emissions from thawing sub-aquatic permafrost. Although no terrestrial surveys were performed at Goltsovoye Lake, the IPGG performed extensive land surveys over Yedoma and Alas permafrost in between Uomullyakh-Kyuel Lagoon and Goltsovoye Lake with a 5 m electrode spacing.

Terrestrial surveys

Uomullyakh-Kyuel Lagoon
For terrestrial surveys at Uomullyakh-Kyuel Lagoon, a total of 64 one-dimensional soundings were carried out at 12 locations along an active layer monitoring transect (refer to Section *Active Layer Survey*) with an electrode spacing of 5 m and the ISP. The active layer profile started in the lagoon's shallow northern waters close to camp and progressed further north perpendicular to shore for a total length of 170 m. The profile crossed an occasionally inundated zone with scarce vegetation, a small bluff, and undisturbed upland permafrost tundra. At 9/12 sounding locations, surveys were taken with the geoelectric cable oriented perpendicular to Uomullyakh-Kyuel Lagoon's shoreline and thus parallel with the active layer transect. At 6/12 sounding locations, surveys were taken with the geoelectric cable oriented parallel to Uomullyakh-Kyuel Lagoon's shoreline and thus perpendicular to the active layer transect. While the orientation of the cable affects the half-space and thus the resistivity of the subsurface medium in which the electrical current propagates, the surface position below which the apparent resistivity depth points are located, remains the same. At the sounding locations, the surveys included variations in receiver voltage range (5 volts and 15 volts) and the array type. The arrays used were Reciprocal Wenner Schlumberger (Figure 4.1-11(a)), Wenner Schlumberger (Figure 4.1-11(c)), Dipole-Dipole-A (Figure 4.1-11(d)), and Dipole-Dipole-B (Figure 4.1-11(e)). The active layer transect was also surveyed by the IPGG using a 2.5 m electrode spacing and a Wenner Schlumberger array configuration.

Polar Fox Lagoon
For terrestrial surveys at Polar Fox Lagoon, a total of 13 one-dimensional soundings were carried out at 3 locations on a land bridge separating salty Polar Fox Lagoon and a smaller freshwater lake to the north. Since both water bodies exist within the same basin, the land bridge was likely flooded in the past. Furthermore, remote sensing imagery dating back to 1951 shows that the land bridge has been drying up and/or growing in extent over the past several decades. Therefore, the goal of this investigation was to determine if the land bridge overlies a currently re-freezing talik. The surveys were carried out with the ISP, a 10 m electrode spacing, 5 volt and 15 volt receiver voltages, as well as both Reciprocal Wenner Schlumberger and Wenner Schlumberger arrays.

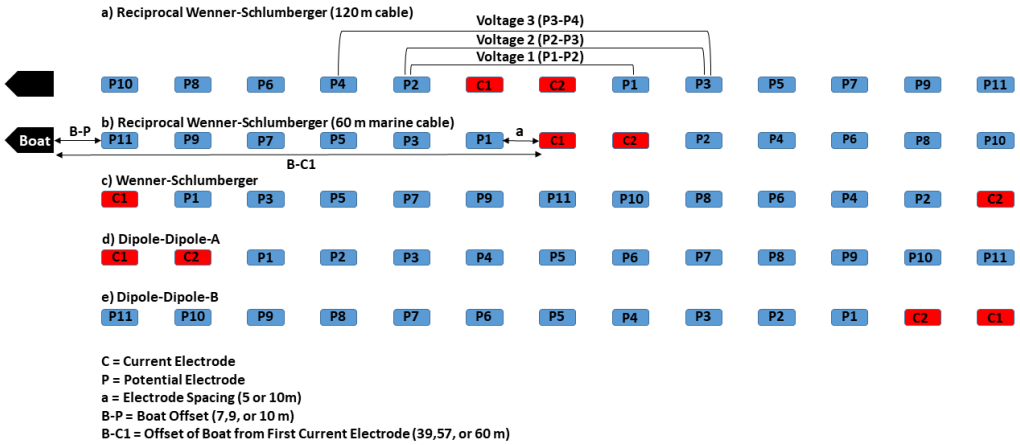

Figure 4.1-11: *The different array configurations used included the Reciprocal Schlumberger configuration for the 120 m cable (a), the Reciprocal Schlumberger configuration for the 60 m marine cable (b), the Wenner Schlumberger array (c), the Dipole-Dipole-A setup (d), and the Dipole-Dipole-B configuration (e). For each array type, 10 voltages were recorded simultaneously for each measurement point using the current electrodes and a pair of potential electrodes. The potential electrode pairs follow the P1-P2,P2-P3,P3-P4,P4-P5,P5-P6,P6-P7,P7-P8,P8-P9,P9-P10, and P10-P11 sequence for all array types.*

Ground-penetrating radar

Ground-penetrating radar (GPR) transmits electromagnetic waves (approx. 10 to 1000 MHz) into the subsurface and records reflections at boundaries between materials with different dielectric constants. Since the dielectric constant of a soil sharply decreases as water freezes to form ice, GPR has proven to be effective at mapping unfrozen/frozen soil interfaces, as well as ground ice bodies (e.g. Angelopoulos et al., 2013; Moorman et al., 2003). GPR surveys were performed at a small alas lake in between Goltsovoye Lake and Uomullyakh-Kyuel Lagoon, Uomullyakh-Kyuel Lagoon's sand bar, as well as the active layer transect described in *Section Active Layer Survey*. To maximize the possibility of detecting deep unfrozen/frozen soil boundaries, the 50 MHz MALA Geoscience rough terrain antenna was used for all surveys. Since saltwater severely attenuates GPR signals (e.g. Annan, 2004), no surveys were carried out in the waters of Uomullyakh-Kyuel and Polar Fox Lagoons. The small Alas lake was a site of particular interest during the spring expedition to its small size, proximity to camp, and promising initial GPR results. 50 MHz profiles from the spring showed structures below the lake-bottom reflector, but it was unclear whether the structures were real or artefacts generated by a combination of side reflections from the lake edges and multiple reflections from the ice/water and water/sediment interfaces. Therefore, the south to north profile line was repeated in summer by towing the antenna behind a small inflatable kayak (Figure 4.1-13). The antenna was wrapped in thin plastic film to keep it dry and six empty water bottles were attached to the antenna to make it float. The rationale for investigating Uomullyakh-Kyuel Lagoon's sand bar with the GPR was to map the underlying frozen soil bulb geometry that the authors suspect is forming due to permafrost aggradation. Even with 50 MHz, the vertical resolution of GPR is superior to ERT surveys with a 5 m electrode spacing. To maximize resolution in the near-surface, 200 MHz GPR surveys were attempted, but they failed due to equipment problems. In total, 2 north-south and 2 west-east profiles were taken in both possible directions at the ERT transect location. Lastly, south to north, as well as north to south GPR profiles were carried out along the active layer transect. In this scenario, the exploration of penetration depth as a function of distance away from the shoreline was of particular interest. Since electrically conductive saltwater attenuates GPR signals, changes in penetration depth across the survey line could detect lateral transitions of salty sediment, particularly below the occasionally submerged sandy beach. An overview of GPR surveys is presented in Figure 4.1-12 and a detailed summary of profile settings and start/end coordinates are shown in Table A.4-3.

Figure 4.1-12: *GPR Profiles*

Figure 4.1-13: *Floating 50 MHz ground-penetrating radar survey at a small alas lake between Goltsovoye Lake and Uomullyakh-Kyuel Lagoon*

Radiometry

Radiometric measurements included above-water and in-water measurements with different instruments (discussed below). For a better orientation of light and sky conditions during the measurements, photos of the sky and the water were taken according to the view angles of the

measurements. All measurements were carried out with an anchored boat to avoid strong drift. The duration of all measurements at one station took between 30 and 60 minutes. Only at good light conditions (clear sky) radiometric measurements were carried out. However, sky conditions changed for some stations during the period of measurement. These changing conditions have to be filtered during the data analysis.

Above-water
Above-water radiometric measurements were taken at selected stations using a handheld 3-radiometer (Hamamatsu). The radiometer provides high resolution hyperspectral measurements of the downwelling irradiance (Ed), downwelling radiance (Lsky) and the total upwelling radiance (Lu) (Figure. 4.1-14).
An absolute radiometric calibration was done for each radiometer before the expedition using a spectralon plate and a FEL lamp as a spectral irradiance reference standard. For each measurement the dark current of the radiometers were measured which will be subtracted from the measured intensities. Intercalibration of all 3 sensors were done taking a grey spectralon plate for both radiance sensors.

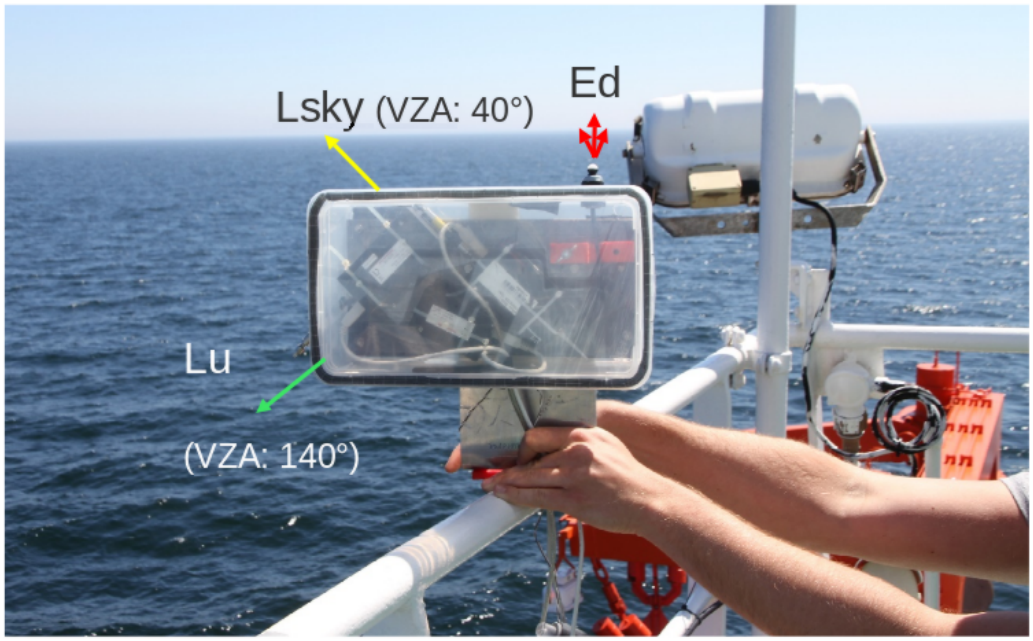

Figure 4.1-14: *Handheld 3-Radiometer with 2 radiance and 1 irradiance spectroradiometers*

In-water
In addition to above-water radiometric measurements, in-water radiometric measurements were taken at the same stations with two TRIOS Ramses irradiance sensors (Figure. 4.1-15). The in-water downwelling and upwelling irradiance (Ed and Eu) was measured at different depths depending on the transparency of the water. In-water measurements will provide information about the penetration depth of light into the water and about the spectral characteristics of the water at different water depths. Above- and in-water radiometric measurements were taken mainly in sunny conditions without cloud overcast. At some stations radiometric measurements were taking in overcast situation. To normalize in-water irradiance measurements, continuous above water irradiance measurements were taken throughout the in-water measuring period. The calibration of TRIOS Ramses sensors was done at TRIOS laboratory. Additional dark current measurements were done during the expedition. One sensor on the frame (Figure. 4.1-15) was equipped with a pressure and inclination sensor for a better quality control of the measurements. Intercalibration measurements of both irradiance

sensors as well as the irradiance sensor installed on the handheld 3-radiometer were taken in sunny conditions.

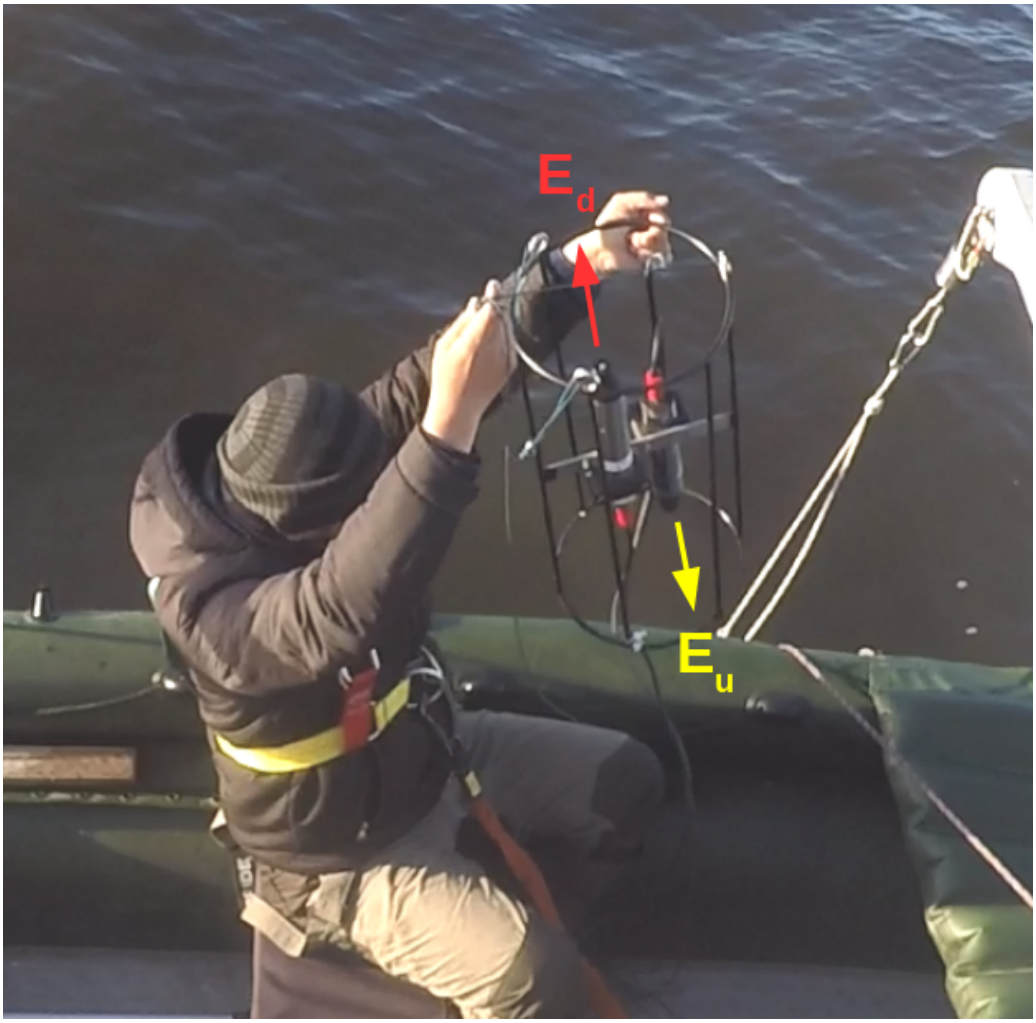

Figure 4.1-15: *Metal frame with two TRIOS Ramses sensor for Irradiance (uplooking sensor for downwelling Irradiance Ed and downlooking sensor for upward irradiance Eu)*

Microtops measurements

Atmospheric parameters such as aerosol optical thickness, direct solar irradiance, and water vapor column were obtained with a Microtops II Sunphotometer. The instrument has 5 spectral bands with centre wavelengths at 380, 440, 500, 675, 870 nm. These measurements are made for additional information for atmospheric correction of satellite images.

Water chemistry

Water column conductivity and temperature were determined with a Sontek CastAway CTD sensor, which measured electrical conductivity with a 6-electrode flow through cell, temperature with a thermistor and water pressure. Locations were automatically saved using onboard GPS, ideally prior to and following each cast.

Water samples were collected for biogeochemical constituents of the water such as suspended particulate matter (SPM), chlorophyll-a (chl-a), coloured dissolved organic matter (cDOM) and dissolved organic carbon (DOC). Furthermore, water samples for stable isotopes, pH, cations and anions were collected. At the majority of stations, only surface water was collected directly into the sampling bottle. At some stations with a higher water depth, also deep water was collected with

an UWITEC^{TM} water sampler. Water samples for SPM (0.5 l) were filtered through pre-rinsed, and pre-weighed 47 mm diameter Whatman GF/F filters with a pore size of 0.7 μm. The filters were dried (50 °C) and the filter weights will be determined at the OSL in St. Petersburg.
For chlorophyll-a, 0.5 l water was filtered through 0.7 μm Whatman GF/F. Further analysis will be done at the OSL in St. Petersburg. The pigments will be extracted from the concentrated algal sample in an aqueous solution of acetone. The chlorophyll-a concentration will be determined spectrophotometrically with a fluorometer TD Trilogy and a spectrophotometer SPECORD 200 by measuring the absorbance (optical density, OD) of the extract at various wavelengths. The resulting absorbance measurements are then applied to a standard equation.
Water for cDOM (0.2 l) was filtered through 0.22 μm GSWP filters. The filter was pre-washed with approx.20 ml Milli-Q water and approx. 20 ml of the seawater sample. After washing the filter, 250 ml of seawater was filtered. 50 ml of the filtrate was used to rinse the storage bottles. The rest of the filtrate (100 ml) was filled into two storage bottles and stored in a dark and cold place. The CDOM analysis will be carried out with a SPECORD 200 spectrophotometer at the OSL in St. Petersburg.
Water samples for DOC were filtered through a pre-rinsed disposable GF/F syringe prefilter 0.7 μm pore size. 20 ml filtrate was filled into a glass vial and 25 ul of 30 % HCl was added for conservation.
At most surface water sampling stations, samples were collected for the analyses of stable isotopes of water (30 ml), major cations/total elements (15 ml, filtered through 0.45 μm pore size cellulose acetate filters and conserved with 65 % HNO_3), major anions (8 ml, filtered through 0.45 μm pore size cellulose acetate filters) and pH and electrical conductivity were measured within 24 hours using a WTW field probe. All samples were kept cool in the field and during transport from the field. Water level was monitored at irregular intervals using staff gauges graduated at 2 cm intervals inserted into the sediment. Four staff gauges spread out over a distance of about 50 m were required to cover the range of water levels between minimum and maximum water levels observed during the field camp. Measurements were made by observing the height of the water on one of the staff gauges. Simultaneous measurements were made when water covered more than one staff gauge to provide correspondence between gauges.
Water column electrical conductivity, salinity and temperature were measured using a Sontek CastAway CTD with built-in GPS. The CTD was placed in recording mode, held beneath the water surface for approx. 10 seconds to allow temperature equilibration, then allowed to fall through the water column in a controlled manner, and then retrieved. Data were recorded during both downward and upward travel.
Sediments were sampled for dating at AWI's MICADAS $\delta^{14}C$ dating laboratory. This included sediment samples, thawed and frozen, from the eroding coastal bluff at Cape Mamontovy Klyk, and offshore surface sediments. Samples were collected using an ice hammer and spoon, collected in glass jars that had been previously purified at temperatures sufficiently high to burn off carbon compounds and covered with foil.
Coastline position was measured relative to terrestrial benchmarks at Cape Mamontovy Khayata on the Bykovsky Peninsula (approx. 71.7837°N, 129.4131°E) and on Muostakh Island, south of the Peninsula (approx. 71.6116°N, 129.9449°E). For these purposes the distance between the benchmark and edge of the undisturbed tundra at the upper edge of the coastal bluff were measured to the nearest centimetre using a measuring tape. Direction was chosen based on the shortest distance between the benchmark and the bluff edge. These measurements continue long-term series of point measurements of coastline position (e.g. Overduin et al., 2015).

Results

Meteorological observations

Air temperatures during the field campaign varied between 0 and 19 °C. Precipitation fell as rain and reached up to a recorded 7 mm/d, although undercatch due to high wind speeds probably skewed these results towards lower than actual values (Figure. 4.1-16). Winds of up to 14 m/s blew mostly from the northwest and northeast and wind direction was highly variable, changing at times more than once a day (Figure. 4.1-17,4.1-18). Air pressure rose and fell repeatedly over a period of approx. 3 - 5 days, with a generally decreasing trend from over 1020 hPa at the beginning of the field season on July 13, to less than 1000 hPa by August 4th. These variations were roughly paralleled by changes in water level in Uomullyakh-Kyuel Lagoon (Figure. 4.1-18). Changes in water level were sometimes very rapid (Figure 4.1-19), for example a variation of half a meter in less than 12 hours on July 23-24. The result of these changes included rapidly changing bathymetry in the lagoon and high rates of discharge or inflow at the two open channels between the lagoon and Tiksi Bay.

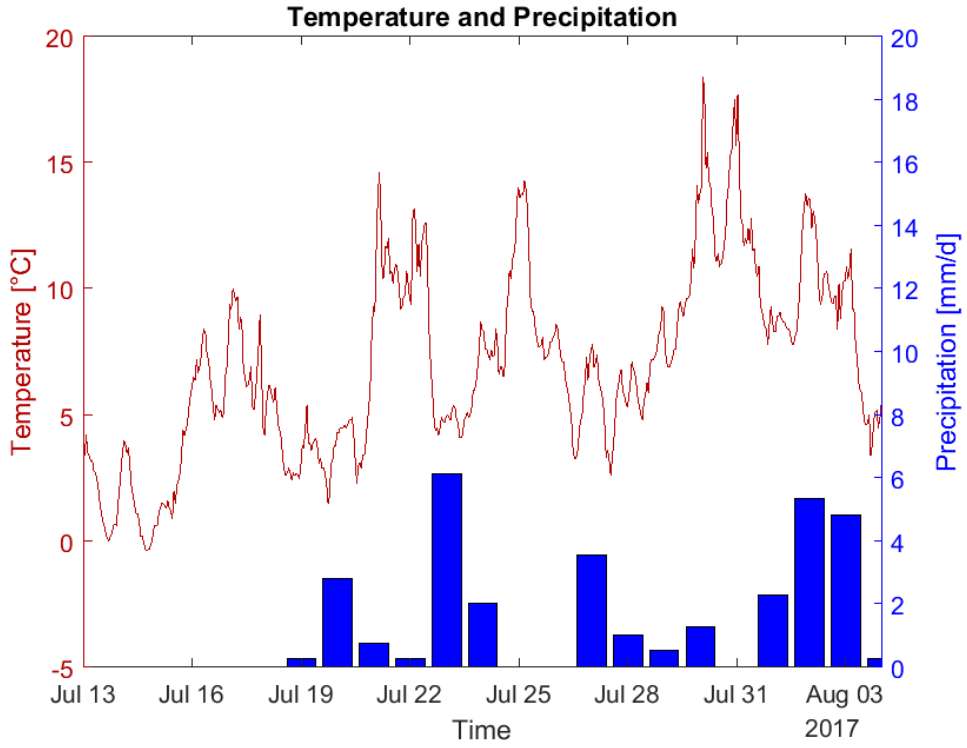

Figure 4.1-16: *Air temperature and precipitation per day during the expedition*

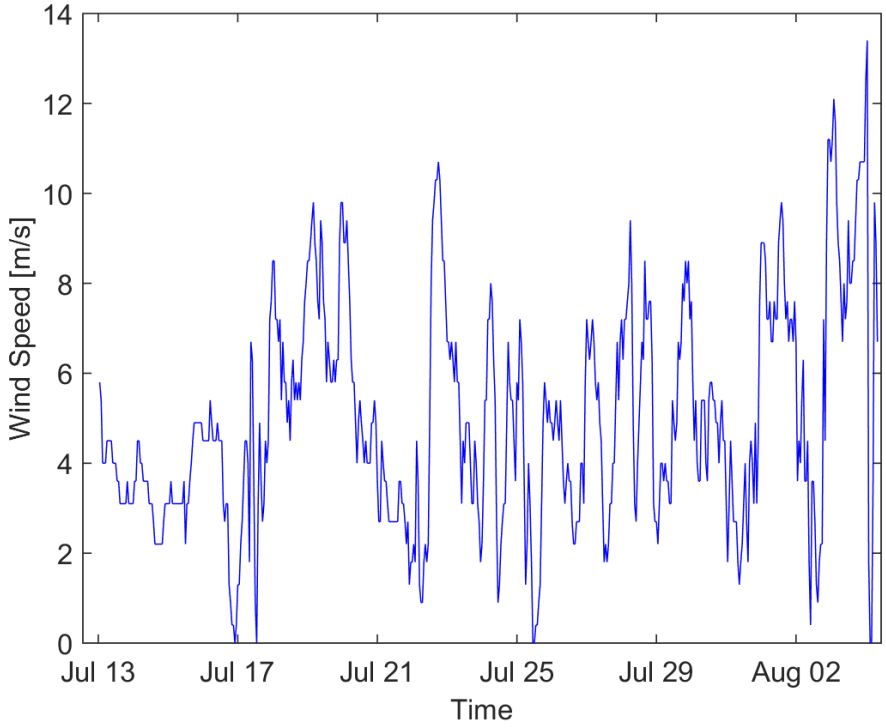

Figure 4.1-17: *Hourly wind speed*

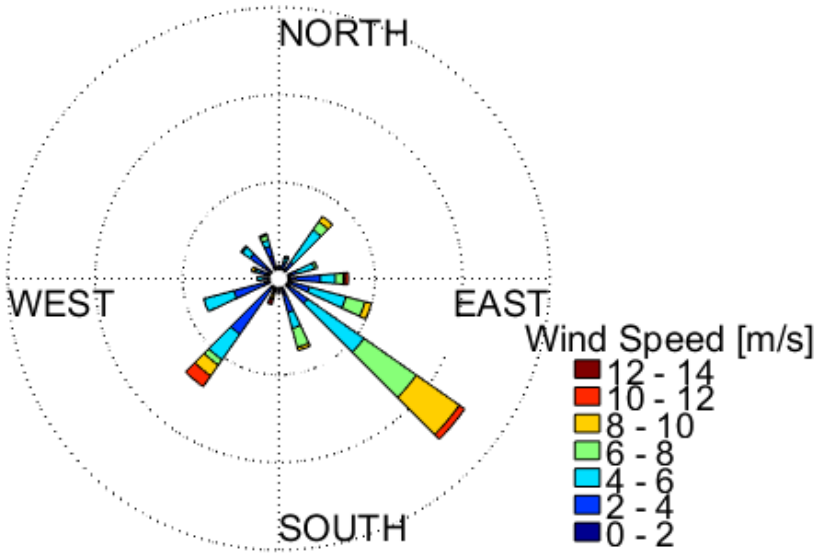

Figure 4.1-18: *Wind rose*

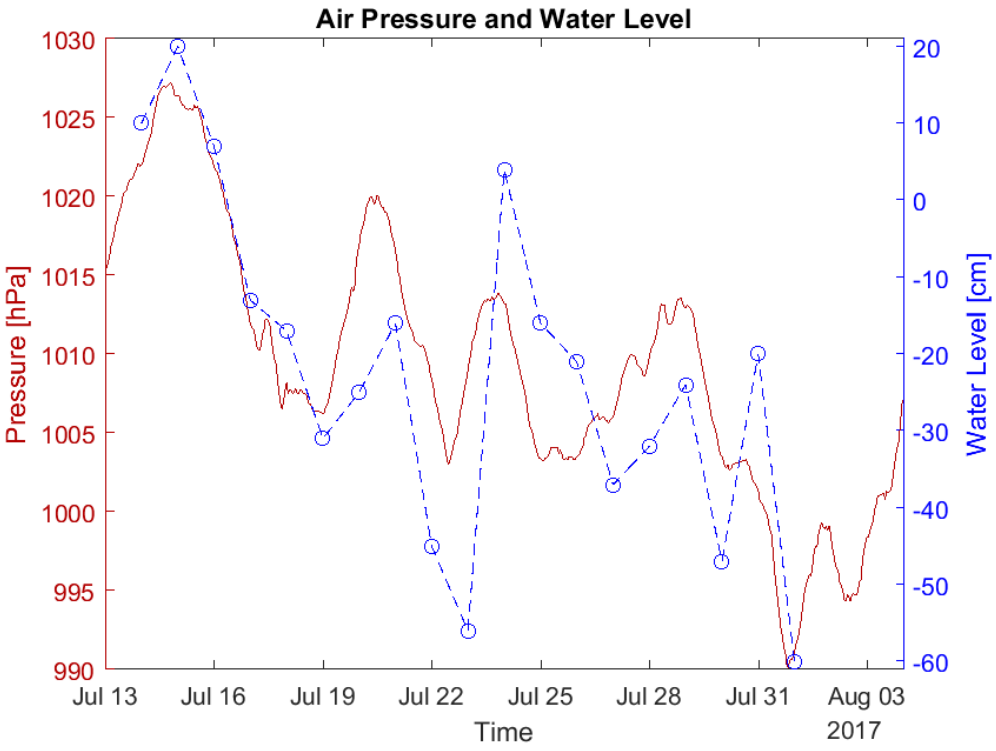

Figure 4.1-19: *Air pressure and water level during the expedition*

4.2 Bibliography

Annan A.P. (2004): Ground penetrating radar principles, procedures and applications.

Angelopoulos M.C., Pollard W.H., Couture N.J. (2013): The application of CCR and GPR to characterize ground ice conditions at Parsons Lake, Northwest Territories. Cold Regions Science and Technology 85, pp. 22-33.

Kneisel C., Hauck C., Fortier R., Moorman B. (2008): Advances in geophysical methods for permafrost investigations. Permafrost and Periglacial Processes 19 (2), pp. 157-178.

Moorman B.J., Robinson S.D., Burgess M.M. (2003): Imaging periglacial conditions with ground-penetrating radar. Permafrost and Periglacial Processes 14 (4), pp. 319-329.

Overduin P.P., Westermann S., Yoshikawa K., Haberlau T., Romanovsky V., Wetterich, S. (2012): Geoelectric observations of the degradation of nearshore submarine permafrost at Barrow (Alaskan Beaufort Sea). Journal of Geophysical Research 117. F02004, doi:10.1029/2011JF002088.

Overduin P.P., Haberland C., Ryberg T., Kneier F., Jacobi T., Grigoriev M.N., Ohrnberger M. (2015): Submarine permafrost depth from ambient seismic noise: Geophysical Research Letters. doi:10.1002/2015GL065409.

Overduin P.P., Blender F., Bolshiyanov D.Y., Grigoriev M.N., Morgenstern A., Meyer H. (2017): Russian-German Cooperation: Expeditions to Siberia in 2016, Berichte zur Polar- und Meeresforschung 709, pp. 295.

Romanovskii N.N., Hubberten H.W., Gavrilov A.V., Tumskoy V.E., Kholodov A.L. (2004): Permafrost of the east Siberian Arctic shelf and coastal lowlands. Quaternary Science Reviews 23 (11), pp. 1359-1369.

Appendix

A.1 List of Participants

Table A.1-1: List of Participants in Samoylov Island Campaign

No.	Name	Institution	Duration
Samoylov Island			
1	Aboukrat Maxime	EPFL	16.07.17–14.08.17
2	Abramova Ekaterina	LDR	02.04.17–15.05.17 and 19.06.17–01.09.17
3	Alekseev Andrey	USP	16.07.17–01.08.17
4	Alekseev Ivan	NSU	30.07.17–25.08.17
5	Alekseev Viktor	ZIN-RAS	19.06.17–05.07.17
6	Alekseeva Natalia	IPGG SB RAN, NSU	02.04.17-28.04.17
7	Anders Katharina	AWI B	03.09.17–26.09.17
8	Asseng Jölund	AWI B	18.07.17-09.08.17
9	Assmann Volkmar	AWI P	16.07.17-26.09.17
10	Avdeev Denis	IPGG, NSU	30.07.17–25.08.17
11	Aybulatov Denis	UM	11.04.17–28.04.17
12	Beckebanze Lutz	UH	02.07.17–01.08.17
13	Bobrov Nikita	USP	02.07.17–18.07.17
14	Boike Julia	AWI P	03.09.17–26.09.17
15	Bolshiyanov Dmitry	AARI	30.06.17–22.08.17
16	Bolshiyanova Olga	AARI	30.07.17–01.09.17
17	Bonne Jean-Louis	AWI B	02.04.17–21.04.17
18	Bornemann Niko	AWI P	03.09.17–26.09.17
19	Bussmann Ingeborg	AWI H	12.04.17–28.04.17
20	Chertoprud Elena	UM	30.07.17–01.09.17
21	De Staercke Vincent	EPFL	16.07.17–14.08.17
22	Esin Egor	IPGG, NSU	11.07.17–25.07.17
23	Evgrafova Svetlana	SIF	30.07.17–01.09.17
24	Fage Aleksey	IPGG, NSU	11.07.17–25.07.17
25	Fedorova Irina	AARI	11.04.17–28.04.17
26	Grigorevskaya Alina	IPGG, NSU	11.07.17–29.07.17
27	Grotheer Hendrik	AWI B	02.07.17–01.08.17
28	Gukov Stepan	YRC	18.07.17-09.08.17
29	Haberland Christian	GFZ	not on board
30	Hoffmann Kirstin	AWI P	02.04.17–28.04.17
31	Izokh Nadezhda	IPGG, NSU	30.07.17–25.08.17
32	Kartozia Andrey	IPGG, NSU, IGM	05.07.17–29.07.17
33	Kaufmann Oliver	UH	03.09.17–26.09.17
34	Krueger Frank	UP	18.07.17-09.08.17
35	Kufner Sofia-Katerina	GFZ	18.07.17-09.08.17
36	Laboor Sebastian	AWI P	03.09.17–13.09.17
37	Lange Stephan	AWI P	03.09.17–26.09.17
38	Lashchinskiy Nikolay	IPGG, CSBG	01.08.17–23.08.17
39	Mathieu Laura	EPFL	16.07.17–14.08.17
40	Meyer Hanno	AWI P	23.08.17–03.09.17
41	Michaelis Rune	AWI S	30.07.17–22.08.17

No.	Name	Institution	Duration
Samoylov Island			
42	Mikhaltsov Nikolay	IPGG NSU	30.07.17–25.08.17
43	Morgenstern Anne	AWI P	20.08.17–13.09.17
44	Nikitich Polina	IPGG NSU ISSA	11.07.17–29.07.17
45	Nitzbon Jan	AWIP	03.09.17–26.09.17
46	Olenchenko Vladimir	IPGG, NSU	11.07.17–25.07.17
47	Papenmeier Svenja	AWI S	30.07.17–22.08.17
48	Pascal Léa	EPFL	16.07.17–14.08.17
49	Peresypkin Dmitri	YRC	18.07.17-09.08.17
50	Petrunin Sergey	YRC	18.07.17-09.08.17
51	Pravkin Sergey	AARI	30.06.17–01.09.17
52	Praz Christophe	EPFL	16.07.17–14.08.17
53	Pudrikov Pavel	IPGG, NSU	30.07.17–25.08.17
54	Radevitch Anastasija	IPGG, NSU	30.07.17–25.08.17
55	Rehder Zoé	UH	02.04.17–21.04.17
56	Rüggen Norman	UH	03.09.17–26.09.17
57	Sachs Torsten	GFZ P	03.09.17–26.09.17
58	Sander Lasse	AWI S	30.07.17–22.08.17
59	Schaer Mathieu	EPFL	16.07.17–14.08.17
60	Schneider Waldemar	AWI P	30.03.17–21.04.17 and 02.07.17–01.09.17
61	Schreiber Peter	AWI P	03.09.17–26.09.17
62	Sennikov Nikolay	IPGG, NSU	30.07.17–25.08.17
63	Shadrina Alexandra	USP	06.07.17–01.08.17
64	Sosnovtsev Konstantin	IPGG, NSU	11.07.17–25.07.17
65	Stoof Günter	AWI P	02.04.17–21.04.17 and 02.07.17–26.09.17
66	Tatarchenko Ksenia	EPFL	16.07.17–14.08.17
67	Titov Alexey	USP	02.07.17–18.07.17
68	Tsibizov Leonid	IPGG, NSU	05.07.17–29.07.17
69	Tsukanov Nikolay	RAS	18.07.17-09.08.17
70	Tuktarov Rustam	YRC	18.07.17-09.08.17
71	Wiltshire Karen	AWI S	13.08.17–22.08.17
72	Winterfeld Maria	AWI B	02.07.17–01.08.17
73	Wischhoefer Philipp	UC	30.07.17–01.09.17
74	Wotte Anja	UC	30.07.17–01.09.17
75	Zogg Dimitri	EPFL	16.07.17–14.08.17

Table A.1-2: List of Participants in Bykovsky Drilling Campaign: Spring 2017

No.	Name	Institution	Duration
Bykovsky Peninsula Spring		*06.04.17-24.04.17*	
1	Angelopoulos Michael	AWI-P	06.04.17-24.04.17
2	Biskaborn Boris	AWI-P	05.04.17-24.04.17
3	Bussmann Ingeborg	AWI-H	05.04.17-24.04.17 (13.04.17-24.04.17 on Samoylov Island)
4	Dobrobaba Viktor	HT	06.04.17-24.04.17
5	Golikov Nikita	IPGG	06.04.17-24.04.17
6	Grigoriev Mikhail	MPI, IPGG	06.04.17-24.04.17
7	Grosse Guido	AWI-P	05.04.17-12.04.17
8	Kahl Jan	AWI-P	06.04.17-24.04.17
9	Kallmeyer Jens	GFZ	05.04.17-12.04.17
10	Kamanin Sergey	HT	06.04.17-24.04.17
11	Kitte Axel	GFZ	06.04.17-24.04.17
12	Kulikov Valeri	HT	06.04.17-24.04.17
13	Liebner Susanne	GFZ	13.04.17-24.04.17
14	Maslov Alexandr	MPI	06.04.17-24.04.17
15	Maximov Georgii	MPI	06.04.17-24.04.17
16	Nasyrov Juri	HT	06.04.17-24.04.17
17	Ostreldin Stanislay	NEFU	06.04.17-24.04.17
18	Overduin Paul	AWI-P	05.04.17-12.04.17
19	Plotnikov Andrey	IPGG	13.04.17-24.04.17
20	Pravkin Sergey	AARI	06.04.17-24.04.17
21	Scherstnev Alexey	Timer LLC	12.04.17-18.04.17
22	Schirrmeister Lutz	AWI-P	06.04.17-24.04.17
23	Schiyan Alexander	HT	06.04.17-24.04.17
24	Strauss Jens	AWI-P	06.04.17-24.04.17
25	Tsapenko Victor	IPGG	06.04.17-24.04.17
26	Zimmermann Heike	AWI-P	05.04.17-12.04.17

Table A.1-3: List of Participants in Summer Bykovsky Peninsula Campaign

No.	Name	Institutuion	Duration
Bykovsky Peninsula Summer		*09.07.17-08.08.17*	
1	Angelopoulos Michael	AWI-P	12.07.17-4.08.17
2	Esin Egor	I. IPGG NSU	25.07.17-30.07.17
3	Fage Aleksey	N. IPGG NSU	25.07.17-30.07.17
4	Grigoriev Mikhail	MPI	31.07.17-04.08.17
5	Juhls Bennet	WeW-FU	12.07.17-04.08.17
6	Kartozia Andrey	A. NSU IGM	30.07.17-04.08.17
7	Maximov Georgy	MPI	12.07.17-04.08.17
8	Nikitich Polina	A. NSU ISSA	30.07.17-04.08.17
9	Olenchenko Vladimir	V. IPGG NSU	25.07.17-30.07.17
10	Overduin Pier Paul	AWI-P	12.07.17-04.08.17
11	Sosnovtsev Konstantin	A. IPGG NSU	25.07.17-30.07.17

Table A.1-4: List of Participating Institutions

Abbr.	Institution
AARI	Arctic and Antarctic Research Institute, St. Petersburg, Russian Federation
AWI-B	Alfred Wegener Institute Helmholtz Centre for Polar and Marine Research, Bremerhaven, Germany
AWI-H	Alfred Wegener Institute Helmholtz Centre for Polar and Marine Research, Helgoland, Germany
AWI-P	Alfred Wegener Institute Helmholtz Centre for Polar and Marine Research, Potsdam, Germany
AWI-S	Alfred Wegener Institute Helmholtz Centre for Polar and Marine Research, List/Sylt, Germany
CSBG	Central Siberian Botanical Garden of Siberian Branch Russian Academy of Sciences, Novosibirsk, Russian Federation
EPFL	Ecole Polytechnique Fédérale de Lausanne - Geneva Global, Lausanne, Switzerland
GFZ	Helmholtz Centre Potsdam – GFZ German Research Centre for Geosciences, Potsdam, Germany
HT	Hydrobase Tiksi
IGM	V.S. Sobolev Institute of Geology and Mineralogy of Siberian Branch Russian Academy of Sciences, Novosibirsk, Russian Federation
IPGG	Trofimuk Institute for Petroleum Geology and Geophysics, Siberian Branch, Russian Academy of Sciences, Novosibirsk, Russian Federation
ISSA	Institute of Soil Sciences and Agrochemistry, Novosibirsk, Russian Federation
LDR	Lena Delta Reserve, Tiksi, Yakutia, Russian Federation
NEFU	North-Eastern Federal University, Yakutsk, Russian Federation
NSU	Novosibirsk State University, Novosibirsk, Russian Federation
RAS	P.P.Shirshov Institute of Oceanology of the Russian Academy of Sciences, Moscow, Russian Federation
SIF	V.N. Sukachev Institute of Forest, Krasnoyarsk, Academgorodok, Russian Federation
TIMER LLC	TIMER LLC
UC	University of Cologne, Institute of Geology and Mineralogy, Cologne, Germany
UH	University of Hamburg, Institute of Soil Science, Hamburg, Germany
UM	Moscow State University, Moscow, Russian Federation
UP	University of Potsdam, Postdam, Germany
USP	University of St. Petersburg, Saint-Petersburg, Russian Federation
WeW-FU	Institute of Space Sciences, Freie Universitaet Berlin, Berlin, Germany
YRC	Yakutsk Branch Federal Research Center Geophysical Survey Russian Academy of Sciences
ZIN-RAS	Zoological Institute of Russian Academy of Science, Saint Petersburg, Russian Federation

A.2 Measurements at Research Station Samoylov Island and Lena Delta

Table A.2-1: List of water samples and planned analyses

Sample No	Sample location	Depth (surface=0.2h bottom=0.8h)	Date	Main ions	Isotope	DOC	CDOM	Biogens
A1	Main Channel. point N1	Surface	9.04	+	+	+	+	+
A2	Main Channel. point N1	Bottom	9.04	+	+	+	+	+
A3	Main Channel. point N2	Surface	11.04	+	+	+	+	+
A4	Main Channel. point N2	Bottom	11.04	+	+	+	+	+
A5	Main Channel. point N3	Surface	12.04	+	+	+	+	+
A6	Main Channel. point N3	Bottom	12.04	+	+	+	+	+
A7	Olenekskaya Channel	Surface	15.04	+	+	+	+	+
A8	Olenekskaya Channel	Bottom	15.04	+	+	+	+	+
B1	Lake Banya-2	Surface	20.04	+	+	+	+	+
B2	Lake Banya-2	Bottom	20.04	+	+	+	+	+
B3	Molo Lake	Surface	21.04	+	+	+	-	+
B4	Molo Lake	Bottom	21.04	+	+	+	+	+
B5	Lake N10	Surface	21.04	+	+	+	+	+
B6	Lake N10	Bottom	21.04	+	+	+	+	+
B7	Lake Banya-3	Surface	22.04	+	+	+	+	+
B8	Lake Banya-3	Bottom	22.04	+	+	+	+	+
B9	Lake N9	3m	22.04	+	+	+	+	+
B10	Lake Banya-1	Surface	22.04	+	+	+	+	+
B11	Lake Banya-1	Bottom	22.04	+	+	+	+	+
B12	Fish Lake	Surface	22.04	+	+	+	+	+
B13	Fish Lake	Bottom	22.04	+	+	+	+	+
B14	Lake N11	1.7m	23.04	+	+	+	+	+

Sample No	Sample location	Depth (surface=0.2h bottom=0.8h)	Date	Main ions	Isotope	DOC	CDOM	Biogens
C1	Main Channel surface ice	-	9.04	+	+	+	+	+
C2	Lake Banya-3 water from sediment	-	22.04	+	+	+	+	-
C3	Main Channel snow	-	9.04	-	+	+	+	-
C4	Molo Lake snow	-	21.04	-	+	+	+	-
C5	Lake Banya-3 deep snow	-	22.04	-	+	+	+	-
C6	Olenekskaya Channel snow	-	15.04	-	+	+	+	-
C7	Main Channel deep ice	-	9.04	-	+	+	+	-
C8	Olenekskaya Channel surface ice	-	15.04	-	+	+	+	-
C9	Olenekskaya Channel deep ice	-	15.04	-	+	+	+	-
C10	Lake Banya-3 surface snow	-	22.04	-	+	+	+	-
C11	Molo Lake ice	-	21.04	-	+	+	+	-
F1	Talik N1	6 m	13.04	+	-	-	-	-
F3	Talik N3	-	13.04	+	-	-	-	-
F4	Talik N4	-	13.04	+	-	-	-	-

Table A.2-2: List of express-analyses and lab results

Sample No	Conductivity [μS/cm]	pH	Dissolved oxygen [mg/liter] (% of saturation)	permanganate index [mg atomic oxygen/liter]	Chromaticity [pt-co degrees]
A1	581	7.1	-	-	33
A2	494	7.44	-	-	44
A3	519	7.82	-	-	33
A4	524	7.73	-	-	30
A5	507	7.81	-	-	40
A6	502	7.84	-	-	30
A7	495	7.72	-	-	30
A8	506	7.7	-	-	27
B1	185	7.42	15.17 (116%)	17.7	40
B2	162	7.37	10.77 (82%)	9.82	48
B3	140	7.32	18.19 (139%)	9.37	44
B4	142	7.38	17.66 (135%)	6.36	33
B5	144	7.9	10.92 (83%)	7.84	56
B6	143	7.04	12.04 (92%)	4.56	48
B7	232	9.46	12.08 (92%)	16.22	96
B8	225	8.3	17.13 (130%)	14	77
B9	168	7.39	11.32 (86%)	20.47	178
B10	277	7.01	10.61 (81%)	12.63	89
B11	277	7.27	7.92 (60%)	11.58	142
B12	152	7.33	11.53 (88%)	8.83	40
B13	-	-	6.82 (52%)	8.53	44
B14	131	6.98	7.79 (59%)	7.88	37
C1	107	7.72	-	-	30
C2	238	6.95	-	-	44
C3	7	6.6	-	-	37
C4	13	7.07	-	-	33
C5	14	6.73	-	-	20
C6	17	7.19	-	-	37
C7	-	-	-	-	192
C8	47	7.27	-	-	40
C9	6	6.39	-	-	23
C10	47	5.05	-	-	168
C11	3	7.68	-	-	96

Table A.2-3: Water samples from various channels

Location	Snow on ice [m]	Depth of a channel or lake [m]	Ice thickness [m]	Max. velocity	vertical	Samples for water chemistry	Samples for turbidity	CO_2/ PO/ CH_4
Olenekskaya Channel, near station	0.43	4.7	1.17	Not measured	Under ice	-	+	+/-/-
		+0.04 - water level on ice						
Tumatskaya Channel	0.67	10.9	1.30	No velocity	On 10 m depth	+	+	+/-/-
		+0.12 - water level on ice			On 5 m depth	+	+	+/-/-
					On 1.5 m depth	+	+	+/-/-
Main Channel, vertical 1	0.63	25.3	1.45	0.041+	On 17 m depth	-	+	+/+/+
		+0.08 - water on ice		0.114 m/sec	under ice	+	+	+/+/+
Main Channel, vertical 2	0.4	19.5	1.85	0.047+	On 17 m depth	-	+	+/+/+
				0.112 m/sec	under ice	+	+	+/+/+
Main Channel, vertical 3	0.32	14.3	1.80	0.045+	On 14.5 m depth	-	+	+/+/-
		-0.02 - water under ice surface		0.061 m/sec	on 8.5 m depth	+	+	+/+/-
					on 2.5 m depth	+	+	+/+/-

Location	Snow on ice [m]	Depth of a channel or lake [m]	Ice thick-ness [m]	Max. veloc-ity	vertical	Sam-ples for wa-ter chem-istry	Sam-ples for tur-bid-ity	CO_2/ PO/ CH_4
Main Channel, vertical 4	0.8	19	2.50	0.073+	Under ice	+	+	+/+/+
		+0.28 - water on ice surface		0.1 m/sec	on 16.4 m	-	+	+/+/-
					on 9 m	-	+	+/+/+
Main Channel, vertical 5	0.6	18	1.10	0.045+	Under ice	+	+	+/+/+
		+0.10 - water on ice surface		0.092 m/sec	on 16.4 m depth	-	+	+/+/-
					on 9 m depth	-	+	+/+/-
Main Channel, vertical 6	0.42	14.3	1.10	0.02	Under ice	+	+	+/+/-
		-0.02 - water under ice surface		m/sec	on 6.4 m depth	+	+	+/+/
					”on 12.5 m depth”	+	+	+/+/-
Main Channel, vertical 7	0.82	2.4	1.60	No	On	+	+	+/+/-
		+0.15 - water under ice surface		velocity	middle of the vertical			
Bykovskaya Channel, vertical 1	With-out snow, 3-5 cm max	9.2	1.95	0.117+	On 2.3 depth	+	+	+/+/+
		-0.15 - water under ice surface		0.143 m/sec	on 7 m depth	+	+	+/+/+
					on 8.5 m depth	-	+	+/+/-

Location	Snow on ice [m]	Depth of a channel or lake [m]	Ice thick-ness [m]	Max. veloc-ity	vertical	Sam-ples for wa-ter chem-istry	Sam-ples for tur-bid-ity	CO_2/ PO/ CH_4
Bykovskaya Channel, vertical 2	With-out snow	14 -0.16 - water under ice surface	2	0.127+ 0.182 m/sec		-	-	-
Bykovskaya Channel, vertical 2	With-out snow	4 -0.15 - water under ice surface	1.90	0.020 m/sec	Under ice	+	+	+/+/-
Olenek-skaya Channel	0.4, snow was with a lot of sand	2.8 -0.02 m under ice	1.1	0+0.042 m/sec	Under ice on 2.5 m depth	- -	+ +	+/+/+ +/+/-

Table A.2-4: List of measurement points of water and suspended material sampling

Date	Channel	ice thick-ness [m]	sampling depth [m]	pH	Conductivity [μS/cm]	O2 [mg/l]
15.04.2017	Olenekskaya (nearby station)	1.17	integrate	7.76	443	7.7
17.04.2017	Tumatskaya hydro section	1.3	under ice	7.49	411	7.58
			5	7.4	431	
			10	7.51		3.97
19.04.2017	Main Channel vert.2	1.85	2.5			5.62
			8.5			7.3
			14.5			6.46
20.04.2017	Main Channel vert.4	2.5	under ice	7.38	532	6.89
			9	7.33	517	6.23
			16.4	7.47	526	6.6
	Main Channel vert.6	1.1	2	7.34	461	7
			6	7.34	457	5.98
			12.5	7.19	455	6.69
21.04.2017	Main Channel vert.7	1.6	2.4	7.26	449	6.9
			integral		453	6.97
22.04.2017	Bykovskaya vert.1	1.95	under ice	7.36	468	6.89
			5	7.29	470	6.99
			8.5	7.34	471	6.74
25.04.2017	Olenekskaya hydrosection	2.5	under ice	7.4	437	6.5
			2.5	7.34	447	7.35

Table A.2-5: List of water samples of Samoylov lakes and planned analyses

Lake name	**Position of sampling on vertical**	**Depth on vertical [m]**	**Ice thickness [m]**	**snow on ice [m]**	**water on/ under ice [m]**	**Main ions**	**CO_2**	**Permanganate oxyd.**	**DOC**	**CDOM**	**Nutrients**
Polygonal crack	water was under pressure	0.7					+				+
Molo Lake	under ice	5.5	1.4			+	+	+	+	+	+
Molo Lake	bottom	5.5	1.4			+	+	+	+	+	+
North Lake	under ice	5	1.4	0.34		+	+	+	+	+	+
North-East Lake	very fast sampling. surface	4	1.45	1.23	0.35	+	+	+	+	+	+
North-East Lake	bottom. beetles in water	4	1.45	1.23	0.35	+	+	+	+	+	+
East lake	samples from 2.5m; hydrogen sulphide smell	3.25	1.4	0.3		+	+	+	+	+	+
East lake	under ice	3.25	1.4	0.3		+	+	+	+	+	+
South Lake	under ice	3.5	1.5	0.1		+	+	+	+	+	+
South Lake	bottom samples; hydrogen sulphide smell	3.5	1.5	0.1		+	+	+	+	+	+
Shallow Lake	surface	4.6	1.4	0.3		+	+	+	+	+	+
Shallow Lake	bottom	4.6	1.4	0.3		+	+	+	+	+	+

Table A.2-6: Concentration of CO_2 and Permanganate oxidation in water of channels and lakes

Point of sampling	**Carbon Dioxide concentration [mg/l]**	**Permanganate Oxidation [mgO/l]**
Tumatskaya. 1m	8	-
Tumatskaya. 2m	5.9	-
Main Channel. vert.1. 17m	6	3.6
Main Channel. vert.1. under ice	6.7	9
Main Channel. vert.3. 3.6m	6.5	8.8
Main Channel. vert.3. 8.5m	6.3	8.1
Main Channel. vert.3. 14.5m	8.3	7.8
Main Channel. vert.4. under ice	5.8	7.2
Main Channel. vert.4. 9m	7.2	7.9
Main Channel. vert.4. 16.4m	6	8.6
Main Channel. vert.6. under ice	5.9	7.6
Main Channel. vert.6. 6m	7.2	8.2
Main Channel. vert.6. 12m	6.6	8.2
Main Channel. vert.7. under ice	8.1	10.1
Fish Lake. surface	5.3	3.3
Fish Lake. integral	6.6	2.95
Banya-1 Lake. surface	15.7	8.2
North Lake	5.1	9.4
Molo Lake. surface	5.3	8.3
Molo Lake. 5m	17.2	6.8
North-East Lake. surface	16.5	8.7

Table A.2-7: List of water samples (surface and bottom), zooplankton and benthos samples, and planned analyses

Date	Sample location	Latitude [°N]	Longitude [°E]	Zoo-plankton littoral	Zoo-plankton pelagial	Ben-thos	Main ions	Iso-tope	DOC	CDOM	Bio-gens
08.07. 2016	Fish Lake	72.37383	126.4893	+	+	+	+	+	+	+	+
09.07. 2016	Northeast Lake	72.38333	126.50045	+	+	+	+	+	+	+	+
09.07. 2016	Shallow II	72.36667	126.49548	+	+	+	+	+	+	+	+
10.07. 2016	Northern Lake	72.38333	126.4863	+	+	+	+	+	+	+	+
11.07. 2016	Eastern Lake	72.36667	126.5188	+	+	+	+	+	+	+	+
11.07. 2016	Shallow	72.36667	126.5111	+	+	+	+	+	+	+	+
12.07. 2016	Molo	72.36667	126.49731	+	+	+	+	+	+	+	+
13.07. 2016	Seregino Lake	72.38751	126.48408	+	+	+	+	+	+	+	+
14.07. 2016	Fish Lake	72.37383	126.47263	+	+	+	+	+	+	+	+
18.07. 2016	Fish Lake	72.36667	126.5111	+	+	+	+	+	+	+	+
16.07. 2016	Lake on Kurungnakh Island	72.29488	126.19963	+	+	+	+	-	+	+	+
18.07. 2016	Eastern Lake	72.36667	126.5188	+	+	+	+	+	+	+	+
18.07. 2016	Molo	72.36667	126.49731	+	+	+	+	+	+	+	+
21.07. 2016	Fish Lake	72.37383	126.4893	+	+	+	+	+	+	+	+
23.07. 2016	Molo	72.36667	126.49731	+	+	+	+	+	+	+	+
23.07. 2016	Shallow	72.36667	126.5111	+	+	+	+	+	+	+	+
23.07. 2016	Eastern Lake	72.36667	126.5188	+	+	+	+	+	+	+	+
23.07. 2016	Reinder	72.38165	126.4992	+	+	+	+	+	+	+	+
26.07. 2016	Bannoe 2	72.36851	126.50096	+	+	+	+	+	+	+	+
26.07. 2016	Southern Lake	72.36911	126.51255	+	+	+	+	+	+	+	+
27.07. 2016	Molo	72.36667	126.49731	+	+	+	+	+	+	+	+
27.07. 2016	Shallow	72.36667	126.5111	+	+	+	+	+	+	+	+
27.07. 2016	Eastern Lake	72.36667	126.5188	+	+	+	+	+	+	+	+
27.07. 2016	Fish Lake	72.37383	126.4893	-	-	+	+	+	+	+	+

Table A.2-8: List of express-analyses and lab results

Sample location	Date	T surface	Dissolved oxygen [mg/liter] (% of saturation)	Dissolved oxygen [mg/l]	pH	Redox potential (Eh), [mV]	Conductivity [μS/cm]	Sample depth [m]
Fish Lake	08.07. 2016	8.2	125.3	14.45	7.33	-43	82	5.4
Northeast Lake	09.07. 2016	7.3	90.7	10.7	6.04	-44	70	3.1
Shallow II	09.07. 2016	7.7	99.3	11.72	5.16	-94	65	2.9
Northern Lake	10.07. 2016	6.9	87	10.5	6.7	9	62	5
Eastern Lake	11.07. 2016	6.4	87	10.64	7.67	-46	43	4.6
Shallow	11.07. 2016	5	87.7	11.12	7.64	-43	54	3.4
Molo	12.07. 2016	6.7	89.3	10.7	7.72	-52	67	6
Seregino Lake	13.07. 2016	7	90.3	10.95	7.72	-45	37	7.4
Fish Lake	14.07. 2016	7.3	90.8	10.83	7.86	-53	83	5
Fish Lake	18.07. 2016	7.1	91.7	10.96	7.66	-42	54	2.7
Lake on Kurungnakh Island	16.07. 2016	6.7	86.2	10.7	8	-59.8	118	5.8
Eastern Lake	18.07. 2016	9.2	92.8	10.52	7.86	-50	43	4
Molo	18.07. 2016	9.9	93.5	10.53	8.08	-62	67	5.5
Fish Lake	21.07. 2016	9.4	89.3	10.24	8.06	-64	84	5.5
Molo	23.07. 2016	10.1	90.5	10.42	7.9	-56	69	5.5
Shallow	23.07. 2016	11.3	91.2	9.9	7.74	-59	59	2.2
Eastern Lake	23.07. 2016	10.3	91.4	10.06	7.6	-39	45	4.5
Reindeer	23.07. 2016	11.4	90.6	9.77	7.9	-57	100	2.8

Sample location	**Date**	**T surface**	**Dissolved oxygen [mg/liter] (% of saturation)**	**Dissolved oxygen [mg/l]**	**pH**	**Redox potential (Eh), [mV]**	**Conductivity [μS/cm]**	**Sample depth [m]**
Bannoe 2	26.07. 2016	10.3	72.1	7.96	7.55	-38	85	12
Southern Lake	26.07. 2016	11	96.1	10.79	7.59	-44	114	3.5
Molo	27.07. 2016	10.5	98.6	10.9	7.7	-50	70	5.5
Shallow	27.07. 2016	10.8	96.7	10.65	7.59	-45	61	2.5
Eastern Lake	27.07. 2016	11.2	86.6	9.5	6.62	11	61	4.5
Fish Lake	27.07. 2016	10.5	99.2	10.99	6.32	-87	28	5.2

Table A.2-9: Measurement points of surface sediment sampling

Surface samples	Date	Point	Latitude [°N]	Longitude [°E]	Location
16-Tik-01	08.07.2016	Fish Lake	72.37383	126.4893	Samoylov Island
16-Tik-02	09.07.2016	Northeast lake	72.38333	126.50045	Samoylov Island
16-Tik-03	09.07.2016	Shallow II lake	72.36667	126.49548	Samoylov Island
16-Tik-04	10.07.2016	Northern Lake	72.38333	126.4863	Samoylov Island
16-Tik-05	11.07.2016	East lake	72.36667	126.5188	Samoylov Island
16-Tik-06	11.07.2016	Shallow Lake	72.36667	126.5111	Samoylov Island
16-Tik-07	12.07.2016	Molo Lake	72.36667	126.49731	Samoylov Island
16-Tik-08	13.07.2016	Seregino lake	72.38751	126.48408	Kurungnakh Island
16-Tik-09	14.07.2016	Pond in a Polygon	72.37105	126.4713	Samoylov Island
16-Tik-10	16.07.2016	Eastern lake	72.29488	126.19963	Kurungnakh Island
16-Tik-11	23.07.2016	Reindeer	72.38165	126.4992	Samoylov Island
16-Tik-12	26.07.2016	Bannoe II	72.36851	126.50096	Samoylov Island
16-Tik-13	26.07.2016	Southern lake	72.36911	126.51255	Samoylov Island

Table A.2-10: Measurement points of cores sampling

Core samples	Date	Point	Latitude [°N]	Longitude [°E]	Length [cm]	Location
16-Tik-07, 1A	12.07.2016	Molo Lake	7237806	126.49731	32	Samoylov Island
16-Tik-07, 1B	12.07.2016	Molo Lake	72.37806	126.49731	30	Samoylov Island
16-Tik-10, 1A	16.07.2016	Eastern Lake	72.29488	126.19963	28	Kurungnakh Island
16-Tik-10, 1B	16.07.2016	Eastern Lake	72.29488	126.19963	25	Kurungnakh Island

Table A.2-11: Calculation of water discharge and suspended sediment load (Olenekskaya Channel, old station Chay-Tumus/Olenekskaya Channel, Olenekskaya gauge line/Tumatskaya Channel, gauge line/Trofimovskaya Channel, gauge line)

Sounding on the vertical	distance from a standing start	depth on the vertical [m]	Average velocity on the vertical [m/sec]	Average turbidity on the vertical [g/l]	Average velocity between the verticals [m/sec]	Average turbidity between verticals [g/l]	Squer between verticals [m^2]	water discharge between verticals [m^3/sec]	Sediment discharge between verticals [kg/sec]
Level of left bank	0	-	-	-	-	-	-	-	-
Vertical 1	170	17.9	0.46	0.032	0.46	0.032	304	141	4.53
Vertical 2	290	14.1	0.45	0.034	0.46	0.033	1.207	553	18.24
Vertical 3	415	5.5	0.21	0.013	0.33	0.024	1.901	625	14.69
Level of right bank	-	-	-	-	0.21	0.013	2.186	453	5.88
Q (m3/s)	-	-	-	-	-	-	-	1.772	43

Level of right bank	0	-	-	-	-	-	-	-	-
Vertical 4	120	6.8	0.48	0.008	0.48	0.008	472	228	1.71
Vertical 3	380	11.3	0.78	0.021	0.63	0.014	2.312	1.455	20.42
Vertical 2	500	7.1	0.57	0.019	0.67	0.02	1.033	694	13.65
Vertical 1	680	2.6	0.28	0.014	0.42	0.016	896	378	6.11
Level of left bank	-	-	-	-	0.28	0.014	216	59	0.81
Q (m3/s)	-	-	-	-	-	-	-	2.815	43

Level of right bank	0	-	-	-	0.33	0.027	341.1	112	3.01
Vertical 4	50	12	0.33	0.027	0.45	0.028	847.5	385	10.9
Vertical 3	110	14.9	0.58	0.03	0.58	0.058	2.769	1.602	92.6
Vertical 2	330	10.8	0.58	0.086	0.53	0.048	2.332	1.228	58.8
Vertical 1	670	5.8	0.47	0.01	0.47	0.01	232	110	1.1
Level of left bank	-	-	-	-	-	-	-	-	-
Q (m3/s)	-	-	-	-	-	-	-	3.437	167

Sounding on the vertical	**distance from a standing start**	**depth on the vertical [m]**	**Average velocity on the vertical [m/sec]**	**Average turbidity on the vertical [g/l]**	**Average velocity between the verticals [m/sec]**	**Average turbidity between verticals [g/l]**	**Squer between verticals [m^2]**	**water discharge between verticals [m^3/sec]**	**Sediment discharge between verticals [kg/sec]**
Level of left bank	3.2	-	-	-	-	-	-	-	-
Vertical 5	2.3	10.3	0.641	0.022	0.641	0.022	6.662	4.271	95
Vertical 4	1.8	13.9	0.93	0.031	0.786	0.027	6.851	5.381	144
Vertical 3	1.4	11.7	0.833	0.056	0.881	0.044	5.086	4.483	196
Vertical 2	960	7.9	0.738	0.02	0.786	0.038	4299	3377	129
Vertical 1	500	5.3	0.701	0.015	0.72	0.017	3.219	2.316	40
Level of right bank	0	-	-	-	0.701	0.015	1.827	1.281	19
Q (m3/s)	-	-	-	-	-	-	-	21.11	622

Table A.2-12: List of Hydrochemical express-analyses

N. of sample	pH	Eh [mV]	Conductivity [μSm/cm]	O2 [mg/l]	O2 [%]	Place
1	7.33	-43	82	14.45	125.3	Fish Lake
2	6.04	-44	70	10.7	90.7	Northeastern Lake
3	5.16	-94	65	11.72	99.3	Shallow-2 Lake
4	6.7	-90	62	10.5	87	Northern Lake
5	7.64	-43	54	10.64	87.7	Shallow Lake
6	7.67	-46	43	11.12	89.3	Eastern Lake
7	7.72	-52	67	10.7	90.3	Molo Lake
8	7.72	-45	37	10.95	90.8	Kurungnakh-1 Lake
9	8	-59,8	118	10.7	86.2	Kurungnakh-2 Lake
10	7.55	-38	85	7.96	72.1	Bannoe-2 Lake
11	7.59	-44	114	10.79	96.1	Southern Lake
12	8.06	-61	113	6.43	59.5	Trofimovskaya Channel, Right Coast
13	7.74	-45	103	7.55	67.4	Trofimovskaya Channel, Average Vertical
14	7.98	-61	110	7.25	76.7	Trofimovskaya Channel, Left Coast
15	7.99	-60	103	10.93	91.4	Bykovskaya Channel, Vertical 1
16	7.84	-51	103	10.85	91.4	Bykovskaya Channel, Vertical 2
17	7.59	-49	104	11.21	90.7	Bykovskaya Channel, Vertical 3
18	7.81	-	113	-		Olenekskaya Channel, 40 km downstream of Gusinka, Vertical 1
19	-	-	113	-		Olenekskaya Channel, 40 km downstream of Gusinka, Vertical 2
20	7.85	-	113	12.7	119.4	Olenekskaya Channel, 40 km downstream of Gusinka, Vertical 3
21	7.83	-	120	8.63	82.8	Olenekskaya Channel, Gusinka, Vertical 1

N. of sample	pH	Eh [mV]	Conductivity [μSm/cm]	O2 [mg/l]	O2 [%]	Place
22	7.84	-	120	9.03	86.7	Olenekskaya Channel, Gusinka, Vertical 2
23	7.94	-	119	9.6	86.6	Olenekskaya Channel, Gusinka, Vertical 3
24	7.85	-53	125	8.78	85.6	Olenekskaya Channel, Chay-Tumus, Vertical 1
25	7.91	-58	125	8.81	85.5	Olenekskaya Channel, Chay-Tumus, Vertical 2
26	7.8	-51	124	8.87	85.8	Olenekskaya Channel, Chay-Tumus, Vertical 3
27	7.78	-50	118	9.33	86.1	Olenekskaya Channel, g/s, Vertical 1
28	7.67	-43	130	8.8	85.4	Olenekskaya Channel, Main g/s, Vertical 3
29	7.56	-38	132	8.52	83.7	Olenekskaya Channel, Main g/s, Vertical 4
30	8.01	-73	131	8.86	88.7	Tumatskaya Channel, Vertical 1
31	7.77	-56	133	8.2	82.5	Tumatskaya Channel, Vertical 2
32	7.62	-42	133	8.2	82.7	Tumatskaya Channel, Vertical 3
33	7.58	-38	133	8.14	83	Tumatskaya Channel, Vertical 4

Table A.2-13: Stations along the Lena River and samples for water chemistry

No.	Point	Coordinates [°]	Date	Turbidity [mg/l]	Main Ions	nut-rients	CDOM	DOC
1	Lena River	N 62.34672 E 130.07481	08.07.17	5.71	+	+	+	+
2	Lena River	N 62.61236 E 129.81428	08.07.17	7.4	+	+	+	+
3	Lena River. estuary of the Aldan river	N 63.05575' E 129.68675	09.07.17	9.92	+	+	+	+
4	Lena River. Sangar	N 63.88336 E 127.55617	09.07.17	0.61	+	+	+	+
5	Estuary of the Vilyi river	N 64.37563 E 126.40169	09.07.17	3.95	+	+	+	+
6	Lena River	N 64.46891 E 126.06431	10.07.17	2.79	+	+	+	+
7	Lena River	N 65.85083 E 124.21056	14.07.17	2.61	+	+	+	+
8	Lena River	N 66.29233 E 123.87022	14.07.17	4.93	+	+	+	+
9	Lena River. Zhi-gansk	N 66.78069 E 123.39658	16.07.17	15.12	+	+	+	+
10	Lena River	N 67.58778 E 123.01211	16.07.17	4.46	+	+	+	+
11	Lena River	N 68.05689 E 123.31778	17.07.17	9.06	+	+	+	+
12	Lena River	N 68.81269 E 124.01561	18.07.17	3.56	+	+	+	+
13	Lena River	N 69.62944 E 125.01028	18.07.17	3.53	+	+	+	+
14	Lena River. Sekhtyah	N 69.91414 E 125.12361	18.07.17	8.31	+	+	+	+
15	Lena River. Kusyur	N 70.52917 E 126.13936	19.07.17	7.83	+	+	+	+
16	Lena River	N 71.4' E 127.25947	19.07.17	4.54	+	+	+	+

No.	Point	Coordinates [°]	Date	Turbidity [mg/l]	Main Ions	nut-rients	CDOM	DOC
17	Lena River. Tit - Ary	N 71.99353 E 127.08333	20.07.17	4.92	+	+	+	+
18	Tumats-kaya Channel	N 72.41583 E 126.4542	24.07.17		+	+	+	+
19	Tumats-kaya Channel	N 72.41583 E 126.4542	24.07.17		+	+	+	+
20	Lake Banya 1	N 72.36897 E 126.4867	24.07.17		+	+	+	+
21	Olenek-skaya Channel	N 72.29622 E 126.07358	25.07.17		+	+	+	+
22	Olenek-skaya Channel	N 72.29622 E 126.07358	25.07.17		+	+	+	+
23	Trofi-movskaya Channel	N 72.43816 E 126.65127	26.07.17		+	+	+	+
24	Trofi-movskaya Channel	N 72.43872 E 126.65127	26.07.17		+	+	+	+
25	Fish Lake (cental part)	N 72.43203 E 126.62117	27.07.17		+	+	+	+
26	Fish Lake (cental part)	N 72.43203 E 126.62117	27.07.17		+	+	+	+
27	The Fish Lake	N 72.43203 E 126.62117	27.07.17		+	+	+	+
28	Molo Lake	N 72.37833 E 126.49678	27.07.17		+	+	+	+
29	Shallow Lake	N 72.37365 E 126.48745	28.07.17		+	+	+	+
30	Bykovs-kaya Channel	N 72.4125 E 126.87528	28.07.17		+	+	+	+

Table A.2-14: Hydrometrical parameters, water discharges and suspended material for the Main Channels of the Lena Delta

No	Channel	Profile	Date	position	Coordinates [°]	Channel width [m]	Max depth [m]	Water Discharge [m^3/s]	Mean turbidity [mg/L]	Sediment load [kg/s]
1	Olenekskaya	gauge line	25.07.17	left bank	N 72.29362 E 126.0701	770	5.1	757.4	3.94	2.984
				right bank	N 72.29475 E 126.07842					
2	Tumatskaya	gauge line	24.07.17	left bank	N 72.41405 E 125.4426	630	12.5	451.4	4.98	2.25
				right bank	N 72.41658 E 126.45915					
4	Bykovskaya	gauge line	28.07.17	point 1	N 72.4166 E 126.86425	770	15.1	5.313	3.34	17.74
				point 2	N 72.41403 E 126.86883					
				point 3	N 72.41153 E 126.86905					
5	Trofimovskaya	gauge line	26.07.17	point 4, close to the left bank	N 72.43682 E 126.61665	3.220	12.7	11.5	5.64	64.79
				point 3	N 72.43787 E 126.62817					
				point 2	N 72.43877 E 126.65198					
				point 1, close to right bank	N 72.43921 E 126.67007					

Table A.2-15: Hydrochemistry of lakes on Samoylov Island in surface waters

No	Point	Coordinates [°]	Date	Physico-chemical parameters			
				water temperature [°C]	Conductivity [μS/cm]	pH	O2 [mg/l]
1	Banya 1 Lake	N 72.36897 E 126.4867	24.07.17	8.9	84	8.51	11.65
2	Banya 2 Lake	N 72.36941 E 126.50478	24.07.17	9.1	91	-	11.53
3	Fish Lake	N 72.43203 E 126.62117	27.07.17	9	77	7.37	11.49
4	Molo Lake	N 72.37833 E 126.49673	27.07.17	8.7	65	7.53	11.35
5	Shallow Lake	N 72.37365 E 126.48745	28.07.17	7.7	48	7.4	11.7

Table A.2-16: Water parameters (temperature, oxygen concentration, pH, conductivity) and preserved samples for later analysis (Chlorophyll-a (CHl-a), Phytoplankton (PHp), Phytobenthos (Phb), Hydrochemistry (Hc), Primary production (PP) of plankton and benthos) for pond I

Pond I	**measure-ments**	**N 72.37008°**	**E 126.48325°**	**sampling**					
date	**ToC water**	**O_2 [mg/l]**	**pH**	**C [μS/cm]**	**Chl-a**	**Php**	**Phb**	**Hc**	**PP**
30.06.	12.4	7.48	7.03	25	-	-	-	-	X
02.07.	10.8	7.15	7.24	26	X	X	X	-	X
08.07.	12.6	7.76	7.36	26	-	-	-	-	X
10.07.	12.5	8.52	7.74	25	X	X	X	-	X
17.07.	12.7	8.6	7.37	30	-	-	-	X	X
19.07.	5.5	7.07	7.38	34	X	X	X	-	X
25.07.	10	7.5	7.4	36	-	-	-	X	X
27.07.	8.6	7.49	6.9	36	X	X	X	-	X
01.08.	12.6	6.28	7.13	41	-	-	-	-	X
02.08.	10.6	6.74	7	41	-	-	-	X	-
03.08.	9.8	6.16	6.65	43	X	X	X	-	X
08.08.	10.8	6.59	7.04	42	-	-	-	X	X
10.08.	11.2	6.06	6.97	48	X	X	X	-	X
14.08.	9.3	7.15	7.33	48	-	-	-	-	X
16.08.	8.2	7.54	7.37	50	X	X	X	X	X
21.08.	9.1	8.15	7.42	55	-	-	-	-	X
22.08.	9.5	8.27	7.41	53	-	-	-	X	-
23.08.	9	8.28	7.39	54	X	X	X	-	X

Table A.2-17: Water parameters (temperature, oxygen concentration, pH, conductivity) and preserved samples for later analysis (Chlorophyll-a (CHl-a), Phytoplankton (PHp), Phytobenthos (Phb), Hydrochemistry (Hc), Primary production (PP) of plankton and benthos, and Zooplankton (ZP) samples for pond II

Pond II	**N 72.37086°**		**E 126.48292°**							
measurements					**sampling**					
date	**ToC water**	**O2 [mg/l]**	**pH**	**C μS/cm**	**Chl-a**	**Php**	**Phb**	**Hc**	**ZP**	**PP**
26.06.	15.8	8.24	7.42	46	-	-	-	-	X	X
28.06.	9.6	7.37	7.61	42	X	X	X	-	-	X
04.07.	8.2	8.14	7.88	51	-	-	-	-	X	X
06.07.	4.5	7.92	7.75	53	X	X	X	-	-	X
07.07.	6	7.45	7.61	49	-	-	-	-	X	-
11.07.	13.8	7.96	7.08	54	-	-	-	-	X	-
12.07.	9.8	7.1	7.72	55	-	-	-	-	-	X
14.07.	9.7	8.05	7.58	54	X	X	X	-	X	X
17.07.	12.4	7.63	7.53	53	-	-	-	X	X	-
18.07.	9				-	-	-	-	-	-
20.07.	5	8.02	7.65	56	-	-	-	-	X	X
22.07.	9.9	8.01	7.62	57	X	X	X	-	-	X
23.07.	8.3				-	-	-	-	X	-
24.07.	9	7.89	7.5	58	-	-	-	X	-	-
26.07.	10				-	-	-	-	X	-
28.07.	7.1	7.84	7.34	59	-	-	-	-	X	X
30.07.	8.5	7.53	7.54	60	X	X	X	X	-	X
01.08.	12.3				-	-	-	-	X	-
02.08.	10.6	6.74	7	41	-	-	-	-	-	-
04.08.	6.4	8.42	7.35	63	-	-	-	-	X	-
05.08.	9.7	8.34	7.51	62	-	-	-	-	-	X
07.08.	9.4	7.63	7.49	64	X	X	X	X	X	X
10.08.	11.4	6.33	7.38	73	-	-	-	-	X	-
11.08.	7.1	7.67	7.53	75	-	-	-	-	-	X
13.08.	8.9	8.27	7.6	75	X	X	X	X	X	X
17.08.	10.2	8.02	7.66	78	-	-	-	-	-	X
18.08.	10.2				-	-	-	-	X	-
19.08.	9.2	8.15	7.59	78	X	X	X	-	-	X
21.08.	9.1	8.82	7.65	79	-	-	-	X	X	-
25.08.	7.9	9.22	7.7	82	-	-	-	-	X	-

Table A.2-18: Sample locations and types, and sample types. The abbreviation n.d. means not determined.

Station name	Latitude N [decimal degree]	Longitude E [decimal degree]	water depth [m]	description	sampled depths	sample types
L17-01	72.3849	126.4832	surface sample	Samoylov; North Lake outflow	surface	DIC. DOC. POC
L17-04	72.3847	126.4873	4	Samoylov; North Lake center	surface; 1.5m; 4m	DIC. DOC. POC
L17-05	72.3852	126.4805	surface sample	Samoylov; Katya Lake (on floodplain. downstream of North Lake)	surface	DIC. DOC. POC
L17-06	72.3894	126.4833	surface sample	Samoylov; outflow floodplain into Lena River. downstream of Katya Lake	surface	DIC. DOC. POC
L17-07	72.3956	126.6787	9.4	Lena-West. Main Channel at Stolb	surface; 4m; 8m	DIC. DOC. POC
L17-08	72.3998	126.7061	24	Lena-Mid. Main Channel at Stolb	surface; 12m; 21m	DIC. DOC. POC
L17-09	72.3998	126.7267	17.2	Lena-East. Main Channel at Stolb	surface; 4m; 8m	DIC. DOC. POC
L17-10	72.3839	126.4861	surface	Samoylov; polygon pond north	surface	DIC. DOC. POC
L17-11	72.2828	126.4854	surface	Samoylov; polygon pond middle	surface	DIC. DOC. POC
L17-12	72.3837	126.4851	surface	Samoylov; polygon pond south	surface	DIC. DOC. POC
L17-13	72.2934	126.1998	5	Kurungnakh; Oval Lake center	surface; 2m; 4m	DIC. DOC. POC
L17-14	72.2920	126.1935	surface	Kurungnakh; Oval Lake outflow	surface	DIC. DOC. POC
L17-15	72.2943	126.1543	surface	Kurungnakh; Lucky Lake outflow	surface	DIC. DOC. POC

Station name	Latitude N [decimal degree]	Longitude E [decimal degree]	water depth [m]	description	sampled depths	sample types
L17-16	72.2814	126.1930	surface	Kurungnakh; outflow to Lena River (downstream of Lucky Lake)	surface	DIC. DOC. POC
L17-17	72.2988	126.1748	∼4.0	Kurungnakh; Lucky Lake center	surface; 1.5m; 3m	DIC. DOC. POC
L17-18	72.3956	126.6787	n.d.	Lena-West. Main Channel at Stolb	surface	DIC. DOC. POC
L17-19	72.3989	126.7061	n.d.	Lena-Mid. Main Channel at Stolb	surface; 12m; 21m	DIC. DOC. POC
L17-20	72.3989	126.7221	n.d.	Lena-East. Main Channel at Stolb	surface	DIC. DOC. POC

Table A.2-19: General characteristics of the sampling stations in the area of the Samoylov Island Resear (August 2017)

Sample number	Island	Date	Type of water body	Sampling depth [m]	Bottom	Water body size [m]	Latitude	Longitude
L-1	SI	Aug. 1. 17	Pond	0.5	Mosses and silt	5 x 5	72.37	126.48333
L-2	SI	Aug. 2. 17	Lake	0.5	Claim and silt	100 x 150	72.37361	126.49028
L-3	SI	Aug. 2. 17	Pond	0.5	Mosses and silt	50 x 5	72.37083	126.47139
L-4	SI	Aug. 3. 17	Lake	0.5	Silt with detritus	500 x 100	72.36889	126.50389
L-5	SI	Aug. 3. 17	Lake	0.6	Silt with detritus	350 x 100	72.36806	126.48944
L-6	SI	Aug. 3. 17	Lake	0.5	Mosses and detritus. green algae	50 x 20	72.36861	126.47528
L-7	SI	Aug. 4. 17	Lake	0.6	Silt with detritus	80 x 50	72.36639	126.50528
L-8	SI	Aug. 4. 17	Lake	0.5	Silt with detritus	370 x 50	72.36889	126.51361
L-9	SI	Aug. 4. 17	Lake	0.6	Sand with silt	150 x 80	72.37056	126.51861
L-10	SI	Aug. 4. 17	Lake	0.5	Silt with detritus	350 x 75	72.37639	126.51639
L-11	SI	Aug. 4. 17	Lake	0.6	Silt with detritus	70 x 20	72.3825	126.50444
L-12	SI	Aug. 4. 17	Lake	0.5	Silt with detritus	160 x 45	72.38417	126.49833
L-13	SI	Aug. 4. 17	Lake	0.6	Sand with silt	330 x 75	72.38472	126.49167
L-14	KI	Aug. 5. 17	Lake	0.5	Silt with detritus	550 x 150	72.35694	126.23111
L-15	KI	Aug. 5. 17	Stream	0.3	Mosses	10 x 50	72.34972	126.22889
L-16	KI	Aug. 5. 17	Pond	0.5	Mosses and silt	5 x 5	72.33667	126.20472
L-17	KI	Aug. 5. 17	Lake	0.7	Silt with detritus	420 x 300	72.32611	126.22222
L-18	KI	Aug. 5. 17	Lake	0.5	Silt with detritus	70 x 150	72.31806	126.24278
L-19	KI	Aug. 5. 17	Pond	0.5	Silt with detritus	20 x 40	72.31417	126.25194

Sample number	Island	Date	Type of water body	Sampling depth [m]	Bottom	Water body size [m]	Latitude	Longitude
L-20	KI	Aug. 5. 17	Lake	0.4	Sand	850 x 420	72.32028	126.25972
L-21	OK	Aug. 6. 17	Lake	0.6	Claim and silt	100 x 200	72.45694	126.29361
L-22	OK	Aug. 6. 17	Pond	0.6	Silt with detritus	5 x 5	72.45778	126.29583
L-23	OK	Aug. 6. 17	Pond	0.6	Silt with detritus	5 x 5	72.45861	126.30361
L-24	OK	Aug. 6. 17	Lake	0.6	Sand	25 x 100	72.45917	126.30222
L-25	OK	Aug. 6. 17	Pond	0.6	Silt with detritus	6 x 9	72.45917	126.30028
L-26	TA	Aug. 7. 17	Lake	0.4	Sand	1000 x 500	71.96778	127.09167
L-27	TA	Aug. 7. 17	Pond	0.4	Silt with detritus	10 x 5	71.96556	127.08889
L-28	TA	Aug. 7. 17	Pond	0.2	Silt with detritus	5 x 5	71.96528	127.0875
L-29	KI	Aug. 9. 17	Lake	0.5	Sand	200 x 200	72.28444	126.20722
L-30	KI	Aug. 9. 17	Lake	0.5	Sand and mosses	100 x 50	72.28611	126.19694
L-31	KI	Aug. 9. 17	Lake	0.5	Sand	700 x 800	72.29194	126.19778
L-32	KI	Aug. 9. 17	Pond	0.4	Silt with detritus	5 x 5	72.29278	126.18417
L-33	KI	Aug. 9. 17	Pond	0.6	Silt with detritus	80 x 30	72.29056	126.17056
L-34	KI	Aug. 12. 17	Pond	0.4	Mosses and detritus	5 x 6	72.28167	126.18083
L-35	KI	Aug. 12. 17	Lake	0.5	Sand with detritus	30 x 20	72.28056	126.15444
L-36	KI	Aug. 12. 17	Lake	0.6	Sand	460 x 172	72.28333	126.13833
L-37	KI	Aug. 12. 17	Lake	0.4	Sand	200 x 100	72.29	126.12333
L-38	KI	Aug. 12. 17	Pond	0.4	Mosses and detritus	15 x 7	72.28167	126.17028
L-39	ABA	Aug. 17. 17	Lake	0.4	Silt with detritus	70 x 10	72.385	126.41472

Sample number	Island	Date	Type of water body	Sampling depth [m]	Bottom	Water body size [m]	Latitude	Longitude
L-40	ABA	Aug. 17. 17	Pond	0.5	Silt with detritus and mosses	8 x 13	72.38472	126.40861
L-41	ABA	Aug. 17. 17	Pond	0.2	Mosses and detritus	5 x 5	72.38694	126.39778
L-42	ABA	Aug. 17. 17	Pond	0.6	Sand with detritus	7 x 10	72.39333	126.37556
L-43	ABA	Aug. 17. 17	Lake	0.4	Sand	300 x 30	72.42111	126.39528
L-44	MS	Aug. 18. 17	Pond	0.4	Silt with detritus	8 x 10	72.39278	126.92944
L-45	MS	Aug. 18. 17	Lake	0.5	Silt with detritus	30 x 40	72.39056	126.92889
L-46	MS	Aug. 18. 17	Lake	0.5	Silt with detritus	70 x 90	72.38778	126.93917
L-47	MS	Aug. 18. 17	Pond	0.5	Mosses and detritus	3 x 3	72.39056	126.95694
L-48	MS	Aug. 18. 17	Lake	0.4	Sand with detritus	100 x 120	72.39778	126.96111
L-49	MS	Aug. 18. 17	Lake	0.5	Sand with detritus	50 x 40	72.39694	126.98472
L-50	SI	Aug. 24. 17	Lake	0.5	Sand and silt with detritus	100 x 150	72.375	126.51333
L-51	SI	Aug. 25. 17	Lake	0.5	Detritus with sand	300 x 100	72.3775	126.50278
L-52	SI	Aug. 25. 17	Stream	0.4	Silt with detritus	600 x 60	72.3875	126.48194

Table A.2-20: Hydrological characteristics and type of macrophytes at the sampling stations in the area of the Samoylov Island Research Station (August 2017)

Sample number	Temperature [°C]	Mineralization [ppm]	pH	Macrophyte
L-1	13.3	55.8	7.13	Carex
L-2	12.5	70.42	7.1	Carex
L-3	13.7	118	7.2	Mosses and Carex
L-4	11	115	8.4	Carex
L-5	14.2	33	7.2	Arctophyla
L-6	10.1	67	7	Carex; Arctophyla
L-7	9	60	8.1	Carex
L-8	8.4	54	8	Carex
L-9	6.6	55	7.8	Carex; Arctophyla
L-10	7	19	7.9	Carex
L-11	8	32	7.8	Carex; Arctophyla
L-12	9.2	30	7.6	Carex
L-13	8.5	87	7.6	Carex; Arctophyla
L-14	10.7	12	8.2	Carex; Arctophyla
L-15	15.7	11	7.6	Carex and mosses
L-16	12	15	7	Carex; Hippuris vulgaris
L-17	11	17	7.3	Carex
L-18	13.7	16	7	Carex
L-19	12.8	19	7.1	Carex
L-20	12.8	28	7.4	None
L-21	10.5	55	7.1	Carex
L-22	9.8	30	7.2	Carex
L-23	10.6	26	7.1	Carex
L-24	10.2	23	7.3	Carex
L-25	10.3	11	7.1	Carex; Hippuris vulgaris
L-26	13.5	31	7.1	Carex
L-27	19.5	14	7.3	Carex
L-28	20	12	6.3	Carex
L-29	12.2	37	7.6	Carex
L-30	12.6	26	7.3	Arctophyla
L-31	12.4	52	8	Arctophyla
L-32	17.2	22	7.9	Carex; Nostoc
L-33	13	12	7	Arctophyla
L-34	8.2	21	7.6	Carex
L-35	8.8	41	7.3	Carex
L-36	10	36	6.9	Arctophyla
L-37	9.7	39	7	Arctophyla
L-38	8.7	17	7.1	Carex
L-39	10.8	85	7.5	Arctophyla; Nostoc
L-40	10.6	26	8.8	Arctophyla; Carex; Nostoc
L-41	12.5	41	7.8	Caltha
L-42	12	36	7.6	None

Sample number	Temperature [°C]	Mineralization [ppm]	pH	Macrophyte
L-43	14.2	106	7.7	Arctophyla
L-44	11.7	19	7.8	Carex; Comarum
L-45	12.2	15	7.5	Arctophyla; Carex
L-46	12.8	13	7.6	Arctophyla (many)
L-47	13.2	21	7	Arctophyla; Utricularia; Comarum
L-48	11.3	27	6.9	Arctophyla
L-49	11.2	34	7.5	None
L-50	9.2	29	7.8	Carex
L-51	8.9	38	7	Carex
L-52	8.3	62	7.2	Arctophyla

Table A.2-21: Soil samples

Label	Coordinates	Analyses
Samoylov Island		
C1	N 72.36813; E 126.4764	Magnetic properties; granulometric composition; losses of inginition; total C; N; pH; bulk density; soil moisture
C2	N 72.36792; E 126.48035	
C3	N 72.36763; E 126.4826	
C4	N 72.3672; E 126.48579	
C6	N 72.3747; E 126.47826	
C12	N 72.36627; E 126.50077	
C15	N 72.366576; E 126.490719	
C17	N 72.365983; E 126.507187	
C20	N 72.37552; E 126.524123	
C23	N 72.384978; E 126.482722	
C26	N 72.388396; E 126.484621	
C27	N 72.387827; E 126.482658	
C30	N 72.383688;E 126.502508	
C31	N 72.38374; E 126.502937	
C32	N 72.373302; E 126.495935	
C33	N 72.374428; E 126.49829	
C34	N 72.375375; E 126.489797	
C35	N 72.375775; E 126.49041	
C36	N 72.37953; E 126.491	
C5	N 72.366; E 126.50352	Morphological description
C7	N 72.37289; E 126.47807	
C8	N 72.37384; E 126.49065	
C9	N 72.38153; E 126.48543	
C10	N 72.389443; E 126.485433	
C11	N 72.36827; E 126.48096	
C13	N 72.36615; E 126.50795	
C14	N 72.36678; E 126.50994	
C16	N 72.365999; E 126.503199	
C18	N 72.368497; E 126.515143	
C19	N 72.374718; E 126.525298	
C21	N 72.378283; E 126.518297	
C22	N 72.383785; E 126.502663	
C24	N 72.385142; E 126.483793	
C25	N 72.385962; E 126.483738	
C28	N 72.371085;E 126.484915	
C29	N 72.37236; E 126.491448	

Label	Coordinates	Analyses
Kurungnakh Island		
K1	N 72.324622; E 126.256312	Magnetic properties; granulometric composition; losses of inginition; total C; N; pH; bulk density; soil moisture
K2	N 72.324407; E 126.255597	
K3	N 72.324482; E 126.25575	
K4	N 72.32389; E 126.254558	
K5	N 72.323372; E 126.253515	
K6	N 72.289113; E 126.18857	
K7	N 72.289335; E 126.187965	
K8	N 72.289538; E 126.18724	
K9	N 72.289593; E 126.187255	
K10	N 72.289877; E 126.186745	
K11	N 72.290533; E 126.18508	
K12	N 72.291023; E 126.181357	
K13	N 72.291005; E 126.18061	
K14	N 72.29102; E 126.180227	
K15	N 72.2913; E 126.178358	

Table A.2-22: Samples of surface/pond/stream water, snow and ice in the Lena River Delta

Site	Day	Lat [°]	Lon [°]	Sample type	Planned analyses			
					DOC	Isotopes	cDOM	Cations /Anions
LD17_A_01	06.09. 2017	72.33432	126.2897	surface water	x	x	-	-
LD17_A_02	06.09. 2017	72.33352	126.27306	surface water	x	x	-	-
LD17_A_03	06.09. 2017	72.33361	126.27375	surface water	x	x	-	-
LD17_A_04	06.09. 2017	72.333	126.27374	surface water	x	x	-	-
LD17_A_05	06.09. 2017	72.33355	126.27481	surface water	x	x	-	-
LD17_A_06	06.09. 2017	72.33306	126.27914	surface water	x	x	-	-
LD17_A_07	06.09. 2017	72.33271	126.27974	surface water	x	x	-	-
LD17_A_08	06.09. 2017	72.33263	126.28436	surface water	x	x	-	-
LD17_A_09	07.09. 2017	72.37459	126.26376	surface water	x	x	-	-
LD17_A_10	07.09. 2017	72.37294	126.26057	surface water	x	x	-	-
LD17_A_11	07.09. 2017	72.37319	126.24567	surface water	x	x	-	-
LD17_A_12	07.09. 2017	72.37343	126.24543	surface water	x	x	-	-
LD17_A_13	07.09. 2017	72.37363	126.24317	snow	-	x	-	-
LD17_A_14	09.09. 2017	72.37423	126.23818	surface water	x	x	-	-
LD17_A_15	09.09. 2017	72.36745	126.25417	surface water	x	x	-	-
LD17_A_17	12.09. 2017	72.37079	126.48263	pond water	-	x	-	-
LD17_A_18	12.09. 2017	72.37008	126.48338	pond water	-	x	-	-
LD17_A_19	15.09. 2017	72.36601	126.256725	pond water	-	x	-	-
LD17_A_20	19.09. 2017	72.37083	126.48248	pond water	-	x	-	-

Site	Day	Lat [°]	Lon [°]	Sample type	Planned analyses			
					DOC	Isotopes	cDOM	Cations/Anions
LD17_A_21	19.09.2017	72.37079	126.48263	pond water	-	x	-	-
LD17_A_22	19.09.2017	72.37008	126.48338	pond water	-	x	-	-
LD17_A_23	19.09.2017	72.37008	126.48338	pond water	-	-	-	-
LD17_A_24	12.09.2017	72.37079	126.48263	pond water	-	-	-	-
LD17_A_25	12.09.2017	72.37008	126.48338	pond water	-	-	-	x
LD17_A_26	12.09.2017	72.37079	126.48263	pond water	-	-	-	x
LD17_A_27	15.09.2017	72.36601	126.256725	stream water	-	-	-	x
LD17_A_28	19.09.2017	72.370831	26.48248	pond water	-	-	-	x
LD17_A_29	19.09.2017	72.37079	126.48263	pond water	-	-	-	x
LD17_A_30	19.09.2017	72.37008	126.48338	pond water	-	-	-	x
LD17_A_31	12.09.2017	72.37079	126.48263	pond water	-	-	-	x
LD17_A_32	12.09.2017	72.37008	126.48338	pond water	-	-	-	x
LD17_A_33	15.09.2017	72.36601	126.256725	stream water	-	-	-	x
LD17_A_34	19.09.2017	72.37083	126.48248	pond water	-	-	-	x
LD17_A_35	19.09.2017	72.37079	126.48263	pond water	-	-	-	x
LD17_A_36	19.09.2017	72.37008	126.48338	pond water	-	-	-	x
LD17_A_37	12.09.2017	72.37079	126.48263	pond water	-	-	x	-
LD17_A_38	12.09.2017	72.37008	126.48338	pond water	-	-	x	-
LD17_A_39	19.09.2017	72.37083	126.48248	pond water	-	-	x	-

Site	Day	Lat [°]	Lon [°]	Sample type	Planned analyses			
					DOC	Isotopes	cDOM	Cations /Anions
LD17_A_40	19.09. 2017	72.37079	126.48263	pond water	-	-	x	-
LD17_A_41	19.09. 2017	72.37008	126.48338	pond water	-	-	x	-
LD17_A_42	19.09. 2017	72.37079	126.48263	pond water	x	-	-	-
LD17_A_43	12.09. 2017	72.37008	126.48338	pond water	x	-	-	-
LD17_A_44	15.09. 2017	72.36601	126.256725	stream water	x	-	-	-
LD17_A_45	19.09. 2017	72.37083	126.48248	pond water	x	-	-	-
LD17_A_46	19.09. 2017	72.37079	126.48263	pond water	x	-	-	-
LD17_A_47	19.09. 2017	72.37008	126.48338	pond water	x	-	-	-

Table A.2-23: Terrestrial laser scanning (TLS) data of the ground surface has been acquired for six plots on Samoylov and Kurungnakh. Respective datasets, coordinate locations and dates of acquisition are listed in the table below. Data is stored in the scanner own software format (RiSCAN).

Date	Location	Location [N-E]	Area [m]	Project name
08.09. 2017	Kurungnakh	72.36571 126.27275	15x20	ld2017_kurungnakh_20170908.RiSCAN
09.09. 2017	Kurungnakh	72.36785 126.25751	10x10	ld2017_kurungnakh_20170909.RiSCAN
12.09. 2017	Samoylov	72.36996 126.48093	20x20	ld1709_samoylov_soil_20170912.RiSCAN
14.09. 2017	Kurungnakh	72.36236 126.26695	20x25	ld2017_kurungnakh_20170914.RiSCAN
18.09. 2017	Kurungnakh	72.3661 126.25635	15x15	ld2017_kurungnakh_20170918.RiSCAN
19.09. 2017	Samoylov	72.37424 126.49529	15x15	ld2017_samoylov_20170919.RiSCAN

Table A.2-24: GNSS data was acquired using the station's system in differential mode. Surveys are listed by date with respective project names, locations and point counts. Projects are stored in the Leica GNSS system format for post-processing of the data using the logged base station and rover data.

Date	Location	App. Location [N-E]	Project name	Point count	Area of interest
6.9. 2017	Kurungnakh	72.33441 126.28727	TEV2017ANNE	118	Thermoerosional valley (TEV)
7.9. 2017	Kurungnakh	72.37349 126.2492	JAN2017TEV	12	TEV profile
8.9. 2017	Kurungnakh	72.36563 126.27332	JAN2017TEV	13	TLS positioning (s. above) and reference points of the ground surface
9.9. 2017	Kurungnakh	72.36742 126.2542	JAN2017TEV	116	TEV profile; TLS positioning (s. above) and reference points of the ground surface
10.9. 2017	Sardakh	72.57153 127.24147	LD2017SARDAKH	104	Borehole with subsurface temperature measurements
12.9. 2017	Samoylov	72.36985 126.48101	LD2017_SAMOYLOV1	68	TLS positioning (s. above) and reference points of the ground surface
13.9. 2017	Samoylov	72.37026 126.48299	LD2017_SAMOYLOV1	31	Cliff and old station building (monitoring); Polygon with subsidence monitoring setup
14.9. 2017	Kurungnakh	72.36237 126.26674	LD2017 KURUN JAN	51	TLS positioning (s. above) and reference points of the ground surface
15.9. 2017	Kurungnakh	72.36541 126.25116	LD2017 KURUN JAN	49	TEV profile; Positioning of subsidence monitoring stations
18.9. 2017	Kurungnakh	72.3661 126.25635	KUR20170918	16	TLS positioning (s. above) and reference points of the ground surface

Table A.2-25: List of samples

Point name	Coordinates	Height above the river [m]	Sample number	Analysis
Mammoth mountain1	62.948889N 134.000583E	12-85	3021/1	Spore and pollen/diatom
			3021/2	OSL dating
			3021/2	Spore and pollen/diatom
			3021/3	Spore and pollen/diatom
			3021/4	Spore and pollen/diatom
			3021/5	Spore and pollen/diatom
			3021/6	Spore and pollen/diatom
			3021/7	Spore and pollen/diatom
			3021/8	Spore and pollen/diatom
			3021/9	Spore and pollen/diatom
			3021/10	Spore and pollen/diatom
			3021/11	OSL dating
			3021/11	Spore and pollen/diatom
			3021/12	Radiocarbon dating
			3021/12	Spore and pollen/diatom
			3021/13	Spore and pollen/diatom
			3021/14	Spore and pollen/diatom
			3021/15	Spore and pollen/diatom
			3021/16	OSL dating
			3021/16	Spore and pollen/diatom
Mammoth mountain2	62.968889N 133.951028E	10-58	3022/1	Spore and pollen/diatom
			3022/2	Spore and pollen/diatom
			3022/3	OSL dating
			3022/3	Spore and pollen/diatom
			3022/4	Spore and pollen/diatom
			3022/5	Radiocarbon dating
			3022/5	Spore and pollen/diatom
			3022/6	OSL dating
			3022/6	Spore and pollen/diatom
Kullarata	63.136028N 133.694222E	32	3024/1	OSL dating
			3024/1	Spore and pollen/diatom
Ust'-Tatta	63.022944N 133.437389E	7	3025/1	Radiocarbon dating
Big Chabada Lake	61.992722N 129.36125E	160-165	3026/1	Spore and pollen/diatom
			3026/2	Spore and pollen/diatom
			3026/3	Spore and pollen/diatom
			3024/4	Spore and pollen/diatom
			3026/5	Spore and pollen/diatom
			3026/6	OSL dating
			3026/6	Spore and pollen/diatom
Mouth of the Vilyuy River	64.366667N 126.401556E	3	3015/2	Radiocarbon dating

Point name	Coordinates	Height above the river [m]	Sample number	Analysis
Ulahan-Kistyah island	64.791972N 125.384361E	1.5-7	3027/1	Radiocarbon dating
			3027/2	Spore and pollen/diatom
			3027/3	Spore and pollen/diatom
			3027/4	Radiocarbon dating
			3027/5	Radiocarbon dating
			3027/6	Spore and pollen/diatom
			3027/7	Spore and pollen/diatom
			3027/8	Spore and pollen/diatom
Tungus-Khaya	64.890389N 125.245139E	7.5-10	3028/1	Spore and pollen/diatom
			3028/2	Spore and pollen/diatom
			3028/3	OSL dating
			3028/4	Spore and pollen/diatom
Mouth of the Menkere River	68.032778N 123.327389E	33-35	3029/1	OSL dating
			3029/2	Spore and pollen/diatom
			3029/3	Spore and pollen/diatom
			3029/4	Spore and pollen/diatom
			3029/5	Spore and pollen/diatom
Duoldanga-Aryita island	68.101139N 123.328722E	1.5	3030/1	Radiocarbon dating
Mouth of the Natara River	68.401889N 123.924417E	30	3031/1	OSL dating
			3031/2	Spore and pollen/diatom

Table A.2-26: List of measurement points of water and suspended material sampling

Name pf point	Data	Latitude [N]	Longitude [E]	Note
Fish Lake	08.07.2016	72.37383°	126.4893°	Samoylov Island
North-Eastern Lake	09.07.2016	72.38425°	126.50045°	Samoylov Island
Shallow-2 Lake	09.07.2016	72.38216°	126.49548°	Samoylov Island
Northern Lake	10.07.2016	72.38455°	126.4863°	Samoylov Island
Shallow Lake	11.07.2016	72.36667°	126.5188°	Samoylov Island
Eastern Lake	11.07.2016	72.36667°	126.5111°	Samoylov Island
Molo Lake	12.07.2016	72.36667°	126.49731°	Samoylov Island
Kurungnakh-1 Lake	13.07.2016	72.38751°	126.48408°	Kurungnakh Island
Kurungnakh-2 Lake	16.07.2016	72.29488°	126.19963°	Kurungnakh Island
Banya Lake	26.07.2016	72.36851°	126.50096°	Samoylov Island
Southern Lake	26.07.2016	72.36911°	126.51255°	Samoylov Island
Trofim Main Bed	19.07.2016	72.42705°	126.6378°	Trofimovskaya Channel
Bykovskaya Channel	20.07.2016	72.4043°	126.78283°	Bykovskaya Channel
40 km downstream of Gusinka	25.07.2016	72.65385°	124.35846°	Olenekskaya Channel
Gusinka	26.07.2016	72.5058°	125.28621°	Olenekskaya Channel
Chay Tumus	26.07.2016	72.359°	125.67116°	Olenekskaya Channel
Oleneks Gauging Station	27.07.2016	72.29613°	126.09445°	Olenekskaya Channel
Tumatskaya	28.07.2016	72.41663°	126.46028°	Tumatskaya Channel

Table A.2-27: Calculation of water discharge and suspended sediment load (Bykovskaya Channel/Olenekskaya Channel, 40 km below Gusinka/and Olenekskaya Channel, old station Gusinka

Sounding on the vertical	distance from a standing start	depth on the vertical [m]	Average velocity on the vertical [m/sec]	Average turbidity on the vertical [g/l]	Average velocity between the verticals [m/sec]	Average turbidity between verticals [g/l]	Squer between verticals [m^2]	water discharge between verticals [m^3/sec]	Sediment discharge between verticals [kg/sec]
Level of right bank	0	-	-	-	-	-	-	-	-
Vertical 4	100	9	0.79	0.047	0.79	0.047	1.1	874	40.71
Vertical 3	210	3.6	1.53	0.05	1.15	0.048	1.339	1.553	74.62
Vertical 2	510	9.9	0.56	0.041	1.04	0.045	3.989	4.15	188.18
Vertical 1	960	13.6	0.89	0.051	0.72	0.046	1.097	790	36.25
Level of left bank	-	-	-	-	0.89	0.051	209	185	9.35
Q (m^3/s)	-	-	-	-	-	-	-	7.551	349.11

Level of left bank	0	-	-	-	-	-	-	-	-
Vertical 1	900	8	0.44	0.032	0.22	0.032	1.173	258	8.26
Vertical 2	550	5.9	0.36	0.02	0.4	0.026	1.249	500	12.99
Vertical 3	300	5	0.18	0.035	0.27	0.027	2.523	681	18.7
Level of right bank	1.14	-	-	-	0.09	0.035	1.234	111	3.88
Q (m^3/s)	-	-	-	-	-	-	-	1.55	44

Level of right bank	0	-	-	-	-	-	-	-	-
Vertical 2	100	8.9	0.94	0.021	0.94	0.021	731	685	14.38
Vertical 1	210	4	0.8	0.032	0.87	0.027	960	832	22.06
Vertical 3	290	8.9	0.49	0.049	0.65	0.04	455	294	11.82
Level of right bank	-	-	-	-	0.49	0.049	352	174	8.46
Q (m^3/s)	-	-	-	-	-	-	-	1.985	57

Table A.2-28: Comparing of measured water discharge and sediment load with meanings

Cross section	**Area of cross section [m^2]**	**Measured water discharge in July 2016 [m^3/s]**	**Average annual water discharge [m^3/s /(period)]**	**Measured flow of sediment in July 2016 [kg/s]**	**Average annual flow of water [kg/s /(period)]**
Olenekskaya Chanel (40km downstream of Gusinka)	6.179	1.55	2.886 /(1977-2004)	43.82	-
Olenekskaya Chanel (Gusinka)	2.497	1.985	2.886 /(1977-2004)	56.72	-
Olenekskaya Chanel (Chay-Tumus)	5.598	1.772	2.886 /(1977-2004)	43.35	-
Olenekskaya Chanel (Olenekskyi Gauging Station)	4.928	2.815	2.886 /(1977-2004)	42.7	38.64/(1977-2004)
Bykovskaya Channel	7.945	7.653	10.564/(1951-2004)	355.05	131.80/(1968-2004)
Trofimovskaya Channel	6.522	21.11	24.767 /(1977-2004)	622.29	387.70/(1977-2004)
Tumatskaya Channel	27.944	3.437	10.776/(1977-2004)	166.53	66.41/(1977-2004)

A.3 Supplementary material: Drilling Campaign on Bykovsky Peninsula - Spring 2017

Table A.3-1: Core description - PG 2410

Core	**PG 2410**
Location name	Uomullyakh-Kyuel Lagoon
Coordinates	N 71.730869°, E 129.274831°
Personnel	Schirrmeister/Strauss
Location unit	BYK17-1-1
Sampling date	08.- 11.04. 2017
snow thickness	na
ice thickness	120 cm
water depth	0 cm

Table A.3-2: Core description - PG 2411

Core	**PG 2411**
Location name	Ozero Pestsa (Polar Fox Lagoon)
Coordinates	N 71.74303°, E 129,3383°
Personnel	Schirrmeister/Strauss
Location unit	BYK17-3-1
Sampling date	14.-17.04.2017
snow thickness	15 cm
ice thickness	155 cm
water depth	330 cm

Table A.3-3: Core description - PG 2412

Core	**PG 2412**
Location name	Ozero Golzovoye (Golzovoye Lake)
Coordinates	N 71.74515°, E 129.30217°
Personnel	Schirrmeister/Strauss
Location unit	BYK17-2-1
Sampling date	18.-21.04.2017
snow thickness	na
ice thickness	195 cm
water depth	510 cm

Table A.3-4: Drilling log of the deep core PG 2410

PG-No	Length [cm]	Depth [cm]		Sample [cm]			Packing type	Sediment type	Colour	Cryo-structure	Visible OM	Additional observa-tions	core barrel [mm]
		from	to	No	from	to							
PG2410-01	6	120	126	na	na	na	whirlpak	layered	black to dark grey	frozen	not visible	salty taste, ice thickness 120 cm, frozen to the bottom, no liquid water	146
PG2410-02	59	126	185	na	na	na		clayish silt, sparse fine sand	black to dark grey			salty taste	146
PG2410-02				-1	126	130	whirlpak	clayish silt, sparse fine sand	black to dark grey	unfrozen		salty taste	146
PG2410-02				-2	130	145	whirlpak	clayish silt, sparse fine sand	black to dark grey	unfrozen		salty taste	146
PG2410-02				-3	145	150	whirlpak	clayish silt, sparse fine sand	black to dark grey	unfrozen		salty taste	146
PG2410-02				-4	150	185	core foil	clayish silt, sparse fine sand	black to dark grey	unfrozen to 170, deeper 170 frozen		salty taste	146
PG2410-03	100	185	285	na	na	na	core foil	to 250: layered, silty, sparsely fine sand	black to dark grey	frozen to 250, layered, 0.5 cm between layers, unfrozen 250 to 285		salty taste	146
core loss	20				185	205							

PG-No	Length [cm]	Depth [cm]		Sample [cm]			Packing type	Sediment type	Colour	Cryo-structure	Visible OM	Additional observa-tions	core barrel [mm]
		from	to	No	from	to							
PG2410-04	80	285	365	na	na	na		clayish silt, sparse fine sand	black to dark grey	unfrozen		salty taste	146
PG2410-04				-1	285	292	whirlpak	clayish silt, sparse fine sand	black to dark grey	unfrozen		salty taste	146
PG2410-04				-2	292	300	whirlpak	clayish silt, sparse fine sand	black to dark grey	unfrozen		salty taste	146
PG2410-04				-3	300	305	whirlpak	clayish silt, sparse fine sand	black to dark grey	unfrozen		salty taste	146
PG2410-04				-4	305	310	whirlpak	clayish silt, sparse fine sand	black to dark grey	unfrozen		salty taste	146
PG2410-04				-5	310	315	whirlpak	clayish silt, sparse fine sand	black to dark grey	unfrozen		salty taste	146
PG2410-04				-6	315	322	whirlpak	clayish silt, sparse fine sand	black to dark grey	unfrozen		salty taste	146
PG2410-04				-7	322	350	core foil	clayish silt, sparse fine sand	black to dark grey	unfrozen		salty taste	146
PG2410-04				-8	350	355	whirlpak	clayish silt, sparse fine sand	black to dark grey	unfrozen		salty taste	146
PG2410-04				-9	355	360	whirlpak	clayish silt, sparse fine sand	black to dark grey	unfrozen		salty taste	146
PG2410-04				-10	360	365	whirlpak	clayish silt, sparse fine sand	black to dark grey	unfrozen		salty taste	146

PG-No	Length [cm]	Depth [cm]		Sample [cm]			Packing type	Sediment type	Colour	Cryo-structure	Visible OM	Additional observa-tions	core barrel [mm]
		from	to	No	from	to							
PG2410-05	115	365	480				whirlpak	parallel structures, clayish silt	black to dark grey	unfrozen		salty taste, relatively dry	146
PG2410-05				-1	365	375	whirlpak	parallel structures, clayish silt	black to dark grey	unfrozen		salty taste, relatively dry	146
PG2410-05				-2	375	395	whirlpak	parallel structures, clayish silt	black to dark grey	unfrozen		salty taste, relatively dry	146
PG2410-05				-3	395	420	core foil	parallel structures, clayish silt	black to dark grey	unfrozen		salty taste, relatively dry	146
PG2410-05				-4	420	435	whirlpak	parallel structures, clayish silt	black to dark grey	unfrozen		salty taste, relatively dry	146
PG2410-05				-5	435	450	whirlpak	parallel structures, clayish silt	black to dark grey	unfrozen		salty taste, relatively dry	146
PG2410-05				-6	450	480	core foil	parallel structures, clayish silt	black to dark grey	unfrozen		salty taste, relatively dry	146
PG2410-06	175	480	655						blackish	unfrozen			146
PG2410-06				-1	480	500	whirlpak	silty fine sand	dark grey	unfrozen		salty taste	146
PG2410-06				-2	500	510	whirlpak	medium to coarse sand, rounded grains	greyish black	unfrozen	plant remains, rootlets	salty taste	146
PG2410-06				-3	510	515	whirlpak	medium sand, rounded grains	greyish black	unfrozen	plant remains	salty taste	146

PG-No	Length [cm]	Depth [cm]		Sample [cm]			Packing type	Sediment type	Colour	Cryo-structure	Visible OM	Additional observa-tions	core barrel [mm]
		from	to	No	from	to							
PG2410-06				-4	515	520	whirlpak	medium to coarse sand	greyish black darker than above	unfrozen	plant remains	salty taste	146
PG2410-06				-5	520	530	whirlpak	fine sand	darker than above	unfrozen	woody remains	salty taste	146
PG2410-06				-6	530	540	whirlpak	fine sand	darker than above	unfrozen	woody remains	salty taste	146
PG2410-06				-7	540	555	whirlpak	silty sand	darker than above	unfrozen	woody remains	salty taste	146
PG2410-06				-8	555	655	core foil	555-625: like above, 625 - 655 more silty clay	black to dark grey	unfrozen		salty taste	146
PG2410-07	100	655	755				core foil	clayish silt, at 755 sandy part	black to dark grey	unfrozen		salty taste	146
core loss	100				755	775						core loss due to pressure air 'explosion'	
PG2410-08	160	775	935					down to 825: clayish, 825 - 865: clayish fine sand, parallel structures, here more greyish		775 to 865 unfrozen, frozen (sandy with pebbles) from 865, except 870-875 (unfrozen)		salty taste	146
PG2410-08				-1	775	880	core foil		greyish black	unfrozen		salty taste	146

PG-No	Length [cm]	Depth [cm]		Sample [cm]			Packing type	Sediment type	Colour	Cryo-structure	Visible OM	Additional observa-tions	core barrel [mm]
		from	to	No	from	to							
PG2410-08				-2	880	890	whirlpak	sandy	greyish black	frozen		salty taste	146
PG2410-08				-3	890	900	whirlpak	clayish silt	greyish black	unfrozen		salty taste	146
PG2410-08				-4	900	920	whirlpak	sandy	greyish black	frozen		salty taste	146
PG2410-08				-5	920	935	whirlpak	sandy	greyish black	frozen		salty taste	146
PG2410-09	105	935	1040					935 - 960: silty fine sand, 940-945: coarse sand layer, 1015 - 1020: coarse sand with pebbles	greyish black	unfrozen		salty taste	127
PG2410-09				-1	935	1000	core foil		greyish black	unfrozen		salty taste	127
PG2410-09				-2	1000	1040	core foil		greyish black	unfrozen		salty taste	127
PG2410-10	160	1040	1200					silty fine sand, lower part with brighter layers/dots	dark to medium grey	unfrozen	dark layers and dots	salty taste	127
core loss	50				1040	1090						crash, wire rope drill, core crush	

PG-No	Length [cm]	Depth [cm]		Sample [cm]			Packing type	Sediment type	Colour	Cryo-structure	Visible OM	Additional observa-tions	core barrel [mm]
		from	to	No	from	to							
PG2410-10				-1	1090	1135	core foil	at 1165 a stone 2cm coarse sand, sparse pebbles	dark to medium grey	unfrozen		salty taste	127
PG2410-10				-2	1135	1200	core foil		dark to medium grey	unfrozen		salty taste	127
PG2410-11	100	1265	1365					silty down to 1315 silty, deeper 1315 sand with pebbles, at 1330 pebble 2,5 cm thick		unfrozen		salty taste, detail picture of silt/sand border at 1315	127
core loss	65				1200	1265						new wire rope without enough tension, core was stuck and crushed	
PG2410-11				-1	1265	1320	core foil			unfrozen		salty taste	127
PG2410-11				-2	1320	1365	core foil			unfrozen		salty taste	127
PG2410-12	165	1365	1530					sandy silt (fine and medium sand)	greenish grey				127
PG2410-12				-1	1365	1400	bag			unfrozen		not salty any more	127
PG2410-12				-2	1400	1485	bag		dark grey	unfrozen		Mixed sample, "Com-pressed air explosion"	127

PG-No	Length [cm]	Depth [cm]		Sample [cm]			Packing type	Sediment type	Colour	Cryo-structure	Visible OM	Additional observa-tions	core barrel [mm]
		from	to	No	from	to							
PG2410-12				-3	1485	1505	core foil	at 1505 fine to coarse sand, rounded pebbles up to 1 cm	brownish grey	unfrozen			127
PG2410-12				-4	1505	1520	whirlpak	from 1505 to 1530 medium to coarse sand	brownish grey	unfrozen			127
PG2410-12				-5	1520	1530	whirlpak	from 1505 to 1530 sandy silt (fine and medium sand)	brownish grey	unfrozen			127
PG2410-13	140	1530	1670					at 1605 sandy, below to 1650 finer material, below 1650 sandy again, 1605 to 1650 sandy layers	greenish grey	unfrozen		at 1575 layer with woody remains	127
PG2410-13				-1	1530	1580	whirlpak			unfrozen		slightly muddy	127
PG2410-13				-2	1550	1580	whirlpak	1650 - 1670, sandy with silty fine sand layered, 3-4 cm thick		unfrozen			127
PG2410-13				-3	1580	1670	core foil			unfrozen		see detailed picture	127

PG-No	Length [cm]	Depth [cm]		Sample [cm]			Packing type	Sediment type	Colour	Cryo-structure	Visible OM	Additional observa-tions	core barrel [mm]
		from	to	No	from	to							
PG2410-14	150	1670	1820					1670 - 1690: medium sand with silt layers, 1730 to 1765 sample like above, core better preserved: alternating layers sand and silt, river?				not to little bit salty	127
PG2410-14				-1	1670	1690	whirlpak			unfrozen			127
core loss	40				1690	1730							
PG2410-14				-2	1730	1745	whirlpak			unfrozen			127
PG2410-14				-3	1745	1760	whirlpak			unfrozen			127
PG2410-14				-4	1760	1765	whirlpak			unfrozen			127
PG2410-14				-5	1765	1775	whirlpak	medium sand with rounded grains		frozen		problems with extruding the core, this frozen part was expected to be there	127
PG2410-14				-6	1775	1785	whirlpak			unfrozen			127
PG2410-14				-7	1785	1792	whirlpak	silty alternating layers		unfrozen			127
PG2410-14				-8	1792	1805	whirlpak	no layers, medium sands		frozen			127
PG2410-14				-9	1805	1820	whirlpak	no layers, medium sands		unfrozen			127

PG-No	Length [cm]	Depth [cm]		Sample [cm]			Packing type	Sediment type	Colour	Cryo-structure	Visible OM	Additional observa-tions	core barrel [mm]
		from	to	No	from	to							
PG2410-15	190	1820	2010					1860-1900: medium sand and grey, 1900 - 1970: silty clayey, finely layered, dark grey layers 1-2 cm, bright sandy layers 5-10 mm, 1970 - 1982: medium sandy, grey-dark grey, 1992 - 2000: silty with sandy layers					127
core loss	45				1820	1865							
PG2410-15				-1	1865	1885	whirlpak	medium sand		unfrozen		not salty any more	127
PG2410-15				-2	1885	1900	whirlpak	medium sand		unfrozen			127
PG2410-15				-3	1910	1965		silt with clayish parts, finely		unfrozen			127
PG2410-15				-4	1965	2000				unfrozen			127
PG2410-15				-5	2000	2010		sandy layer, fine medium sand		frozen			127
PG2410-16	70	2010	2080					2010 - 2080: sandy parts frozen,		unfrozen			127
PG2410-16				-1	2010	2030	whirlpak			unfrozen			127

PG-No	Length [cm]	Depth [cm]		Sample [cm]			Packing type	Sediment type	Colour	Cryo-structure	Visible OM	Additional observa-tions	core barrel [mm]
		from	to	No	from	to							
PG2410-16				-2	2030	2033	whirlpak	medium sand		frozen			127
PG2410-16				-3	2033	2045	whirlpak	medium sandy horizon with plant remains	greyish	unfrozen	plant remains		127
PG2410-16				-4	2045	2053	whirlpak	medium sandy with coarse sand		unfrozen	plant remains		127
PG2410-16				-5	2053	2080	whirlpak	medium sandy with coarse sand		unfrozen	plant remains		127
PG2410-17	270	2080	2350										107
PG2410-17				-1	2080	2100	whirlpak	medium sand with coarse sand fragments		frozen			107
PG2410-17				-2	2100	2170	core foil	medium sand with coarse sand fragments, at 2070: up to 1 cm pebbles		frozen			107
PG2410-17				-3	2170	2270	core foil	2250-2275: layered sand (1 cm) and fine sand (2 mm)		frozen			107
PG2410-17				-4	2270	2290	whirlpak	2275-2335: fine sand with coarse sand inclusions		frozen			107
PG2410-17				-5	2290	2305	whirlpak	2275-2335: fine sand with coarse sand inclusions		frozen			107

PG-No	Length [cm]	Depth [cm]		Sample [cm]			Packing type	Sediment type	Colour	Cryo-structure	Visible OM	Additional observations	core barrel [mm]
		from	to	No	from	to							
PG2410-17				-6	2305	2315	whirlpak	2275-2335: fine sand with coarse sand inclusions		frozen			107
PG2410-17				-7	2315	2330	whirlpak	2275-2335: fine sand with coarse sand inclusions		frozen			107
PG2410-17				-8	2330	2335	whirlpak	2275-2335: fine sand with coarse sand inclusions		frozen			107
PG2410-17				-9	2335	2350	whirlpak	fine sand /coarse sand		frozen	organic remains at 2342	see detailed picture	107
PG2410-18	430	2350	2780					medium to coarse sand	grey to dark grey	unfrozen, but potentially thawed by 4 times drilling		was cored with different coring diameters	107
core loss	100				2350	2450							
PG2410-18				-1	2450	2470	whirlpak			unfrozen		due to drilling (?)	107
PG2410-18				-2	2470	2500	whirlpak			unfrozen		due to drilling (?)	107
PG2410-18				-3	2500	2525	whirlpak			unfrozen		due to drilling (?)	107
PG2410-18				-4	2525	2550	whirlpak			unfrozen		due to drilling (?)	107
PG2410-18				-5	2550	2590	core foil			unfrozen		due to drilling (?)	107
PG2410-18				-6	2590	2600	whirlpak			unfrozen		due to drilling (?)	107
PG2410-18				-7	2600	2620	whirlpak			unfrozen		due to drilling (?)	107
PG2410-18				-8	2620	2640	whirlpak			unfrozen		due to drilling (?)	107

PG-No	Length [cm]	Depth [cm]		Sample [cm]			Packing type	Sediment type	Colour	Cryo-structure	Visible OM	Additional observa-tions	core barrel [mm]
		from	to	No	from	to							
PG2410-18				-9	2640	2660	whirlpak			unfrozen (due to drilling?)		very crumbly	107
PG2410-18				-10	2660	2675	whirlpak			unfrozen (due to drilling?)		very crumbly	107
PG2410-18				-11	2675	2705	whirlpak			unfrozen (due to drilling?)		very crumbly	107
PG2410-18				-12	2705	2725	whirlpak			unfrozen		due to drilling?	107
PG2410-18				-13	2725	2750	core foil			unfrozen		due to drilling?	107
PG2410-18				-14	2750	2780	whirlpak			unfrozen		due to drilling?	107
PG2410-19	150	2780	2930					medium to coarse sand		unfrozen		2 times empty barrel, core 3rd time	107
PG2410-19				-1	2780	2790	whirlpak			unfrozen		due to drilling (?)	107
PG2410-19				-2	2790	2830	core foil			unfrozen		due to drilling (?)	107
PG2410-19				-3	2830	2840	whirlpak			unfrozen		due to drilling (?)	107
PG2410-19				-4	2840	2855	whirlpak			unfrozen		due to drilling (?)	107
PG2410-19				-5	2855	2875	whirlpak			unfrozen		due to drilling (?) drill material thawed	107
PG2410-19				-6	2875	2895	whirlpak			unfrozen			107

PG-No	Length [cm]	Depth [cm]		Sample [cm]			Packing type	Sediment type	Colour	Cryo-structure	Visible OM	Additional observa-tions	core barrel [mm]
		from	to	No	from	to							
PG2410-19				-7	2895	2915	whirlpak			unfrozen		drill material thawed	107
PG2410-19				-8	2915	2930	whirlpak			unfrozen		drill material thawed	107
PG2410-20	120	2930	3050					2930 -2965: fine to medium sand, medium grey, no visible organic, 2965-2980: Layer with black organic dots, some coarse sand grains, 2980-3005: fine medium, medium grey, 3005 - 3020: organic remains, 3020-3050: fine to medium sand		unfrozen		due to drilling (?)	107
PG2410-20				-1	2930	2950	whirlpak			unfrozen		due to drilling (?)	107
PG2410-20				-2	2950	3020	core foil			unfrozen		due to drilling (?) for Russian colleagues	107
					3020	3025				unfrozen			107
PG2410-20				-3	3025	3035	whirlpak			unfrozen		due to drilling (?)	107
PG2410-20				-4	3035	3050	whirlpak			unfrozen		due to drilling (?)	107

PG-No	Length [cm]	Depth [cm]		Sample [cm]			Packing type	Sediment type	Colour	Cryo-structure	Visible OM	Additional observa-tions	core barrel [mm]
		from	to	No	from	to							
PG2410-21	100	3050	3150					medium sand, with parts of coarse sand		unfrozen	at 3095 and 3135: plant remains	a little bit salty again	107
core loss	25				3050	3075						25 cm core loss, groundwa-ter channel (?), lot of water above the core	
PG2410-21				0	3050	3075	whirlpak	water sample				puddle around the borehole	107
PG2410-21				-1	3075	3090	whirlpak			unfrozen		due to drilling (?)	107
Russian colleagues					3090	3010		sampled by Russian colleagues				due to drilling (?)	
PG2410-21				-2	3100	3150	core foil			unfrozen (due to drilling?)		due to drilling (?)	107
PG2410-22	30	3150	3180					medium sand with coarse and	medium grey	unfrozen	no organic visible	again water above core, infiltration by layer above (?)	107
PG2410-22				0	3150		whirlpak	water sample				puddle around the borehole	107
PG2410-22				-1	3150	3157	whirlpak					very wet	107
PG2410-22				-2	3157	3164	whirlpak					very wet	107
PG2410-22				-3	3164	3170	whirlpak						107
PG2410-22				-4	3170	3180	whirlpak						107

PG-No	Length [cm]	Depth [cm]		Sample [cm]			Packing type	Sediment type	Colour	Cryo-structure	Visible OM	Additional observa-tions	core barrel [mm]
		from	to	No	from	to							
PG2410-23	150	3180	3330				whirlpak	3185-3270: unfrozen, fine to medium sand with some pebbles (0.5 - 2 cm), 3240 - 3345: layer with pebbles, 3270 - 3330: frozen, coarse sand with some rounded pebbles.	3180 - 3185: frozen, including a big stone (4 cm), 3185-3270: unfrozen			50 cm of drilling mud above were removed, probably crumbling material fall from above	89
PG2410-23				-1	3180	3190	whirlpak			frozen			89
PG2410-23				-2	3190	3205	whirlpak			unfrozen			89
PG2410-23				-3	3205	3220	whirlpak			unfrozen			89
PG2410-23				-4	3220	3230	whirlpak			unfrozen			89
PG2410-23				-5	3230	3245	whirlpak	with a bigger stone		unfrozen			89
PG2410-23				-6	3245	3270	whirlpak			unfrozen			89
for Russian colleagues					3270	3280							
PG2410-23				-7	3280	3330	core foil			frozen			89
PG2410-24	20	3330	3350							unfrozen		because of drilling (?)	73
PG2410-24				0	3330		whirlpak	water sample				directly from the core barrel	73
PG2410-24				-1	3330	3340	packed like a core			unfrozen		because of drilling (?)	73
PG2410-24				-2	3340	3350	whirlpak			unfrozen		packed with the final drilling crown. Very dry due to long drilling	73

Table A.3-5: Drilling log of the deep core PG 2411

PG-No	Length [cm]	Depth [cm]		Sample [cm]			Packing type	Sediment type	Colour	Cryo-structure	Visible OM	Additional observa-tions	core barrel [mm]
		from	to	No	from	to							
PG2411-01	300	330	630				core foil	330-355: fine sands silt, dark grey, plant remains, salty, 355-365: silt fine sand, dark grey, salty, 365-400: clayey silty material, dark to medium grey, not salty, 400-440: silty, slightly layered, dark grey, shell remains, not salty		unfrozen		all cohesive material, core of 300 cm compacted to 110 cm–¿ de-compaction in lab with adjusting depth!!! 403-409: sample Russian colleague	146
PG2411-02	360	630	990										107
core loss	90				630	720						core drilled two times and dropped: destruction of the upper part?	
PG2411-02				-1	720	750	whirlpak	silty material	black, dark grey	unfrozen	some organic remain	salty taste again	
PG2411-02				-2	750	780	whirlpak	like above, fine grains	black, dark grey	unfrozen			

PG-No	Length [cm]	Depth [cm]		Sample [cm]			Packing type	Sediment type	Colour	Cryo-structure	Visible OM	Additional observa-tions	core barrel [mm]
		from	to	No	from	to							
PG2411-02				-3	780	990	core foil	785 -795: like above, but border to more sandy sediments, 795 - 870: sandy silty (medium sand)		795 - 870 : half frozen, 870 - 990: frozen, ice lenses		880-890: sample Russian colleagues	
PG2411-03	220	990	1210									drilled in the second try, lost in the 1st try, detailed picture of the pebble horizon (portrait orientation picture)	
core loss	130				990	1120						destroyed while drilling the same core the second time	
PG2411-03				-1	1120	1135	whirlpak	medium sand	dark grey	unfrozen		not salty any more	
PG2411-03				-2	1135	1155	whirlpak	medium sand with pebbles (up to 2 cm, rounded)	dark grey	unfrozen		not salty any more	
PG2411-03				-3	1155	1195	core foil	medium to coarse sand		half frozen to unfrozen		not salty any more, unfrozen due to drilling (?)	
PG2411-03				-4	1195	1210	whirlpak	medium to coarse sand		half frozen to unfrozen		not salty any more, unfrozen due to drilling (?)	

PG-No	Length [cm]	Depth [cm]		Sample [cm]			Packing type	Sediment type	Colour	Cryo-structure	Visible OM	Additional observa-tions	core barrel [mm]
		from	to	No	from	to							
PG2411-04	400	121(	1610					fine sand		unfrozen	1460-1500: organic remains visible, 1500-1610: fewer, but still visible	not salty, core lost once, drilled in the second try, water above the core	
core loss	250				1210	1460						core dropped in the first try and was destroyed in the second try	
PG2411-04				-1	1460	1535	core foil						
PG2411-04				-2	1535	1610	core foil						
PG2411-05	50	1610	1660										
core loss	20				1610	1630							
PG2411-05				0	1610		whirlpak					water above core, directly taken from the barrel	
PG2411-05				-1	1630	1650	whirlpak	fine sand		unfrozen			
PG2411-05				-2	1650	1660	whirlpak	medium sand, equal-grained		unfrozen		very dry due to drilling	
PG2411-06	195	166(	1855									detail picture woody horizon	
core loss	130				1660	1790							

PG-No	Length [cm]	Depth [cm]		Sample [cm]			Packing type	Sediment type	Colour	Cryo-structure	Visible OM	Additional observations	core barrel [mm]
		from	to	No	from	to							
PG2411-06				-1	1790	1800	whirlpak	fine sand	medium grey	unfrozen	no organic		
PG2411-06				-2	1800	1810	whirlpak	fine sand	medium grey	unfrozen	no organic		
PG2411-06				-3	1810	1815	whirlpak			unfrozen	woody horizon		
PG2411-06				-4	1815	1855	core foil	medium to coarse sand with pebbles, layered	medium grey	frozen		detail picture of pebbles	
PG2411-07	130	1855	1985										
core loss	85				1855	1940							
PG2411-07				-1	¿1855		whirlpak	wood samples, was above the core		unfrozen		wood samples, was above the core	
PG2411-07				-2	1940	1950	whirlpak	medium to coarse sand		unfrozen			
PG2411-07				-3	1950	1965	whirlpak	medium to coarse sand, visible transparent quartz grains		unfrozen			
PG2411-07				-4	1965	1985	whirlpak	medium to coarse sand, visible transparent quartz grains		unfrozen			
PG2411-08	65	198¦	2050										
core loss	45				1985	2030						core loss due to water above the core, washed away	

PG-No	Length [cm]	Depth [cm]		Sample [cm]			Packing type	Sediment type	Colour	Cryo-structure	Visible OM	Additional observa-tions	core barrel [mm]
		from	to	No	from	to							
PG2411-08				-1	2030	2040	whirlpak	fine sand, layered with medium sand	greenish dark grey	unfrozen		not salty	
PG2411-08				-2	2040	2050	whirlpak, packed like a core?	medium sand with pebbles	dark grey	frozen		not salty	
PG2411-09	70	2050	2120									depth on the pictures do not fit to the depth! New depth with paper noted.	
PG2411-09				-1	2050	2055	whirlpak	fine to medium sand, some fine pebbles	medium grey	unfrozen		not salty	
PG2411-09				-2	2055	2065	whirlpak	medium to coarse sand	medium grey	unfrozen		not salty	
PG2411-09				-3	2065	2085	whirlpak	medium to coarse sand, some fine pebbles (5-10 mm)	medium grey	unfrozen		not salty	
PG2411-09				-4	2085	2095	whirlpak	medium to coarse sand, pebbles up to 3 cm		unfrozen		not salty	
PG2411-09				-5	2095	2105	whirlpak	fine to medium sand, some fine pebbles (1 cm, rounded), dried through drilling process		unfrozen		not salty, core piece intact	

PG-No	Length [cm]	Depth [cm]		Sample [cm]			Packing type	Sediment type	Colour	Cryo-structure	Visible OM	Additional observations	core barrel [mm]
		from	to	No	from	to							
PG2411-09				-6	2105	2115	whirlpak	medium to coarse sand		unfrozen	wooden piece	not salty, core piece intact	
PG2411-09				-7	2115	2120	whirlpak	fine to middle sand, no pebbles		unfrozen (thawed due to drilling?		not salty	
PG2411-10	145	2120	2265					2195-2245: fine to medium sand, layered, crumbly					
core loss	75				2120	2195						water above core, which washed away the upper part during extrusion	
PG2411-10				-1	2195	2215	whirlpak	fine to medium sand, layered, crumbly		unfrozen			
PG2411-10				-2	2215	2235	whirlpak	fine to medium sand, layered, crumbly		unfrozen			
PG2411-10				-3	2235	2245	whirlpak	fine to medium sand, layered, crumbly		unfrozen	piece of wood at 2243		
PG2411-10				-4	2245	2265	bag packed like a core	fine to medium sand, layered, one piece of core		unfrozen			

PG-No	Length [cm]	Depth [cm]		Sample [cm]			Packing type	Sediment type	Colour	Cryo-structure	Visible OM	Additional observa-tions	core barrel [mm]
		from	to	No	from	to							
PG2411-11	25	2265	2290				core foil	2265-2280: medium to coarse sand, layered like below, with pebbles, medium grey, 2280-2290: layered, medium grey and dark grey layers 1 cm, medium sand		unfrozen		no water above core, not salty, deepening casing and cleaning casing with bigger core diameter before	
PG2411-12	80	2290	2370							unfrozen		core dropped at the first try	
PG2411-12				-1	2290	2370	core foil	medium to coarse sand	medium grey	unfrozen			
PG2411-12				-2	2370	2440	core foil	medium to coarse sand	medium grey	unfrozen			
PG2411-12				-3	2440	2500	core foil	medium to coarse sand, stone up to 4 cm at 2460 to 2470	medium grey	unfrozen			
PG2411-13	140	2500	2640					2500-2570: medium to coarse sand, grey, wet, with some pebbles, 2570-2630: medium to coarse sand, gravely, at 2630 big rounded pebble, 2630-2640: coarse sand to fine pebbles, medium grey		unfrozen		50 drilling mud removed before taking pictures	

PG-No	Length [cm]	Depth [cm]		Sample [cm]			Packing type	Sediment type	Colour	Cryo-structure	Visible OM	Additional observa-tions	core barrel [mm]
		from	to	No	from	to							
PG2411-13				-1	2500	2520	whirlpak			unfrozen			
PG2411-13				-2	2520	2540	whirlpak			unfrozen			
PG2411-13				-3	2540	2560	whirlpak			unfrozen			
PG2411-13				-4	2560	2580	whirlpak			unfrozen			
PG2411-13				-5	2580	2600	whirlpak			unfrozen			
PG2411-13				-6	2600	2620	whirlpak			unfrozen			
PG2411-13				-7	2620	2635	whirlpak			unfrozen			
PG2411-13				-8	2635	2640	whirlpak			unfrozen			
PG2411-14	110	2640	2750					2640-2715: medium to coarse sand, medium to dark grey, 2715-2750: layered fine sand		unfrozen	organic remains in a layer at 2735 (de-tailed photo-graph)	not salty	
PG2411-14				-1	2640	2660	whirlpak			unfrozen			
PG2411-14				-2	2660	2680	whirlpak			unfrozen			
PG2411-14				-3	2680	2750	core foil			unfrozen			
PG2411-15	90	2750	2840					medium to coarse sand, some rounded pebbles, layered fine to medium sand, layered	dark grey	unfrozen		drilling mud removed above core	
PG2411-15				-1	2750	2785	core foil		medium and dark grey	unfrozen			
PG2411-15				-2	2785	2840	core foil			unfrozen			
PG2411-16	70	2840	2910		2840	2910	core foil	medium to coarse sand, crumbly, not-cohesive, river deposits	dark grey	unfrozen		core dropped once, than continued with smaller diameter, packed in core foil, but not really a core	

PG-No	Length [cm]	Depth [cm]		Sample [cm]			Packing type	Sediment type	Colour	Cryo-structure	Visible OM	Additional observa-tions	core barrel [mm]
		from	to	No	from	to							
PG2411-17	195	2910	3105					2985- 3015: coarse sand with pebbles, very wet, 3015-3055: fine to medium sand, 3055-3070: medium to coarse sand (2-3 cm) rounded, 3070-3105: medium to fine sand		unfrozen		16.4.17 drilling the hole day with no core material, just inflowing water and sand: drilling mud	
core loss					2910	2985						everything unfrozen, put with spade into the sampling half-pipe	
PG2411-17				-1	2985	3030	core foil			unfrozen			
PG2411-17				-2	3030	3105	core foil			unfrozen			
PG2411-18		3105	3150				core foil	medium to coarse sand with pebbles (2 cm), rounded, lower part from drilling crown, dried				no core, but packed in core foil	
core loss	25				2910	2935							
PG2411-17(2)	140	2935	3075										
PG2411-17(2)				-1	2935	3005	core foil			2970-2985: frozen			
PG2411-17(2)				-2	3005	3075	core foil			unfrozen			

Table A.3-6: Drilling log of the deep core PG 2412

PG-No	Length [cm]	Depth [cm]		Sample [cm]			Packing type	Sediment type	Colour	Cryo-structure	Visible OM	Additional observa-tions	core barrel [mm]
		from	to	No	from	to							
PG2412-1	400	510	910					510-550: silty material, fine sand, dark grey, plant remains, shells, 550-610: silty fine sand, partly clayish, shells, 610-675: fine sand to silt, shells, drier than above, 675-725: fine sand to silt, shells, higher density, 725-755: fine to medium sand, no shells	dark grey	unfrozen		4 m core compacted to 2.4 m, freshwater again breaks out at 550-552, 724-725,608-610 cm depth, 754-755 samples Russian colleagues	
PG2412-1				-1	510	550	core foil	silty material, fine sand, dark grey, plant remains, shells	dark grey	unfrozen			
PG2412-1				-2	550	610	core foil	silty fine sand, partly clayish, shells	dark grey	unfrozen			
PG2412-1				-3	610	675	core foil	fine sand to silt, shells, drier than above	dark grey	unfrozen			
PG2412-1				-4	675	755	core foil	fine sand to silt, shells, higher density, 725-755: fine to medium sand, no shells	dark grey	unfrozen		at 730 a bit of core loss	

PG-No	Length [cm]	Depth [cm]		Sample [cm]			Packing type	Sediment type	Colour	Cryo-structure	Visible OM	Additional observa-tions	core barrel [mm]
		from	to	No	from	to							
PG2412-2	195	910	1105					910-930: silty fine sand, very wet, sparse plant remains, 930-970: medium to coarse sand, 970-980: fine to medium sand, 980-1040: fine to medium sand, dark grey, 1040-1105: fine sand silty , silt layers 1-2 mm thick, 1060: sandy layer		unfrozen		1100-1105, 980-982, 1039-1040 samples Russian colleagues	
PG2412-2				-1	910	930	bag	silty fine sand, very wet, sparse plant remains,		unfrozen			
PG2412-2				-2	930	950	bag	medium to coarse sand		unfrozen			
PG2412-2				-3	950	970	bag	medium to coarse sand		unfrozen			
PG2412-2				-4	970	980	bag	fine to medium sand		unfrozen			
PG2412-2				-5	980	1040	core foil	fine to medium sand	dark grey	unfrozen			
PG2412-2				-6	1040	1100	core foil	fine sand silty , silt layers 1-2 mm thick, 1060: sandy layer		unfrozen			
PG2412-3	135	1105	1240					silty fine sand, some pebbles, 2-4 mm, sparse plant remains, Taberite?	dark grey	unfrozen		methane comes out of the hole, good core quality	
PG2412-3				-1	1105	1180	core foil			unfrozen			

PG-No	Length [cm]	Depth [cm]		Sample [cm]			Packing type	Sediment type	Colour	Cryo-structure	Visible OM	Additional observa-tions	core barrel [mm]
		from	to	No	from	to							
PG2412-3				-2	1180	1240	core foil			unfrozen		1182-1184, 1182-1184 samples Russian colleagues	
PG2412-4	350	1240	1590					1360-1430: medium sand, very crumbly, pushed out of the barrel, maybe not stratigraphical correct, 1430-1470: fine sand, equal-grained, 1470-1590: silty fine sand, at 1575 pebbles (10-15-20 mm)		unfrozen		sample Russian colleague: 1585-1590	
PG2412-4					1240	1360	whirlpak	medium sand, very crumbly		unfrozen			
PG2412-4				-1	1360	1380	whirlpak	medium sand, very crumbly		unfrozen			
PG2412-4				-2	1380	1400	whirlpak	medium sand, very crumbly		unfrozen			
PG2412-4				-3	1400	1430	whirlpak	medium sand, very crumbly		unfrozen			
PG2412-4				-4	1430	1460	whirlpak	fine sand, equal-grained		unfrozen			
PG2412-4				-5	1460	1480	whirlpak	silty fine sand		unfrozen			
PG2412-4				-6	1480	1590	core	silty fine sand, at 1575 pebbles (10-15-20 mm)		unfrozen			
PG2412-5	165	1590	1755					1590-1605: silty, 1605-1740: like above, fine sand layer at 1715, 1740-1755: more fine sand	medium to dark grey	unfrozen	no plant remains visible,	samples Russian colleagues: 1605-1608, 1672-1675	

PG-No	Length [cm]	Depth [cm]		Sample [cm]			Packing type	Sediment type	Colour	Cryo-structure	Visible OM	Additional observations	core barrel [mm]
		from	to	No	from	to							
PG2412-5				-1	1590	1670	core			unfrozen			
PG2412-5				-2	1670	1755	core			unfrozen			
PG2412-6	165	1755	1920					1755-1770: fine sand, 1770-1785: silty fine sand, 1785-1805: fine sand, 1805-1840 silt with fine sand, 1840-1920: fine sand, layered	fine sand, medium grey, fine sand, dark grey	unfrozen	woody remains at 1905 (detailed picture)	samples Russian colleagues: 1825-1830, 1915-1920	
PG2412-6				-1	1755	1825	core foil			unfrozen		samples Russian colleagues	
PG2412-6				-2	1825	1830				unfrozen			
PG2412-6				-2	1830	1920	core foil			unfrozen		samples of Russian colleagues	
PG2412-6				-2	1915	1920				unfrozen			
PG2412-7	130	1920	2050					1920-1950: fine sand, 1950-1985: silty fine sand, 1985-2035: fine sand, 2035-2050: fine sand with big woody remains	medium grey, dark grey	unfrozen, evaporated (?)	plant remains at 2020, 2035-2050: big woody remains	big woody remains (detailed picture)	
PG2412-7				-1	1920	1975	core foil	fine sand	medium grey	unfrozen, evaporated (?)			
					1975	1980		silty fine sand	dark grey	unfrozen, evaporated (?)		samples Russian colleagues	
PG2412-7				-2	1980	2035	core foil	fine sand		unfrozen, evaporated (?)			

PG-No	Length [cm]	Depth [cm]		Sample [cm]			Packing type	Sediment type	Colour	Cryo-structure	Visible OM	Additional observa-tions	core barrel [mm]
		from	to	No	from	to							
PG2412-7				-3	2035	2050	whirlpak	fine sand with big woody remains		unfrozen, evaporated (?)	big woody remain		
PG2412-8	325	2050	2375					fine sand	medium grey	unfrozen			
core loss	85				2050	2135						core lost 2 times, retrieved 3rd try, core loss of the upper part due to repeated drilling	
PG2412-8				-1	2135	2150	whirlpak			unfrozen			
PG2412-8				-2	2150	2215	core foil			unfrozen		samples Russian colleagues	
PG2412-8					2215	2220				unfrozen			
PG2412-8				-3	2220	2300	core foil			unfrozen		samples Russian colleagues	
PG2412-8				-4	2300	2365	core foil			unfrozen			
					2365	2375							
PG2412-9	265	2375	2640					2375-2510: fine sand, not layered, 2510-2570: becomes coarser, medium sand with coarse sand, partly layered, 2570-2640: fine sand, layered	medium grey	unfrozen			

PG-No	Length [cm]	Depth [cm]		Sample [cm]			Packing type	Sediment type	Colour	Cryo-structure	Visible OM	Additional observa-tions	core barrel [mm]
		from	to	No	from	to							
PG2412-9				-1	2375	2443	core foil	fine sand, not layered	medium grey	unfrozen		packed in core foil, but from spate into the subsam-pling pipe, not sure if it is strati-graphically correct samples Russian colleagues	
					2443	2445		fine sand, not layered	medium grey			packed in core foil, but from spate into the subsam-pling pipe, not sure if it is strati-graphically correct samples Russian colleagues	
PG2412-9				-2	2445	2510	core foil	fine sand, not layered	medium grey	unfrozen			
PG2412-9				-3	2510	2565	core foil	medium sand with coarse sand, partly layered		unfrozen			
					2565	2570		medium sand with coarse sand, partly layered				samples Russian colleagues	
PG2412-9				-4	2570	2635	core foil	fine sand, layered	medium grey	unfrozen			
					2635	2640		fine sand, layered		unfrozen		samples Russian colleagues	

PG-No	Length [cm]	Depth [cm]		Sample [cm]			Packing type	Sediment type	Colour	Cryo-structure	Visible OM	Additional observa-tions	core barrel [mm]
		from	to	No	from	to							
PG2412-10	265	2650	2915					2640-2770: fine sand, 2780-2790: layered, fine and medium sand layers, 2790-2830: fine sand, 2830-2835: layer of pebbles (detail picture), 2835-2850: medium to fine sand, with coarse sand, 2850-2920: fine to medium sand,	medium grey	unfrozen	piece of wood at 2670 (detail picture), at 2715, 2875 and 2910: woody re-mains, 2985: woody horizon (detail picture)	50 cm of mud above core, removed	
PG2412-10				-1	2640	2700	core foil	fine sand	medium grey	unfrozen			
PG2412-10				-2	2700	2780	core foil	fine sand	medium grey	unfrozen			
PG2412-10				-3	2780	2845	core foil	layered, fine and medium sand layers	medium grey	unfrozen			
PG2412-10								layered, fine and medium sand layers	medium grey	unfrozen		samples Russian colleagues	
PG2412-10				-4	2850	2913	core foil	medium to fine sand, with coarse sand	medium grey	unfrozen			
					2913	2915		fine to medium sand, medium grey	medium grey	unfrozen		samples Russian colleagues	

PG-No	Length [cm]	Depth [cm]		Sample [cm]			Packing type	Sediment type	Colour	Cryo-structure	Visible OM	Additional observa-tions	core barrel [mm]
		from	to	No	from	to							
PG2412-11	170	2915	3085					2915-2975: fine sand, silty layer at 2940-2942, 2975-3022: fine sand, medium grey, 3022-3025: pebble layer (detail picture), 3015-3065: fine sand with medium sand, at 3047 again with pebbles, 3065-3085: layered (detail picture) silty and medium sand layers, at 3080 layer with coarse sand and pebbles	medium grey,	unfrozen		water come out of the casing when uplifting barrel, approx. 50 cm drilling mud removed above core	
PG2412-11				-1	2915	2974	core foil	fine sand, silty layer at 2940-2942	medium grey	unfrozen		samples Russian colleagues packed into core foil, but from spate into the sub-sampling pipe, not 100% sure if it is strati-graphically correct	
					2974	2975		fine sand, silty layer at 2940-2942	medium grey	unfrozen			
PG2412-11				-2	2975	3025	core foil	fine sand, medium grey		unfrozen			
PG2412-11				-3	3025	3084	core foil	fine sand with medium sand		unfrozen			

PG-No	Length [cm]	Depth [cm]		Sample [cm]			Packing type	Sediment type	Colour	Cryo-structure	Visible OM	Additional observations	core barrel [mm]
		from	to	No	from	to							
					3084	3085		fine sand with medium sand		unfrozen		samples Russian colleagues	
					3085	3087		fine sand with medium sand				samples Russian colleagues	
PG2412-12	85	3085	3170				core foil	3085-3110: coarse sand with medium sand, 3110-3115: medium sand, 3115-3170: fine sand, with coarse sand at 3160		unfrozen	3120-3130 with woody remains		
PG2412-13	125	3170	3295					3170-3205: fine sand, very wet, groundwater pathway (?), 3205-3295: fine sand		unfrozen		90 cm of "core-shaped" material removed, drilling mud?	
PG2412-13				-1	3170	3185	whirlpak			unfrozen			
PG2412-13				-2	3185	3205	whirlpak			unfrozen			
PG2412-13				-3	3205	3220	whirlpak			unfrozen			
PG2412-13				-4	3220	3235	whirlpak			unfrozen			
					3235	3237						samples Russian colleagues	
PG2412-13				-5	3237	3295	core foil			unfrozen			
PG2412-14	35	3260	3295					silty fine sand, dense	medium grey	unfrozen		actually over the drill core, but taken, since not sure whether the piece stuck on the previous day, looks like core	

PG-No	Length [cm]	Depth [cm]		Sample [cm]			Packing type	Sediment type	Colour	Cryo-structure	Visible OM	Additional observa-tions	core barrel [mm]
		from	to	No	from	to							
PG2412-14	130	3295	3425					3295-3300: silty fine sand, dense, 3300-3385: fine sand, with pebbles (2x2 cm), 3385-3395: layers (1-3 cm), silty sand and fine sand layers, 3395-3422: woody horizon, 3422-3425: sand	medium grey, dark grey	unfrozen	3395-3422: woody horizon, big wood remains		
PG2412-14				-1	3260	3327	core foil	fine sand, with pebbles (2x2 cm		unfrozen		samples Russian colleagues	
					3327	3330		layers (1-3 cm), silty sand and fine sand layers	dark grey	unfrozen	big wood remains		
PG2412-14				-2	3330	3395	core foil						
PG2412-14				-3	3395	3405	whirlpak	woody horizon		unfrozen	big wood remains		
PG2412-14				-4	3405	3415	whirlpak	woody horizon		unfrozen	big wood remains		
PG2412-14				-5	3415	3425	whirlpak	woody horizon		unfrozen	big wood remains		
PG2412-15	85	3425	3510					3450-3505: silty fine sand with big plant remains, 3505-3510: medium sand	bright to medium grey	unfrozen	3450-3505: big plant remains	approx. 1 m core-like drilling mud above the core, removed, still to much core, segment is to long, pictures do not fit to scale	

PG-No	Length [cm]	Depth [cm]		Sample [cm]			Packing type	Sediment type	Colour	Cryo-structure	Visible OM	Additional observa-tions	core barrel [mm]
		from	to	No	from	to							
PG2412-15				-1	3425	3430	whirlpak	fine sand	dark to medium grey	(half-)frozen	plant remains visible		
PG2412-15				-2	3430	3435	whirlpak	fine sand	dark to medium grey	(half-)frozen	plant remains visible		
PG2412-15				-3	3435	3445	whirlpak	fine sand	dark to medium grey	(half-)frozen	plant remains visible		
PG2412-15				-4	3445	3450	whirlpak	fine sand	dark to medium grey	(half-)frozen	plant remains visible		
PG2412-15				-5	3450	3460	whirlpak	medium sand	bright to medium grey	frozen			
PG2412-15				-6	3460	3470	whirlpak	medium sand	bright to medium grey	frozen			
PG2412-15				-7	3470	3480	whirlpak	medium sand	bright to medium grey	frozen			
PG2412-15				-8	3480	3510	core	medium sand	bright to medium grey	frozen			
PG2412-15(2)	85	3425	3510					3425-3455: un layered fine sand, layered fine sand, alternate bedding, sparse plant remains, 3490-3510: fine sand with big plant remains	medium to dark grey	frozen			
PG2412-15(2)				-1	3425	3455	core			frozen		mysterious 2nd core from the same depth like above, but frozen and core, not mud!	

PG-No	Length [cm]	Depth [cm]		Sample [cm]			Packing type	Sediment type	Colour	Cryo-structure	Visible OM	Additional observa-tions	core barrel [mm]
		from	to	No	from	to							
PG2412-15(2)				-2	3455	3510	whirlpak			frozen			
PG2412-16	155	3510	3665					3550-3570: fine sand with a lot of woody remains, 3570-3605: fine sand , no plant remains, 3605-3665: fine sand, fluvial (?)	medium grey	frozen	3550-3570: a lot of woody remain		
core loss	40				3510	3550						part of the core was not able to extrude from the barrel: was invasively extruded one day later and was composed of the woody horizon visible in the cores above	
PG2412-16				-1	3550	3595				frozen		samples Russian colleagues	
					3595	3605							
PG2412-16				-2	3605	3625				frozen			
PG2412-16				-3	3625	3645				frozen			
PG2412-16				-4	3645	3650				frozen			
PG2412-16				-5	3650	3650				frozen			

A.4 Supplementary material: Summer Campaign on Bykovsky Peninsula

Table A.4-1: Water Resistivity Surveys

Site	Date	System	Filename	Range [V]	Tx Voltage [V]	Electrode Spacing [m]	Coordinate Offset [m] to First Current Electrode (Ca)	Array	Lat (Start; End)	Lon (Start; End)
Uomullyakh-Kyuel Lagoon	15.07. 2017	PRO	Uomullyakh_Lagoon_ 150717_Survey1A	5	100	10	-60	Reciprocal Wenner Schlumberger	71.7326 ; 71.7326	129.2808 ; 129.2742
	15.07. 2017		Uomullyakh_Lagoon_ 150717_Survey2	5	50	10	-60		71.7313 ; 71.7287	129.2724 ; 129.2751
	15.07. 2017		Uomullyakh_Lagoon _150717_Survey4	5	50	10	-60		71.7309 ; 71.7347	129.2735 ; 129.2695
	15.07. 2017		Uomullyakh_Lagoon_ 150717_Survey5	5	50	10	-60		71.7325 ; 71.7291	129.2690 ; 129.2738
	15.07. 2017		Uomullyakh_Lagoon_ 150717_Survey6	5	50	10	-60		71.7308 ; 71.7321	129.2752 ; 129.2767
	17.07. 2017	MARINE	Uomullyakh_Lagoon_ Land_to_Water_Merge	5	48	10	-60		71.7346 ; 71.7316	129.2991 ; 129.2942
	17.07. 2017		Uomullyakh_Lagoon_ 170717_Survey2	5	48	10	-60		71.7319 ; 71.7322	129.2859 ; 129.2779
	17.07. 2017		Uomullyakh_Lagoon_ 170717_Survey3	5	48	10	-60		71.7313 ; 71.7314	129.2770 ; 129.2774
	17.07. 2017		Uomullyakh_Lagoon_ 170717_Survey4	5	48	10	-60		71.7339 ; 71.7351	129.2843 ; 129.2896
	18.07. 2017		Uomullyakh_Lagoon_ 180717_Survey1	5	48	10	-60		71.7356 ; 71.7335	129.2940 ; 129.2671
	18.07. 2017		Uomullyakh_Lagoon_ 180717_Survey2	5	48	10	-60		71.7339 ; 71.7354	129.2734 ; 129.2776
	18.07. 2017		Uomullyakh_Lagoon_ 180717_Survey3	5	48	10	-60		71.7351 ; 71.7295	129.2732 ; 129.2767
	18.07. 2017		Uomullyakh_Lagoon_ 180717_Survey4	5	48	10	-60		71.7293 ; 71.7246	129.2726 ; 129.2439
	18.07. 2017		Uomullyakh_Lagoon_ 180717_Survey6	5	48	10	-60		71.7261 ; 71.7349	129.2509 ; 129.2981

Site	Date	System	Filename	Range [V]	Tx Voltage [V]	Electrode Spacing [m]	Coordinate Offset [m] to First Current Electrode (Ca)	Array	Lat	Lon
									(Start; End)	(Start; End)
Uomullyakh-Kyuel Lagoon	18.07.2017	MARINE	Uomullyakh_Lagoon_180717_RecipWenner_Sounding1	5	48	10	0	Reciprocal Wenner Schlumberger	71.7241 ; 71.7241	129.2445 ; 129.2445
	18.07.2017		Uomullyakh_Lagoon_180717_RecipWenner_Sounding2	5	48	10	0		71.7366 ; 71.7366	129.2738 ; 129.2738
	18.07.2017		Uomullyakh_Lagoon_180717_Wenner_Sounding1	5	48	10	0	Wenner Schlumberger	71.7241 ; 71.7241	129.2445 ; 129.2445
	18.07.2017		Uomullyakh_Lagoon_180717_Wenner_Sounding2	5	48	10	0		71.7366 ; 71.7366	129.2738 ; 129.2738
	20.07.2017		Uomullyakh_Lagoon_200717_Offshore_to_SandBar_Merge	5	48	10	-60	Reciprocal Wenner Schlumberger	71.7287 ; 71.7304	129.2955 ; 129.2929
	20.07.2017		Uomullyakh_Lagoon_200717_perp_to_sandbar_S_to_N	5	48	10	-60		71.7304 ; 71.7355	129.2928 ; 129.2706
	20.07.2017		Uomullyakh_Lagoon_200717_Survey2	5	48	10	-60		71.7346 ; 71.7343	129.2784 ; 129.2903
	20.07.2017		Uomullyakh_Offshore_200717_Survey1	5	48	10	-60		71.7293 ; 71.7326	129.2946 ; 129.3245
	20.07.2017		Uomullyakh_Offshore_200717_Survey2	5	48	10	-60		71.7322 ; 71.7286	129.3193 ; 129.2878
	20.07.2017		Uomullyakh_Offshore_200717_Survey3	5	48	10	-60		71.7290 ; 71.7323	129.2954 ; 129.3269
	20.07.2017		Uomullyakh_Offshore_200717_Survey4	5	48	10	-60		71.7321 ; 71.7320	129.3205 ; 129.3186
	20.07.2017		Uomullyakh_Offshore_200717_Survey5_SegmentA	5	48	10	-60		71.7288 ; 71.7292	129.3205 ; 129.3143
	20.07.2017		Uomullyakh_Offshore_200717_Survey5_SegmentB	5	48	10	-60		71.7288 ; 71.7273	129.3103 ; 129.2975

Site	Date	System	Filename	Range [V]	Tx Voltage [V]	Electrode Spacing [m]	Coordinate Offset [m] to First Current Electrode (Ca)	Array	Lat (Start; End)	Lon (Start; End)
Uomullyakh-Kyuel Lagoon	20.07.2017	MARINE	Uomullyakh_Offshore_200717_Survey6	5	48	10	-60	Reciprocal Wenner Schlumberger	71.7314 ; 71.7284	129.3236 ; 129.3272
	20.07.2017		Uomullyakh_Lagoon_200717_Sounding1_RecipWenner	5	48	10	0		71.7363 ; 71.7363	129.2859 ; 129.2859
	20.07.2017		Uomullyakh_Lagoon_200717_Sounding1_Wenner	5	48	10	0	Wenner	71.7363 ; 71.7363	129.2859 ; 129.2859
Polar Fox Lagoon	24.07.2017	MARINE	Polar_Fox_240717_Survey3	5	48	10	-60	Reciprocal Wenner Schlumberger	71.7413 ; 71.7475	129.3419 ; 129.3340
	26.07.2017		Polar_Fox_Land_to_Water_Merge	5	48	10	-57		71.7442 ; 71.7417	129.3250 ; 129.3454
	26.07.2017		Polar_Fox_260717_Survey1	5	48	10	-57		71.7431 ; 71.7444	129.3444 ; 129.3462
	26.07.2017		Polar_Fox_260717_Survey2	5	48	10	-57		71.7453 ; 71.7472	129.3439 ; 129.3274
	26.07.2017		Polar_Fox_260717_Survey3	5	48	10	-57		71.7457 ; 71.7402	129.3317 ; 129.3381
	26.07.2017		Polar_Fox_260717_Survey4	5	48	10	-57		71.7419 ; 71.7458	129.3388 ; 129.3424
Uomullyakh-Kyuel Lagoon	28.07.2017	MARINE	Uomullyakh_Lagoon_280717_Survey1	5	48	10	-57	Reciprocal Wenner Schlumberger	71.7346 ; 71.7309	129.2881 ; 129.2880
	28.07.2017		Uomullyakh_Lagoon_280717_Survey2	5	48	10	-57		71.7314 ; 71.7331	129.2824 ; 129.2661
	28.07.2017		Uomullyakh_Lagoon_280717_Survey3	5	48	10	-57		71.7324 ; 71.7253	129.2653 ; 129.2558
	28.07.2017		Uomullyakh_Lagoon_280717_Survey4	5	48	10	-57		71.7275 ; 71.7330	129.2569 ; 129.2486

Site	Date	System	Filename	Range [V]	Tx Voltage [V]	Electrode Spacing [m]	Coordinate Offset [m] to First Current Electrode (Ca)	Array	Lat (Start; End)	Lon (Start; End)
Uomullyakh-Kyuel Lagoon	28.07.2017	MARINE	Uomullyakh_Lagoon_280717_Survey5	5	48	10	-57	Reciprocal Wenner Schlumberger	71.7321 ; 71.7319	129.2543 ; 129.2635
	28.07.2017		Uomullyakh_Lagoon_280717_Survey6	5	48	10	-57		71.7319 ; 71.7316	129.2635 ; 129.2872
	28.07.2017		Uomullyakh_Lagoon_280717_Survey7	5	48	10	-57		71.7328 ; 71.7364	129.2874 ; 129.2895
Goltsovoye Lake	31.07.2017	MARINE	Goltsovoe_310717_Survey03	15	100	5	-39	Reciprocal Wenner Schlumberger	71.7429 ; 71.7472	129.2999 ; 129.3032
	31.07.2017		Goltsovoe_310717_Survey04	15	100	5	-39		71.7463 ; 71.7418	129.3044 ; 129.3031
	31.07.2017		Goltsovoe_310717_Survey05	15	100	5	-39		71.7429 ; 71.7440	129.3048 ; 129.3075
	31.07.2017		Goltsovoe_310717_Survey06	15	100	5	-39		71.7430 ; 71.7452	129.3011 ; 129.3114
	31.07.2017		Goltsovoe_310717_Survey07	15	100	5	-39		71.7454 ; 71.7455	129.3077 ; 129.2990
	31.07.2017		Goltsovoe_310717_Survey08	15	100	5	-39		71.7450 ; 71.7435	129.3018 ; 129.3094
	31.07.2017		Goltsovoe_310717_Survey09	15	100	5	-39		71.7442 ; 71.7456	129.3072 ; 129.2990
	31.07.2017		Goltsovoe_310717_Survey10	15	100	5	-39		71.7463 ; 71.7471	129.3015 ; 129.3053
	31.07.2017		Goltsovoe_310717_Survey11	15	100	5	-39		71.7464 ; 71.7450	129.3049 ; 129.3026
	31.07.2017		Goltsovoe_310717_Survey12	15	100	5	-39		71.7446 ; 71.7429	129.3012 ; 129.2982
	31.07.2017		Goltsovoe_310717_Survey13	15	100	5	-39		71.7440 ; 71.7467	129.2986 ; 129.3006

Site	Date	System	Filename	Range [V]	Tx Voltage [V]	Electrode Spacing [m]	Coordinate Offset [m] to First Current Electrode (Ca)	Array	Lat	Lon
									(Start; End)	(Start; End)
Goltsovoye Lake	31.07.2017	MARINE	Goltsovoe_310717_Survey14	15	100	5	-39	Reciprocal Wenner Schlumberger	71.7468 ; 71.7470	129.3034 ; 129.3067
	31.07.2017		Goltsovoe_310717_Survey15	15	100	5	-39		71.7466 ; 71.7426	129.3081 ; 129.3078
	31.07.2017		Goltsovoe_310717_Survey16	15	100	5	-39		71.7429 ; 71.7438	129.3047 ; 129.2985
	31.07.2017		Goltsovoe_310717_Survey17	15	100	5	-39		71.7446 ; 71.7471	129.3002 ; 129.3045
	31.07.2017		Goltsovoe_310717_Survey18	15	100	5	-39		71.7463 ; 71.7445	129.3064 ; 129.3109
	31.07.2017		Goltsovoe_310717_Survey19	15	100	5	-39		71.7447 ; 71.7452	129.3076 ; 129.2990
	31.07.2017		Goltsovoe_310717_Survey20	15	100	5	-39		71.7443 ; 71.7431	129.3010 ; 129.3085
	31.07.2017	PRO	Goltsovoe_310717_Survey21	15	100	5	-39		71.7437 ; 71.7466	129.3096 ; 129.3086
	31.07.2017		Goltsovoe_310717_Survey22	15	100	5	-39		71.7465 ; 71.7464	129.3057 ; 129.3000
	31.07.2017		Goltsovoe_310717_Survey23	15	100	5	-39		71.7460 ; 71.7460	129.3028 ; 129.3102
	31.07.2017		Goltsovoe_310717_Survey24	15	100	5	-39		71.7454 ; 71.7438	129.3111 ; 129.3103
	31.07.2017		Goltsovoe_310717_Survey25	15	100	5	-39		71.7435 ; 71.7424	129.3067 ; 129.2986

Site	Date	System	Filename	Range [V]	Tx Voltage [V]	Electrode Spacing [m]	Coordinate Offset [m] to First Current Electrode (Ca)	Array	Lat		Lon	
									(Start; End)		(Start; End)	
Uomullyakh-Kyuel Lagoon	02.08. 2017	MARINE	Uomullyakh_Lagoon_ 020817_on_sandbar_S_to_N_Merge	5/15	24	5	0	Reciprocal Wenner Schlumberger	71.7293 ; 71.7298		129.2940 ; 129.2935	
Bykovsky Channel	03.08. 2017	PRO	Bykovsky_Channel_Survey1	15	100	10	-57	Reciprocal Wenner Schlumberger	72.0601 ; 72.0601		129.2463 ; 129.2465	
	03.08. 2017		Bykovsky_Channel_Survey2	15	100	10	-57		72.0587 ; 72.0577		129.2440 ; 129.2410	
	03.08. 2017		Bykovsky_Channel_Survey3	15	100	10	-57		72.0562 ; 72.0418		129.2402 ; 129.2316	
	03.08. 2017		Bykovsky_Channel_Survey4	15	100	10	-57		72.0429 ; 72.0432		129.2290 ; 129.2266	
	03.08. 2017		Bykovsky_Channel_Survey5	15	100	10	-57		72.0442 ; 72.0461		129.2219 ; 129.2062	
	03.08. 2017		Bykovsky_Channel_Survey6	15	100	10	-57		72.0475 ; 72.0490		129.2096 ; 129.2141	

Table A.4-2: Terrestrial Resistivity Surveys; *System used for all values: PRO*

Site	Date	Filename	Range [V]	Tx Voltage [V]	Electrode Spacing [m]	Array	Electrode 1 LONG; LAT	Electrode 13 LONG; LAT	Midpoint LONG;LAT
Omullyakh-Kyuel Lagoon	14.07.2017	AL_Profile1_+_0m_ RecipWenner_15Vrange_perpendicular	15	Max	5	Reciprocal Wenner Schlumberger	129.2996 ; 71.7345	129.2983 ; 71.7348	129.2990 ; 71.7343
		AL_Profile1_+_0m_ RecipWenner_5Vrange_perpendicular	5	Max	5		129.2996 ; 71.7345	129.2983 ; 71.7348	129.2990 ; 71.7343
		AL_Profile1_+_0m_ Wenner_15Vrange_perpendicular	15	Max	5	Wenner Schlumberger	129.2996 ; 71.7345	129.2983 ; 71.7348	129.2990 ; 71.7343
		AL_Profile1_+_0m_ Wenner_5Vrange_1	5	Max	5		129.2990 ; 71.7347	129.2997 ; 71.7351	129.2994 ; 71.7349
		AL_Profile1_+_0m_ Wenner_5Vrange_2	5	Max	5		129.2990 ; 71.7347	129.2997 ; 71.7351	129.2994 ; 71.7349
		AL_Profile1_+_0m_ Wenner_5Vrange_3	5	Max	5		129.2990 ; 71.7347	129.2997 ; 71.7351	129.2994 ; 71.7349
		AL_Profile1_+_0m_ Wenner_5Vrange_perpendicular	5	Max	5		129.2996 ; 71.7345	129.2983 ; 71.7348	129.2990 ; 71.7343
		AL_Profile1_+_30m_ Wenner_5Vrange	5	Max	5		129.2994 ; 71.7349	129.3000 ; 71.7354	129.2997 ; 71.7351
		AL_Profile1_+_30m_ RecipWenner_15Vrange_perpendicular	15	Max	5	Reciprocal Wenner Schlumberger	129.2999 ; 71.7348	129.2985 ; 71.7350	129.2991 ; 71.7347
		AL_Profile1_+_30m_ RecipWenner_5Vrange_perpendicular	5	Max	5		129.2999 ; 71.7348	129.2985 ; 71.7350	129.2991 ; 71.7347
		AL_Profile1_+_30m_ Wenner_15Vrange_perpendicular	15	Max	5	Wenner Schlumberger	129.2999 ; 71.7348	129.2985 ; 71.7350	129.2991 ; 71.7347
		AL_Profile1_+_60m_ Wenner_5Vrange	5	Max	5		129.2997 ; 71.7351	129.3003 ; 71.7356	129.3000 ; 71.7354
		AL_Profile1_+_60m_ RecipWenner_5Vrange_perpendicular	5	Max	5	Reciprocal Wenner	129.3004 ; 71.7351	129.2989 ; 71.7353	129.2996 ; 71.7349
		AL_Profile1_+_60m_ Wenner_5Vrange_perpendicular	5	Max	5	Wenner	129.3004 ; 71.7351	129.2989 ; 71.7353	129.2996 ; 71.7349

Site	Date	Filename	Range [V]	Tx Voltage [V]	Electrode Spacing [m]	Array	Electrode 1 LONG; LAT	Electrode 13 LONG; LAT	Midpoint LONG;LAT
Uomullyakh-Kyuel Lagoon	14.07.2017	AL_Profile1_+_70m_ RecipWenner_5Vrange_perpendicular	5	Max	5	Reci-procal Wenner	129.3005 ; 71.7352	129.2989 ; 71.7354	129.2997 ; 71.7351
		AL_Profile1_+_70m_ Wenner_5Vrange_perpendicular	5	Max	5	Wen-ner	129.3005 ; 71.7352	129.2989 ; 71.7354	129.2997 ; 71.7351
		AL_Profile1_+_80m_ RecipWenner_5Vrange_perpendicular	5	Max	5	Reci-procal Wenner	129.3006 ; 71.7353	129.2990 ; 71.7355	129.2998 ; 71.7352
		AL_Profile1_+_80m_ Wenner_5Vrange_perpendicular	5	Max	5	Wenner Schlum-berger	129.3006 ; 71.7353	129.2990 ; 71.7355	129.2998 ; 71.7352
		AL_Profile1_+_90m_ Wenner_15Vrange	15	Max	5	Wenner Schlum-berger	129.3000 ; 71.7354	129.3007 ; 71.7359	129.3003 ; 71.7356
		AL_Profile1_+_90m_ RecipWenner_15Vrange_perpendicular	15	Max	5	Reci-procal Wenner	129.3008 ; 71.7354	129.2991 ; 71.7356	129.2999 ; 71.7353
		AL_Profile1_+_90m_ Wenner_15Vrange_perpendicular	15	Max	5	Wenner Schlum-berger	129.3008 ; 71.7354	129.2991 ; 71.7356	129.2999 ; 71.7353
		AL_Profile1_+_90m_ Wenner_5Vrange_perpendicular	5	Max	5	Wenner Schlum-berger	129.3008 ; 71.7354	129.2991 ; 71.7356	129.2999 ; 71.7353
		AL_Profile1_+120m_ RecipWenner_5Vrange	5	Max	5	Reci-procal Wenner	129.3003 ; 71.7356	129.3010 ; 71.7361	129.3007 ; 71.7359
		AL_Profile1_+120m_ Wenner_5Vrange	5	Max	5	Wen-ner	129.3003 ; 71.7356	129.3010 ; 71.7361	129.3007 ; 71.7359
	30.07.2017	AL_Profile1_+_15m_ DipoleDipoleA_15Vrange_2	15	Max	5	Dipole-Dipole A	129.2999 ; 71.7353	129.2993 ; 71.7348	129.2996 ; 71.7350
		AL_Profile1_+_15m_ DipoleDipoleA_5Vrange_3	5	Max	5		129.2999 ; 71.7353	129.2993 ; 71.7348	129.2996 ; 71.7350
		AL_Profile1_+_15m_ DipoleDipoleB_15Vrange	15	Max	5	Dipole-DipoleB	129.2999 ; 71.7353	129.2993 ; 71.7348	129.2996 ; 71.7350

Site	Date	Filename	Range [V]	Tx Voltage [V]	Electrode Spacing [m]	Array	Electrode 1 LONG; LAT	Electrode 13 LONG; LAT	Midpoint LONG;LAT
Uomullyakh-Kyuel Lagoon	30.07.2017	AL_Profile1_+_15m_DipoleDipoleB_5Vrange_2	5	Max	5	Dipole-DipoleB	129.2999 ; 71.7353	129.2993 ; 71.7348	129.2996 ; 71.7350
		AL_Profile1_+_15m_RecipWenner_15Vrange_2	15	100	5	Reciprocal Wenner Schlumberger	129.2999 ; 71.7353	129.2993 ; 71.7348	129.2996 ; 71.7350
		AL_Profile1_+_15m_RecipWenner_5Vrange_3	5	100	5		129.2999 ; 71.7353	129.2993 ; 71.7348	129.2996 ; 71.7350
		AL_Profile1_+_15m_Wenner_15Vrange_2	15	100	5	Wenner Schlum-berger	129.2999 ; 71.7353	129.2993 ; 71.7348	129.2996 ; 71.7350
		AL_Profile1_+_15m_Wenner_5Vrange_2	5	100	5		129.2999 ; 71.7353	129.2993 ; 71.7348	129.2996 ; 71.7350
		AL_Profile1_+_50m_DipoleDipoleA_15Vrange	15	100	5	Dipole-DipoleA	129.3003 ; 71.7356	129.2997 ; 71.7351	129.3000 ; 71.7353
		AL_Profile1_+_50m_DipoleDipoleA_5Vrange	5	100	5		129.3003 ; 71.7356	129.2997 ; 71.7351	129.3000 ; 71.7353
		AL_Profile1_+_50m_DipoleDipoleB_15Vrange	15	100	5	Dipole-DipoleB	129.3003 ; 71.7356	129.2997 ; 71.7351	129.3000 ; 71.7353
		AL_Profile1_+_50m_DipoleDipoleB_5Vrange	5	100	5		129.3003 ; 71.7356	129.2997 ; 71.7351	129.3000 ; 71.7353
		AL_Profile1_+_50m_RecipWenner_15Vrange	15	100	5	Reciprocal Wenner Schlumberger	129.3003 ; 71.7356	129.2997 ; 71.7351	129.3000 ; 71.7353
		AL_Profile1_+_50m_RecipWenner_5Vrange	5	100	5		129.3003 ; 71.7356	129.2997 ; 71.7351	129.3000 ; 71.7353
		AL_Profile1_+_50m_Wenner_15Vrange	15	100	5	Wenner Schlum-berger	129.3003 ; 71.7356	129.2997 ; 71.7351	129.3000 ; 71.7353
		AL_Profile1_+_50m_Wenner_5Vrange	5	100	5		129.3003 ; 71.7356	129.2997 ; 71.7351	129.3000 ; 71.7353

Site	Date	Filename	Range [V]	Tx Voltage [V]	Electrode Spacing [m]	Array	Electrode 1 LONG; LAT	Electrode 13 LONG; LAT	Midpoint LONG;LAT
Uomullyakh-Kyuel Lagoon	30.07.2017	AL_Profile1_+_80m_DipoleDipoleA_15Vrange	15	100	5	Dipole-Dipole A	129.3006 ; 71.7358	129.3000 ; 71.7353	129.3003 ; 71.7356
		AL_Profile1_+_80m_DipoleDipoleA_5Vrange	5	100	5		129.3006 ; 71.7358	129.3000 ; 71.7353	129.3003 ; 71.7356
		AL_Profile1_+_80m_DipoleDipoleB_15Vrange	15	100	5	Dipole-Dipole B	129.3006 ; 71.7358	129.3000 ; 71.7353	129.3003 ; 71.7356
		AL_Profile1_+_80m_DipoleDipoleB_5Vrange	5	100	5		129.3006 ; 71.7358	129.3000 ; 71.7353	129.3003 ; 71.7356
		AL_Profile1_+_80m_RecipWenner_15Vrange	15	100	5	Reciprocal Wenner Schlumberger	129.3006 ; 71.7358	129.3000 ; 71.7353	129.3003 ; 71.7356
		AL_Profile1_+_80m_RecipWenner_5Vrange	5	100	5		129.3006 ; 71.7358	129.3000 ; 71.7353	129.3003 ; 71.7356
		AL_Profile1_+_80m_Wenner_15Vrange	15	100	5	Wenner Schlum-berger	129.3006 ; 71.7358	129.3000 ; 71.7353	129.3003 ; 71.7356
		AL_Profile1_+_80m_Wenner_5Vrange	5	100	5		129.3006 ; 71.7358	129.3000 ; 71.7353	129.3003 ; 71.7356
		AL_Profile1_+110m_DipoleDipoleA_15Vrange	15	100	5	Dipole-Dipole A	129.3009 ; 71.7361	129.3003 ; 71.7356	129.3006 ; 71.7358
		AL_Profile1_+110m_DipoleDipoleA_5Vrange	5	100	5		129.3009 ; 71.7361	129.3003 ; 71.7356	129.3006 ; 71.7358
		AL_Profile1_+110m_DipoleDipoleB_15Vrange	15	100	5	Dipole-Dipole B	129.3009 ; 71.7361	129.3003 ; 71.7356	129.3006 ; 71.7358
		AL_Profile1_+110m_DipoleDipoleB_5Vrange	5	100	5		129.3009 ; 71.7361	129.3003 ; 71.7356	129.3006 ; 71.7358
		AL_Profile1_+110m_RecipWenner_15Vrange	15	100	5	Reciprocal Wenner Schlumberger	129.3009 ; 71.7361	129.3003 ; 71.7356	129.3006 ; 71.7358
		AL_Profile1_+110m_RecipWenner_5Vrange	5	100	5		129.3009 ; 71.7361	129.3003 ; 71.7356	129.3006 ; 71.7358

Site	Date	Filename	Range [V]	Tx Voltage [V]	Electrode Spacing [m]	Array	Electrode 1 LONG; LAT	Electrode 13 LONG; LAT	Midpoint LONG;LAT
Omullyakh-Kyuel Lagoon	30.07.2017	AL_Profile1_+110m_Wenner_15Vrange_2	15	100	5	Wenner Schlumberger	129.3009 ; 71.7361	129.3003 ; 71.7356	129.3006 ; 71.7358
		AL_Profile1_+110m_Wenner_5Vrange	5	100	5		129.3009 ; 71.7361	129.3003 ; 71.7356	129.3006 ; 71.7358
		AL_Profile1_+140m_DipoleDipoleA_15Vrange	15	100	5	Dipole-DipoleA	129.3012 ; 71.7363	129.3006 ; 71.7358	129.3009 ; 71.7361
		AL_Profile1_+140m_DipoleDipoleA_5Vrange	5	100	5		129.3012 ; 71.7363	129.3006 ; 71.7358	129.3009 ; 71.7361
		AL_Profile1_+140m_DipoleDipoleB_15Vrange	15	100	5	Dipole-DipoleB	129.3012 ; 71.7363	129.3006 ; 71.7358	129.3009 ; 71.7361
		AL_Profile1_+140m_DipoleDipoleB_5Vrange	5	100	5		129.3012 ; 71.7363	129.3006 ; 71.7358	129.3009 ; 71.7361
		AL_Profile1_+140m_RecipWenner_15Vrange	15	100	5	Reciprocal Wenner Schlumberger	129.3012 ; 71.7363	129.3006 ; 71.7358	129.3009 ; 71.7361
		AL_Profile1_+140m_RecipWenner_5Vrange	5	100	5		129.3012 ; 71.7363	129.3006 ; 71.7358	129.3009 ; 71.7361
		AL_Profile1_+140m_Wenner_15Vrange	15	100	5	Wenner Schlumberger	129.3012 ; 71.7363	129.3006 ; 71.7358	129.3009 ; 71.7361
		AL_Profile1_+140m_Wenner_5Vrange	5	100	5		129.3012 ; 71.7363	129.3006 ; 71.7358	129.3009 ; 71.7361

Site	Date	Filename	Range [V]	Tx Voltage [V]	Electrode Spacing [m]	Array	Electrode 1 LONG; LAT	Electrode 13 LONG; LAT	Midpoint LONG;LAT
Polar Fox Lagoon	27.07.2017	Polar_Fox_270717_LandBridge_ ReciprocalWenner_15Vrange_Sounding1	15	100	10	Reciprocal Wenner Schlumberger	129.3394 ; 71.7476	129.3388 ; 71.7465	129.3391 ; 71.7470
		Polar_Fox_270717_LandBridge_ ReciprocalWenner_15Vrange_Sounding2A	15	100	10		129.3390 ; 71.7467	129.3396 ; 71.7477	129.3393 ; 71.7472
		Polar_Fox_270717_LandBridge_ ReciprocalWenner_15Vrange_Sounding2B	15	100	10		129.3390 ; 71.7467	129.3396 ; 71.7477	129.3393 ; 71.7472
		Polar_Fox_270717_LandBridge_ ReciprocalWenner_15Vrange_Sounding3	15	100	10		129.3396 ; 71.7476	129.3408 ; 71.7486	129.3402 ; 71.7481
		Polar_Fox_270717_LandBridge_ RecipWenner_5Vrange_Sounding1	5	100	10		129.3394 ; 71.7476	129.3388 ; 71.7465	129.3391 ; 71.7470
		Polar_Fox_270717_LandBridge_ RecipWenner_5Vrange_Sounding2	5	100	10		129.3390 ; 71.7467	129.3396 ; 71.7477	129.3393 ; 71.7472
		Polar_Fox_270717_LandBridge_ RecipWenner_5Vrange_Sounding3	5	100	10		129.3396 ; 71.7476	129.3408 ; 71.7486	129.3402 ; 71.7481
		Polar_Fox_270717_LandBridge_ Wenner_15Vrange_Sounding1	15	100	10	Wenner Schlumberger	129.3394 ; 71.7476	129.3388 ; 71.7465	129.3391 ; 71.7470
		Polar_Fox_270717_LandBridge_ Wenner_15Vrange_Sounding2	15	100	10		129.3390 ; 71.7467	129.3396 ; 71.7477	129.3393 ; 71.7472
		Polar_Fox_270717_LandBridge_ Wenner_15Vrange_Sounding3	15	100	10		129.3396 ; 71.7476	129.3408 ; 71.7486	129.3402 ; 71.7481
		Polar_Fox_270717_LandBridge_ Wenner_5Vrange_Sounding1	5	100	10		129.3394 ; 71.7476	129.3388 ; 71.7465	129.3391 ; 71.7470
		Polar_Fox_270717_LandBridge_ Wenner_5Vrange_Sounding2	5	100	10		129.3390 ; 71.7467	129.3396 ; 71.7477	129.3393 ; 71.7472
		Polar_Fox_270717_LandBridge_ Wenner_5Vrange_Sounding3	5	100	10		129.3396 ; 71.7476	129.3408 ; 71.7486	129.3402 ; 71.7481

Table A.4-3: Ground-Penetrating Radar Surveys; *For all values: Coordinate Offset to Measurement Point is 0m and Frequency is 50MHz.*

Site	Date	Filename	LONG (Start)	LAT (Start)	LONG (End)	LAT (End)
Small Alas Lake	23.07.2017	50_MHz_GPR_Small_Alas_Lake_South_to_North	129.2979	71.7385	129.2979	71.7397
Uomullyakh-Kyuel Lagoon Active Layer Transect	19.07.2017	50_MHz_GPR_ Uomullyakh_Lagoon_AL_Profile_N_to_S	129.3008	71.736	129.2993	71.7348
Uomullyakh-Kyuel Lagoon Active Layer Transect	19.07.2017	50_MHz_GPR_ Uomullyakh_Lagoon_AL_Profile_S_to_N	129.2993	71.7349	129.3008	71.736
Uomullyakh-Kyuek Lagoon Spit	03.08.2017	50_MHz_GPR_ Uomullyakh_Lagoon_Spit_North_to_South	129.2939	71.73	129.2939	71.7294
Uomullyakh-Kyuek Lagoon Spit	03.08.2017	50_MHz_GPR_ Uomullyakh_Lagoon_Spit_South_to_North	129.294	71.7294	129.2939	71.7299
Uomullyakh-Kyuek Lagoon Spit	03.08.2017	50_MHz_GPR_ Uomullyakh_Lagoon_Spit_East_to_West	129.296	71.7298	129.2924	71.7295
Uomullyakh-Kyuek Lagoon Spit	03.08.2017	50_MHz_GPR_ Uomullyakh_Lagoon_Spit_West_to_East	129.292	71.7295	129.2956	71.7297

Table A.4-4: Active Layer Sampling

No	Sample ID	Name	Latitude	Longitude
1	0,10-0,15	Pit 802	71.736	129.3008
2	0,10-0,15	Pit 802	71.736	129.3008
3	0,20-0,25	Pit 802	71.736	129.3008
4	0,20-0,25	Pit 802	71.736	129.3008
5	0,10-0,15	Pit 806	71.7358	129.3006
6	0,25-0,30	Pit 806	71.7358	129.3006
7	0,25-0,30	Pit 806	71.7358	129.3006
8	0,10-0,15	Pit 806	71.7358	129.3006
9	0,05-0,10	Pit 810	71.7356	129.3003
10	0,05-0,10	Pit 810	71.7356	129.3003
11	0,15-0,20	Pit 810	71.7356	129.3003
12	0,15-0,20	Pit 810	71.7356	129.3003
13	Vegetation	Pit 813	71.7354	129.3
14	0,05-0,1	Pit 813	71.7354	129.3
15	0,15-0,20	Pit 813	71.7354	129.3
16	0,25-0,32	Pit 813	71.7354	129.3
17	0.35	Pit 813	71.7354	129.3
18	0,40-0,45	Pit 813	71.7354	129.3
19	0,50-0,55	Pit 813	71.7354	129.3
20	0,03-0,08	Pit 816	71.7352	129.2997
21	0.16	Pit 816	71.7352	129.2997
22	0,28-0,32	Pit 816	71.7352	129.2997
23	0.04	Pit 830	71.7346	129.299
24	0.1	Pit 830	71.7346	129.299
25	0.26	Pit 830	71.7346	129.299
26	0,10-0,15	MetSt	71.7359	129.2999
27	0,10-0,15	MetSt	71.7359	129.2999
28	0,30-0,35	MetSt	71.7359	129.2999
29	0,30-0,35	MetSt	71.7359	129.2999
30	0,35-0,40	Bh 1-1	71.736	129.3008
31	0,40-0,44	Bh 1-1	71.736	129.3008
32	0,45-0,50	Bh 1-1	71.736	129.3008
33	0,55-0,60	Bh 1-1	71.736	129.3008
34	0.65	Bh 1-1	71.736	129.3008
35	0,80-0,85	Bh 1-1	71.736	129.3008
36	0,90-0,95	Bh 1-1	71.736	129.3008
37	0,97-1,02	Bh 1-1	71.736	129.3008
38	1,02-1,10	Bh 1-1	71.736	129.3008
39	1,05-1,12	Bh 1-1	71.736	129.3008
40	1,12-1,22	Bh 1-1	71.736	129.3008
41	1,22-1,35	Bh 1-1	71.736	129.3008
42	1,20-1,25	Bh 1-1	71.736	129.3008
43	0,50-0,55	Bh 2-1	71.7354	129.3001
44	0,55-0,65	Bh 2-1	71.7354	129.3001

No	Sample ID	Name	Latitude	Longitude
45	0,65-0,75	Bh 2-1	71.7354	129.3001
46	0,75-0,82	Bh 2-1	71.7354	129.3001
47	0,82-0,90	Bh 2-1	71.7354	129.3001
48	0,90-1,00	Bh 2-1	71.7354	129.3001
49	1,00-1,10	Bh 2-1	71.7354	129.3001
50	1,10-1,20	Bh 2-1	71.7354	129.3001
51	1,20-1,30	Bh 2-1	71.7354	129.3001
52	0-0,08	Bh 3-1	71.7351	129.2996
53	0,08-0,19	Bh 3-1	71.7351	129.2996
54	0,19-0,27	Bh 3-1	71.7351	129.2996
55	0,27-0,35	Bh 3-1	71.7351	129.2996
56	0,35-0,45	Bh 3-1	71.7351	129.2996
57	0,45-0,54	Bh 3-1	71.7351	129.2996
58	0,54-0,60	Bh 3-1	71.7351	129.2996
59	0,60-0,70	Bh 3-1	71.7351	129.2996
60	0-0,10	Bh 4-1	71.7358	129.3005
61	0,10-0,15	Bh 4-1	71.7358	129.3005
62	0,16-0,25	Bh 4-1	71.7358	129.3005
63	0,25-0,30	Bh 4-1	71.7358	129.3005
64	0,30-0,40	Bh 4-1	71.7358	129.3005
65	0,40-0,46	Bh 4-1	71.7358	129.3005
66	0,47-0,60	Bh 4-1	71.7358	129.3005
67	0,60-0,70	Bh 4-1	71.7358	129.3005
68	0,70-0,80	Bh 4-1	71.7358	129.3005
69	0,80-0,87	Bh 4-1	71.7358	129.3005
70	0,88-1,00	Bh 4-1	71.7358	129.3005
71	1,00-1,09	Bh 4-1	71.7358	129.3005
72	1,10-1,15	Bh 4-1	71.7358	129.3005
73	1,15-1,25	Bh 4-1	71.7358	129.3005
74	1,25-1,35	Bh 4-1	71.7358	129.3005

Table A.4-5: CTD Casts; Radiometric Measurements (Hamamatsu and Ramses); Water Samples (Methane and Biogeochemical)

Station	Site	Date	Time	Lat; Lon	Water-depth [m]	CTD (Depth, Salinity, Temp)	Hamamatsu Radiometry	Ramses Radiometry	SPM	CHL	CDOM	DOC	Isotopes	Cat/An	Secchi
Ben_1	Sea, in front of Omulakh	7/14/2017	2:27:00 AM	71.7157 ; 129.2944	5.47	X	X	-	X	X	X	X	X	X	-
Ben_2	Sea, Cape Muostakh	7/14/2017	4:03:00 AM	71.696 ; 129.5996	5.33	X	X	-	X	X	X	X	X	X	-
Ben_3	Sea, between camp and Cape Muostakh	7/14/2017	5:20:00 AM	71.7207 ; 129.4330	4.1	X	X	-	X	X	X	X	X	X	-
Ben_4	Golzovoe Lake	7/15/2017	4:40:00 AM	71.7419 ; 129.3006	-	-	-	-	X	X	X	X	X	X	-
Ben_5	Small lake	7/15/2017	5:04:00 AM	71.7394 ; 129.2986	0.75	X	-	-	X	X	X	X	X	X	-
Air_Measurement_1	Camp	7/15/2017	10:20:00 AM	71.7394 ; 129.2986	-	-	X	-	-	-	-	-	-	-	-
Ben_6	Sea, in front of Omulakh	7/16/2017	1:25:00 AM	71.7042 ; 129.3053	7.78	X	X	X	X	X	X	X	X	X	X
Ben_7	Sea, Cape Muostakh	7/16/2017	4:52:00 AM	71.6969 ; 129.6211	3.82	X	X	X	X	X	X	X	X	X	X

Station	Site	Date	Time	Lat; Lon	Water-depth [m]	CTD (Depth, Salin-ity, Temp)	Hamamatsu Radiometry	Ramses Radiometry	SPM	CHL	CDOM	DOC	Isotopes	Cat/An	Secchi
Ben_8	Sea, between camp and Cape Muostakh	7/16/ 2017	6:22:00 AM	71.6832 ; 129.5115	7.6	X	X	X	X	X	X	X	X	X	X
Spec-tralon Mea-sure-ment 1	In camp at Omullakh lagoon	7/16/ 2017	9:44:00 AM	71.6842 ; 129.5203	-	-	X	-	-	-	-	-	-	-	-
Ben_9	Omullyakh Lagoon	7/17/ 2017	4:16:00 AM	71.7326 ; 129.2839	1.28	X	X	X	X	X	X	X	X	X	-
Ben_10	Sea, in front of Omulakh	7/17/ 2017	5:09:00 AM	71.7069 ; 129.2700	5.17	X	X	-	X	X	X	X	X	X	X
Ben_11	Lake bykovsky	7/20/ 2017	5:08:00 AM	71.7585 ; 129.3007	-	-	-	-	X	X	X	X	X	X	-
Ben_12	Lake bykovsky	7/20/ 2017	5:20:00 AM	71.7609 ; 129.2967	-	-	-	-	X	X	X	X	X	X	-
Ben_13	Lake bykovsky	7/20/ 2017	6:12:00 AM	71.7589 ; 129.3344	-	-	-	-	X	X	X	X	X	X	-
Ben_14	Lake bykovsky	7/20/ 2017	6:38:00 AM	71.754 ; 129.3207	1.41	X	-	-	X	X	X	X	X	X	-

Station	Site	Date	Time	Lat; Lon	Water-depth [m]	CTD (Depth, Salinity, Temp)	Hamamatsu Radiometry	Ramses Radiometry	SPM	CHL	CDOM	DOC	Isotopes	Cat/An	Secchi
Ben_15	Tiksi Bay, close to Tiksi	7/21/2017	4:41:00 AM	71.6892 ; 129.1023	7.41	X	X	X	X	X	X	X	X	X	X
Ben_16	Tiksi Bay, south west	7/21/2017	6:10:00 AM	71.6462 ; 129.1583	9.77	X	X	X	X	X	X	X	X	X	X
Ben_17	Far out in front of Omullakh	7/21/2017	7:21:00 AM	71.6561 ; 129.3002	10.31	X	X	X	X	X	X	X	X	X	X
Ben_18	In front of Mamontovy Khayata	7/22/2017	10:50:00 AM	71.7864 ; 129.4929	4.45	X	-	-	X	X	X	X	X	X	X
Ben_19	5km out in front of Omullakh Lagoon	7/24/2017	4:38:00 AM	71.701 ; 129.2937	8.52	X	X	X	X	X	X	X	X	X	X
PFL Borehole	Polar Fox Lake at Borehole position	7/26/2017	-	71.7259 ; 129.2806	-	-	-	-	X	X	X	X	X	X	-
Ed_test_camp	In camp at Omullakh lagoon	7/30/2017	2:52:00 AM	71.722 ; 129.2829	-	-	X	X	-	-	-	-	-	-	-
Ben_20	In front of Omullakh Lagoon	7/30/2017	6:50:00 AM	71.722 ; 129.2827	2.79	X	X	X	X	X	X	X	X	X	-

Station	Site	Date	Time	Lat; Lon	Water-depth [m]	CTD (Depth, Salin-ity, Temp)	Hamamatsu Radiometry	Ramses Radiometry	SPM	CHL	CDOM	DOC	Isotopes	Cat/An	Secchi
Ben_21	Tiksi Bay, way to tiksi	7/30/ 2017	7:40:00 AM	71.7011; 129.2251	5.25	X	X	X	X	X	X	X	X	X	-
Ben_22	On yacht, in front of omullkah lagoon	8/2/ 2017	4:58:00 AM	71.6500 ; 129.4375	10.27	X	X	X	X	X	X	X	X	X	X
Ben_23	On yacht, at cape muostakh	8/2/ 2017	7:02:00 AM	71.6838 ; 129.7838	4.43	X	X	X	X	X	X	X	X	X	X
Ben_24	On yacht, in front of bykovsky	8/4/ 2017	10:54:00 PM	71.7623 ; 129.7149	6.47	X	X	X	X	X	X	X	X	X	X
Ben_25	On yacht, 10 km away from bykovsky shore	8/5/ 2017	12:49:00 AM	71.8375 ; 130.0051	10.61	X	X	X	X	X	X	X	X	X	X
Ben_26	On yacht, transect buor khaya	8/5/ 2017	3:12:00 AM	71.9604 ; 130.4435	15.84	X	X	X	X	X	X	X	X	X	-
Ben_27	On yachtl, most far out on transect	8/5/ 2017	6:14:00 AM	72.0675 ; 130.9128	17.24	X	X	X	X	X	X	X	X	X	X
Ben_28	On yacht, on front of Lena Water and Sea water (white foam)	8/5/ 2017	9:55:00 AM	72.0628 ; 129.9914	9.36	X	X	X	X	X	X	X	X	X	X

Die **Berichte zur Polar- und Meeresforschung** (ISSN 1866-3192) werden beginnend mit dem Band 569 (2008) als Open-Access-Publikation herausgegeben. Ein Verzeichnis aller Bände einschließlich der Druckausgaben (ISSN 1618-3193, Band 377-568, von 2000 bis 2008) sowie der früheren **Berichte zur Polarforschung** (ISSN 0176-5027, Band 1-376, von 1981 bis 2000) befindet sich im electronic Publication Information Center **(ePIC)** des Alfred-Wegener-Instituts, Helmholtz-Zentrum für Polar- und Meeresforschung (AWI); see http://epic.awi.de. Durch Auswahl “Reports on Polar- and Marine Research“ (via “browse”/”type”) wird eine Liste der Publikationen, sortiert nach Bandnummer, innerhalb der absteigenden chronologischen Reihenfolge der Jahrgänge mit Verweis auf das jeweilige pdf-Symbol zum Herunterladen angezeigt.

The **Reports on Polar and Marine Research** (ISSN 1866-3192) are available as open access publications since 2008. A table of all volumes including the printed issues (ISSN 1618-3193, Vol. 377-568, from 2000 until 2008), as well as the earlier **Reports on Polar Research** (ISSN 0176-5027, Vol. 1-376, from 1981 until 2000) is provided by the electronic Publication Information Center **(ePIC)** of the Alfred Wegener Institute, Helmholtz Centre for Polar and Marine Research (AWI); see URL http://epic.awi.de. To generate a list of all Reports, use the URL http://epic.awi.de and select “browse”/ ”type” to browse ”Reports on Polar and Marine Research”. A chronological list in declining order will be presented, and pdf-icons displayed for downloading.

Zuletzt erschienene Ausgaben:

Recently published issues:

725 (2018) Russian-German Cooperation: Expeditions to Siberia in 2017, edited by Jens Strauss, Julia Boike, Dmitry Yu. Bolshiyanov, Mikhail N. Grigoriev, Hassan El-Hajj, Anne Morgenstern, Pier Paul Overduin, Annegret Udke

724 (2018) The Expedition PS113 of the Research Vessel POLARSTERN to the Atlantic Ocean in 2018, edited by Volker Strass

723 (2018) The Expedition PS114 of the Research Vessel POLARSTERN to the Fram Strait in 2018, edited by Wilken-Jon von Appen

722 (2018) The Expedition PS112 of the Research Vessel POLARSTERN to the Antarctic Peninsula Region in 2018, edited by Bettina Meyer and Wiebke Weßels

721 (2018) Alfred Wegener im 1. Weltkrieg. Ein Polarforscher und die „Urkatastrophe des 20. Jahrhunderts“, by Christian R. Salewski

720 (2018) The Expedition PS98 of the Research Vessel POLARSTERN to the Atlantic Ocean in 2016, edited by Bernhard Pospichal

719 (2018) The Expeditions PS106/1 and 2 of the Research Vessel POLARSTERN to the Arctic Ocean in 2017, edited by Andreas Macke and Hauke Flores

718 (2018) The Expedition PS111 of the Research Vessel POLARSTERN to the southern Weddell Sea in 2018, edited by Michael Schröder

717 (2018) The Expedition PS107 of the Research Vessel POLARSTERN to the Fram Strait and the AWI-HAUSGARTEN in 2017, edited by Ingo Schewe

716 (2018) Polar Systems under Pressure, 27th International Polar Conference, Rostock, 25 - 29 March 2018, German Society for Polar Research, edited by H. Kassens, D. Damaske, B. Diekmann, D. Fütterer, G. Heinemann, U. Karsten, E.M. Pfeiffer, J. Regnery, M. Scheinert, J. Thiede, R. Tiedemann & D. Wagner

ALFRED-WEGENER-INSTITUT
HELMHOLTZ-ZENTRUM FÜR POLAR-
UND MEERESFORSCHUNG

BREMERHAVEN

Am Handelshafen 12
27570 Bremerhaven
Telefon 0471 4831-0
Telefax 0471 4831-1149
www.awi.de

HELMHOLTZ
GEMEINSCHAFT